

JODY M. KLYMAK

INTRODUCTION TO PHYSICAL OCEANOGRAPHY

UNIVERSITY OF VICTORIA

Copyright © 2022 Jody M. Klymak

PUBLISHED BY UNIVERSITY OF VICTORIA

/

Licensed under the Apache License, Version 2.0 (the “License”); you may not use this file except in compliance with the License. You may obtain a copy of the License at <http://www.apache.org/licenses/LICENSE-2.0>. Unless required by applicable law or agreed to in writing, software distributed under the License is distributed on an “AS IS” BASIS, WITHOUT WARRANTIES OR CONDITIONS OF ANY KIND, either express or implied. See the License for the specific language governing permissions and limitations under the License.

First printing, November 2022

Contents

	<i>I</i>	<i>Overturning circulations</i>	10
1		<i>Estuaries</i>	11
	1.1	<i>Pressure differences</i>	12
	1.2	<i>Estuarine Flow</i>	13
	1.2.1	<i>Salt-wedge estuary</i>	13
	1.2.2	<i>Fjord-type estuary</i>	13
	1.2.3	<i>Flood-plain estuaries</i>	14
	1.2.4	<i>Time-dependence</i>	16
	1.2.5	<i>Topographic blocking (mostly in fjords)</i>	19
	1.3	<i>Quantifying the Circulation</i>	19
	1.3.1	<i>The Conservation of Volume</i>	20
	1.3.2	<i>Calculating volume transport</i>	21
	1.3.3	<i>Conservation of a mass of a substance</i>	21
	1.3.4	<i>Using the concentration and volume transport to calculate advective transport and flux</i>	21
	1.3.5	<i>Application to Estuaries: the Knudsen Relation</i>	23
	1.4	<i>Exercise</i>	25
2		<i>Equation of State and Pressure Gradients</i>	29
	2.1	<i>Temperature</i>	29
	2.1.1	<i>Measurement</i>	30
	2.1.2	<i>In-situ and potential temperature</i>	31

2.2	<i>Salinity</i>	31
2.2.1	<i>Measurement</i>	33
2.3	<i>Pressure</i>	34
2.3.1	<i>Measuring pressure</i>	35
2.4	<i>Calculating density</i>	35
2.4.1	<i>Density relation</i>	36
2.4.2	<i>Potential density</i>	37
2.4.3	<i>Cabbeling</i>	39
2.5	<i>Other seawater properties</i>	40
2.5.1	<i>Sound</i>	40
2.5.2	<i>Light transmission</i>	41
2.5.3	<i>Ice</i>	41
2.6	<i>Pressure Gradients</i>	42
2.6.1	<i>Hydrostatic Pressure</i>	43
2.6.2	<i>Single density fluid</i>	43
2.6.3	<i>Two-density fluid</i>	45
2.7	<i>Pressure gradients</i>	46
2.7.1	<i>Surface pressure gradients</i>	46
2.7.2	<i>Internal pressure gradients</i>	47
2.8	<i>Exercise</i>	49
3	<i>Heat and Salt fluxes</i>	50
3.1	<i>Surface heat fluxes</i>	50
3.1.1	<i>Incoming shortwave radiation</i>	51
3.1.2	<i>Longwave radiation (back radiation)</i>	59
3.1.3	<i>Sensible heat transfer</i>	59
3.1.4	<i>Latent heat losses</i>	60
3.1.5	<i>Integrated Surface Heat Fluxes</i>	62
3.2	<i>Surface freshwater fluxes</i>	64
3.2.1	<i>Evaporation and precipitation patterns</i>	65

3.3	<i>Fluxes and transports in the ocean</i>	67
3.3.1	<i>Advective flux</i>	67
3.3.2	<i>Advective transport</i>	68
3.3.3	<i>Conservation of mass (and heat)</i>	68
3.3.4	<i>Conservation of mass and volume</i>	70
3.4	<i>Diffusive Fluxes</i>	71
3.5	<i>Net flux: advection plus diffusion</i>	73
3.5.1	<i>Turbulent diffusivities</i>	74
3.5.2	<i>Turbulent diffusion</i>	75
3.6	<i>Exercises</i>	78
4	<i>Ocean water masses</i>	81
4.1	<i>Surface distributions of temperature and salinity</i>	82
4.2	<i>Meridional sections</i>	83
4.3	<i>Vertical distributions, and the surface mixed layer</i>	88
4.4	<i>Property-property plots: θ-S plots</i>	93
4.5	<i>Summary</i>	96
4.6	<i>Exercises</i>	98
5	<i>Thermohaline overturning circulation</i>	100
5.1	<i>Inferring the overturning circulation from other tracers</i>	101
5.1.1	<i>Bio-active tracers</i>	101
5.1.2	<i>Radioactive and tracers from the crust</i>	104
5.1.3	<i>Man-made tracers</i>	107
5.2	<i>Deep water formation processes</i>	111
5.2.1	<i>Antarctic Bottom Water</i>	111
5.2.2	<i>North Atlantic Deep Water</i>	111
5.3	<i>Inferring the strength of the overturning circulation from data</i>	113
5.3.1	<i>Inverse results</i>	116
5.3.2	<i>How to make an inverse calculation</i>	119
5.4	<i>Theory of overturning circulation and Sandstrom's theorem</i>	122
5.5	<i>Exercises</i>	125

6	<i>Climate Change; The Effect on the Overturning Circulation and Sea Level</i>	127
6.1	<i>Effect of melting on the overturning circulation</i>	127
6.2	<i>Sea level change</i>	131
6.2.1	<i>Land-fast ice</i>	132
6.2.2	<i>Thermal expansion (steric change)</i>	133
6.3	<i>Future sea level rise</i>	133
6.4	<i>Other reading</i>	134
II	<i>Waves and Tides</i>	137
7	<i>Surface gravity waves</i>	138
7.1	<i>Characterizing waves</i>	139
7.2	<i>Causes</i>	140
7.3	<i>Dispersion relation, phase speed, and particle motion</i>	142
7.4	<i>Orbital motions: velocity of water parcels</i>	143
7.5	<i>Group speed</i>	145
7.6	<i>Energy conservation</i>	150
7.7	<i>Refraction and diffraction</i>	151
7.8	<i>Non-linearity</i>	153
7.9	<i>Exercises</i>	154
8	<i>Tides</i>	157
8.1	<i>Tidal example and describing tides</i>	157
8.2	<i>Tidal forces: Gravity and centrifugal forces on co-orbiting bodies</i>	158
8.3	<i>The reason for various tidal frequencies</i>	162
8.3.1	<i>Twice a day tides</i>	163
8.3.2	<i>Daily tides (diurnal): Tides due to non-equatorial orbits</i>	165
8.3.3	<i>Longer period tides</i>	167
8.4	<i>Dynamic theory of the tides</i>	168
8.4.1	<i>Tidal Resonance</i>	168
8.4.2	<i>Frictional effects</i>	170
8.4.3	<i>Global response</i>	170

8.5	<i>Exercises</i>	172
	<i>III Wind-driven circulations</i>	174
9	<i>Wind-driven circulation overview</i>	175
9.1	<i>Coastal upwelling</i>	175
9.2	<i>North Pacific observations</i>	180
10	<i>Coriolis force and Ekman Balance</i>	193
10.1	<i>Quick review of forces and apparent forces</i>	193
10.2	<i>Centrifugal and Coriolis forces</i>	195
10.2.1	<i>Centrifugal force</i>	195
10.2.2	<i>Coriolis force</i>	197
10.3	<i>Friction force</i>	201
10.3.1	<i>External stresses</i>	202
10.4	<i>Ekman balance</i>	203
10.4.1	<i>The Ekman spiral: fact and fiction</i>	205
10.5	<i>Ekman convergence and divergence</i>	207
10.6	<i>Exercises</i>	210
11	<i>Geostrophic balance and coastal flow</i>	211
11.1	<i>Geostrophic balance</i>	211
11.1.1	<i>Thermal wind</i>	213
11.1.2	<i>Level of no motion and "dynamic height"</i>	214
11.2	<i>Coastal upwelling, complete picture</i>	215
11.2.1	<i>Internal dynamics on shelf</i>	216
11.3	<i>Exercises</i>	220
12	<i>Sverdrup balance and basin-scale circulation</i>	222
12.1	<i>Circulation</i>	223

12.2	<i>Conservation of potential vorticity</i>	224
12.3	<i>Sverdrup transport</i>	226
12.3.1	<i>Alternative derivation: Ekman pumping</i>	228
12.4	<i>Return flow</i>	230
13	<i>Bibliography</i>	232
	<i>Index</i>	237

Foreward

These are the course notes for Descriptive Physical Oceanography, taught at the University of Victoria, School of Earth and Ocean Sciences, a 13-week undergraduate offering.

Unlike many physical oceanography courses, students taking this course are not expected to have vector calculus or differential equations, nor are they expected to have classical mechanics beyond what is typically offered in a first year physics course. Many of the students taking the course have a deep interest in understanding the ocean, and often approach the course with considerable intuition. The challenge of a course like this is to more than just a list of facts, but rather to try and give a feeling for the forces that drive the ocean, without becoming too bogged down in mathematical formalism. As such this course tries to strike a balance between knowing about the various physical phenomena in the ocean and understanding the dynamics that gives rise to them, while still giving the students some practice in practical calculations.

The course is divided into three unequal parts - overturning circulations driven by lateral buoyancy differences and mixing; waves and tides; and wind-driven circulations. We start with estuaries as a nice introduction to overturning circulations, but also because the students do work in Saanich Inlet, and understanding estuaries early is very helpful.

Part I

Overtaking circulations

1

Estuaries



Estuaries are semi-enclosed basins of water that are strongly influenced by freshwater sources (i.e. a river) or evaporation, yet have an opening to the open ocean where salty water can get into the basin. The semi-enclosed nature of the basin allows time for mixing between the fresh and the ocean water, and the density differences created drive a strong *overturning circulation* in the basin, such that much more water is drawn up the estuary than starts out flowing in from the river. Here we attempt to describe how this circulation works. How estuarine circulation occurs is subtle, but not terribly difficult to understand qualitatively. It is, however, not amenable to simple mathematical description, which may explain its omission from basic texts.

It is a little unusual to start a course with something as dynamic as an estuary. We do this as a bit of foreshadowing for the rest of the course, and because Saanich Inlet is an estuary, and we will be considering Saanich Inlet in the context of the course project.

1.1 Pressure differences

Before we start, it is helpful to think about how pressure differences drive flows. A fluid moves due to friction (i.e. the wind blowing over the surface), direct action (i.e. a paddle pushing water), or pressure forces. Pressure forces are unique to fluids, and are the forces that the water can exert on itself. In general they tend to move water so that pressure differences are evened out, i.e. the water pushes itself from high pressure regions to low pressure regions.

If the sea-surface is tilted, then the pressure will be greater where the sea surface is high than where it is low; in figure 1.1, $P_1 > P_2$. This will drive the flow from left to right. *Note* pressure increases with depth, so when we think about how the pressure moves water, we need to think about the pressure along a “geopotential” surface (ie. a surface along which the water would be flat). For our purposes, this is a set distance below the flat surface of the water.

In general, it is a good rule to think that the water will move in the direction that will lead to a flattening of the surface. The resting state of the body of water is to have a flat surface, as indicated with the dashed line at the surface in figure 1.1.

The situation is more complicated if we add density variations. Consider just tipping the interface of a two-layer fluid (figure 1.2), where the lighter fluid floats on top of the denser ($\rho_0 < \rho_1$; tilting this interface is actually hard to do, but just imagine). At first, the pressure difference in the upper layer is zero ($P_3 = P_4$) because the upper interface is not tilted. However, there is more dense water on the left side than the right, so there is a pressure gradient below the interface, $P_1 > P_2$, driving deep water to the right.

This leads to more water on the right hand side than the left side (figure 1.2b). This makes a surface pressure gradient that tends to drive the upper layer to the left ($P_4 > P_3$). This surface pressure gradient is set up *very* quickly, and only involves a tiny amount of water in order to drive the surface-layer flow to the left.

The water column will slosh around for a while, but friction will eventually damp the motions and the interfaces will be flattened as indicated with the dashed lines (figure 1.2c).

Again, the general idea is that the body of water has pressure gradients in it that drive a flow that will tend to flatten the layers.

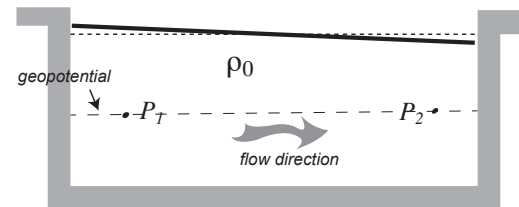


Figure 1.1: A body of water of uniform density with a tilted upper surface. Note that P_1 and P_2 are at the same geopotential height (i.e. their value of z is constant)

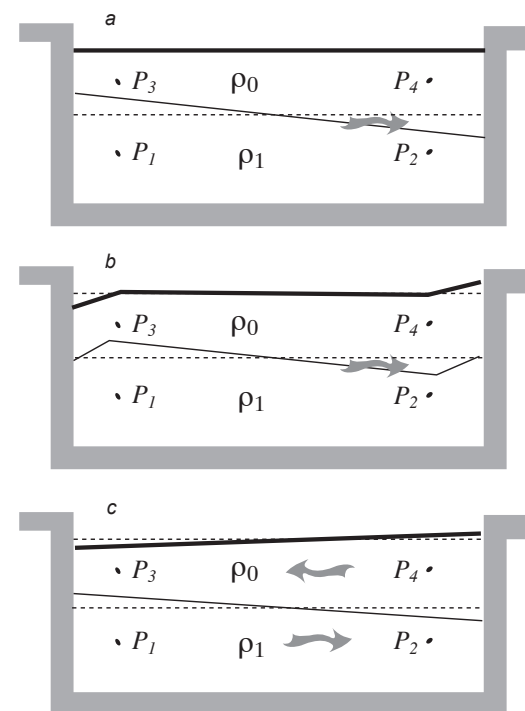
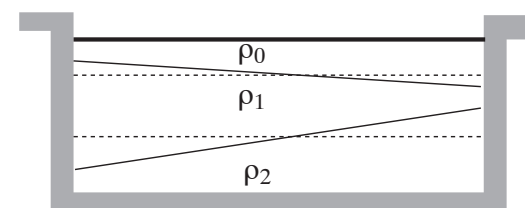


Figure 1.2: A two-layer body water with an interface that is initially tilted. See text for the description.



1.2 Estuarine Flow

1.2.1 Salt-wedge estuary

Estuaries are bodies of water with opposing buoyancy sources at their ends, usually a river at the head and the ocean at the mouth. The buoyancy difference usually arise from the salt content of the water, with fresh water being “lighter”, or more buoyant, than salty water. The simplest situation is a river spills into the ocean, spreads out and becomes a buoyant plume (figure 1.4). If we quantify the river volume transport as R (typically in units of $m^3 s^{-1}$) then in **steady state** the transport out the mouth of the estuary will be $Q_o = R$. The deep ocean layer will be stagnant.

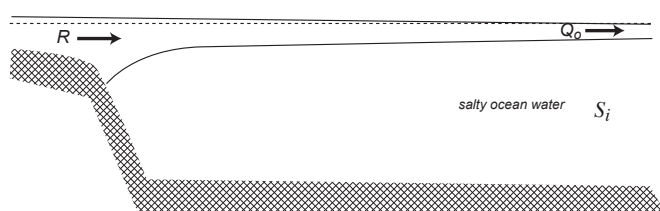


Figure 1.4: A salt-wedge estuary and river plume. The river discharges into the salt water without substantial mixing.

This type of estuary is called a *salt-wedge estuary*. The mouth of the Fraser River is a classic example of a salt-wedge estuary with a spreading plume (figure 1.5). Fresh water runs over salty with a small amount of mixing between the two layers. The salinity goes from 2 psu to 24 psu (1 psu \approx 1 part-per-thousand, or gram of salt per kilogram of water) in just a few meters vertically. This sharp front moves back and forth with the tide, a typical feature of most salt-wedge estuaries.

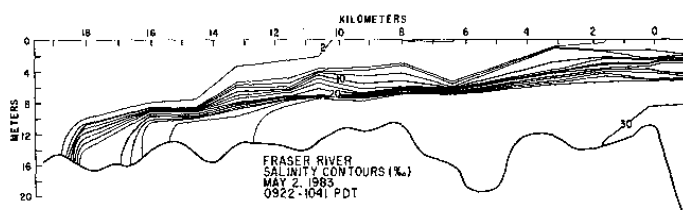


Figure 1.5: Salinity contours in mouth of the Fraser River. Salinity has units of parts per thousand, or ppt. So 1 ppt means 1 gram of salt per kilogram of water. The unit “psu” is also often used, meaning practical salinity unit, with 1 psu = 1 ppt. The river is on the left, the ocean on the right. [Geyer and Farmer, 1989]

1.2.2 Fjord-type estuary

Unlike a *salt-wedge estuary*, most estuaries have an “exchange flow” that is much stronger than the river flow. This flow is driven by vertical mixing that in turn creates tilted “isopycnals”, or constant density surfaces. These tilted isopycnals want to flatten out due to the pressure gradients that are set up, as discussed above.

As an example, imagine the situation pictured in figure 1.6. Here a river flows into salty water. If turbulent mixing is driven by strong tidal flow over the topographic bump in the middle of the estuary, then intermediate-salinity water will be formed. This intermediate-salinity water will be denser than the river water, but lighter than the ocean water, and will set up a flow that is pictured in figure 1.6b.

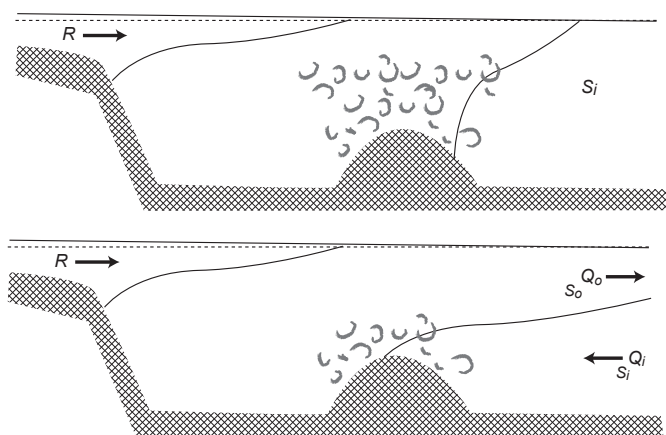


Figure 1.6: The effect of weak local mixing on flow in a fjord-type estuary. Intermediate salinity water is formed by the mixing which drives a flow out to sea. In this figure, “isohalines” are indicated by the contours (constant salinity surfaces) and will correspond to “isopycnals” (constant density surfaces) in most cases.

Determining the steady-state for such a flow is not trivial, and not very conducive to theoretical formulation. However, general tendencies can be determined. If there is more mixing, more intermediate water is formed. In steady state, this intermediate water must be flushed away, so there is a stronger circulation. Conversely, if the mixing is weaker, less intermediate water is produced, weakening the circulation.

1.2.3 Flood-plain estuaries

The more mixing that takes place, the more vertical the isopycnals, and the stronger the exchange flow relative to the river flow. The salt and density fields also become much more complicated. In shallow estuaries, of which the Chesapeake Bay is an excellent example, mixing from bottom stress and the winds tends to affect the whole water column, not just near topographic features. This sets up large along-estuary salinity and density gradients (figure 1.7). These types of estuaries tend to have much stronger amplification of the river flow (R) because of the extra mixing.

An example from an arm of the Chesapeake demonstrates how such an estuary may look (figure 1.8). Up estuary of Maryland Point, the estuary is really a river with no salinity. However, unlike the salt-wedge estuary, there is a gradual horizontal gradient of many kilometers before salty water is found. Note that even at this point the

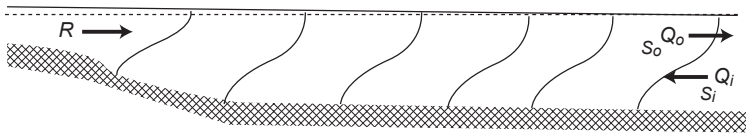


Figure 1.7: A flood-plain estuary schematic. Salinity increases from the head to the mouth, with weak vertical gradients.

water is still only 12 psu, and that the Chesapeake Estuary continues for hundreds more kilometers before open-ocean water is found.

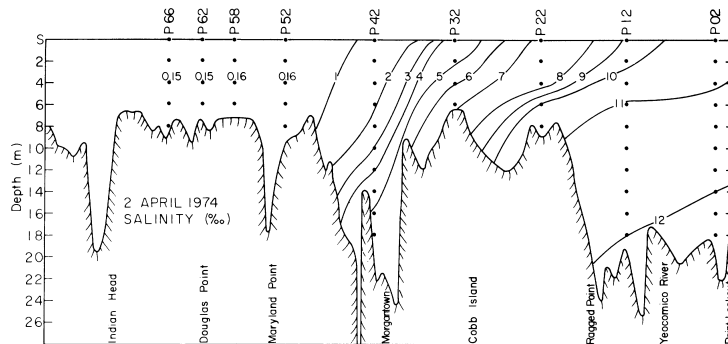


Fig. 8. Salinity section, April 1974.

Figure 1.8: A salinity cross-section from the Upper Potomac estuary, part of the Chesapeake Bay estuarine system [Elliott, 1976].

The whole estuary has been measured and simulated numerous times. A recent example is shown in figure 1.9. Here the upper layer of fresher water can be seen flowing south and seaward. There is a strong return flow in the bottom 20 m. Note that the volume transport of the return flow is not accurately represented by these velocities, since they do not take into account the fact that the Bay widens considerably as it travels further south.

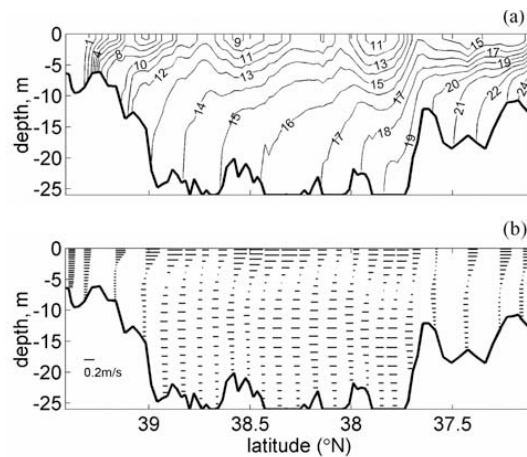


Figure 1.9: A salinity and mean velocity sections from a numerical model of the whole Chesapeake Bay [Li et al., 2005]

Also note the lenses of fresher water that appear along the estuary. These occur because of rivers along the length of the estuary. This

complicates the simple picture given above, but the general trend of the flow remains unchanged.

1.2.4 Time-dependence

Time dependence changes the steady-state balance in estuaries in three main ways. First, the fresh-water input at the head of the estuary can change (figure 1.10). This significantly changes the salinity content of the estuary and the estuarine circulation. Somewhat paradoxically, the increased river flow can lead to a decreased estuarine flow. For instance in the Apr 1968 panel the isopycnals are much less tilted than in the Oct panel, indicating enhanced flow. The balance here, however, is not a perfect one, and determining the exact response if the river forcing changes depends on the mixing response. Strong vertical density gradients caused by fresh water influx can suppress turbulence and hence reduce the mixing required to drive the exchange flow.

A second effect that can change the forcing of an estuary is that the ocean water at the mouth of the estuary can change salinity due to seasonal changes in the open ocean. This tends to be a smaller effect because the salinity differences, even in coastal waters, tend to be less pronounced. However, coastal waters are subject to seasonal changes due to coastal upwelling and downwelling. During upwelling, denser water can be found at the estuary mouth, whereas during downwelling the density can decrease.

Finally, there is a time dependence to the mixing that ultimately drives the enhanced estuarine circulation. The most regular source of time-dependence is the tidal forcing. This varies with the fortnightly (every two weeks) modulation of the tide, and with the long-term perigee/apogee variations of the moon-earth-sun system. More mixing during the *spring* tides leads to *isohalines* that are more tilted (figure 1.11) which therefore drive more circulation.

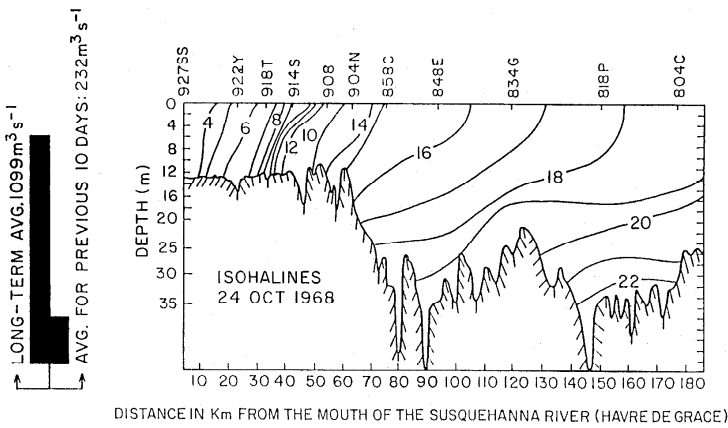
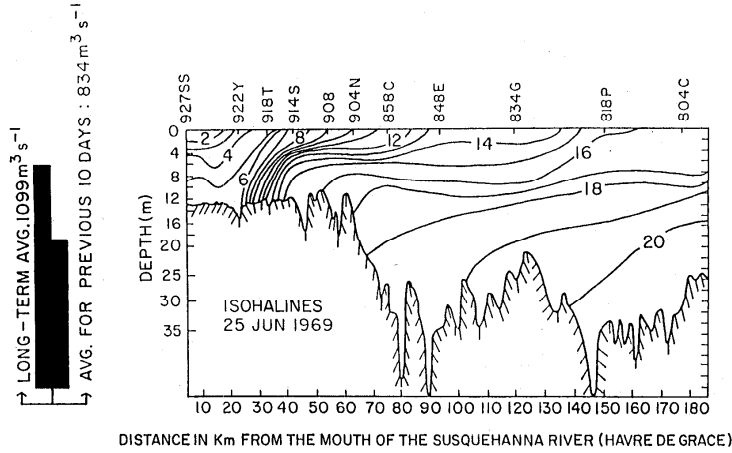
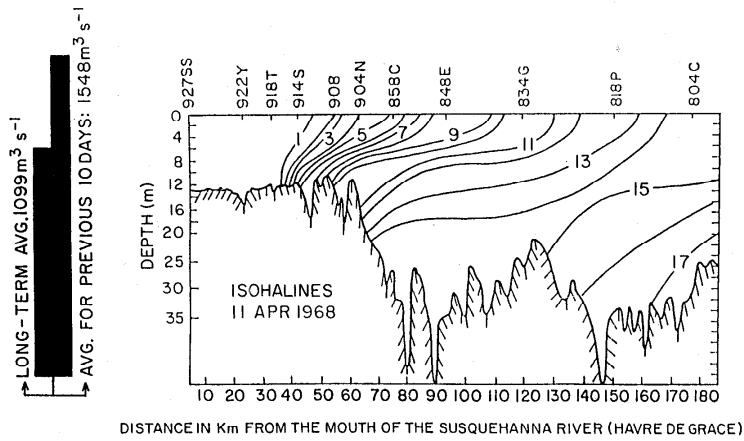


Figure 1.10: Salinity in the Chesapeake as it varies due to river discharge over the year (bars on left) [Schubel and Pritchard, 1986].

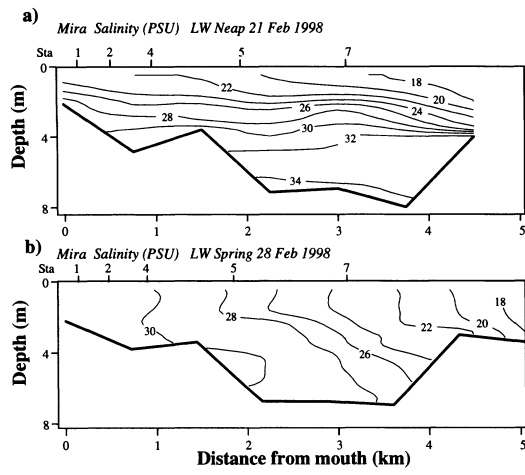


Figure 1.11: Salinity in the Mira estuary (Portugal) during neap and spring tides [Blanton et al., 2000].

1.2.5 Topographic blocking (mostly in fjords)

One final topic is topographic blocking. Fjords are often demarcated from the ocean by underwater sills (terminal moraines left over from glaciations). These sills can be quite tall and sometimes the tides are not strong enough to bring the densest water from the ocean-side of the sill over the sill (figure 1.12a). The estuarine circulation carries on as normal above this depth, but the deep ocean layer does not make it into the landward basin. This is called “blocking”.

However, occasionally strong tides perhaps enhanced by atmospheric forcing will conspire to provide enough energy for the densest water to get over the sill. This dense water will spill over the sill and, if it does not mix, will reach the bottom of the fjord (figure 1.12b). For some fjords this happens every spring-neap cycle. For others only when the spring tide is particularly large, or the water on the seaward side denser than usual.

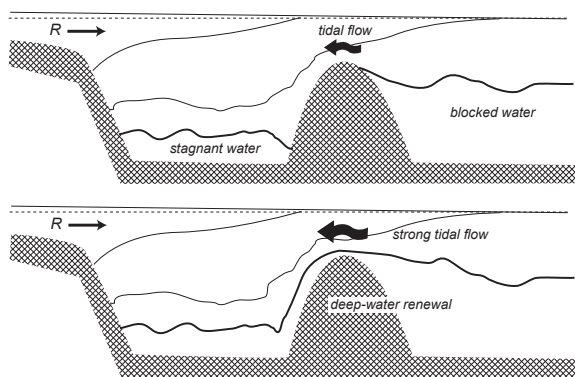


Figure 1.12: A narrow-silled fjord with blocking of deep water, and a deep-water renewal event.

Conversely, if the sill is broad, or has a lot of horizontal constrictions, deep-water renewal can happen on the exact opposite phase of the spring-neap cycle (figure 1.13). During spring tides the incoming dense water is subjected to so much mixing that it is mixed away before it can reach the inner basin. It is only during neap tides with enough velocity to push the dense water into the inner basin, but not so much as to cause excessive mixing that deep-water renewal can take place.

1.3 Quantifying the Circulation

See also, Open University Sec 6.2

Estuaries are a great example of mass and volume conservation. These concepts are very important for all of oceanography (and probably most of science in general). Most people are familiar with the concepts, but laying out the mathematics takes some care (often just

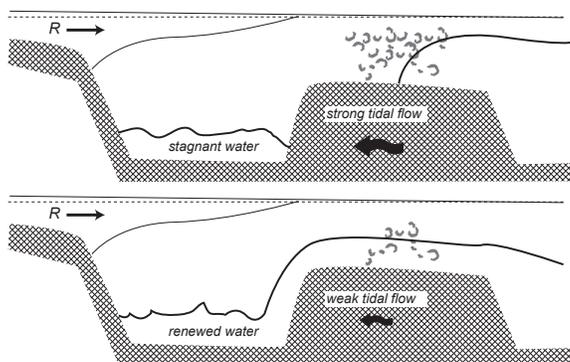


Figure 1.13: A broad-silled fjord with blocking of deep water during spring tides, and a deep-water renewal during neaps.

keeping the units straight!).

In an estuary, water flows in the river mouth, and in and out at the ocean end of the estuary. If everything is in “steady-state” we can write equations that relate the incoming mass of water and mass of salt to the outgoing, and make assumptions about the flow based on those measurements. The discussion below indicates how that is done.

1.3.1 The Conservation of Volume

Suppose we are interested in the dynamics of a body of water, say a rectangular swimming pool. The pool has a hose pumping water into it at a rate of volume transport of $q[\text{m}^3\text{s}^{-1}]$. If its surface area A , how fast is the water rising in the pool?

Here the answer is relatively easy. The speed at which water rises in the pool is $w = q/A$, the volume transport divided by the surface area. Here we have applied the conservation of volume:

$$\frac{dV}{dt} = - \sum_i q_i + \sum_j s_j. \quad (1.1)$$

where V is the volume of fluid in the body we are studying, q_i are individual transports out of (positive) or into (negative) the volume. The last term is the sum of the sources (positive) and sinks (negative) inside the volume, and is included for completeness. For the conservation of volume of water, a sink could be evaporation, and a source rainfall. We differentiate such source and sinks from the “advective” transports (caused by water velocity) because the physics is distinct.

Formally, this should really be conservation of mass in the volume. In which case:

$$\frac{d}{dt} \int_V \rho dV = - \sum_i \rho_i q_i + \sum_j \rho_j s_j. \quad (1.2)$$

where the integration over the volume is summing all the mass in

the volume. However, the density of water only changes by a few percent, so equation (1.1) is a very good approximation.

1.3.2 Calculating volume transport

Volume transports only arise because water is moving from point a to point b. Sometimes we are given the volume transport (in $\text{m}^3 \text{s}^{-1}$), but sometimes we want to report the velocity. i.e. in the swimming pool example above we wanted to know how fast the water was rising (i.e. in ms^{-1}). In the simple case:

$$q_i = A_i u_i \quad (1.3)$$

where A_i is the *cross-sectional area* the water is flowing through, and u_i is a velocity *perpendicular* to that area. In vector calculus we write this as:

$$q_i = \int_A \mathbf{u} \cdot d\mathbf{A} \quad (1.4)$$

where the dot product makes it clear that the flux is perpendicular to the area and the integral sign means that we are summing over many small elements.

1.3.3 Conservation of a mass of a substance

The conservation of a substance (or heat) has essentially the same terms:

$$\underbrace{\frac{d}{dt} \int_V S dV}_{\text{change of amount of stuff}} = \underbrace{\sum_i q_S}_{\text{transport of stuff in}} + \underbrace{\sum_j s_S}_{\text{internal sources}} \quad (1.5)$$

Here the substance, S , is expressed in stuff-per-volume. i.e. g m^{-3} . We often discuss the *mean concentration in a volume* as $\bar{S} = \int_V S dV / V$, in which case the equation simplifies to:

$$V \frac{d\bar{S}}{dt} = \sum_i q_S + \sum_j s_S \quad (1.6)$$

The *transport of stuff* q_S is expressed in units of stuff per time (i.e. g s^{-1}).

1.3.4 Using the concentration and volume transport to calculate advective transport and flux

In fluid mechanics we often measure the concentration of a substance (S) separately from the volume transport q or velocity u . For instance if Chlorine is mixed in a vat at a concentration of $S = 200 \text{ g/m}^3$ and

flows through a pipe at $q_v = 0.01\text{m}^3\text{s}^{-1}$ then the rate of chlorine transport into the pool is:

$$q_S = Sq_v \quad (1.7)$$

and has units gs^{-1} . This is called an *advective transport* of chlorine.

If instead we knew the velocity of the water u and the concentration, then we might have expressed this as a *flux* of chlorine:

$$F_S = Su \quad (1.8)$$

Because velocity is a vector, this flux is more properly written as a vector:

$$\mathbf{F}_S = S\mathbf{u} \quad (1.9)$$

and the flux flows in the same direction as the water. Note that the units of the flux are $\text{gs}^{-1}\text{m}^{-2}$. The *transport* (in g/s) of the material through an area A perpendicular to the flow is thus simply:

$$q_S = F_S A = SuA. \quad (1.10)$$

This can all get confusing if the concentration is expressed as parts per thousand, or some other volume unit like that (i.e. mL/L). This can be dealt with in the same ways, but it requires some extra care with the units.

Box 1.3.1: Examples of conservation of mass

Q: Suppose we have a vat, with volume $V = 10 \text{ m}^3$ of water in it. A hose flows into it at a rate of $0.1 \text{ m}^3/\text{s}$ and a second hose flows out at the same rate. If the concentration of Caffeine in the vat is initially $0 \text{ g}/\text{m}^3$, and $10 \text{ g}/\text{m}^3$ in the hose, what is the rate that caffeine is being added to the tank?

A: it is simply $qC = 1 \text{ g}/\text{s}$.

Q: What rate is caffeine leaving the tank initially?

A: The initial concentration in the tank is zero, so $qC = 0 \text{ g}/\text{s}$.

Q: Assuming the tank is well mixed, what is the rate of change of the concentration in the vat, initially?

A: This is just the rate of change of the amount of caffeine, $1 \text{ g}/\text{s}$ divided by the volume of water in the vat, so $0.1 \text{ gm}^{-3}\text{s}^{-1}$.

Q: New vat, with three hoses. One hose has $C_1 = 10 \text{ g}/\text{m}^3$ of caffeine and flows at $q_1 = 0.1 \text{ m}^3/\text{s}$. The second hose flows in with $C_2 = 5 \text{ g}/\text{m}^3$, and $q_2 = 0.4 \text{ m}^3/\text{s}$. If the vat is well-mixed and in steady state, what is the flow out the third hose, and what is the concentration of the caffeine in the water in the vat?

A: First, in steady state, the volume fluxes equal zero (there can be no net flow into the vat), so $q_1 + q_2 + q_3 = 0$. We know q_1 and q_2 , so we know $q_3 = -0.5 \text{ m}^3/\text{s}$, where the negative sign means water is flowing out.

We also know that there can be no net flow of caffeine, so $C_1q_1 + C_2q_2 + C_3q_3 = 0$. We know everything except for C_3 , so we solve and get $C_3 = \frac{C_1q_1 + C_2q_2}{-q_3} = 6 \text{ g}/\text{m}^3$.

1.3.5 Application to Estuaries: the Knudsen Relation

An application to estuaries is to conserve both volume in the estuary, and salt. Imagine that the flow at the mouth is two layers, one in with a volume transport $Q_i \text{ m}^3\text{s}^{-1}$, and one out with volume transport Q_o , and that the river has a volume transport of R . Suppose the salinity of the lower layer flowing in is S_i in units of parts-per-thousand, and the salinity of the layer flowing out is S_o .

Q: What is the salinity of the river?

Q: What is the salt transport into the fjord in g/s ?

Q: Assuming the fjord is in steady state, write out an equation for the volume budget, and a second equation for the salt budget. i.e the volume transport in equals the volume transport out and the salt transport in is equal to the salt transport out.

Q: Assume R , S_i , and S_o are known. Show that:

$$Q_i = \frac{S_o R}{S_i - S_o}. \quad (1.11)$$

Q: If there is no mixing of the river water, what is S_o , and how big is Q_i ?

Q: If there is lots of mixing, what happens to $S_i - S_o$ and thus Q_i ?

1.4 Exercise

We will practice some of what we have learnt based on a paper about local waters by Masson and Cummins [2004]. As part of your final project you will read about similar processes in Saanich Inlet [Gargett et al., 2003].

Q: Consider figure 1.14, which shows the salinity observed and modeled in the Strait of Juan de Fuca. Based on these plots, where do you think the mixing is the strongest in the Strait?

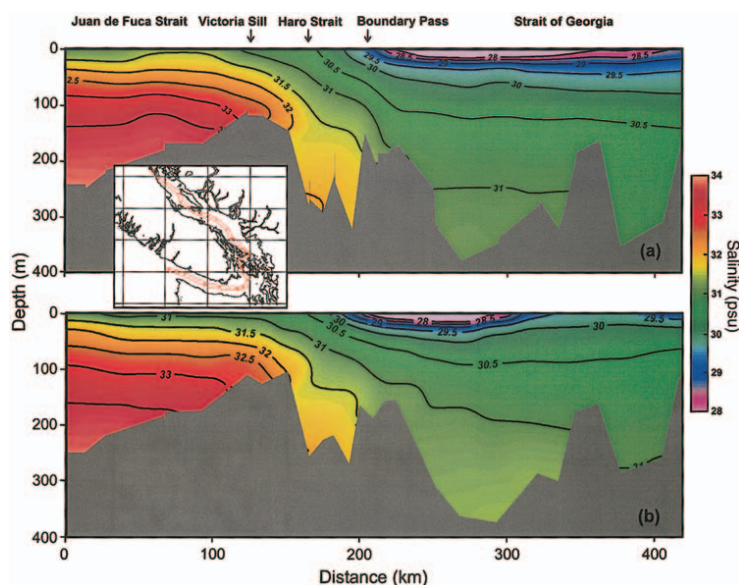


Figure 6. Along-strait section of annual mean salinity from observations (a) and the reference experiment (b).

Figure 1.14: Observed and modeled salinity in the Straits of Juan de Fuca and Georgia [Masson and Cummins, 2004]. The ocean is on the left, and the Fraser River is at Distance = 270 km. The upper plot (a) are the observations and the lower (b) a numerical simulation.

Q: For the flow in figure 1.14, sketch where you think the water is flowing. What happens north of the Fraser river (at Distance = 250 km; make sure you know where north is on this plot)?

Q: Consider figure 1.15, which compares two numerical model runs, one with tides and one without. Which is which, and why? Which has the stronger horizontal circulation?

Q: A seasonal time series of the salinity in Haro Strait is given in figure 1.16. What features of the flow can you identify that indicate the time dependence of the estuarine flow? Pay particular attention to the modeled timeseries (which has better temporal resolution)?

Q: Use the Knudsen relation on the two data plots in figure 1.15 to estimate the exchange flow if the river input is $10^4 \text{ m}^3 \text{ s}^{-1}$. Which case has a stronger exchange, a) or b)?

Q: Suppose the river is suddenly dammed, so $R = 0 \text{ m}^3 \text{ s}^{-1}$. The estuary's average salinity will (initially) change at what rate (in units of psu s^{-1})? Hints: first, you should assume that the estuary adjusts

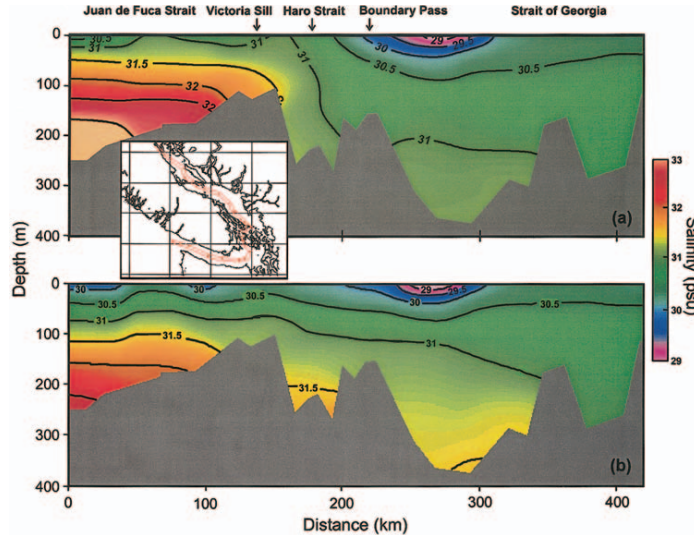


Figure 1.15: Salinity for two model runs, one with and the other without tides [Masson and Cummins, 2004].

so the flux in is equal to the flux out the mouth. Second, you need to estimate the volume of the estuary to answer this questions. Rough numbers are fine, based on the figures above.

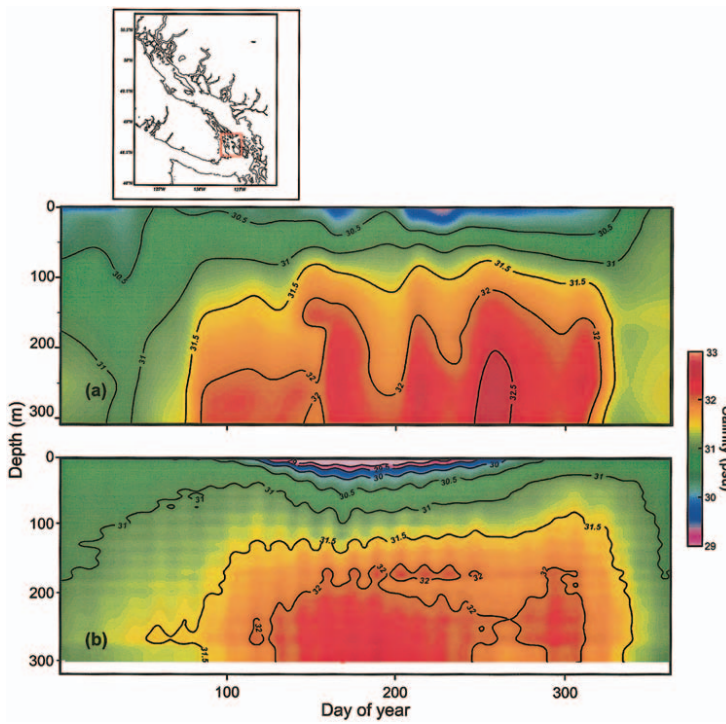


Figure 1.16: Time evolution of observed and modeled salinity in Haro Strait [Masson and Cummins, 2004].

Box 1.4.1: Practice questions (not the exercise!)

Some students are not comfortable with volume and mass balances. If that is the case, try some extra practice questions below. Please ask me if you need more help with these!

- Suppose the water level of a straight-sided pool is observed to rise at 0.01 m/s , and has a surface area of 50 m^2 . There is one hose filling it with speed 4 m/s and cross-sectional area 0.01 m^2 , and a second hose filling it with a cross sectional area of 0.02 m^2 . What is the flow speed in the second hose?
- Suppose a pipe has a diameter of 0.1 m and a flow speed of 1 m/s . If the pipe narrows to 0.05 m what is the flow speed at that part of the pipe (in steady state)?
- Suppose there is a vat with 200 g/m^3 solution of chlorine being fed into the pool through a hose with diameter 0.1 m at a rate fast enough to replace evaporative losses in the pool of $0.01 \text{ m}^3/\text{s}$. What is the transport of chlorine into the pool?
- If the average concentration of chlorine in the pool is initially 50 g/m^3 and 1000 s later is measured to be 55 g/m^3 , what is the volume of the pool?

2

Equation of State and Pressure Gradients

In this chapter we go back now and consider some fundamentals about water that are important to this course. Seawater is a relatively complex substance. As discussed before, lateral density differences can drive lateral circulation, hence it is important to understand and predict how those differences arise. Further, the ocean is a huge reservoir of heat, and understanding its heat content is important for predicting weather and future climate.

2.1 Temperature

Temperature is a thermodynamic property of a substance, the value of which is proportional to the kinetic energy of the random motions of the molecules in the substance (these are called **Brownian motion**). The heat necessary to bring a substance to a given temperature is proportional to the *heat capacity*. In order to change a parcel of water's temperature by ΔT , we need to supply energy proportional to the heat capacity of the water:

$$\Delta E = c_p \Delta T \quad (2.1)$$

where c_p has units of $J C^{-1} kg^{-1}$, and ΔE has units of $J kg^{-1}$. Values for c_p are given in figure 2.1, and note that the heat capacity is not constant, but depends on the temperature of the water, its salinity, and its pressure! The dependence is non-linear, so we usually resort to using a computer to calculate the empirically-derived values. However, for a litre of fresh water ($\approx 1 kg$) at $20^\circ C$ we would need 4180 J of energy to raise the temperature by one degree.

The heat capacity of water is impressive compared to air, where typical values are $1000 J C^{-1} kg^{-1}$. The whole atmosphere has a weight of $\approx 10^4 kg m^{-2}$, so heating the whole atmosphere one degree requires $\approx 10^7 J m^{-2}$. Conversely, the ocean at 4000 m deep and with a density close to $1000 kg m^{-3}$ weighs approximately $4 \times 10^6 kg m^{-2}$, so raising its temperature by one degree requires $16 \times 10^9 J m^{-2}$,

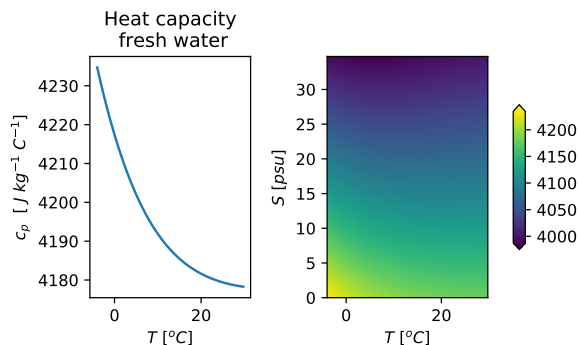


Figure 2.1: Heat capacity of water a) for fresh water as a function of temperature, b) as a function of both salinity and temperature. Both are presented at the sea surface.

more than three orders of magnitude more energy. This helps explain why the ocean is such an important reservoir of heat in the climate system.

2.1.1 Measurement

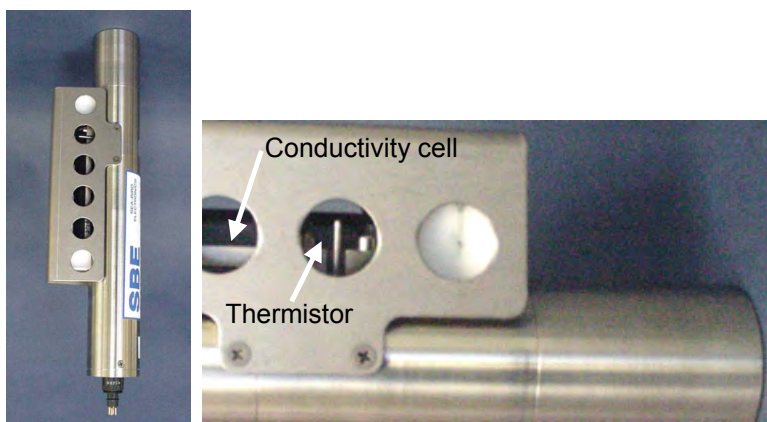


Figure 2.2: a) CTD b) thermistor and conductivity probe on a CTD.

Temperature is measured in the ocean by thermometers. The typical technology is what is called a “**thermistor**”, which is a metal in which the electrical resistance changes proportional to its temperature. Since its relatively easy to design an electronic circuit to measure resistance, this has allowed rapid and automatic measurement of ocean temperatures since such thermistors were first developed in the 1970s.

Once calibrated, quality ocean thermistors are typically accurate to $0.001\ ^{\circ}C$, and are stable to similar levels. It takes time for the thermistor to respond to temperature changes in the ocean, so designing the sensors is a tradeoff between physical robustness and response time. Typical response time is about $0.3\text{--}0.5\ s$, which is quite fast for ocean changes, but can be slow relative to a CTD being lowered in

the ocean.

2.1.2 *In-situ and potential temperature*

Ocean temperatures are largely set at the sea surface either by absorbing sunlight or exchanging heat with the atmosphere, and subsequently modified by ocean mixing. The temperature of the water is thus a powerful *tracer* of where a water mass last saw the surface of the ocean, with warmer waters found near the equator, and colder near the poles.

However, the effect of pressure on the temperature makes it harder to trace where water came from. The temperature of a water parcel that is moved from one depth to a deeper one will increase because the pressure has increased, even if no heat is exchanged with its surroundings during the move (we call this an *adiabatic process*). A thermistor will measure this change. If the parcel is *adiabatically* brought back to the original depth, its temperature will drop again.

In order to remove this adiabatic heating effect, its useful to differentiate between the actual *in-situ* temperature and instead report the *potential temperature*. This is simply the temperature the water would be if it was brought adiabatically to the surface.

The reason for doing this is dramatically illustrated by considering the temperature measured in the Kermadec Trench [Warren, 1973]. The trench is much deeper than the surrounding water, so water in the trench has been there a long time. However, the in-situ temperature increases with depth which might make us think either it is different water, or that there is a heating source from below (figure 2.3, curve labeled with "t"). However, computing the *potential temperature* θ shows that this water is the same potential temperature (*isothermal*) deeper than 5000 m.

Outside of the deepest part of the ocean, the difference between potential and in-situ temperatures are not large (figure 2.4). In the deepest ocean, its clear that the cold tongue of water that originates in the Antarctic Circumpolar Current originates shallower in the water column than we would infer from just looking at the *in-situ* temperature. This improved ability to trace the source of water without accounting for pressure effects is the main motivation for using potential temperature, and most publications will use potential temperature exclusively.

2.2 *Salinity*

Salinity is the measure of dissolved solids in seawater, and is expressed as grams of solids per kilogram of seawater. Because it is

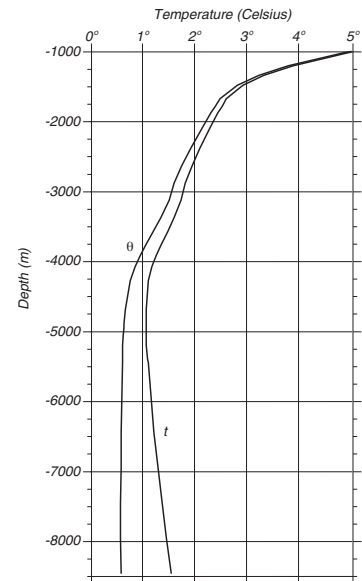


Figure 2.3: CTD data from Kermadec Trench [Warren, 1973] *in situ* temperature and potential temperature. (Figure from Stewart)

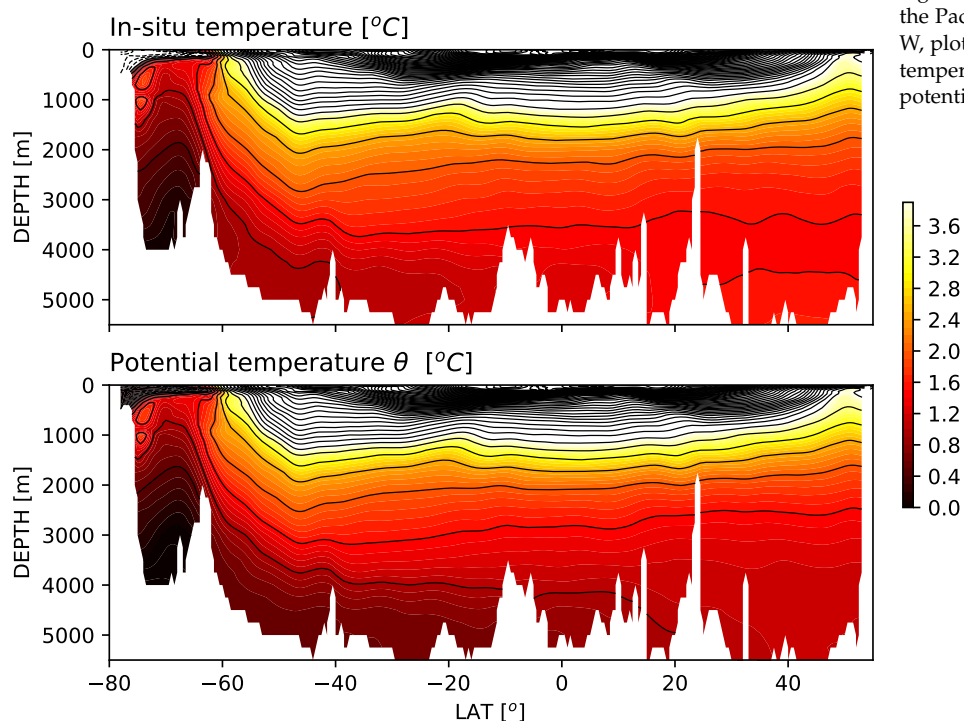


Figure 2.4: North-south sections in the Pacific ocean at a longitude of 150 W, plotted as the measured *in-situ* temperature (upper panel) and the potential temperature, θ (lower panel).

derived from solids in the seawater, salinity is hard to define, and quite hard to accurately measure in the ocean. Oceanographers are greatly aided by the fact that the residence time of a salt ion is very long compared to the mixing timescale of the ocean. While we think of rivers as being composed of fresh water, the input of salt ions largely come from the trace amounts in these rivers. In total, there is $\approx 5 \times 10^{19}$ kg of salt in the ocean, but inputs are $\approx 2.5 \times 10^{12}$ kg/year, so the *residence time* of salt in the ocean is around 20 million years. The overturning time scale of the ocean is 3000 y (at the most), so salt in the ocean is “well-mixed”. This long residence time means that the ratio of salt constituents in the oceans only changes on geological time scales, and thus in the open ocean the ratio of various ions can be considered a constant (closer to river sources the ion ratios can be quite different).

Note, however, that the ratio of the solids that make up the salt being constant does not mean that *salinity* itself is constant. The concentration of salt in a given volume of water depends on how much river water or rain water that parcel has been in contact with, or if it has been subject to evaporation.

2.2.1 Measurement

Chemical oceanographers spent many decades studying the chemical makeup of salt water. The standard way of measuring salinity was to titrate the chloride solids and then use the fact that the ratio of salt ions in the ocean is relatively constant to infer the total salinity. This is done more rarely now, and instead oceanographers measure the *conductivity* of seawater using a conductivity cell. This uses the fact that salt water conducts electricity better than fresh water, and thus the amount of electricity that's able to get from an electrode to an anode through a known quantity of seawater is proportional to the conductivity.

Electric circuits to measure conductivity are relatively straightforward, but the most stable measurements require a good-sized sensing element over which to take the measurement. The conductivity cell in the CTD shown in figure 2.2a is about 15 cm long to allow a stable and accurate estimate. This means that there is a limitation to how fine the vertical resolution of the conductivity estimate is.

The largest challenge in measuring salinity using conductivity is that conductivity is also a strong function of temperature as well as salinity (figure 2.5). That means that we need to have a well-matched temperature measurement at the same time and place as the conductivity measurement in order to back out the salinity. Mismatched sensors lead to a phenomena known as "salinity spiking". It is easily understood if we consider measuring through a temperature interface in water that has a uniform salinity (figure 2.6). If the temperature sensor is lagged compared to the conductivity sensor, the conductivity will go down, but the temperature measured by the temperature sensor will not until a deeper depth. When the salinity is calculated from these two measurements, there will be a sharp discontinuity in inferred salinity at the interface because the sensors are not matched up. This is a very hard problem to get rid of, and involves making sure the two sensors are not lagged from one another, and making sure that their signals are smoothed enough that the mismatch in how the sensors respond to changes are smoothed over.

Regardless of measurement issues, the measurement of salinity using conductivity and temperature is very widespread. In order to differentiate such measurements from fundamental chemically based estimates, oceanographers often use the units of "practical salinity units" or "psu". When these units are used, the measurement is almost always from a CTD. More recently, there is a new salinity unit used as part of an update to the equation of state (TEOS10),

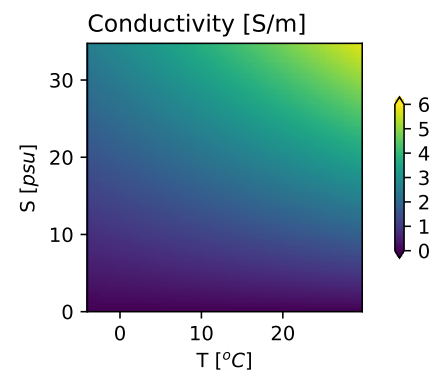


Figure 2.5: Conductivity as a function of temperature and salinity

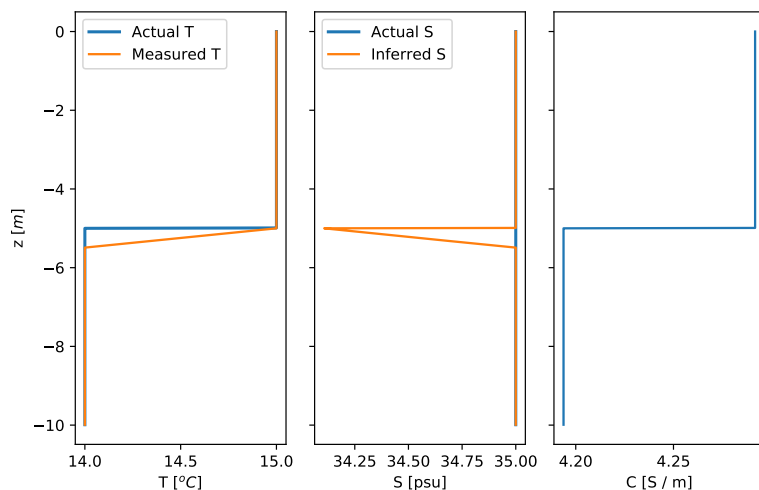


Figure 2.6: Salinity spiking due to conductivity and temperature sensors not being aligned; here the temperature sensor lags the conductivity sensor, so the cold change with depth is registered in the conductivity sensor before the temperature. Note the conductivity change is completely due to temperature.

where salinity is denoted as "absolute salinity" (AS), and the units are g/kg. For this class we will use the older "psu" a.

2.3 Pressure

Pressure is the force per unit area that a parcel of fluid exerts on its neighbours. Remember that in a fluid (gas or liquid), the molecules are in free motion. As discussed above, the more kinetic energy in this motion, the higher the temperature of the fluid. That same kinetic energy exerts itself as a force on any container that holds the molecules. Consider a balloon filled with air. The air inside the balloon is pushing out against the balloon with a certain force per area. This happens because the molecules of air are moving in random motion due to their heat, and some of that momentum is exerted against the balloon's surface. Force always has a direction, but pressure forces are omni-directional or *isotropic*. So in the case of the balloon, the force exerted by the pressure is always perpendicular to the surface of the balloon.

Inside the balloon, the molecules exert a pressure force on one another. If we insert an area element somewhere in the balloon, the molecules on the left side of the barrier exert a force to the right, and the molecules on the right side exert a force to the left. If the pressure is the same on both sides of the area element, then the forces are equal and opposite and the fluid will be stationary. If there are *pressure gradients* inside the balloon, then one side may push harder than the other and the fluid will move. We discuss pressure gradients a great deal in this class and will come back to them below (section 2.7.1).

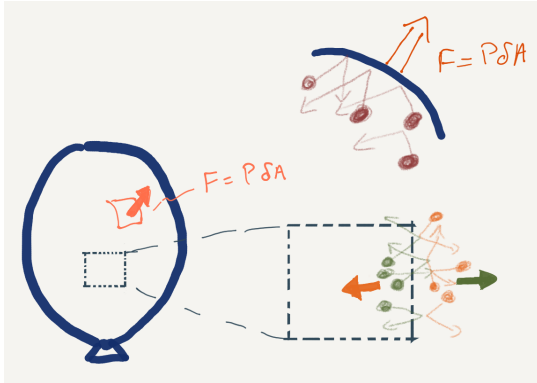


Figure 2.7: Sketch of how molecules in a fluid exert pressure on a balloon and on one another. First blowup is a schematic of air molecules hitting the balloon, second is of molecules on one side of a surface inside the air hitting molecules from the other side and the two sets of molecules therefore exerting a force on one another. Note that in order to get a force we must specify an area element, which we've called δA here.

2.3.1 Measuring pressure

This is usually relatively straight forward using a **strain gauge**. The CTD is equipped with a pressure gauge that is typically sensitive to better than .0025% of their range. Hence a deep-ocean pressure sensor capable of measuring to 7000 m will have an accuracy of 0.14 dbar.

The units of pressure are “officially” Pascals, with $1 Pa = 1 Nm^{-2}$. However, oceanographers almost always report in the units of “decibars”, where $1 Pa = 10^{-4} dbar$. The reasoning behind this is straight forward: pressure at 1-m depth is $g\rho_0\Delta z = 9.8 \times 1023 \times 1 = 10025 Pa = 1.0025 dbar$. So the pressure at a depth of 1-m is very close to 1 dbar.

2.4 Calculating density

Density is the mass per volume of a substance, and expressed in $kg m^{-3}$. The density of seawater varies from approximately $1000 kg m^{-3}$ for freshwater near the surface at 4 degrees C, to $1050 kg m^{-3}$ in the very deepest ocean, at salinities of 35 psu, temperature $-1^\circ C$ and at a depth of 5000 m. Notable is the fact that density of seawater only varies by about 5% over the world's oceans.

Density differences in seawater give rise to pressure differences, and hence help drive currents in the ocean; less dense water wants to float on top of more-dense water (for example in figure 2.8). Unfortunately, there is no direct way to measure density *in-situ*, and scooping volumes of water out of the ocean to weigh is highly impractical.

Instead, we rely on *empirical* relationships between density and the “state” of the seawater. The state variables that give the density are temperature, salinity, and pressure. Increasing the temperature of water tends to decrease the density (except near the freezing point), while increasing the salinity and pressure tend to increase the den-

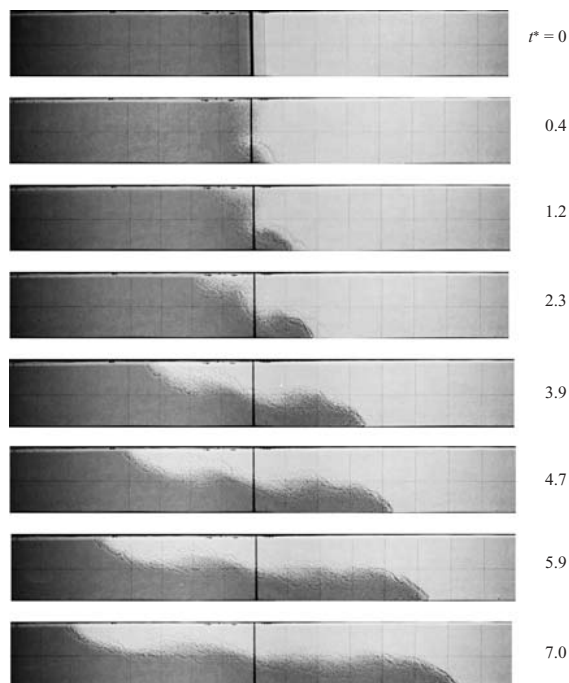


Figure 2.8: Lock exchange with dense water on left and light water on the right. [Shin et al., 2004]

sity.

2.4.1 Density relation

The equation for density is a non-linear function of temperature, salinity, and pressure, and is determined empirically. Various equations of state have been published over the years, but the typically used ones are EOS80 and TEOS-10. See the [TEOS-10](#) website for details and references. The differences between these are subtle, and for our purposes we will use the older EOS80.

The non-linearity of the equation of state is clear in figure 2.9. For a given salinity, the density depends on the temperature in a non-linear fashion, with density changing more quickly with temperature at high temperatures and more slowly at low temperatures, and indeed changing sign at the lowest temperatures, with density dropping again as temperatures get lower. Practically, this means that we must compute the density of seawater on a computer; there are specialized software packages to do this (seawater and/or gsw routines in Matlab, python, or R).

Often, however, it is useful to *linearize* the equation of state if T , S , and P do not vary much. In that case we can write:

$$\rho \approx \rho_0 [1 - \alpha (T - T_0) + \beta (S - S_0) + \gamma (P - P_0)]$$

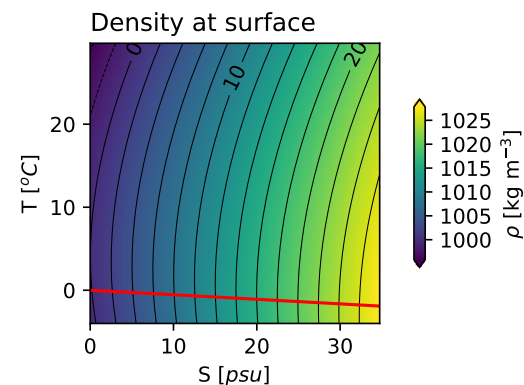


Figure 2.9: Density as a function of T and S at the sea-surface. Contours are the density, the red line is the freezing point at the sea surface.

$$\Delta\rho \approx \rho_0 [-\alpha\Delta T + \beta\Delta S + \gamma\Delta P]$$

α is called the “thermal expansion” co-efficient, and for values $T_0, S_0, P_0 = 15, 30, 0$ is $\alpha \approx 2 \times 10^{-4} [^{\circ}\text{C}^{-1}]$; so for a change of temperature of $+1^{\circ}\text{C}$ the density decreases 0.2 kg m^{-3} . At the same values, $\beta \approx 7 \times 10^{-4} \text{ psu}^{-1}$, so a change of 1 psu increases the density by 0.7 kg m^{-3} . For the same values the value of $\gamma \approx 4.5 \times 10^{-6} \text{ dbar}^{-1}$, so moving a parcel 1 dbar higher pressure will increase its density by $+4.5 \times 10^{-3} \text{ kg m}^{-3}$. Note that γ is relatively linear, so moving to 1000 dbar (i.e. 1000-m deep) increases the density by $+4.42 \text{ kg m}^{-3}$.

2.4.2 Potential density

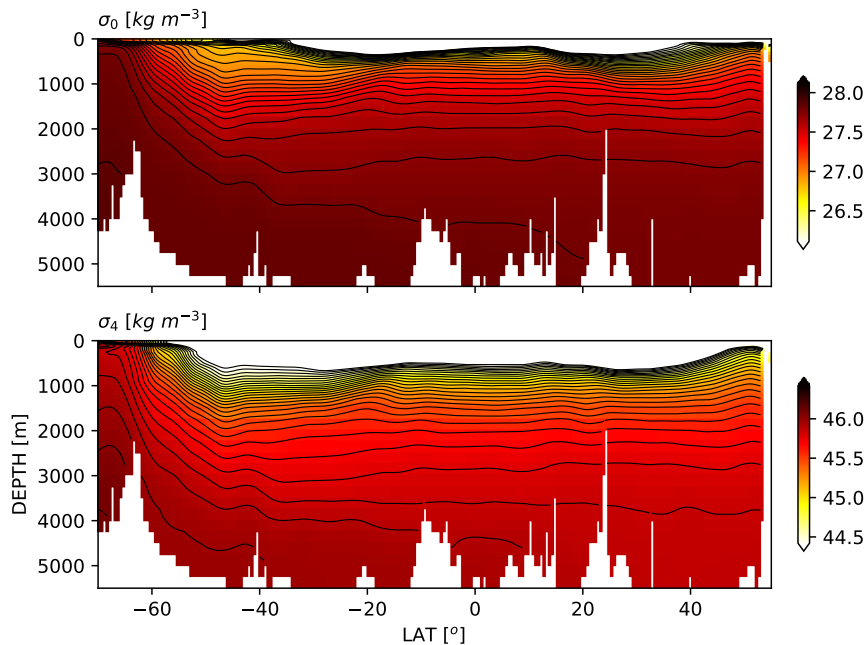


Figure 2.10: Potential density along P16 hydrographic section (north-south along approximately 150 W) relative to the sea surface (top plot) and relative to 4000 dbar (bottom plot). Both are contoured with the same-spaced contour intervals, though the absolute values are different. Note some near-surface contours have been omitted for clarity.

The concept of potential density is similar to that of potential temperature (section 2.1.2), where we would like to remove the pressure effect from the density in order to see where a parcel of water originated. Unfortunately, the non-linearity of the equation of state of seawater makes it impossible to do this cleanly, in that if we change the pressure at one depth, the change of density is not the same if we change it at another depth $\Delta\rho(S, T, \Delta P, P = 0) \neq \Delta\rho(S, T, \Delta P, P = 4000)$. For $S = 30 \text{ psu}$, $T = 15^{\circ}\text{C}$, $\Delta P = 10 \text{ dbar}$ we have 0.0447 kg m^{-3} at 0 dbar, and 0.0412 kg m^{-3} at 4000 dbar. To

deal with this, we calculate the “potential density” relative to a given pressure.

The most commonly used potential density is calculated relative to the surface pressure and is signified as $\sigma_\theta = \rho(S, T, 0) - 1000 \text{ kg m}^{-3}$. Note subtracting 1000 from the density is because all ocean densities are near 1000. Often seen are potential densities relative to 1000-m depth increments in the ocean, signified at $\sigma_1, \sigma_2, \sigma_3, \sigma_4$. Each gives a different view of the density along P16 (figure 2.10). If we adiabatically bring the deep water to the surface it all appears almost the same density, whereas if we bring it to 4000 m there is much more apparent “stratification” (more contour lines per depth). If we are interested in the dynamics of the deep sea, these adjustments are crucial.

The contours of potential density in figure 2.10 are called “isopycnals”.

As a vivid example of how the equation of state depends on both temperature and salinity, again consider the section along P16 in the Pacific (figure 2.11). The potential temperature and salinity is contoured with potential density contours. It is clear that water at a given density is colder and fresher as you move north, and hence both temperature and salinity are necessary to understand the density of the ocean.

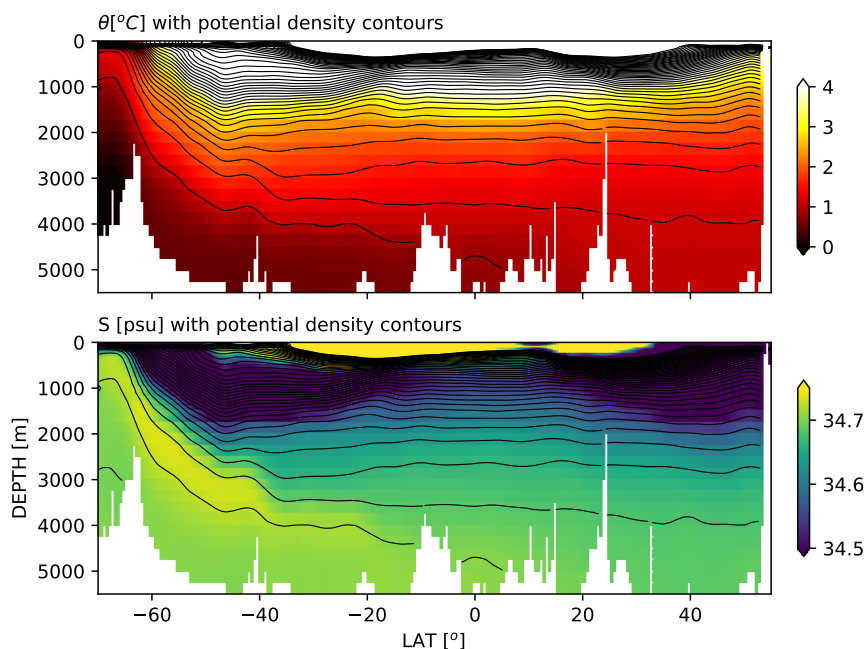


Figure 2.11: Potential temperature and salinity contoured with isopycnals along section P16 in the Pacific Ocean

Another way of looking at the same data that we will use a lot in this course is to plot the data in $\theta - S$ space, where each dot is a

separate measurement of temperature and salinity (figure 2.12). The red data dots are in the south, and blue in the north, and along most isopycnals, the water becomes fresher and colder as profiles from progressively further north are looked at.

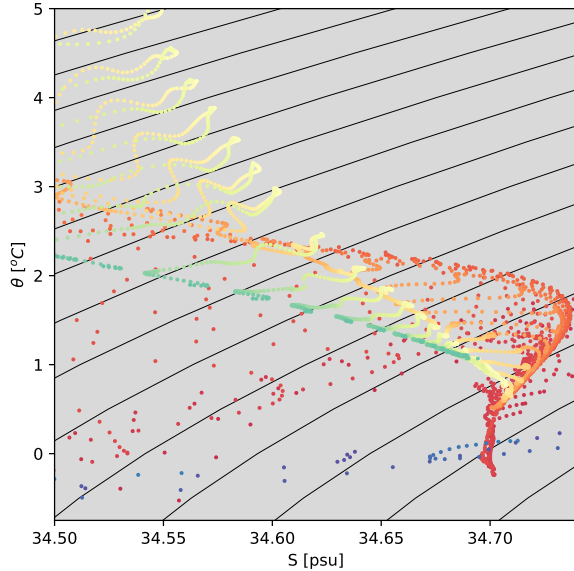


Figure 2.12: Potential temperature as a function of Salinity along P16. Red data points were collected in the south, and blue data points in the north. Isopycnals (relative to atmospheric pressure) are contoured. Note only water below 1000-m is shown here.

2.4.3 Cabbeling

A final note about the equation of state of seawater is the curious effect known as **cabbeling**. As we will discuss in this course, mixing waters of different densities requires energy to overcome the density differences between the water masses. Therefore water tends to be relatively sorted with depth, with dense water under light. However, there exist substantial temperature-salinity (T/S) differences in the ocean, and as we can see from figure 2.9 there is a whole range of T/S properties for any one density contour. It requires very little energy to mix two water parcels on the same *isopycnal*.

However, if we mix two water masses from the same isopycnal, throughout most of the ocean it will lead to a new, slightly denser water mass, as illustrated figure 2.13. If equal volumes of water masses with T/S properties signified by the red dots along the $\sigma_\theta = 24 \text{ kg m}^{-3}$ isopycnal are mixed, their T/S properties fall exactly half way between the parents (green dot). But a water mass with those T/S properties has a density of $\sigma_\theta = 24.022 \text{ kg m}^{-3}$, which is a bit denser than the parent water masses. This curious effect is believed to cause circulation in the ocean, particularly near sharp fronts and at high latitudes where the effect is most pronounced.

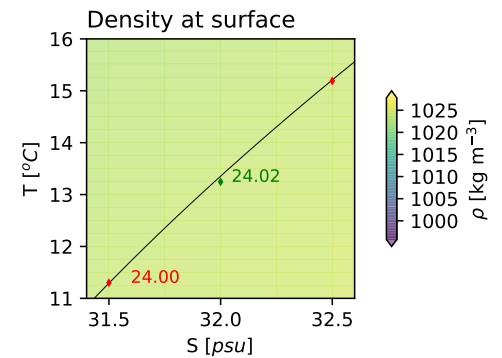


Figure 2.13: Density as a function of T and S at the sea-surface. Contours are the density, the red line is the freezing point at the sea surface.

2.5 Other seawater properties

The properties described above are the main ones dealt with in this course, but there are a few others that are important.

2.5.1 Sound

Sound speed in the water depends on its state variables (S, T, and P), and again can be looked up in empirical fits, typically ranging between 1450 and 1550 m/s (figure 2.14), with higher speeds for warmer and saltier water.

Sound decays in seawater more slowly than in air, with higher frequency sounds decaying over shorter distances. Sound also tends to spread spherically, so its energy falls off with the cube of the distance from the source (i.e. r^{-3}). However, a peculiarity of the sound profile in the ocean means that there is a minimum in the sound speed approximately 500-1000 m deep in the ocean. This occurs because sound speed drops with temperature in the upper kilometer of the ocean, but increases with pressure in the bottom kilometer, where the temperature doesn't change very quickly (figure 2.15). This minimum in the sound speed creates a (sound) waveguide called the **SOFAR** channel (Sound Fixing and Ranging). Waves always refract towards a slower medium, so a sound emitted in the SOFAR channel will start to move upwards and downwards in the water column, but the waves (and hence sound energy) will be refracted back towards the SOFAR channel. This means that instead of sound falling off as r^{-3} , it falls off as r^{-2} , which is much slower. This effect makes it possible for submarines and whales to communicate over long distances using low-frequency sound.

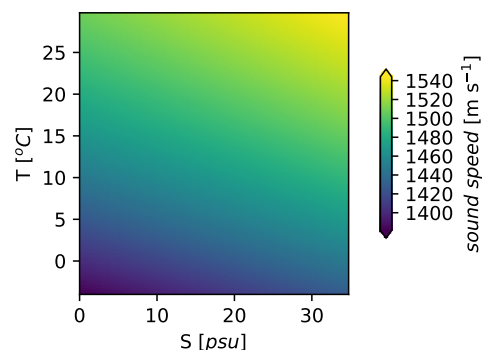


Figure 2.14: Speed of sound in waters as a function of T and S at the sea-surface.

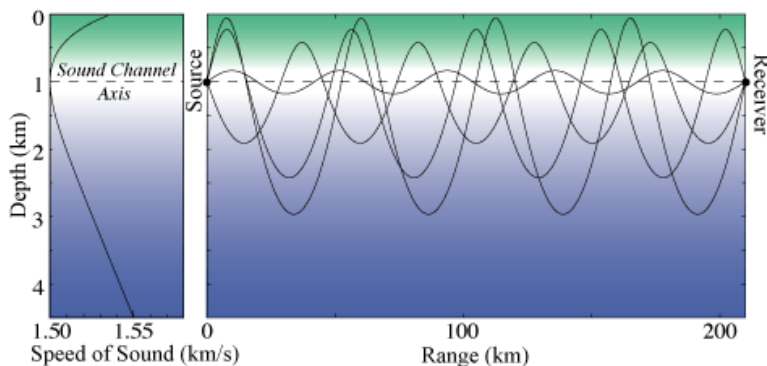


Figure 2.15: Schematic of the SOFAR channel, left is sound speed profile, and on right are sound rays sketched from a source in the SOFAR channel (from [Sound in the Sea](#))

2.5.2 Light transmission

While sound can propagate long distances in the ocean, light cannot. In clear water, less than 10% of incoming light penetrates deeper than 50 m (figure 2.16), with blue light (short wavelengths) getting deeper than red light (long wavelengths). Note that the longer-wavelength red light decays the fastest, whereas longer wavelength sound waves decay more slowly. That's because the decay of light is due to absorption by the water molecules.

The fact that light does not transmit very far in the ocean is an important difference with the atmosphere, where light is relatively transparent to air. It means that radiative heat that comes in from the sun is mostly deposited in the upper few meters of the ocean, and we can think of it as deposited at the surface. It also has profound effect on biological productivity of the ocean, since it means photosynthetic plant growth has to take place in the upper 10s of meters.

2.5.3 Ice

The freezing point of water is indicated in figure 2.9, and is zero degrees for fresh water and decreases to less than zero for salty open-ocean water. The effect of freezing ice on the ocean circulation is profound. Of course, locally it has the effect of insulating the ocean from the atmosphere. Once ice forms on the surface, the loss of heat to the cold atmosphere drops precipitously, as any heat exchange has to propagate through the ice. Further, the effects of wind on the ocean drop, as the wind has to move the more-solid ice floes around before it can have an effect on the ocean below. Of course the ice floes do move, but the effect on the upper ocean is greatly dampened. The wind also generates waves that can propagate under water (*internal waves*), and these are greatly damped by ice cover. Finally, ocean surface waves are radically damped, leading to a calmer sea state, and reduced *fetch* (geography) over which the waves can develop.

The other very important effect of ice on the ocean is for deep- and bottom-water formation. The densest waters in the ocean are formed near ice edges for two reasons. The first is that these regions tend to be cold, and cold water is dense. The second is that when ice freezes the salt crystals are not able to stay in the ice, a process known as *brine rejection*. The salt sinks away from the forming ice and is dissolved in the water underneath the ice-formation region leading to very cold and salty water. This water sinks, and though it mixes as it goes, it remains dense enough to sink to the bottom of the ocean.

Deep-water formation tends to occur in “marginal seas” like the Wedell or Ross Seas off Antarctica, and the Greenland/Iceland seas

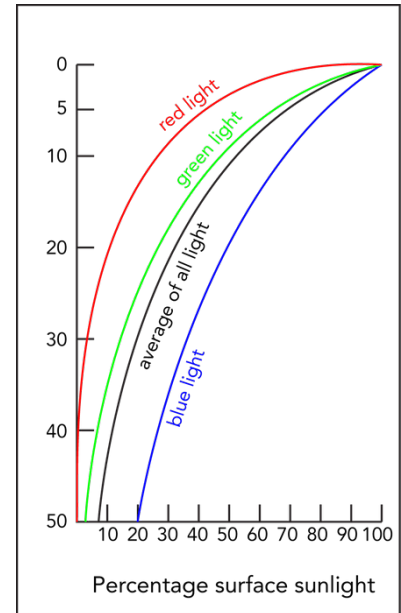


Figure 2.16: Profiles of light penetration in the ocean for different colors. Inouye; Exploring Fluid Earth, U. Hawaii

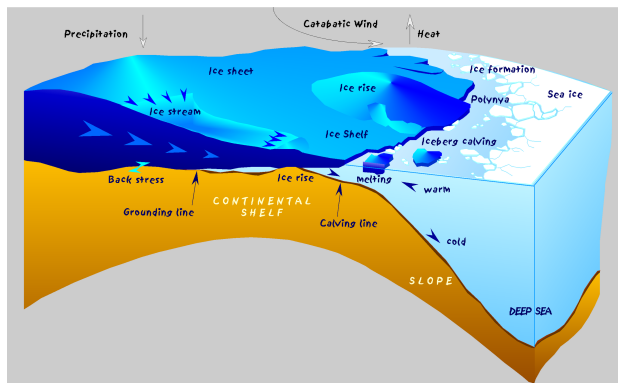


Figure 2.17: Schematic of ice processes off the Antarctic continental shelf. Catabatic winds blow off the continent and push the ice offshore. New ice is formed, dense water produced by brine rejection and cooling, and the dense water sinks, bringing up new warm, fresher water from mid-depth. (From Hannes Grobe, Alfred Wegener Institute for Polar and Marine Research, Bremerhaven, Germany)

in the north. Dense water is produced in these regions at the ice edge, or in breaks in the ice forced by wind or by tidal mixing called **polynyas**. Polynyas tend to dominate the air-sea exchange of heat and brine production because they are open water but exposed to very cold and often windy conditions. The wind forces the polynya to stay open by pushing ice downwind, but also drives dense water formation due to both brine rejection, sensible, and latent heat loss (figure 2.17). This deep water forms **Antarctic bottom water** and **North Atlantic deep water** masses that can be traced throughout the world's oceans as anomalously cold and salty water; the closer the water is observed to the source region, the colder and saltier it is. This water can be clearly seen in T/S sections on the major ocean basins (figure 2.18). We will discuss this substantially more in the next few weeks.

2.6 Pressure Gradients

Pressure is a very important quantity to the dynamics of the oceans, and fluids in general. Pressure *gradients* give rise to net accelerations that cause water to move, often in surprising ways. There was some introduction to this qualitatively in the estuaries discussion. Here we solidify those concepts quantitatively because we need to understand pressure gradients to make progress on understanding how the ocean moves.

To motivate ourselves, recall the demo of sloshing water in a tank (figure 2.19). The surface interface is tilted such that area A is elevated, and area B is depressed. Our intuition might say that the water needs to run downhill, and we may expect a flow, confined to the water surface, of water from area A to area B. Under this hypothesis, what do we expect the dye streak to do? What does the dye stream actually do (approximately)?

To understand what is happening, we must understand pressure

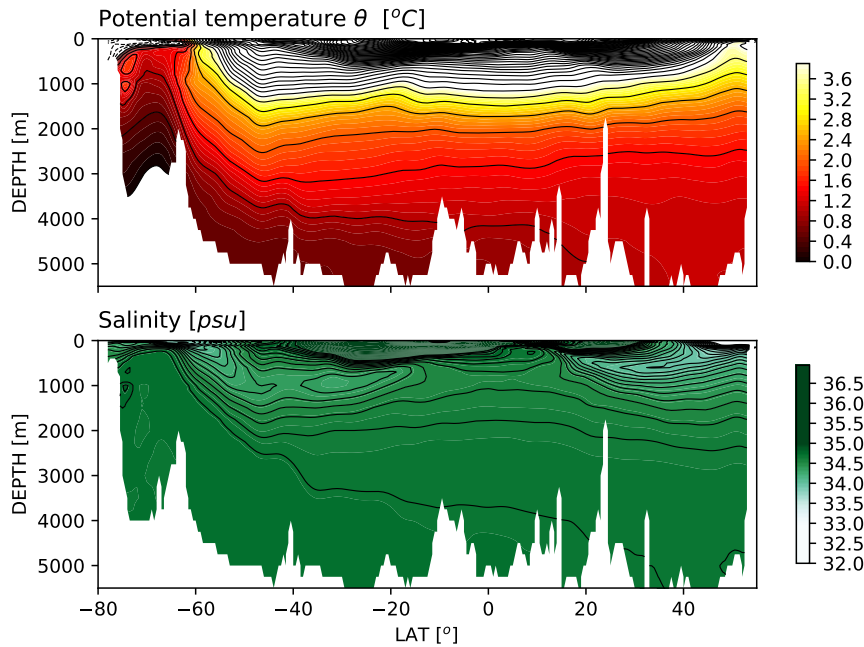


Figure 2.18: North-south sections in the Pacific ocean at a longitude of 150 W of potential temperature, θ and salinity. Note the Antarctic bottom water starting south of -60 Lat, and pouring northwards into the Pacific.

in the fluid. The basic definition was given above (section 2.3)

2.6.1 Hydrostatic Pressure

“Dynamic” pressure happens for fast flows, like those over an airplane wing. Fortunately, in the ocean things are usually slow enough that we can ignore the “dynamic” part, and focus on the “hydrostatic” part.

2.6.2 Single density fluid

“Hydrostatic pressure” is the pressure water parcels exert on one another when the water is not moving. Consider a bucket of water, and think about the forces on a little “cube” of water inside the bucket (figure 2.20, orange cube). Suppose our cube is 0.1 m deep in the bucket. There is a column of water above our little cube that is not moving. The force of gravity wants to pull this column of water down (figure 2.20, green arrow). The force is simply $F_w = mg$, where $g = 9.8 \text{ m s}^{-2}$, the mass $m = \rho V$, where $\rho = 1000 \text{ kg m}^{-3}$ is the density of water, and V is the volume of the column of water $V = (0.1 \text{ m}) \delta x \delta y$. So, the water column is pushing down with force

$$F = \delta x \delta y (0.1 \text{ m}) (9.8 \text{ m s}^{-2}) (1000 \text{ kg m}^{-3})$$

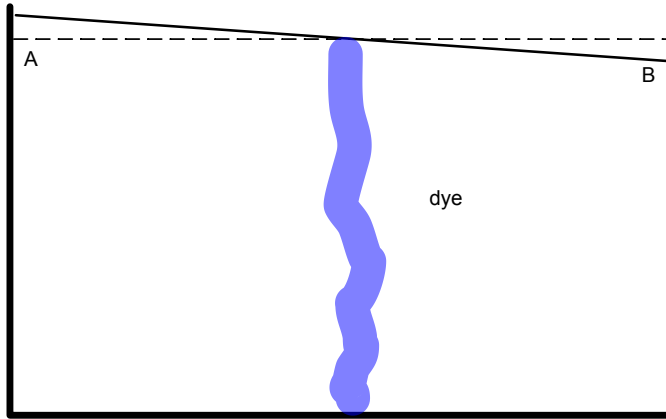


Figure 2.19: A tank with the water surface tilted from equilibrium. The surface wants to flatten, so water must be moved from area A to area B. What is the action of a dye streak through the water column?

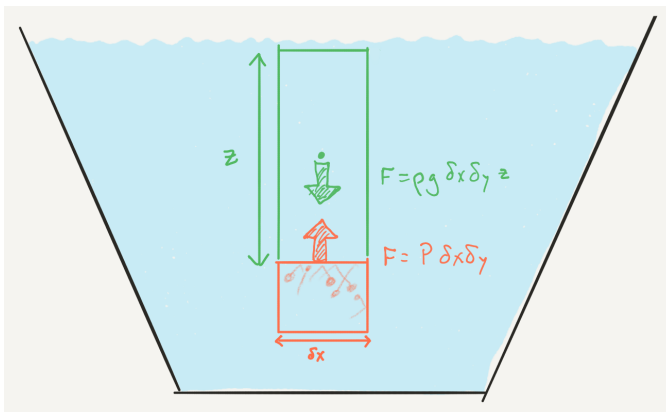


Figure 2.20: The pressure in the small orange box is the weight per area of the water above. δy is in into the page, so $\delta x \delta y$ is the area of the top of the fluid parcel. If the green column of water is static, then the two forces are equal and opposite.

$$\approx \delta x \delta y 980 \text{ N m}^{-2}$$

$$F/A \approx 0.098 \text{ dbar},$$

where we have called $\delta x \delta y$ our area element (i.e. δA from figure 2.7). What provides the force that holds this water up, against gravity? Its the water in our small cube. This water provides a force from directly below $F_p = P \delta x \delta y$ (figure 2.20, orange arrow). If the water is not moving, $F_p = -F_w$, so that the sum of forces in the vertical is zero. We can use this deduction to calculate the pressure at a depth h :

$$P(z = -h) = \rho g h. \quad (2.2)$$

In other words, the pressure is the weight of the water above, per unit area.

It is important to remember that the squishing from the top also causes squishing to the sides, so the water pressurized by the water above also exerts forces on the water in the horizontal direction. If the water beside our small cube has the same pressure forces acting on it, then the water won't move.

2.6.3 Two-density fluid

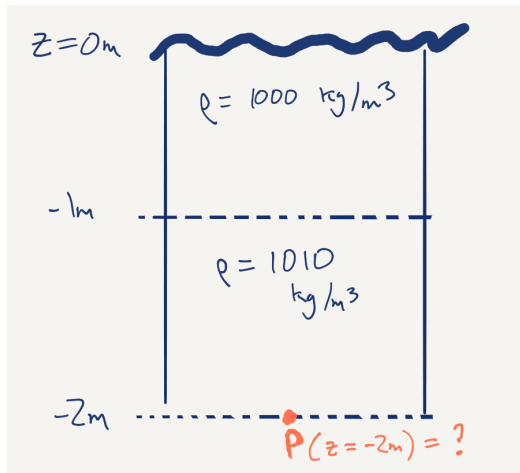


Figure 2.21: Pressure in a two-layer fluid. Imagine the first layer has a different density than the second, and that the densities are (approximately) constant in each layer.

If the density of the water varies due to changes in temperature or salinity, then the weight needs to be calculated by summing up the different densities with depth. i.e. imagine that the first meter, the density is 1000 kg m^{-3} , and for the second meter, the density is 1010 kg m^{-3} (figure 2.21). Then the pressure at 2 m is:

$$P(z) = \int \rho(z) g dz \quad (2.3)$$

$$\approx \sum_{j=1}^n \rho_j g \Delta z_j \quad (2.4)$$

$$= (1000 \times 1 \times 9.8 + 1010 \times 1 \times 9.8) \text{ Nm}^{-2} \quad (2.5)$$

$$= 19698 \text{ Nm}^{-2} \quad (2.6)$$

Adding more layers to the water column, or making the layers different thicknesses is just handled by adding more terms to the sum. Often it is useful to use a computer for this kind of calculation!

2.7 Pressure gradients

2.7.1 Surface pressure gradients

We wouldn't care too much about pressure if it did not cause water to move. Consider a sloshing bathtub, mid-slosh (figure 2.22). In this situation it is intuitively obvious that the water wants to move from left to right, but what force is pushing it? First, where is pressure the highest at point A or point B? These points are both a depth h below the resting depth of the surface of the fluid. Above point A, there is slightly more water due to the "slosh", whereas above point B there is slightly less. Therefore the pressure at point A is greater than at point B. ($P_A(z = -h) = \rho g(h + \eta_A)$ and $P_B(z = -h) = \rho g(h + \eta_B)$, where η is the height of the water above its resting depth. $\eta_A > 0$, and $\eta_B < 0$, therefore $P_A > P_B$).

It should also be obvious that *everywhere* in the fluid the pressure is decreasing to the right along any given depth i.e. $dP/dx < 0$. In fact the *horizontal pressure gradient* can be calculated from

$$P(z = -h) = \rho g(h + \eta) \quad (2.7)$$

and taking the derivative to get the gradient:

$$\frac{dP}{dx}(z = -h) = \rho g \frac{d\eta}{dx}. \quad (2.8)$$

or, the change in the pressure is caused by the slope of the sea surface, $d\eta/dx$.

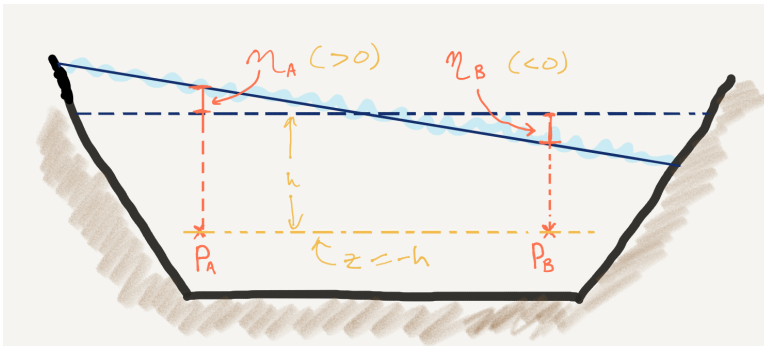


Figure 2.22: Pressure in a sloshing tub. For pressure gradients, we always compare the pressure at the same distance from the surface of the *if it was flat* (i.e. the geoid), which here we have denoted $z = -h$. The sea surface is described as the anomaly from this flat surface, $\eta > 0$ means the surface is above the flat level, and $\eta < 0$ means that it is below.

How does this move the water? Lets consider the force diagram on a block of water inside the tub (figure 2.23) If the pressure is greater on the left hand side, then the force into the block from the left is larger than the force into the block on the right, and the net force $F_A - F_B > 0$, and the block tends to move to the right. Note that in this case $dP/dx < 0$.

Recall Newton's second law of motion:

$$\sum_{i=1}^N F_i = m \frac{du}{dt} \quad (2.9)$$

where du/dt is the acceleration (change of velocity with time). For our block, $m = \rho \delta x \delta y \delta z$, and $F_A = P_A \delta y \delta z$, and $F_B = -P_B \delta y \delta z$, so:

$$P_A - P_B = \rho \delta x \frac{du}{dt} \quad (2.10)$$

or, as δx is made very small:

$$\frac{du}{dt} = -\frac{1}{\rho} \frac{dP}{dx} + (\text{other Forces in } x) \quad (2.11)$$

A question for the reader is to check that this gives the correct sign of the acceleration compared to their intuition.

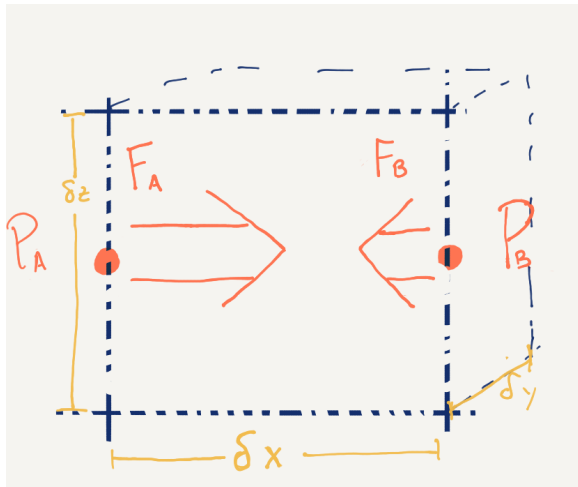


Figure 2.23: Lateral forces across a small hypothetical block.

For the example of the bathtub given above, it should also hopefully be clear that the pressure gradient, and thus the acceleration, does not depend on the depth below the surface. The pressure gradient, dP/dx , only depends on the sea surface tilt, not on z .

2.7.2 Internal pressure gradients

If the fluid has varying density, then the pressure field can be more complicated, and the motions harder to predict. For the simplest

case, consider a two-layer fluid, with a flat upper surface, and a tilted interface between two layers with densities ρ_1 and ρ_2 (figure 2.24) with $\rho_2 > \rho_1$. Again, the pressure is lower on the right than left, so water in the deeper layer has a pressure gradient force from high pressure to low pressure, i.e. to the right.

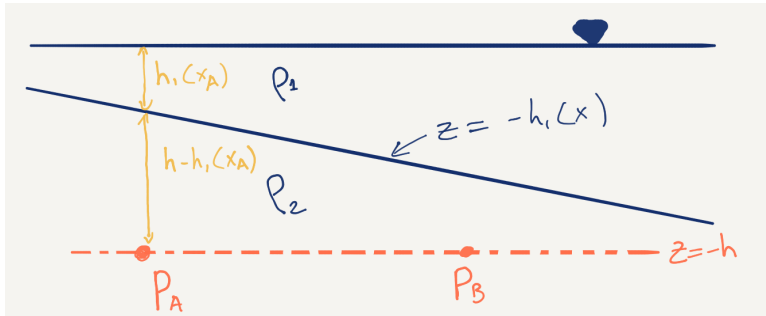


Figure 2.24: How to calculate the pressure gradient in a two-layer fluid.

Mathematically, $P_A(z = -h) = g(\rho_1 h_1(x_A) + \rho_2(h - h_1(x_A)))$, and $P_B(z = -h) = g(\rho_1 h_1(x_B) + \rho_2(h - h_1(x_B)))$. We can estimate the pressure gradient as

$$\frac{dP}{dx} \approx \frac{P_B - P_A}{x_B - x_A} = g(\rho_1 - \rho_2) \frac{h_1(x_B) - h_1(x_A)}{x_B - x_A} = -g(\rho_2 - \rho_1) \frac{dh_1}{dx} \quad (2.12)$$

So again, the pressure gradient depends on the slope of the interface, except this time, the interface is between the two densities.

Of course, the cases can be combined (figure 2.25). There can be a surface tilt, and many interface tilts. While care needs to be taken to keep track of all the layer thicknesses, and the algebra looks messy on the page, the fundamental idea is to simply calculate the weight of the water about the point of interest, including the effect of the local sea-surface elevation.

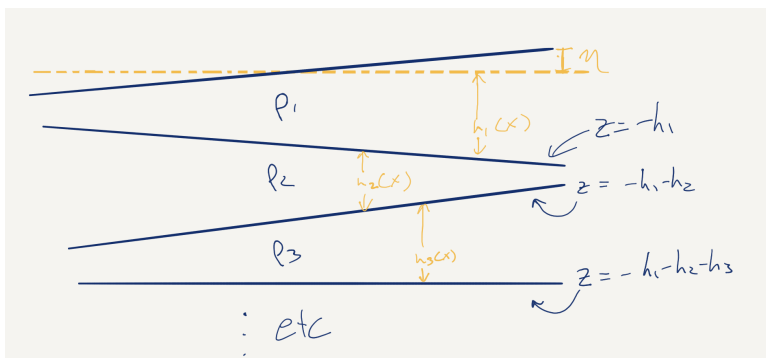


Figure 2.25: Many-layer fluid.

2.8 Exercise

A cruise goes out and makes temperature measurements at two locations 25 km apart as follows:

z	T_A	T_B
10	10.4	10.1
30	8.7	8.4
50	4.7	5.2
70	4.1	4.8

The density of fresh water at 10°C is 1008 kg m^{-3} . What is the *approximate* density at each location where a temperature measurement was taken?

What direction would you expect the water to be flowing at each depth?

Approximate the strength and sign of the horizontal hydrostatic pressure *gradient* at 20, 40, 60 and 80 m, assuming a flat sea surface. Make sure you write out the equation so I can check your math. Does your answer make sense with the answer above? Hint: discretize the water column by assuming that it consists of 4 20-m layers of water, each with a constant temperature. Also, don't round off your density values too much!

What must the difference in the sea surface height be at the two stations for your estimated horizontal pressure gradient to be zero at 40 m?

3

Heat and Salt fluxes

The ocean is moved by three main forcings - friction from the winds, body forces due to astronomical forcing i.e. the tides, and differences in buoyancy forcing. This section discusses the buoyancy forcing. The buoyancy of water is how dense it is, and as we saw in the previous chapter, it is determined by the temperature of the water and how much salt it has in it (and of course the pressure).

This is crucially important for the circulation of the ocean. We already saw how estuaries have differential buoyancy forcing due to a freshwater source at the head of the estuary being more buoyant than the salty ocean water. Buoyancy forcing by fresh water is also important on a global scale. Perhaps even more important is the differential heating, with the ocean gaining heat near the equator and losing it near the poles. This transport of heat is approximately 30% of the poleward transport of heat, the rest is done by the atmosphere. However, it also drives the overturning circulation of the global ocean.

Like an estuary, if the ocean only had heating and cooling at the surface the total volume transport of water in the overturning circulation would be weak. However, mixing brings heat to great depths in the ocean and this creates pressure gradients that move a large slow overturning.

3.1 Surface heat fluxes

Most heat exchange in the ocean occurs at the surface, with short wave radiation passing through the atmosphere and impacting the ocean, and then the ocean losing heat to back radiation, latent heat flux, and heating and cooling from direct contact with the atmosphere.

An estimate of the net heat flux in the ocean is given in figure 3.1 and spatially in figure 3.2e. Recall that heat is specified in units of Joules, where 1 Joule is the energy (or heat) required to warm a kilogram of water one degree Kelvin. Heat fluxes are a rate of heating,

and hence are in units of Watts, or Joules per second. If we want to make a map like figure 3.2e, then we want to know the rate of heating per area, and we plot in units of Watts per meter squared, or W m^{-2} . The average over the surface area of the ocean is shown in figure 3.1.

Overall, there is a net input from shortwave radiation of about $H_{SW} = 170 \text{ W m}^{-2}$ once sunlight penetrates the cloud cover (figure 3.1). There is a net longwave radiation of $H_{LW} = 53 \text{ W m}^{-2}$ just due to the temperature of the water and the temperature of the atmosphere and clouds above. The remaining two terms are “sensible” heat loss, which is just due to the temperature difference diffusing across the sea surface ($H_{sensible} = 16 \text{ W m}^{-2}$), and the “latent” heat loss due to evaporation, which is the largest loss ($H_{latent} = 100 \text{ W m}^{-2}$).

Note that the estimate in figure 3.1 has a net warming of 0.8 W m^{-2} , which is due to global warming. We can consider the average heating for a $D = 4000\text{-m}$ deep ocean using this number. The heat capacity of water is $c_p = 4.2 \times 10^3 \text{ J kg}^{-1} \text{ K}^{-1}$, and the density 1030 kg m^{-3} , so the rate of temperature change is $dT/dt = H_{net}/(D\rho c_p) = 0.0015 \text{ K/y}$, or greater than 600 years to increase by 1 degree at the current rate. This of course does not mean climate change is not important to the ocean - much of this change is confined to the upper few hundred meters, and climate change strongly affects winds that drive much of the ocean circulation.

3.1.1 Incoming shortwave radiation

The spatial distribution of these fluxes and their net magnitudes indicate that, unsurprisingly, the net incoming shortwave radiation is strongest at the equator (figure 3.2a). This radiation comes from the sun, and is modified as it passes through the atmosphere. Of course it includes all wavelengths of radiation, but it is very much dominated by short scale radiation, so it is called “shortwave”.

Estimating the radiation coming from the sun and impacting the ocean would be a simple matter depending only on the tilt of the earth, and to a (much) lesser extent whether the sun is in aphelion or perihelion. However, the atmosphere severely modifies the net flux reaching the earth, due to ozone and clouds. Indeed, much of the east-west spatial variability to the shortwave surface fluxes is due to clouds. For instance, the inter-tropical convergence zone can be clearly seen just north of the equator (figure 3.2a) as a region of reduced incoming radiation.

Given this, it is important to realize that it is very difficult to make accurate estimates of the incoming radiation over the full expanse of

the ocean. Satellites make this easier, because they give a good idea of cloud cover, but the thickness of the clouds and their humidity all matter to making an estimate. Radiation can be measured with **radiometers**, but these need ships, moorings, or other platforms to make direct measurements. Hence estimates of shortwave radiation are derived from empirical models.

Some idea of the magnitude of the problem can be seen by considering the net heat flux of 1.2 PW (figure 3.2e) integrated over the entire global ocean (1 PW is 10^{15} Watts). The volume of the oceans is approximately 1.335×10^{18} m³. The heat capacity of water is 4180 J kg⁻¹ and its density approximately 1030 kg m⁻³. Using these numbers, this 1.2 PW discrepancy in the annual mean would lead to a one-degree warming of the ocean over 140 years. This would be quite large and rapid, even on the scale of anthropogenic climate change, and this net should be considered a bound on how accurate the various terms of the budget are, rather than a direct estimate of how fast the ocean is warming.

We can see the effect of the earth's tilt and changing cloud cover if we look at seasonal averages of the shortwave radiation (figure 3.3a, figure 3.4a, figure 3.5a, figure 3.6a). Not surprisingly, during the boreal winter, the net radiation is low in the northern hemisphere, than in the boreal summer.

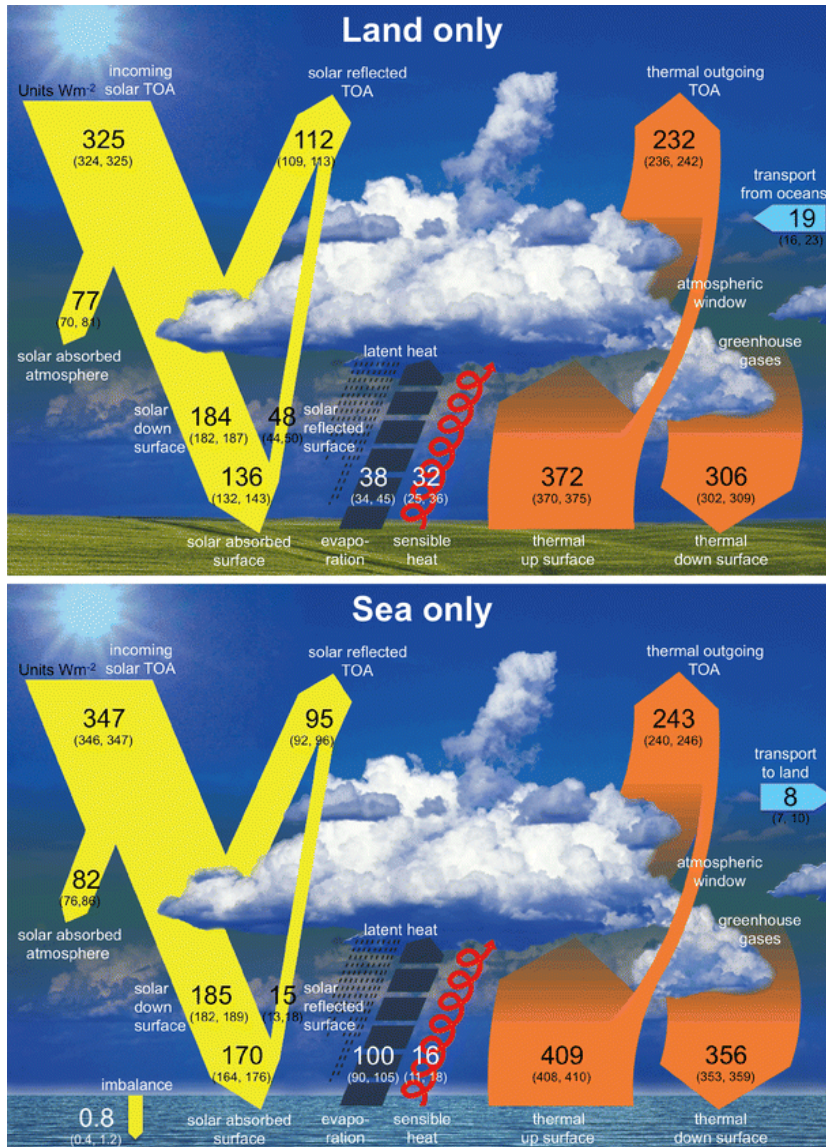


Figure 3.1: Heat fluxes over land and ocean, units of W m^{-2} . Note the net “thermal”, or longwave back radiation is $H_{LW} = 53 \text{ W m}^{-2}$ [Wild et al., 2015]. “Solar absorbed” is the same as H_{SW} below, and “evaporation” is the same as H_{latent} . Note the error bounds next to each estimate. The estimated net imbalance is the warming of the oceans due to global warming.

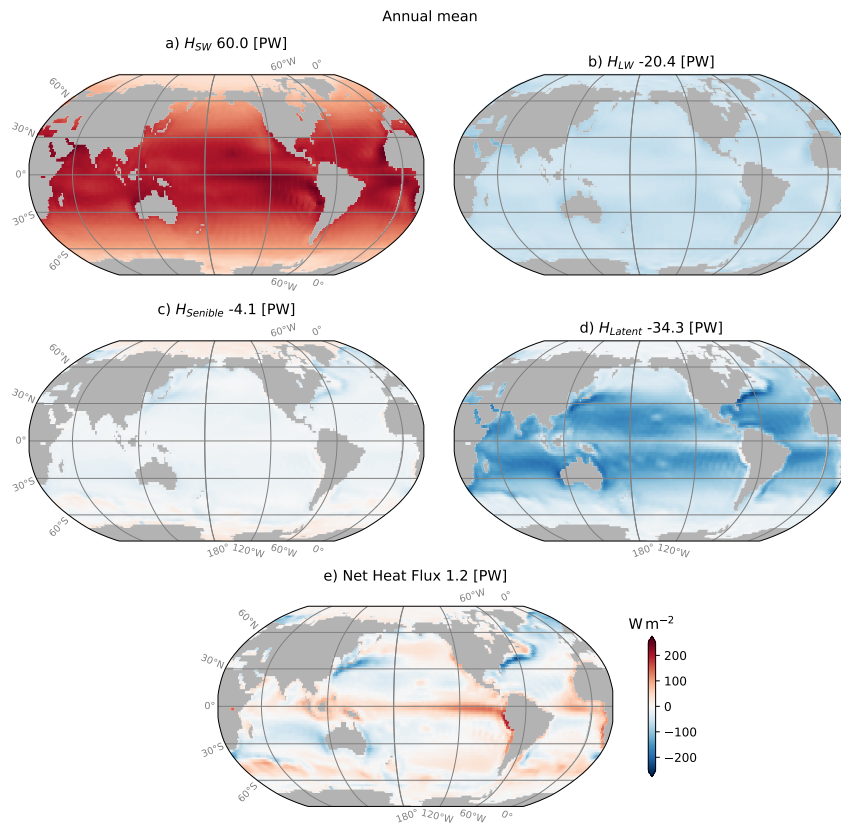


Figure 3.2: Net surface heat fluxes, annually averaged. a) Net shortwave heat flux, b) net longwave flux, c) sensible heat flux, d) latent heat flux and e) net heat flux. Data source: NCEP1 reanalysis.

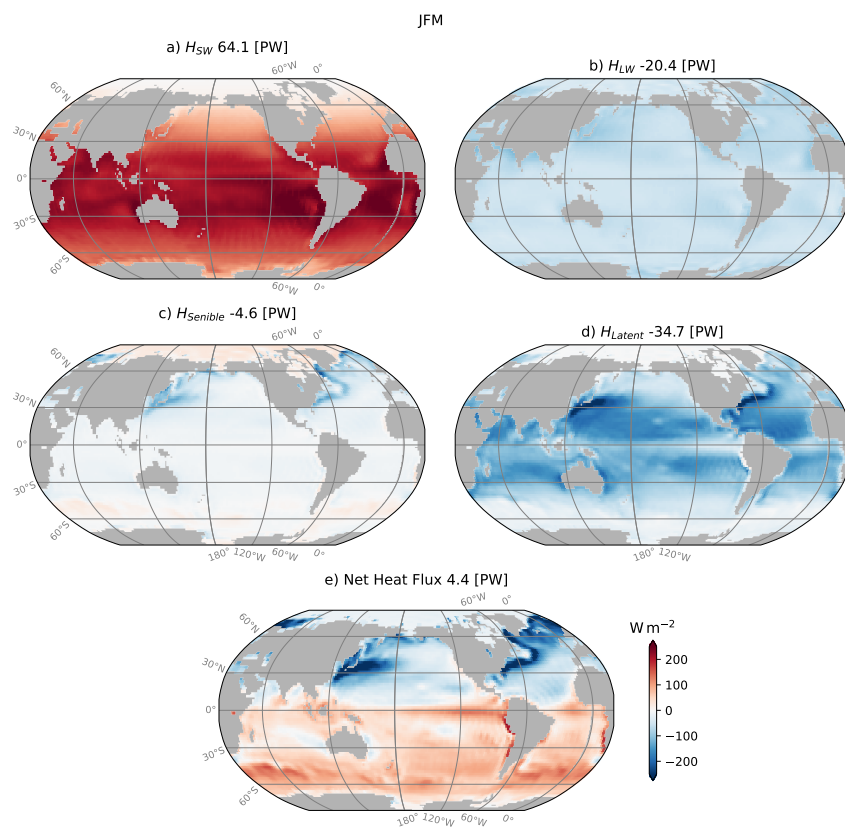


Figure 3.3: Net surface heat fluxes, January to March. a) Net shortwave heat flux, b) net longwave flux, c) sensible heat flux, d) latent heat flux and e) net heat flux. Data source: NCEP1 reanalysis.

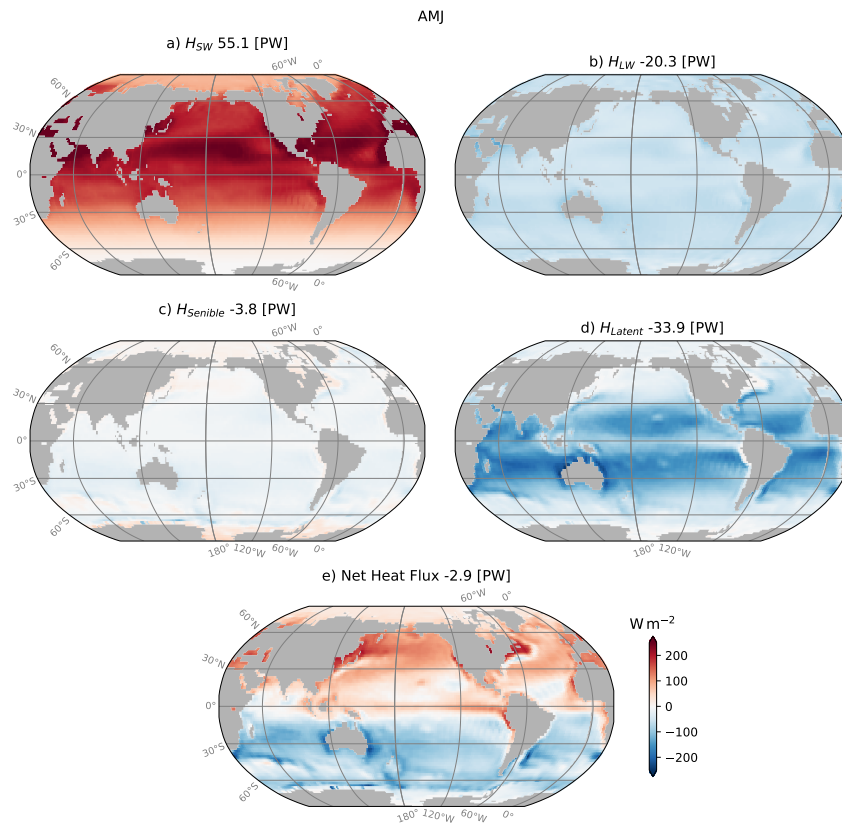


Figure 3.4: Net surface heat fluxes, April to June. a) Net shortwave heat flux, b) net longwave flux, c) sensible heat flux, d) latent heat flux and e) net heat flux. Data source: NCEP1 reanalysis.

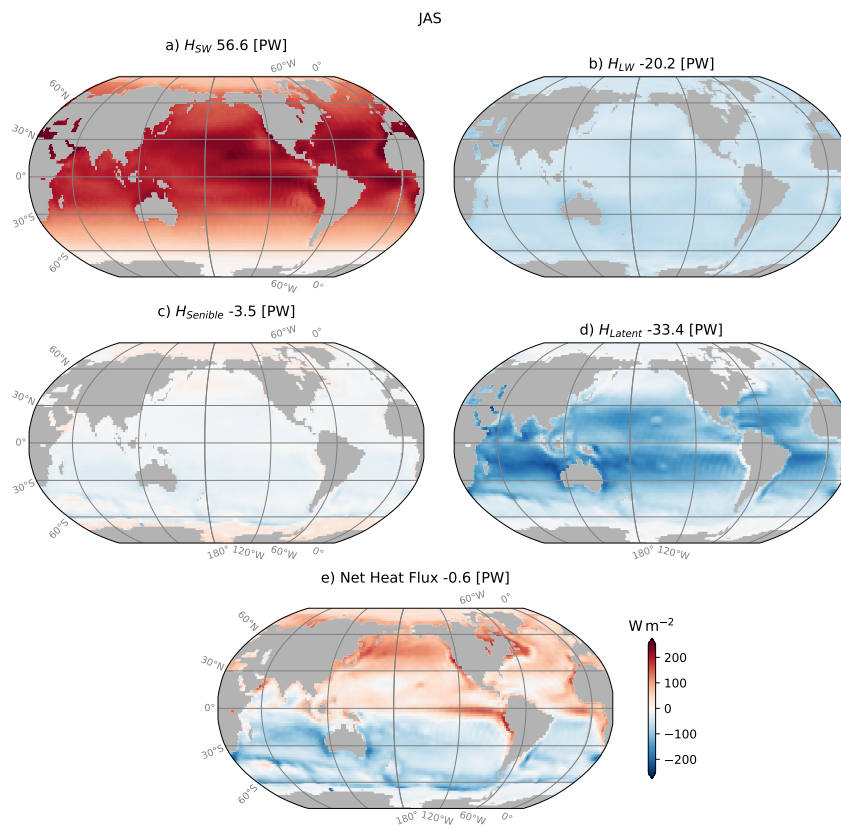


Figure 3.5: Net surface heat fluxes, July to September. a) Net shortwave heat flux, b) net longwave flux, c) sensible heat flux, d) latent heat flux and e) net heat flux. Data source: NCEP1 reanalysis.

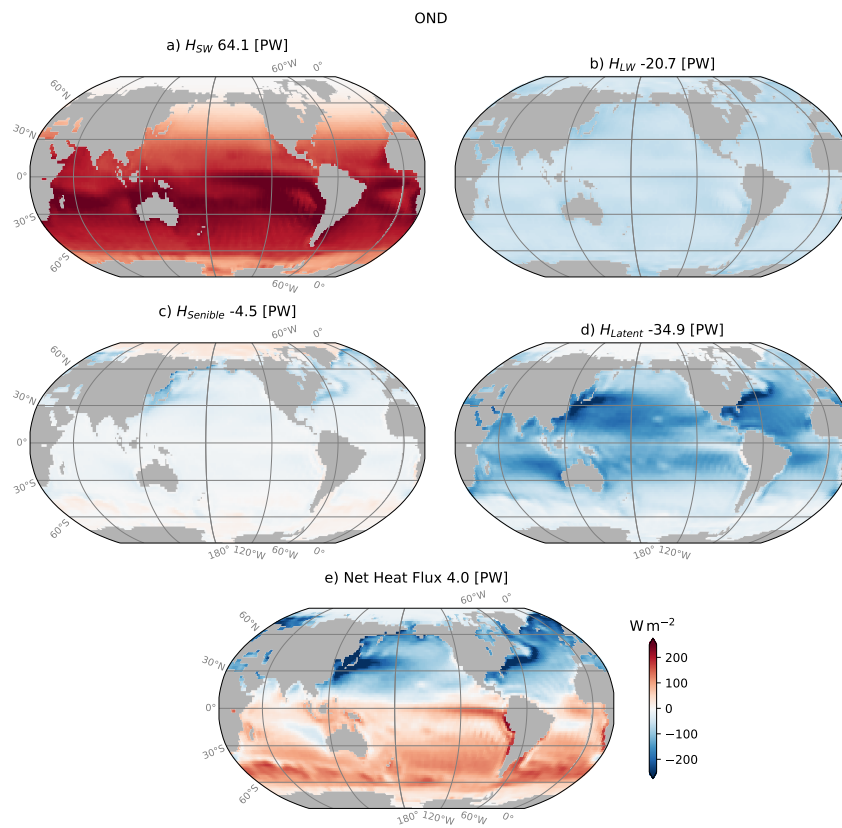


Figure 3.6: Net surface heat fluxes, October to December. a) Net shortwave heat flux, b) net longwave flux, c) sensible heat flux, d) latent heat flux and e) net heat flux. Data source: NCEP1 reanalysis.

3.1.2 Longwave radiation (back radiation)

The earth and ocean emit radiation back into the atmosphere due to their temperature due to blackbody radiation. If there were no atmosphere, then H_{LW} would depend on temperature of the water to the fourth power, the Stefan-Boltzman constant, and the emissivity of the water. If this were the case, the ocean would have very large spatial differences in H_{LW} that depended the sea surface temperature. That is not the case (figure 3.2b) because the atmosphere acts as a strong insulator, and back-reflects much of the emission. Hence, the *net* longwave radiation is surprisingly uniform. This is true spatially, as well as temporally (figure 3.3b, figure 3.4b, figure 3.5b, figure 3.6b). It is indeed surprising that the net back radiation is strongest in the winter when the sea surface is usually colder.

This again points to the difficulty in estimating this flux. As with shortwave radiation it requires radiometers to measure directly, and some correlation with atmospheric forcing must be made to come up with a net value.

3.1.3 Sensible heat transfer

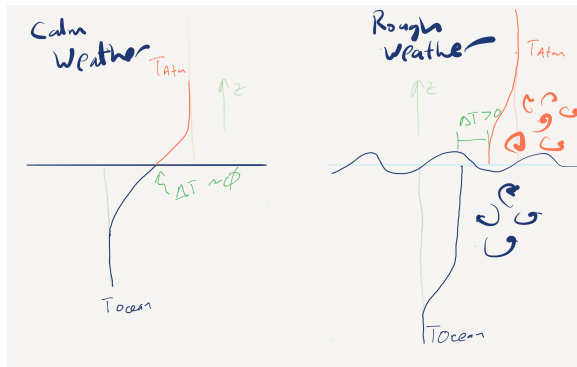


Figure 3.7: Sketch of ocean and atmospheric temperature profiles. During calm weather and stable conditions (warm atmosphere compared to ocean), there is only weak sensible heat transfer. If there is turbulence in the atmosphere or in the ocean, then the transfer can be greatly enhanced.

Sensible heat transfer is the weakest term, despite the fact it is probably what most people think of as how heat is transferred, i.e. when the atmosphere is cold the ocean loses heat and when it is warm it gains heat. The heat exchange is usually assumed to be driven by the temperature difference between the top of the ocean and the atmosphere, i.e. $H_{Sensible} \approx k(T_{air} - T_{ocean})$ where k is a transfer co-efficient ($W K^{-1}$). However, the temperature of the upper ocean and lower atmosphere of course depends on the flux. So if there is only weak mixing of heat by upper ocean turbulence, the temperature profiles will rapidly equilibrate in thin layers at the interface (figure 3.7a). Conversely, if there is substantial mixing, the temperature difference between the two layers can remain large

because heat is mixed away from the interface.

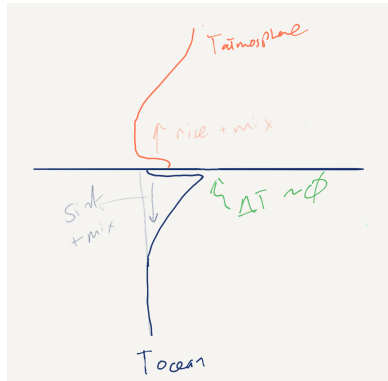


Figure 3.8: Sketch of ocean and atmospheric temperature profiles. During calm weather and stable conditions (warm atmosphere compared to ocean), there is only weak sensible heat transfer. If there is turbulence in the atmosphere or in the ocean, then the transfer can be greatly enhanced.

If the interfaces are unstable, then the ocean (and atmosphere) will tend to “convect”. i.e. if the atmosphere at sea level is colder than the ocean, then the cooling of the ocean will lead to cold water on top of warm water and that water will sink. As it does so, it mixes with the warm water below, and the mixed layer will tend to deepen. Again, mechanical mixing by the wind can enhance this process.

Needless to say, parameterizing these effects to come up with maps like figure 3.2c, has required many years of effort and specialized instrumentation figure 3.9. Measured heat fluxes, as we will see below, are notoriously hard to collect, as are the forcing parameters for those heat fluxes, involving wind speed, ocean current speed, and parameterization for the strength of turbulence in the lower atmosphere and ocean. For an overview of the state of the art, and the pressing need to improve these measurements see ?.

The sensible heat losses show a relatively straight forward patterns with the seasons, with a bit of warming of the ocean in the summer, and substantial cooling in the winter (figure 3.3c to figure 3.6c) . Particularly for the winters there is substantial east-west asymmetry in the ocean’s basins, for instance in figure 3.3c, there is strong losses off Japan and the Eastern US, centred at around 40 N. This is due to dry cold winds off the continents, blowing from west to east with the Jet Stream coming into contact with warm water being advected north by the Kuroshio and Gulf Stream.

3.1.4 Latent heat losses

Latent heat losses are those due to heat used to evaporate water. Evaporation occurs when the atmospheric humidity, q , is less than 100%. During evaporation water mass is transferred from the ocean to the atmosphere, and the heat stored in that water is transferred from the ocean to the atmosphere. This transfer is not 100% efficient



Figure 3.9: Platforms used to measure heat fluxes in the ocean, from ?.

because some energy is used to achieve the evaporation, but it does result in a substantial transfer of heat.

The strength of this transfer depends on the humidity of the ocean directly at the air-sea interface, and hence, just like for the sensible heat transfer, it depends on the turbulence in the atmospheric “boundary layer” - if the layer is turbulent because there are strong winds and/or convection, then the moist near-interface air is mixed more thoroughly and the evaporation and exchange of heat is enhanced. Note that indirectly the exchange depends on the temperature difference between the ocean and the air as cool air has relatively little moisture, and warm water is more readily evaporated.

Again, this leads to seasonal changes in the heat flux that mean more evaporative heat flux occurs in the winter than the summer, (figure 3.3d to figure 3.6d). Further there are clear east-west asymmetries across the basins with the western boundaries at mid-latitude being conspicuous for their evaporative heat loss. This is because cold dry continental air blows west-east across the warm western boundary currents at these latitudes, leading to substantial evaporation.

3.1.5 Integrated Surface Heat Fluxes

The maps in figure 3.2 to figure 3.6 can be integrated to get the net heat flux over the year (figure 3.10). Remember that there is a geometric effect of the area of the earth per degree of latitude at the pole goes to zero, whereas it is very large at the equator. Keeping this in mind, the integral around the globe for each degree shows that there is a net heat input at the equator, and losses to the north and south. Interestingly, in the southern hemisphere, there is a net heat *input* into the ocean between the subpolar band of 40 and 60 S. The general lack of land mass at these latitudes means that the air has largely equilibrated with the ocean in terms of both temperature and humidity and hence the sensible and latent heat fluxes are negligible. Note the same thing happens in the North Pacific but is masked in the net by the north Atlantic and the fluxes in the Kuroshio (figure 3.2e)

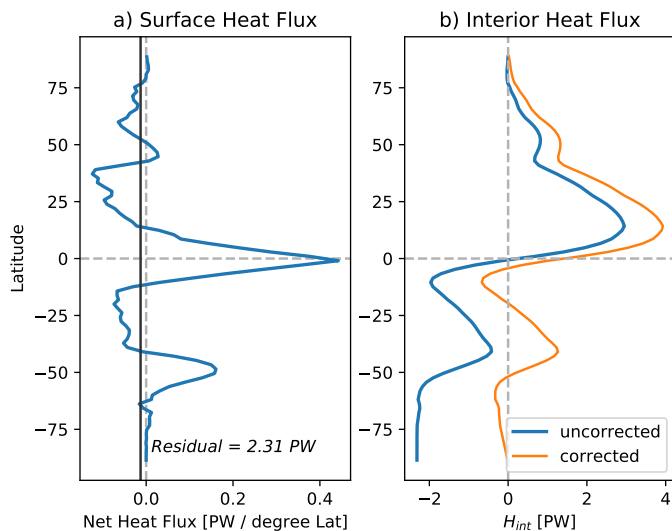


Figure 3.10: a) Globally integrated annual-mean surface heat flux per one degree of latitude. The sum of the heat flux is shown as the “residual”, and is about 4% of the net incoming radiation. b) the inferred heat transport carried by the ocean, computed by integrating the curve in (a). Negative heatflux means heat is flowing from north to south. Theoretically, this should come to zero, so this curve requires correction (orange curve is a crude correction).

As noted above, the 2.3 PW of residual heating is likely a result of error in the estimate rather than a robust idea of how fast the ocean is heating. 2.3 PW is 4% of the total incoming flux, and the estimates likely have more than 4% error in total, so the net flux is not significantly different from zero.

On moderate time scales it is often helpful to think of the ocean as being in steady-state, so in this case it is helpful to think of the ocean as not changing temperature. On the other hand, if there is a net flux of heat into the ocean at some latitude, and a net flux out at another latitude, either the ocean where there is a net heatflux in is getting warmer and warmer, or it is transporting heat to the region where it loses heat, as sketched in figure 3.11.

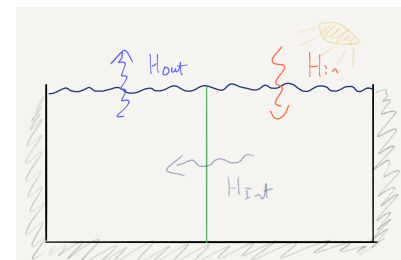


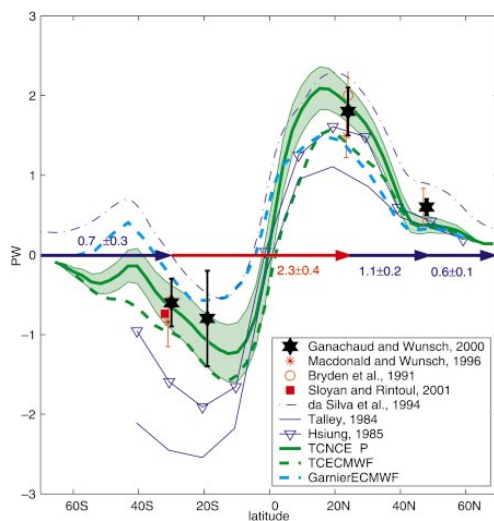
Figure 3.11: Schematic two-box representation where the right-hand box is being heated, the left-hand box cooled, and a heat flux in the interior of the box is assumed to be from warm to cold.

Extending this idea to many boxes is straight forward, but we have to remember that the boxes have a heat source both at the surface, and an interior flux on both sides of the box. (figure 3.12). If we assume steady state and that these heat fluxes balance, then we have $H_{in}^{(N)} = H_{in}^{(N-1)} + H_S^{(N)}$ where the bracketed superscripts refer to the cell number. Surface fluxes are defined as positive into the ocean, and interior fluxes are defined as positive if they are to the north. We can also write this as $\Delta H_{in}^{(N)} = H_S^{(N)}$ and we can see that if we have a positive heat flux into the ocean, then the northward heat flux must grow. Because this relation starts at a pole, where the interior heat flux is zero, the interior heatflux at any given latitude is the sum of the surface fluxes to the south of that latitude:

$$H_{in}^{(N)} = \sum_{i=0}^N H_S^{(i)} \quad (3.1)$$

This gives us the curve in figure 3.10b, which shows northward heatflux in the northern hemisphere and southwards in the southern hemisphere. Again, there is a residual heat flux, so this procedure does not yield a completely sensible curve with large southwards heatflux at the southernmost ocean cell, so a correction is applied that removes the mean flux.

Direct estimates of the interior fluxes have also been made from ocean-based measurements, and a number of these are compared in figure 3.13. The level of variability in these estimates indicates the difficulties in making these types of estimates, even if the patterns make the sense.



If we look at these fluxes by ocean basin, then there are substantial

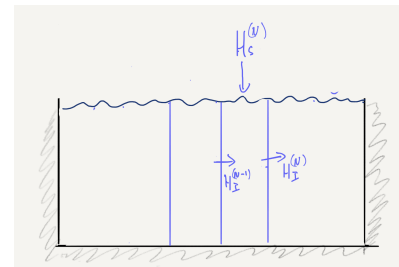


Figure 3.12: Schematic two-box representation where the right-hand box is being heated, the left-hand box cooled, and a heat flux in the interior of the box is assumed to be from warm to cold.

Figure 3.13: Estimates of heat transport by the world's oceans [?].

differences between the Atlantic ocean and the Pacific/Indian Oceans in terms of the structure of the heat flux. In the Atlantic ocean the heat flux is everywhere north. This is because the heat flux at the equator is relatively weak, and there is substantial heat flux in the south Atlantic.

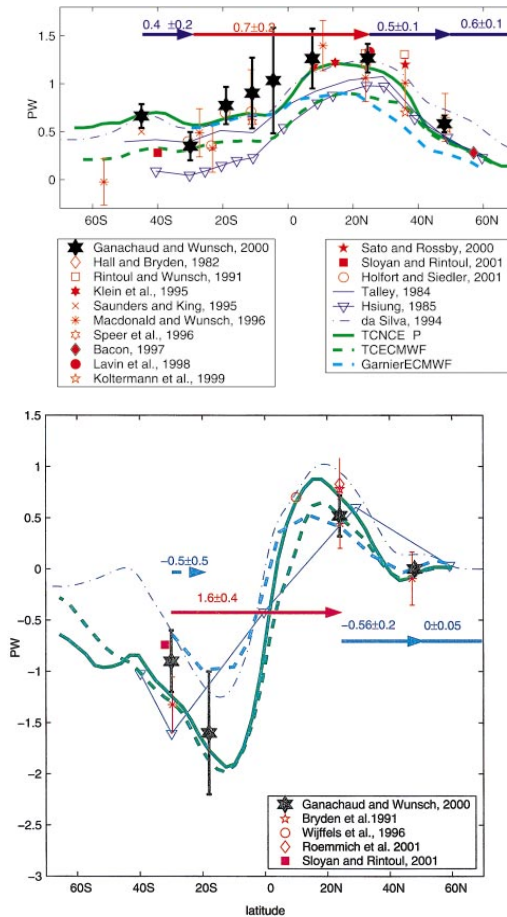


Figure 3.14: Estimates of heat transport in the Atlantic (upper panel) and Pacific and Indian oceans (lower panel)[?].

We have said nothing about what drives these heat fluxes, however, the basic idea is that warm water is less dense, and hence more buoyant, whereas cold water is less buoyant. Just like in an estuary, this creates north-south pressure gradients that drive the warm water northwards.

Make a demo about this!

3.2 Surface freshwater fluxes

The ocean has a large reservoir of salinity compared to the rate of inputs (from rivers) and outputs (from forming **evaporites**), to the point that the mass of salt in the ocean can be regarded as a constant

on the timescale of decades to centuries. Given the volume of the ocean is approximately $1.335 \times 10^{18} \text{ m}^3$, and a typical density is 1030 kg m^{-3} , and salinity is $S \approx 35 \text{ ppt}$, the mass of salt in the oceans is approximately $4.5 \times 10^{19} \text{ kg}$. Conversely, rivers deliver on the order of $3 \times 10^{12} \text{ kg}$ of salt per year, so, in order to increase ocean salinity by one part per thousand, it would take more than 450,000 years of salt input. Given that much of this input is balanced by output to forming evaporites, we tend to think of the salt balance as not changing over sub-geological timescales.

Of course this doesn't mean that salinity is constant in the ocean! Salinity is almost zero in rivers, and is zero in rainfall and at locations where these meet the ocean the salinity drops. Conversely if there is evaporation and ice formation, then salinity is left behind and the ocean is saltier in those locations. When we think about the large-scale budgets then, we often think of them as freshwater budgets, with the understanding that these are also salinity budgets.

3.2.1 *Evaporation and precipitation patterns*

As noted above, evaporation is complicated to estimate because it depends on the temperature difference of the ocean and atmosphere, the humidity of the atmosphere, and all of those parameters depend on the turbulence near the boundary between the two fluids. Many of the spatial patterns of evaporation are the same as those for latent heat loss (figure 3.15a), with evaporation largest where cold dry air passes over warm ocean currents.

Freshwater re-enters the ocean via precipitation and rivers. The precipitation patterns are largely driven by the **Hadley cell** circulation of the atmosphere, with large upward motion at the equator driving strong rainfall there (figure 3.15). The subpolar latitudes see more rainfall as well because there is also rising air in the midlatitude cell, centred at about 60 degrees. Dry air predominates at the subtropical latitudes where this air tends to be subsiding.

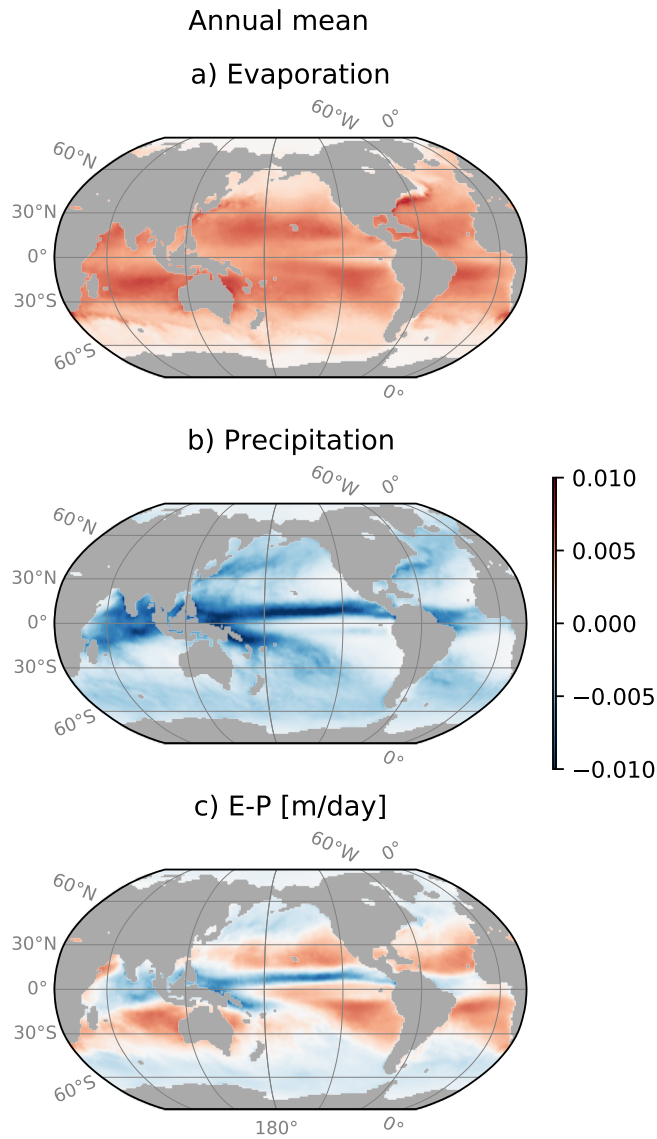


Figure 3.15: Annual average evaporation and precipitation (from ECMWF-CERA-20c re-analysis).

The net pattern of evaporation minus precipitation generally says that moisture is removed from the oceans in a band from approximately 5 degrees to 35 degrees, and in the net, precipitates near the equator and north of 40 degrees. As with heat, this necessitates a transport of freshwater from places of excess precipitation to places of excess evaporation if the ocean is to stay in approximate steady state (figure 3.16).

3.3 Fluxes and transports in the ocean

We saw in the previous section that heat and freshwater can enter and leave the ocean at the surface. We also *inferred* that it must be transported from sources to sinks at the surface if the ocean is believed to be in a quasi-steady state. We call this an *inverse estimate* because we infer the inner workings of the ocean from its external forcing. In this chapter we start grappling with *how* that transport takes place, and how we might quantify and measure it. There are actually *many* processes involved in the transport of heat from the equator poleward, and trying to understand them all is one of the main challenges of oceanography. Given that, this chapter only gives some tools to start understanding fluxes and transports, and as such uses some simple examples.

Note that temperature, (or heat), for instance, can change at a location away from the surface in two possible ways. Currents can bring water with a different temperature from somewhere else; we call this an *advective flux*. Conversely the water can exchange heat via mixing, both at the large scale (stirring) and ultimately at the small scale (molecular diffusion). We call this a *diffusive flux*.

3.3.1 Advective flux

Advective fluxes are changes carried by gradients in the fluid. So, imagine a river with a contaminant C in it, measured with units of g m^{-3} (figure 3.17), and the river is seen to have higher concentrations of contaminant upstream than downstream. The river flows to the right with a speed u [m s^{-1}]. If we stand at some point on the river bank, say $x = x_0$, and measure the concentration over time, clearly, the concentration will be seen to be increasing. Hopefully it is also clear that it is increasing at a rate that depends on how strong the gradient is and how fast the flow is. If there were no gradient, then the concentration at x_0 would be constant, whereas if the gradient is strong the change will be faster.

We can easily quantify this if we know the gradient of C with

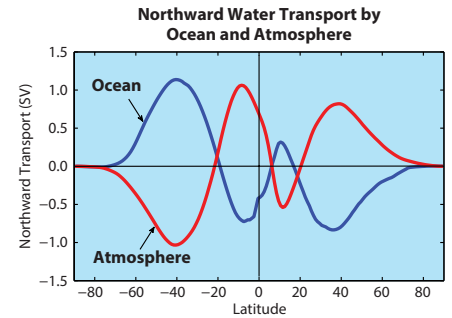


Figure 3.16: Net annual fresh-water transport [from Schmitt, 2018, Fig. 5]. The ocean curve is estimates by integrating the net surface flux curve integrated from figure 3.15, as described above for heat. The atmospheric curve is estimated from the ERA moisture transport simulations.

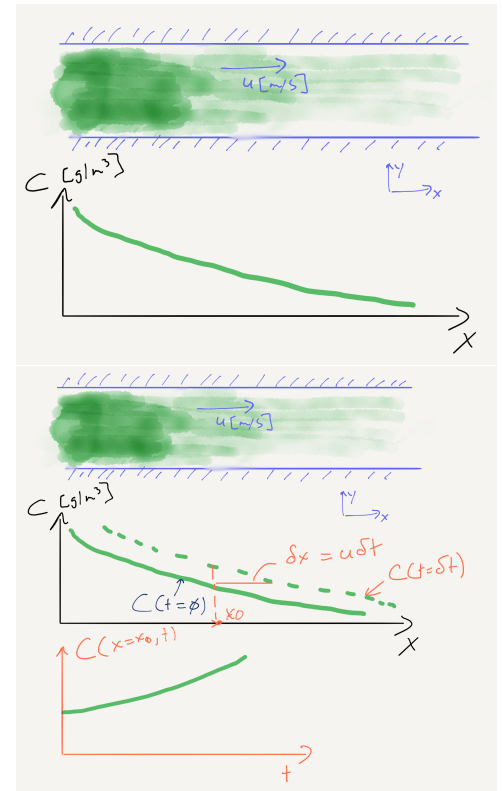


Figure 3.17: Sketch of a river with a gradient of a contaminant.

x , dC/dx and the speed of the river u . At $x = x_0$, the concentration at a time $t = \delta t$ is $C(t = \delta t) \approx C(t = 0) - \delta x \frac{dC}{dx}$, where the approximation is very good so long as dC/dx doesn't change much over the distance δx . Here δx is just the distance the river has travelled in time δt , and is therefore given by $\delta x = u\delta t$. So we can predict the new concentration based on things we can measure as $C(t = \delta t) \approx C(t = 0) - u \delta t \frac{dC}{dx}$. We allow δt to become very small then we can write this as a differential:

$$\frac{dC}{dt} = -u \frac{dC}{dx} + \text{other directions} + \text{diffusive fluxes} \quad (3.2)$$

Note the minus sign, which accords with the sketch in figure 3.17 where $dC/dx < 0$ because the concentration decreases in the positive x direction.

The term $-u \frac{dC}{dx}$ is the *advective flux* in the x -direction. Note that it has units of $\text{gm}^{-2}\text{s}^{-1}$ and can be thought of as mass per time per area of the flow. We can think of a river as only having one spatial dimension, but if there is more than one direction that can have gradients, as is often the case in the ocean, we may also be interested in the flux in the y -direction ($-v \frac{dC}{dy}$) and the vertical ($-w \frac{dC}{dz}$).

3.3.2 Advective transport

Note the units of an advective *flux* are concentration per time (in this case $\text{gm}^{-3}\text{s}^{-1}$). However, now imagine we have a lake that the river is flowing into, and we want to know how quickly the total amount of contaminant in the lake is increasing or decreasing. In this case we want the amount of contaminant per time that the river is carrying into the lake (i.e. in units of g s^{-1}). In this case, we need to know not only how fast the river is moving, but also what its cross-sectional area is to get an *advective transport* via:

$$F_C = -u \delta A \rho C \quad [\text{g s}^{-1}] \quad (3.3)$$

The term $Q = u \delta A$ is a volume transport, and usually has units of $\text{m}^3 \text{s}^{-1}$.

3.3.3 Conservation of mass (and heat)

Transports get used to create mass balance equations. Since we know mass must be conserved (plus or minus releasing nuclear energy), the rate of change of the mass of a contaminant in a volume of water must be equal to the net transports of the contaminant into the volume. A simple situation is to imagine a lake with two rivers, one feeding the lake and one draining it. Suppose we measure the cross sectional area of the river, and the velocity to get Q_{in} , and that

we measure the concentration of a contaminant in the river to be C_{in} . Suppose the river that drains the lake does so at the same rate ($Q_{out} = Q_{in}$) and the concentration is C_{out} . Then the rate of change of mass in the lake is simply:

$$\frac{dM_C}{dt} = Q_{in}C_{in} - Q_{out}C_{out} \quad (3.4)$$

where again, the rate of change is in g/s . Sometimes we want to express this as a rate of change of the average concentration in the lake \bar{C}_{lake} (where the overline emphasizes a volume average), in which case we would write as

$$\frac{d}{dt} (\bar{C}_{lake}V) = Q_{in}C_{in} - Q_{out}C_{out}, \quad (3.5)$$

where V is the volume of the lake. If indeed $Q_{in} = Q_{out}$ then V is a constant and

$$V \frac{d}{dt} \bar{C}_{lake} = Q_{in} (C_{in} - C_{out}). \quad (3.6)$$

The conservation of heat is very similar to the conservation of mass of a contaminant, but if the temperature range is not too large we can assume the heat capacity of water, c_p , is constant and think of this as the conservation of temperature:

$$\frac{d}{dt} (\rho c_p \bar{T}_{lake}V) = Q_{in}T_{in}\rho_{in}c_p - Q_{out}T_{out}\rho_{out}c_p \quad (3.7)$$

or if we assume density doesn't change very much with temperature we get an equation for temperature:

$$\frac{d}{dt} (\bar{T}_{lake}V) \approx Q_{in}T_{in} - Q_{out}T_{out} \quad (3.8)$$

which we lazily call the "heat" equation.

The conservation of salt is just the same as any other contaminant, but again, we just have to be careful of units. Salinity is parts per thousand, so to get weight per volume, we need to multiply by the density of the water to get a mass equation:

$$\frac{d}{dt} (\rho \bar{S}_{lake}V) \approx \rho_{in}Q_{in}S_{in} - \rho_{out}Q_{out}S_{out} \quad (3.9)$$

but again we just drop the density to get:

$$\frac{d}{dt} (\bar{S}_{lake}V) \approx Q_{in}S_{in} - Q_{out}S_{out} \quad (3.10)$$

The general form of all these equations is written as the rate of change of concentration in a fixed volume is equal to net sum of the inputs and outputs, so generally:

$$\frac{d}{dt} (CV) = \sum_{i=1}^N Q_i C_i \quad (3.11)$$

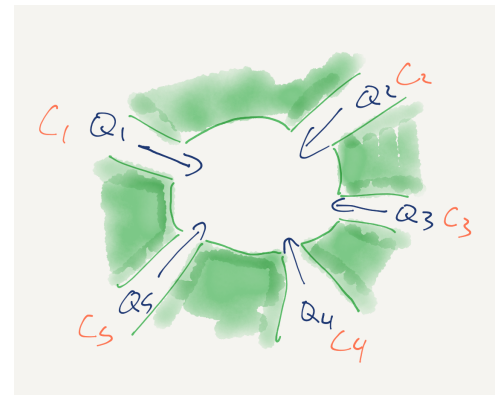


Figure 3.18: Schematic of lake with 5 possible inlets. If $Q_i < 0$ that means the flow is out of the lake.

where the sign of Q_i is chosen to be positive into the volume, and negative if the flow is out of the volume.

Box 3.3.1: Vector form of equation (3.11)

If you have had vector calculus, then equation (3.11) is equivalent to

$$\frac{d}{dt} \int_V C dV = - \oint_A \mathbf{C} \mathbf{u} \cdot d\mathbf{A}, \quad (3.12)$$

where $d\mathbf{A}$ is defined as positive pointing out of the volume.

The volume integral is the same as the finite sum as we make more and more finite sums.

3.3.4 Conservation of mass and volume

This application of the conservation of mass can be applied to the mass of water as well, but here we usually make a crucial approximation called that the fluid obeys **Incompressible flow**, and that variations of density are small enough to ignore in the mass equation. This may seem counter intuitive, but it arises because the density of water does not vary much through the world's oceans (chapter ??).

For the mass of water, the conservation equation for our two-river lake is

$$\frac{dM}{dt} = Q_{in}\rho_{in} - Q_{out}\rho_{out} \quad [\text{kg s}^{-1}] \quad (3.13)$$

where ρ_{in} and ρ_{out} are the inflowing and outflowing density of the water in the lake. Suppose also that $\bar{\rho}_{lake}$ is the average density in the lake, then we can write

$$\frac{d}{dt} (\bar{\rho}_{lake} V) = Q_{in}\rho_{in} - Q_{out}\rho_{out} \quad [\text{kg s}^{-1}] \quad (3.14)$$

At a fundamental level, the incompressible flow approximation just says that $\bar{\rho}_{lake} \approx \rho_{in} \approx \rho_{out}$ and we can write

$$\frac{d}{dt} V \approx Q_{in} - Q_{out} \quad [\text{m}^3 \text{ s}^{-1}] \quad (3.15)$$

A little more justification is given in Box 3.3.2, but assuming incompressibility of the fluid makes the mathematics significantly easier. Of course one can always be more precise if needed.

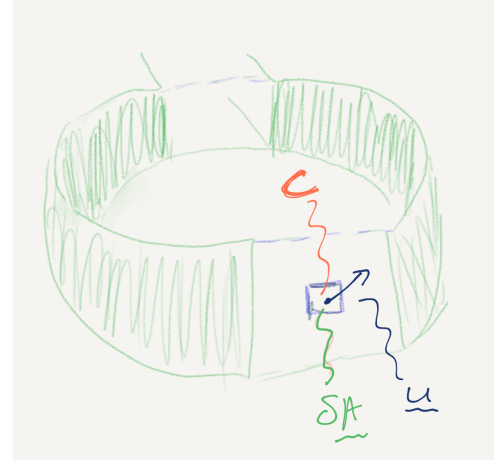


Figure 3.19: Schematic of volume integral. The total integral is the sum of all “open” faces of the area that bounds the lake (i.e. you can only have fluxes out the open sides of the lake).

Box 3.3.2: More justification for dropping ρ

To see why its a good approximation to drop the density from the mass equation and just conserve volume, lets say that $\rho_{in} = \bar{\rho} + \rho'_1$ and $\rho_{out} = \bar{\rho} + \rho'_2$. More formally, we can expand equation (3.14) using the chain rule:

$$V \frac{d}{dt} (\bar{\rho}) + \bar{\rho} \frac{d}{dt} (V) = \bar{\rho} Q_{in} - \bar{\rho} Q_{out} + \rho'_1 Q_{in} - \rho'_2 Q_{out} \quad (3.16)$$

or, dividing by $\bar{\rho}$:

$$V \frac{1}{\bar{\rho}} \frac{d}{dt} (\bar{\rho}) + \frac{d}{dt} (V) = Q_{in} - Q_{out} + \frac{\rho'_1}{\bar{\rho}} Q_{in} - \frac{\rho'_2}{\bar{\rho}} Q_{out} \quad (3.17)$$

A very large density variation in the ocean would be 1%, so all the terms multiplied by $\frac{1}{\bar{\rho}}$ are on order of 1% of the terms that have not been multiplied by this factor. Given that 1% would be a very good estimate of any of the other terms, in a volume budget we usually ignore the small error and use equation (3.15).

As an example, suppose $Q_{in} = 1 \times 10^4 \text{ m}^3 \text{ s}^{-1}$ and $\rho_{in} = 1000 \text{ kg m}^{-3}$, and $Q_{out} = 1.1 \times 10^4$ and $\rho_{out} = 1005$, and $\bar{\rho} = 1002.5$, and $V = 10^{10} \text{ m}^3$. We see that the terms are

$$\frac{1}{\bar{\rho}} \frac{dM}{dt} = 10^3 + 2.5 \text{ m}^3 \text{ s}^{-1} \quad (3.18)$$

and that the second term is far smaller than the first.

Getting at the left-hand term is actually a bit of work and requires an equation of state (chapter 2). The density in the lake changes because of temperature or salinity changes in the body of water from the river. This will give us $V \frac{1}{\bar{\rho}} \frac{d}{dt} (\bar{\rho})$. To make life simple, imagine a linear equation of state that depends only on temperature: $\rho = 1000(1 + \alpha(T - T_0))$ where $\alpha = 2 \times 10^{-4} \text{ [}^\circ\text{C}^{-1}\text{]}$ is a thermal expansion co-efficient.

3.4 Diffusive Fluxes

The other way that the concentration of a contaminant can change in a fluid is for the concentration to diffuse (or heat, or momentum). The diffusion of a contaminant is at the molecular level due to the random motion of the particles in solution (figure 3.20) which acts to homogenize the concentration of the contaminant. This means that the flux of contaminant ($\text{gm}^{-2}\text{s}^{-1}$) is from high concentration to low concentration. Note that diffusive fluxes have exactly the same units

as advective fluxes, and have the same effect on the concentration of the contaminant.

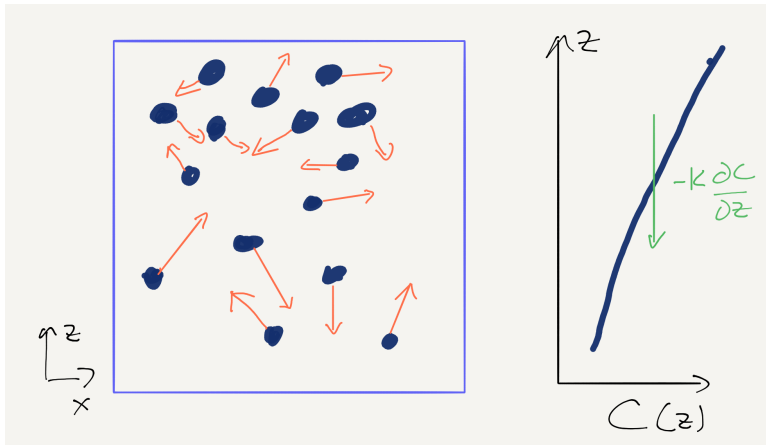


Figure 3.20: Schematic of diffusion of a contaminant. Random motions in the fluid act to homogenize the concentration, with a flux from high concentration to low concentration.

Most contaminants in fluids are assumed to obey *Fick's Law* where the diffusive flux is linearly proportional to the gradient in concentration. i.e. if there is a sharp change in the concentration, the flux is stronger. And of course the flux is always from high concentration to low concentration, so we need a minus sign:

$$F = -K_C \frac{dC}{dz} \quad (3.19)$$

where K_C is the *diffusion co-efficient*, and has units of $\text{m}^2 \text{s}^{-1}$. The sign of this flux indicates whether the flux is in the positive z -direction, or the negative. So in figure 3.20b, the $dC/dz > 0$ so the net diffusive flux of C is downwards.

The Diffusion co-efficient K varies by the contaminant, or if temperature or momentum are being considered. For salinity $K \sim 10^{-9} \text{ m}^2 \text{ s}^{-1}$, where the exact co-efficient depends on the salinity and temperature of the water. For temperature, it is two orders of magnitude larger $K \sim 10^{-7} \text{ m}^2 \text{ s}^{-1}$, because the transfer of heat does not require molecules to trade position, but rather for vibrational energy (heat) to be transferred, which is a more efficient process.

Of course, if we have a two- or three-dimensional distribution of the contaminant, then we need to consider the gradients in each direction. i.e. going back to the example of the river, the diffusive flux would be in the same direction as flow, since the high concentration is coming from upstream, so in this case the flux is $-KdC/dx$.

3.5 Net flux: advection plus diffusion

So, let us go back to considering how to determine how quickly the concentration changes at a given point in a fluid (figure 3.21) by looking at a box in our river. There is a flux from up stream (F_L) and one going downstream (F_R), so the net flux is $F_L - F_R$. The rate of change is then given by

$$\delta x W H \frac{dC}{dt} = (F_L - F_R) W H \quad (3.20)$$

, where W is the width of the channel, and H the depth, and allowing $\delta x \rightarrow 0$

$$\frac{dC}{dt} = -\frac{dF}{dx} \quad (3.21)$$

So, if $F_L > F_R$ the concentration will increase in the volume.

At any given point, the flux in the x -direction is given by the advective plus the diffusive flux $F = uC - K\frac{dC}{dx}$, and the full conservation of mass is given by:

$$\frac{dC}{dt} = -u\frac{dC}{dx} + K\frac{d^2C}{dx^2} + \text{other directions} \quad (3.22)$$

Again, as discussed above, we can also think of this by considering the sum of fluxes across a number of inlets and outlets, but now with both advective and diffusive fluxes:

$$\frac{d}{dt}(CV) = \sum_{i=1}^N F_i = \sum_{i=1}^N \left(Q_i C_i - A_i K \frac{dC}{dn} \right) \quad (3.23)$$

where A_i is the area element the flux is passing through, and dC/dn is a gradient, defined as positive into the volume.

Finally given these two types of fluxes, its possible for a gradient of a property to exist in the ocean and a mean flow, if the mean flow is balanced by diffusion. Imagine if the river in figure 3.21 were flowing from right to left, then the advective flux would be to the left and the diffusive flux would be to the right, and it would be possible for the two fluxes to be in balance, and the concentration of contaminant to not change.

Box 3.5.1: Vector form of equation (3.23)

Again, if we know a little vector calculus, we can rewrite equation (3.23) as

$$\frac{d}{dt} \int_V C dV = - \oint_A (C\mathbf{u} - K\nabla C) \cdot d\mathbf{A}, \quad (3.24)$$

where $C\mathbf{u}$ is the advective flux, and $-K\nabla C$ is the diffusive flux, both of which are vector quantities.

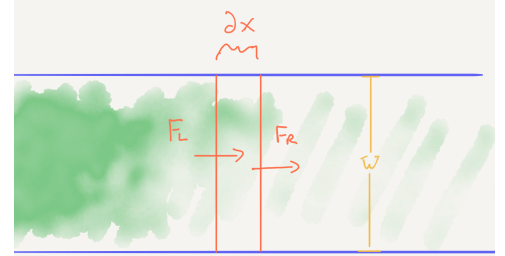


Figure 3.21: Schematic of net flux into a small volume.

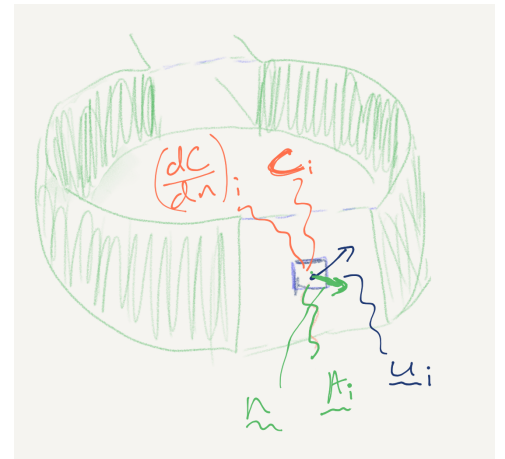
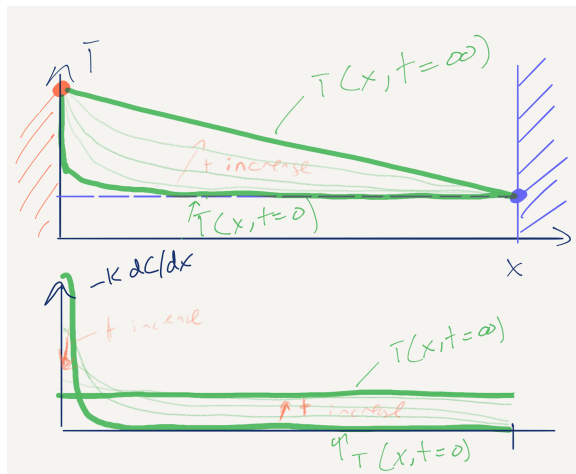


Figure 3.22: Information needed for mass budget across a surface leading out of a lake.

3.5.1 Turbulent diffusivities

Molecular diffusion can be quite slow. The diffusion equation ($\frac{dC}{dt} = -K \frac{d^2C}{dx^2}$) can be solved with exponential functions (see Box 3.5.2) that represent how quickly the solution relaxes to its steady state. E.g. in figure 3.23, the temperature is fixed at two ends of an iron bar, and the initial temperature is cold, then heat will diffuse from the warm side to the cold side until a steady state is reached. In this case, the steady state is a linear temperature gradient so that $d^2T/dx^2 = 0$. How quickly this will happen is given by the exponential approach to the steady state.



TIME SCALE OF DIFFUSION

Figure 3.23: Example diffusion where temperature is fixed on the left and right side of the domain and the temperature all starts out cold. Imagine an iron bar, with one end in a fire and the other end in a pool of water. Heat diffuses in the bar from hot to cold. The steady state is a straight line between the two temperatures.

We can estimate this exponential timescale, quite simply as $\mathcal{T} = L^2/K$, where L is the spatial scale. If we assume a 100-m lateral scale, and a molecular thermal diffusivity of $K = 10^{-7} \text{ m}^2 \text{ s}^{-1}$, we would get a time scale of 10^{11} seconds, or more than 3000 years. If we went all the way to the bottom of the 4000-m deep ocean, the time scale would be greater than 5 million years. All these numbers are 100 times larger for salt.

Box 3.5.2: Solutions to diffusion equation

The diffusion equation $\frac{dC}{dt} = -K \frac{d^2C}{dx^2}$ has solutions of exponential form:

$$C = Ae^{-Kt/x^2} + Be^{Kt/x^2} + C(x, t) \quad (3.25)$$

where the values of A , B , and the function $C(x, t)$ depend on the initial conditions and boundary conditions.

3.5.2 Turbulent diffusion

Clearly, if molecular diffusivity were the only way that diffusion happened, we would just ignore these fluxes. But we saw in chapter 1 that mixing was an essential ingredient to the circulation. What happens in the real ocean is that the flow is often turbulent, and turbulence stirs the fluid, and greatly enhances the efficiency of the molecular diffusion. This is easy to see when you add milk to coffee or tea - if you do not stir the coffee, then the milk will stay in a blob. Net diffusion only happens where there are gradients in the concentration (figure 3.24). Stirring the fluid greatly increase the length of the fluid over which there is a gradient, and often sharpens the gradients. This leads to much more mixing than if the fluid is not stirred.

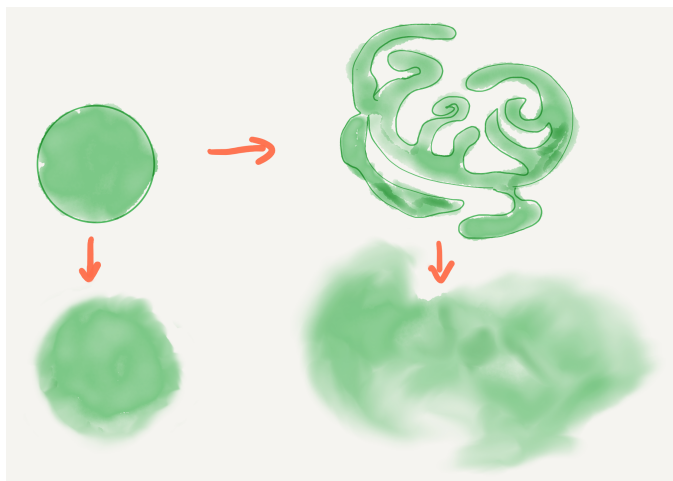


Figure 3.24: 2-D sketch of the difference between diffusion and stirring and diffusion. Of course this happens in three dimensions in the ocean.

Stirring in the ocean is driven by a number of instability processes. *Shear instability* is one such process (figure 3.25) where the flow goes unstable because it has different velocities between layers. In the simulation in figure 3.25, the instability grows and accomplishes significant stirring before it becomes fully three-dimensional turbulence which does more stirring. The result is net mixing and thickened interface between the two layers. A natural example from Admiralty inlet shows that this type of instability is often found in nature (figure 3.26).

A second common instability is *convective instability*. This happens when dense fluid is on top of light fluid, such as happens when you boil water on the stove. A more oceanographic experiment is shown in figure 3.27 where the water is warmed from below. As it rises, there is clear instabilities, however note that these instabilities themselves are actually shear instabilities when looked at closely.

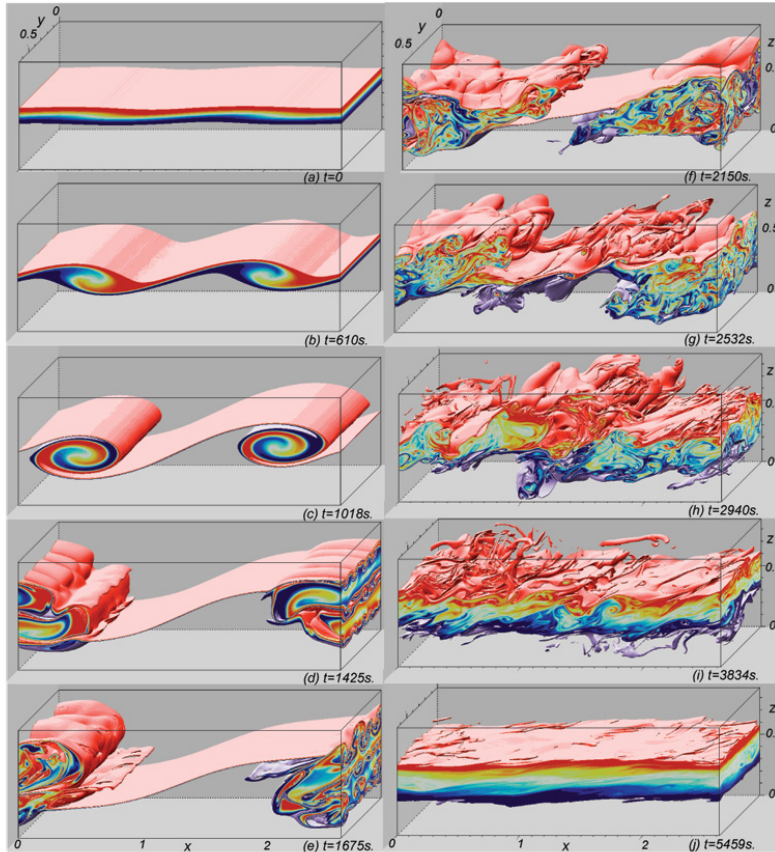


Figure 3.25: Numerical simulation of mixing in the ocean. Here a flow in the upper layer from left to right causes an instability on the temperature interface in the middle. The flow breaks down into turbulence, and the turbulence stirs the fluid driving greatly enhanced mixing. [Smyth et al., 2005]

The effect of turbulence is to greatly increase the rate at which properties are fluxed across interfaces. However the flux still tends to be from regions of high concentration to regions of low concentration. Hence we will often represent these fluxes by a linear flux law. For instance, in the x -direction: $F_x = -K \frac{dC}{dx}$ where now K is a *turbulent diffusivity* rather than a molecular one. When estimated, turbulent diffusivities are *much* larger than molecular diffusivities. Estimates in the open ocean range from molecular levels to $K \sim 10^{-1} \text{ m}^2\text{s}^{-1}$ and levels can reach even higher values in coastal waters where there are strong flows. Estimating turbulence requires sophisticated instrumentation and often simplifying models, and remains a great challenge today to oceanographers. Often the approach to estimating turbulence is to relate the turbulence to external parameters that can be measured or simulated. This has led to many schemes to estimate turbulence in models and ocean calculations.

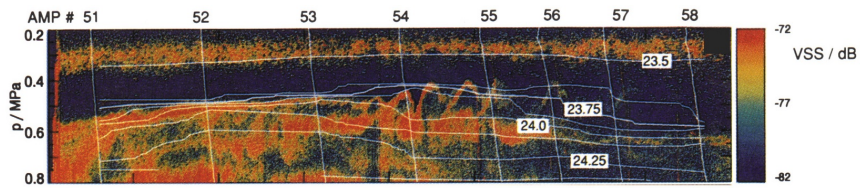


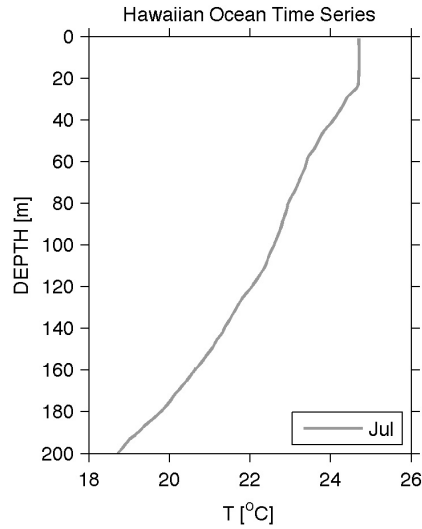
Figure 3.26: Shear instability in the ocean measured at Admiralty Inlet in Puget Sound [Seim and Gregg, 1994].



Figure 3.27: Horizontal convection experiment where the left side of a tank is heated at the bottom, and the right hand side (not shown) is cooled. Water rises, primarily along the left hand wall. <http://rses.anu.edu.au/gfd/AR2005/index.php?p=ar05res>

The consequence of turbulent mixing is that it makes the importance of mixing much more apparent. If the timescale is 10^{11} s for molecular diffusion at $K = 10^{-7} \text{ m}^2 \text{ s}^{-1}$, then it is 10^7 s for $K = 10^{-3} \text{ m}^2 \text{ s}^{-1}$, or 100 days. That starts to matter for long-lasting flows.

3.6 Exercises



Heat budget of the surface mixed layer

- What is the specific heat capacity of water?
- Sketch what the temperature profile would look like if it lost enough heat so that it was a uniform temperature to 100 m?
- How much heat would have to be lost from the surface of the ocean for this to happen? Estimate from the temperature profile and show how you calculated this.
- What is the average heat flux this heat loss would represent if it occurred over 6 months, in W/m^2 . Based on the plots in the reading is this a reasonable net surface heat flux?

Interpret the evolution of the surface mixed layer Based on the following plot, try and answer the following questions:

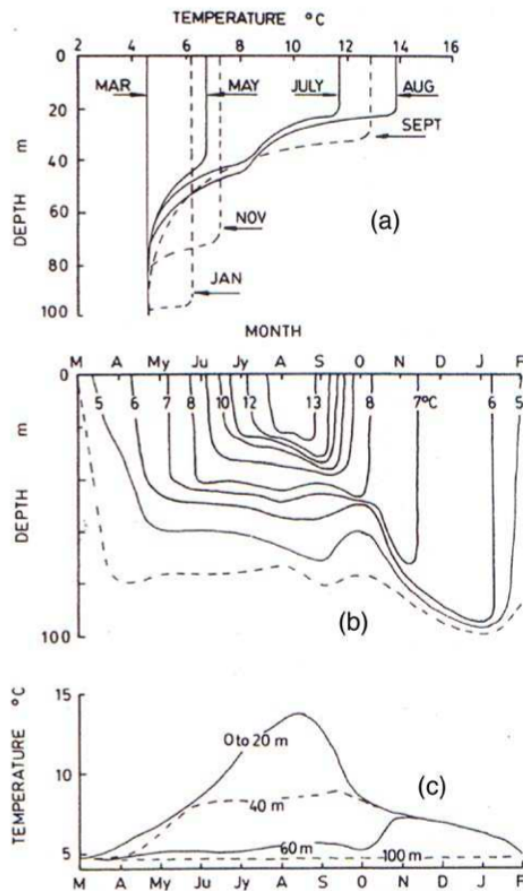


Fig. 4.7. Growth and decay of the seasonal thermocline at 50°N, 145°W in the eastern North Pacific as (a) vertical temperature profiles, (b) time series of isothermal contours, and (c) a time series of temperatures at depths shown.

From Emery et. al. 2007

- Why does the mixed layer deepen in the winter?
- Why does it shoal in the spring and summer?
- Why do you think there is often a spring bloom at Station Papa?
Why does it stop?

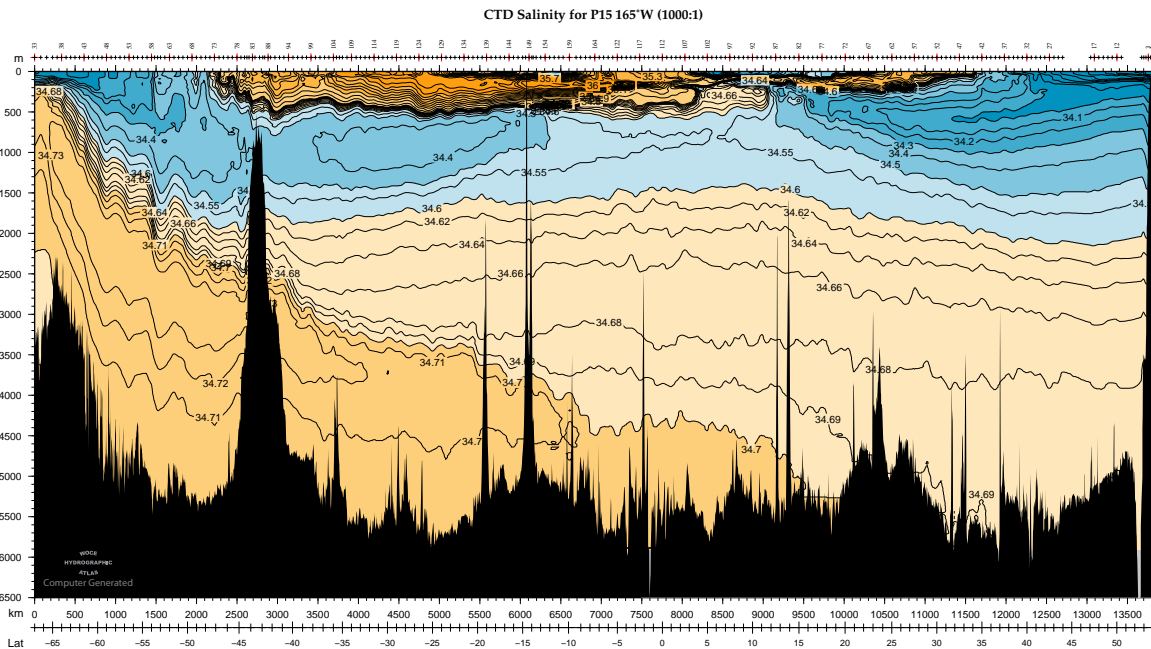
Diffusive fluxes The geometry and units of fluxes are a bit difficult to get clear, so let's practice them here. Consider the following table of data points:

Depth [m]	Concentration Sulfur $g\ m^{-3}$
5	2
15	3
25	6
35	6
45	4
55	2

- Sketch the profile of Sulfur with depth.
- Doing this sort of thing abstractly becomes hard. Lets assume this profile was collected in a column of water that is 65-m deep, 1 m x 1m in the horizontal plane. Divide the column into $10 \times 1 \times 1\ m^3$ blocks centered on our measurements. Approximately, how many grams of Sulfur are there in each of the 6 blocks?
- Approximate the gradient of Sulfur concentration at each the boundaries of each of the boxes (i.e. 10 m, 20 m, etc..).
- If the turbulent diffusivity is $K = 10^{-3}m/s$ what is the diffusive transport across each of the block faces? Make sure you get the direction correct. Report your result in grams/second.
- Consider any one block. You now should know the value and direction of flux (in g/s) across the upper and lower face, and you should know the total grams inside the block. If you assume the flux remains constant for 1000 s, how many grams of Sulfur are in your cell after 1000 s?
- Repeat for all 6 cells (hint, use a computer!) and plot the new sulfur profile after a 1000 s.
- Repeat the procedure 9 more times to get the gradient after 10000 s; (Hint: really use a computer;). Plot the sulfur profile at each timestep.
- Do the changes of the profile correspond to your intuition of how diffusion works?

4

Ocean water masses



Most exchange of ocean heat and freshwater occur at the surface of the ocean, with only minor contributions due to geothermal heatfluxes, and exchange of solutes with the crust. Thus water that is "formed" at the surface tends to retain its signature as it moves through the ocean, leading to the concept of identifiable ocean water masses. These water masses are thought of as having "core" values of temperature and salinity that then are diluted by mixing with other water masses. This approach is of course most effective with water masses that are far from the surface of the ocean where they are not modified, so we concern ourselves primarily with *intermediate* and *deep* water masses here.

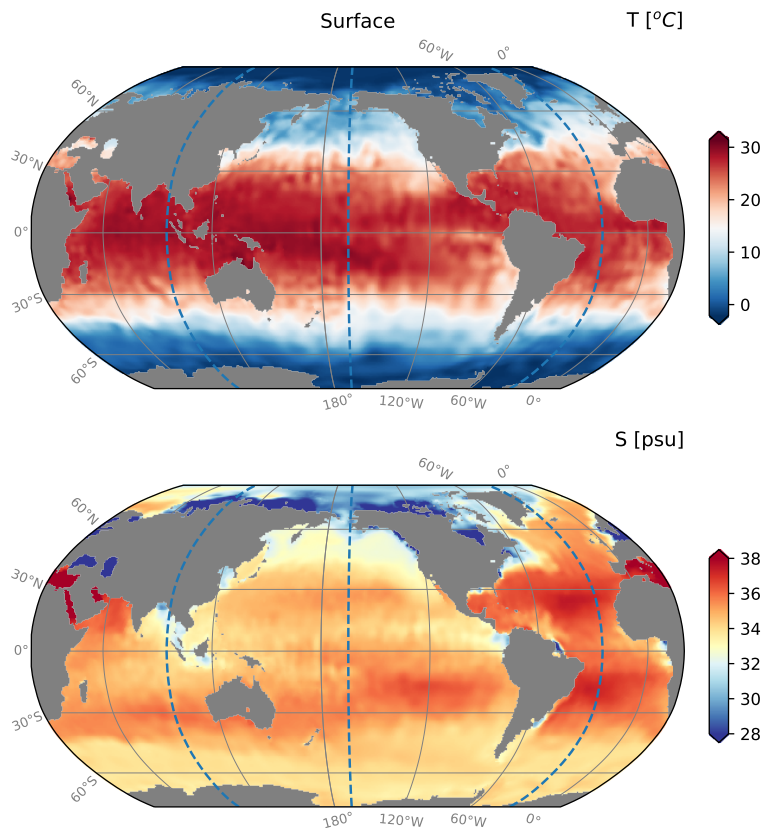
4.1 *Surface distributions of temperature and salinity*

Figure 4.1: Annual average surface temperature and salinity from the [WOCE climatology](#). Dashed lines are sections shown below in the Pacific, Atlantic, and Indian Oceans.

Temperature and salinity distributions at the surface of the ocean follow relatively predictable patterns given the fluxes in chapter ?? (figure 4.1). Warm water is found near the equator, and cold at the poles. There is a relatively sharp delineation between warm waters and cold waters just poleward of approximately 45 degrees, particularly in the Northern Hemisphere, a signature of the separation of the western boundary currents from the continents (like the Gulf Stream) at those latitudes. There is often relatively cool water directly adjacent to the western shore of continents due to upwelling.

Salinity is more complicated with relatively salty surface water at the mid latitudes, and fresher water in the subpolar gyres and the equator. The Mediterranean, Red Sea, and Persian Gulf are very salty, and overall the Atlantic and Indian oceans are much more salty than the Pacific, to no small part because of these marginal seas.

4.2 Meridional sections

Clearly the largest variation at the surface of the ocean in temperature and salinity is in the *meridional* direction (North-south), so we start our exploration of the water masses in the ocean by looking along meridians in the Pacific, Atlantic, and Indian oceans (figure 4.2). There are striking similarities between all three basins, particularly in the Southern hemisphere, with the largest differences in the salinity distribution amongst the oceans.

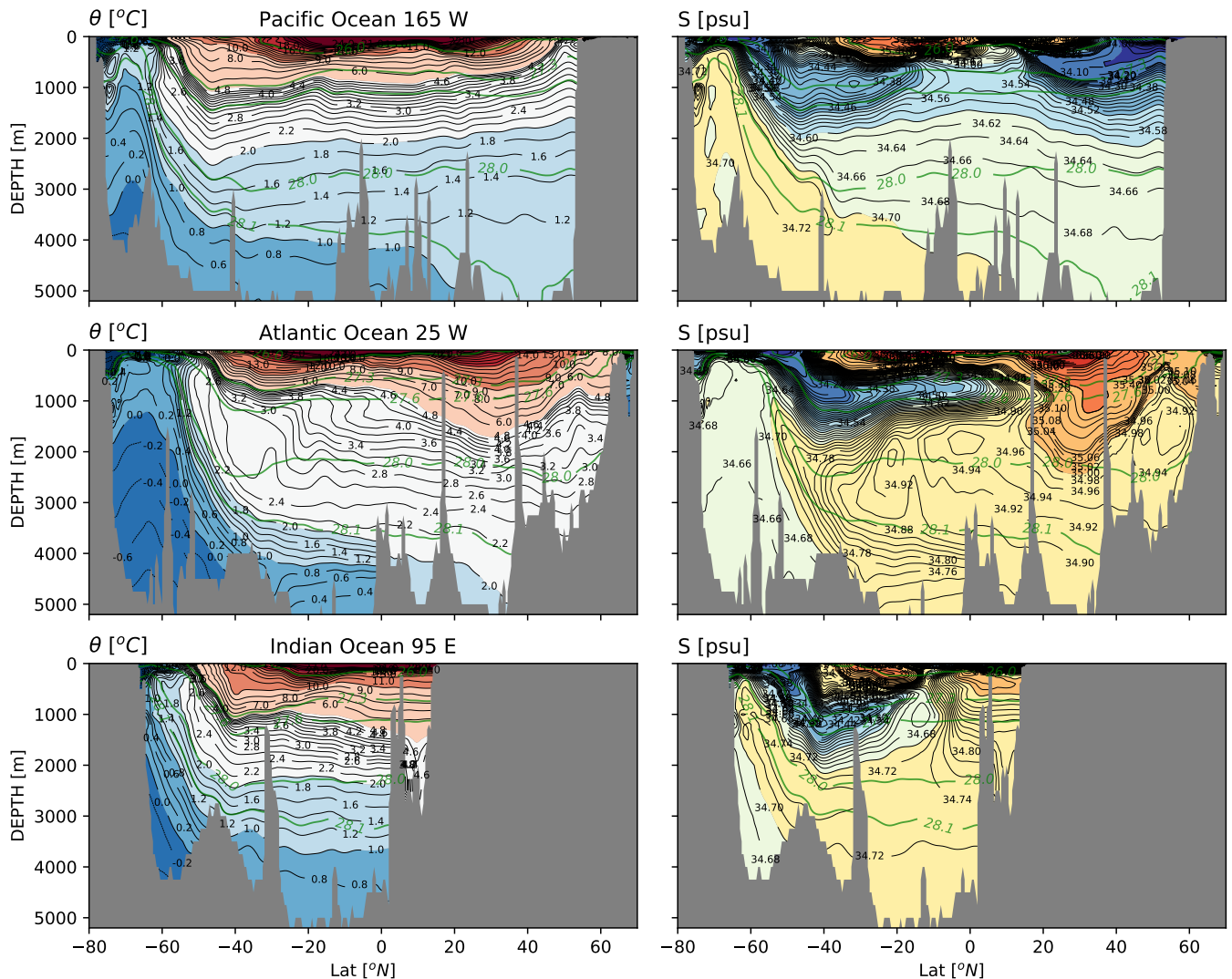


Figure 4.2: North-south cross sections of potential temperature and salinity in the world's oceans. Green contours are levels of constant neutral density. Note the contour levels and colors are non-linear and chosen to highlight ocean water masses. Note the location of these sections is shown in figure 4.1, figure 4.5, and figure 4.4

Surface waters First, in the upper ocean, shallower than 700 m or so, there is a distinct push down of both the isotherms and isohalines

centered around 30 degrees. These surfaces rise at the equator, and then again as we move poleward of 30 degrees. This is the signature of the wind-driven *subtropical gyres*, and will be discussed in later chapters. These surface waters are characterized by relatively warm, salty water. Poleward of these bowls are the *subpolar gyres* which tend to be cooler and significantly fresher.

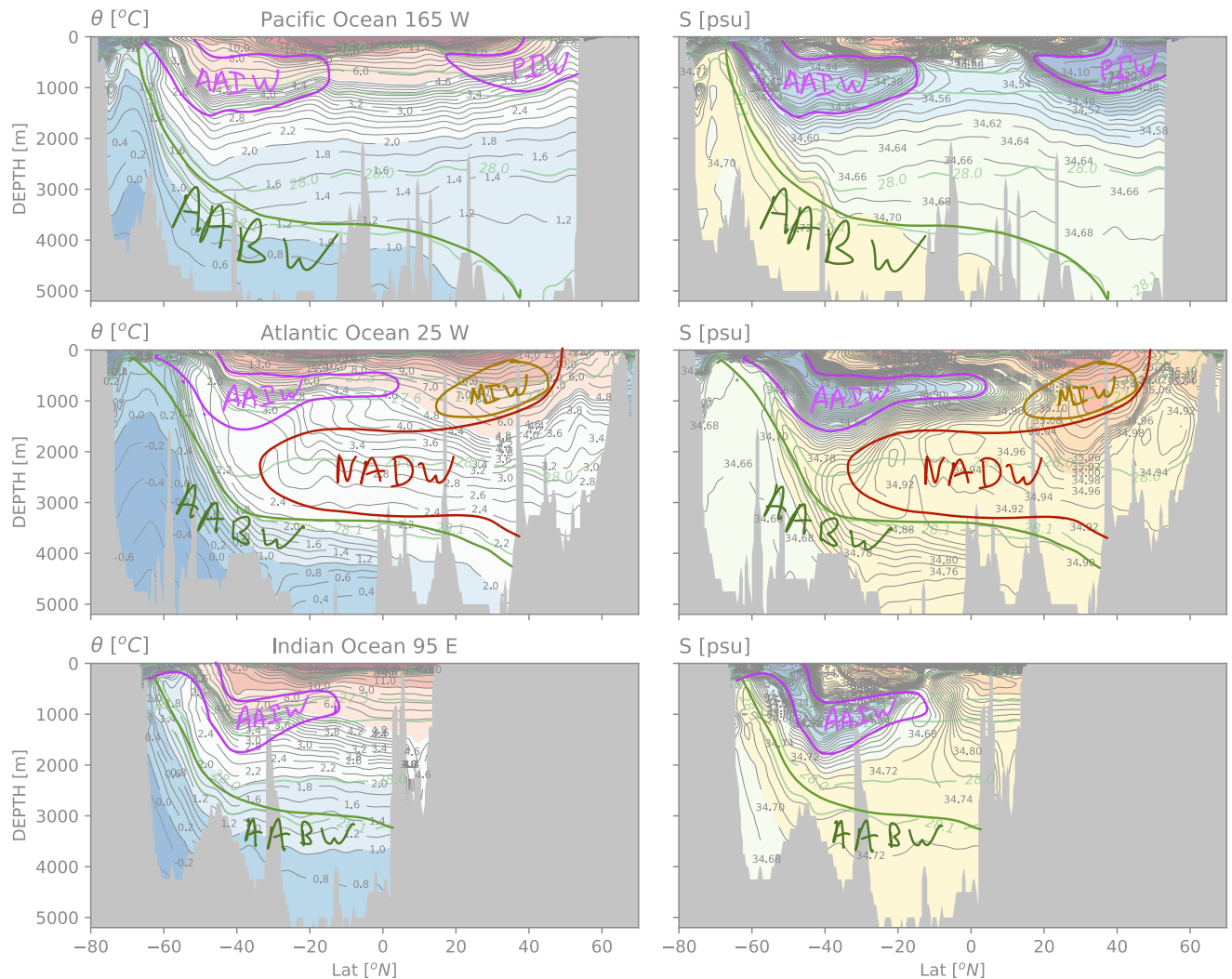


Figure 4.3: As in figure 4.2, with intermediate and deep water masses indicated. AAIW: Antarctic Intermediate Water, PIW: Pacific Intermediate Water, MIW: Mediterranean Intermediate Water, ABW: Antarctic Bottom Water, NADW: North Atlantic Deep Water

Intermediate waters Below the surface water, at depths approximately 1000 m are the Intermediate waters. There is a tongue of fresh cool water found at this depth in all the oceans, clearly connected to the sub-polar gyre in the Southern Ocean, so this water is called *Antarctic Intermediate Water*. This water is found in all the ocean basins as a

northward protruding tongue of water pushed down at around 50 S and then moving up slightly as it moves north (figure 4.3: AAIW). An analogous water mass is found in the North Pacific, and is usually called North-Pacific Intermediate water (figure 4.3: PIW) which originates near 50 N and then is pushed south under the subtropical gyre water.

Finally, there is the very distinct intermediate water mass found in the North Atlantic, called *Mediterranean Intermediate Water* (figure 4.3: MIW). This very salty water is formed in the Mediterranean where salinities exceed 38 psu, which then pours into the North Atlantic as dense water. This water mixes with the ambient water and is diluted, but still has a very robust salinity structure that is found throughout the North Atlantic at the intermediate depths.

Deep and bottom waters Finally, all basins have water along the bottom composed of the densest water in the ocean. It's clear from these cross sections that this water originates in the Southern Ocean (figure 4.3:AABW), where it can be seen *outcropping* south of 60 S, and therefore we call this *Antarctic Bottom Water*. We have the distinct impression that it moves north, as we would expect from the slope of the density surface, and that it becomes diluted with the fresher and warmer above as it moves further north.

The last major water mass is *North Atlantic Deep Water* (figure 4.3: NADW). This water is produced in the Greenland-Iceland Seas, and to a lesser extent the Labrador Sea, and is not as dense as Antarctic Bottom Water. Its density is centred around $\gamma_N \approx 28$, and flows into the ocean above the AABW from the north to the south.

There are many ways to look at these water masses in addition to meridional sections. Surfaces of constant depth (figure 4.4) and surfaces of constant neutral density (figure 4.5) give a useful reference as to where the water masses come from. For instance the Mediterranean water is very clear at $Z = 2000$ m (figure 4.4) as a tongue of salty water. It's also warmer, as can be seen in the contours of temperature, but it is not as obvious due to the colormap. We can see that the fresh intermediate water clearly at 1000 m in the North Pacific is fresher on the west side of the basin than the east.

The deepest surfaces ($Z = 4000$ m) are interesting in that we can see cold salty water pouring in the Pacific (figure 4.4). We note that it preferentially flows in on the west side of the basin, which is due to the Coriolis force turning the flow to the left. This can be seen, somewhat less dramatically, in the other basins. A similar effect happens with the North Atlantic Deep Water, where it flows south, it hugs the western boundary (because it is turning to the right due to the Coriolis force) though it is less obvious to see in these plots.

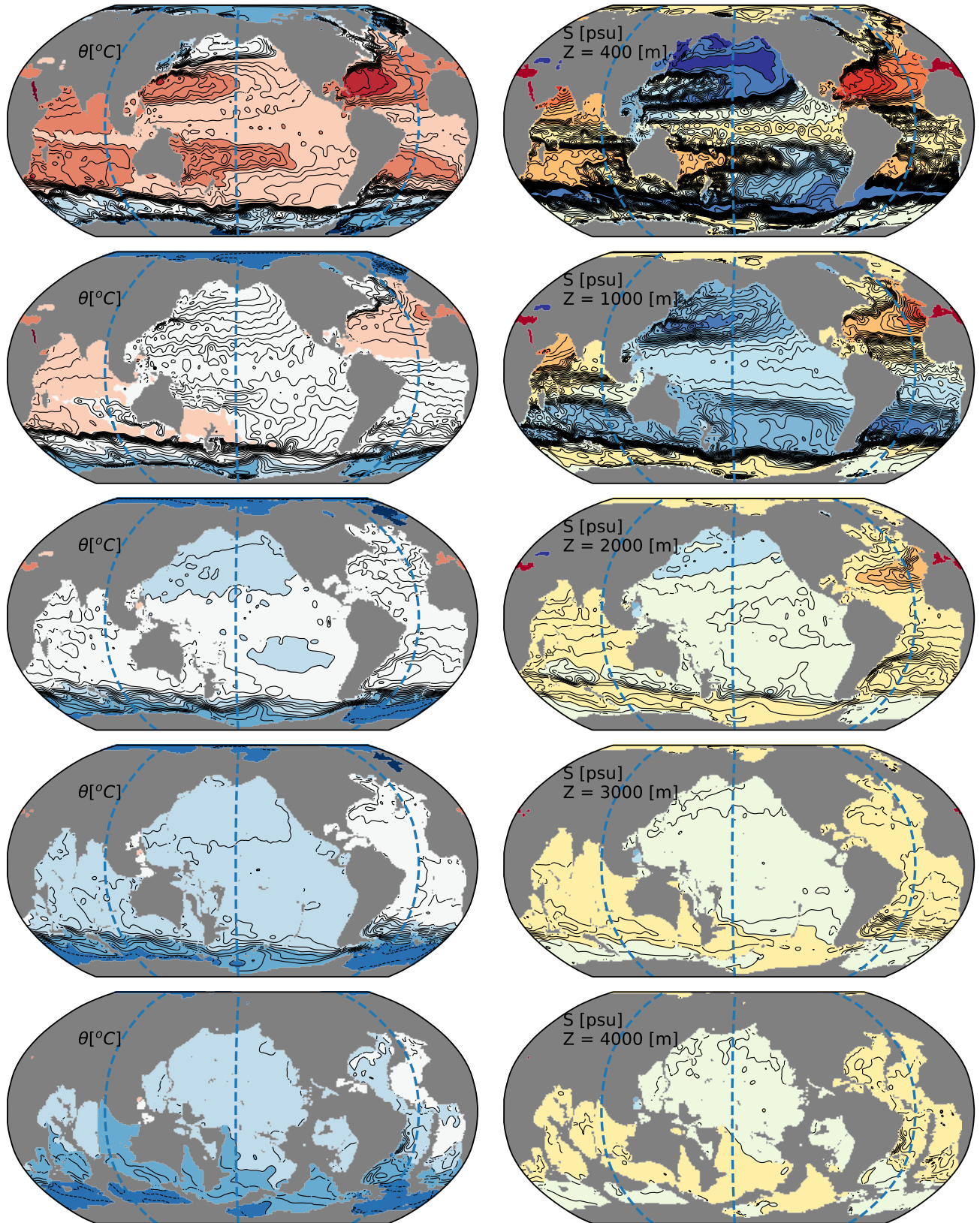


Figure 4.4: Global views of potential temperature and salinity on surfaces of constant depth. Dashed blue lines are sections shown in figure 4.2

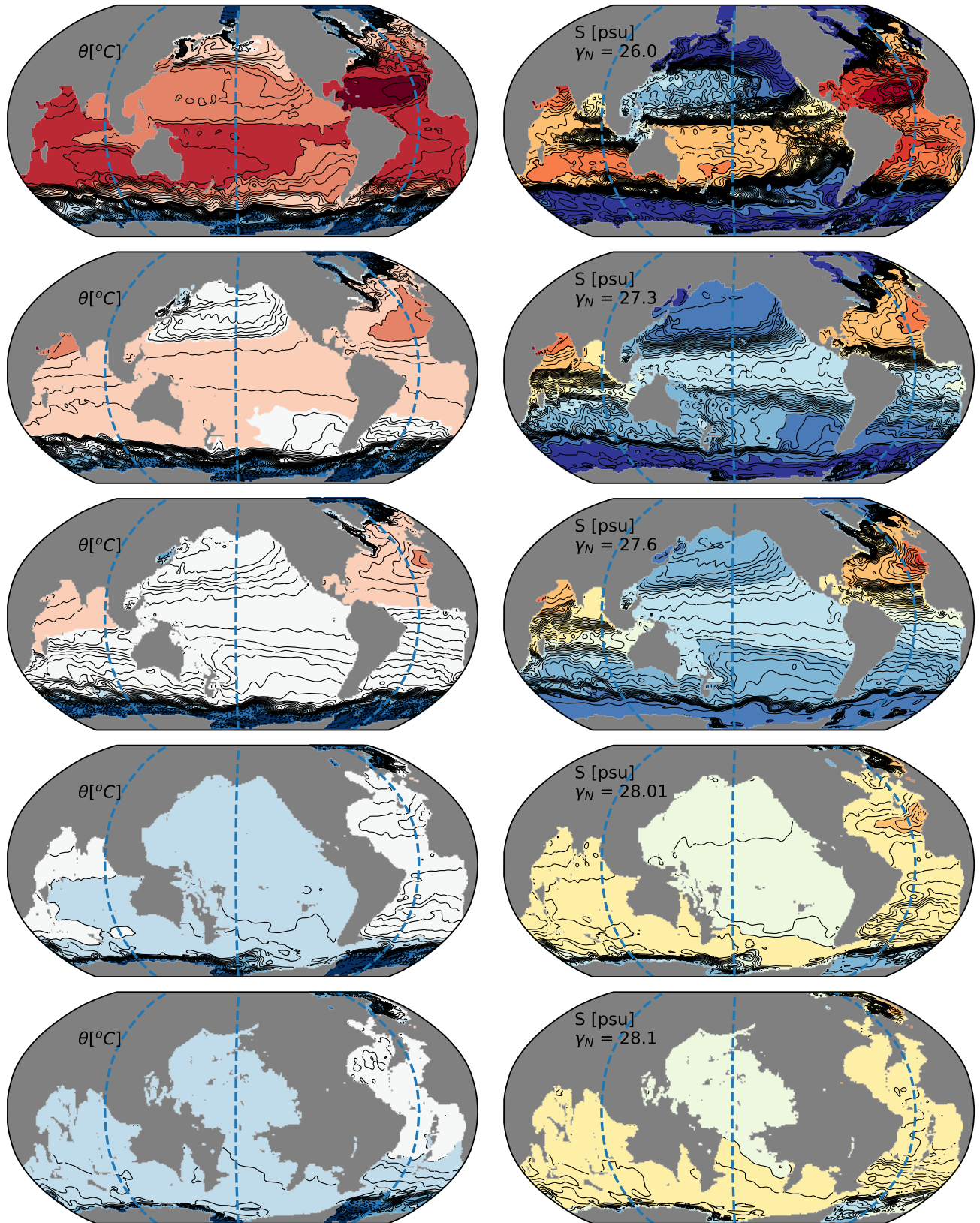


Figure 4.5: Global views of potential temperature and salinity on neutral density surfaces. The surfaces chosen are the same ones contoured in figure 4.2 in green. Dashed blue lines are sections shown in figure 4.2

Overall these plots reinforce the idea that most of the variation is in the meridional direction, with details showing up in the zonal direction. These east-west differences tend to be most pronounced near the coasts, or adjacent to marginal seas like the Mediterranean.

4.3 Vertical distributions, and the surface mixed layer

It is worth re-iterating that the plots made above have very non-linear colormaps, and that most of the ocean's variability is in the upper ocean (figure 4.6) with weak, but very consistent, gradients at depth. This structure applies through much of the ocean with most of the variation taking place across a *thermocline* that is on the order of 1000 m thick, decaying into a relatively homogeneous abyss for the rest of the ocean.

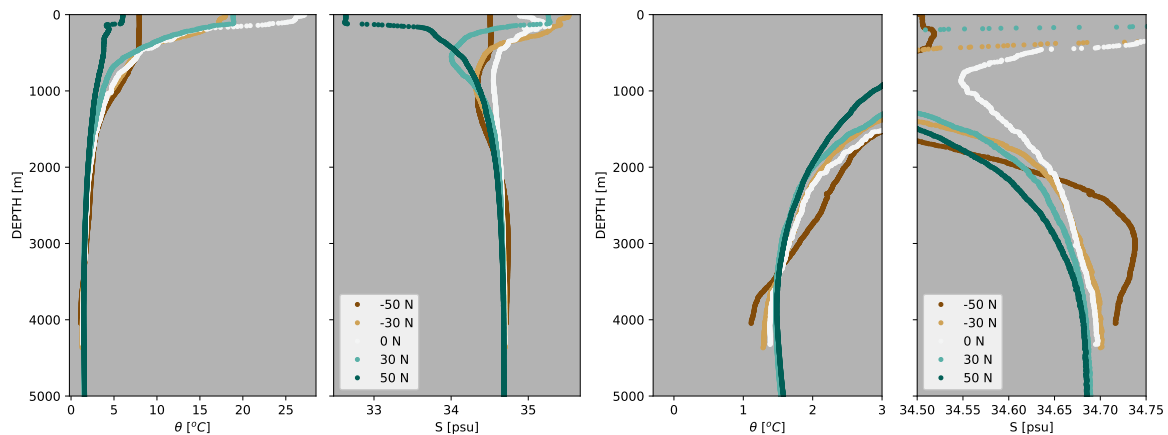


Figure 4.6: Example θ and S profiles from the Pacific Ocean at five different latitudes. The two plots on the right as zoomed version of the plots on the left.

The upper ocean is usually topped by a *mixed layer*, where the action of waves and wind have combined to mix the water uniformly. This can be seen in all the example profiles in figure 4.7, except for the profile at the equator (white) as a region of homogeneous water in both the temperature and salinity profiles. At 50 S, this layer is particularly thick, extending over 150 m deep. In the plot shown it looks like it is much deeper, but there is some slight temperature and salinity difference with depth that stops the water from being completely homogeneous.

The dynamics of the mixed layer are very important given that they mediate the flux of temperature and gasses between the ocean and the atmosphere. There are three things that deepen the mixed layer:

1. Cooling from evaporation and sensible heat loss
2. Mixing from wind-driven turbulence and waves

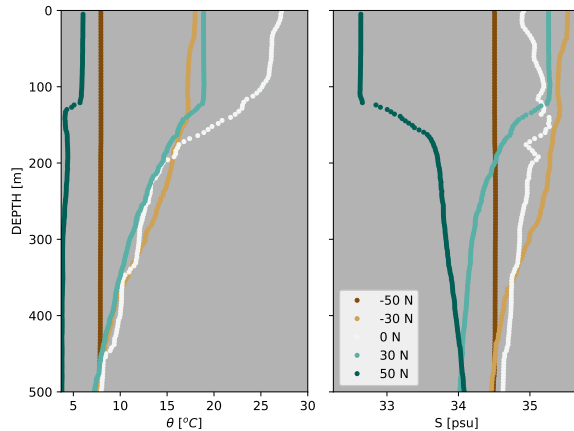


Figure 4.7: Example θ and S profiles from the Pacific Ocean at five different latitudes. The two plots on the right as zoomed version of the plots in figure 4.6.

3. Shear-driven turbulence at the base of the mixed layer.

The first term is relatively straight forward. The second term is hard to parameterize, but accords with our usual understanding of waves as turbulent forces. The last term is because the wind pushes the mixed layer, and hence it develops momentum that is different in speed and direction from the water below. This generates a *shear* and these can go unstable (chapter ??).

The mixed layer will *restratify* due to

1. Heating or freshwater
2. Lateral advection of more buoyant water (often from equator-ward).

This cycle leads to an annual/seasonal cycle of the upper ocean mixed layer (figure 4.8), with cooling in the winter, and warming in the summer. In this case, the mixed layer gets down to about 100 m by later spring, and then starts shoaling again in the summer. This often leads to a situation where there are two thermoclines in the summer; the *permanent thermocline* deeper than 100 m, and a *seasonal thermocline* beneath the summer mixed layer. Note that in this example, the mixed layer is also strongly influenced by salinity, so the concept of the *halocline* is important to understand the annual cycle and why the mixed layer only penetrates to about 100 m.

The mixed layer also evolves on a daily time scale, with warming in the day and cooling at night, of course modified by the wind conditions (figure 4.9). In this example when the ocean is being warmed by the atmosphere, the mixed layer becomes very shallow (figure 4.9B) and turbulence deeper in the water column is suppressed (figure 4.9C). At night the water column cools and turbulence gets to deeper depths.

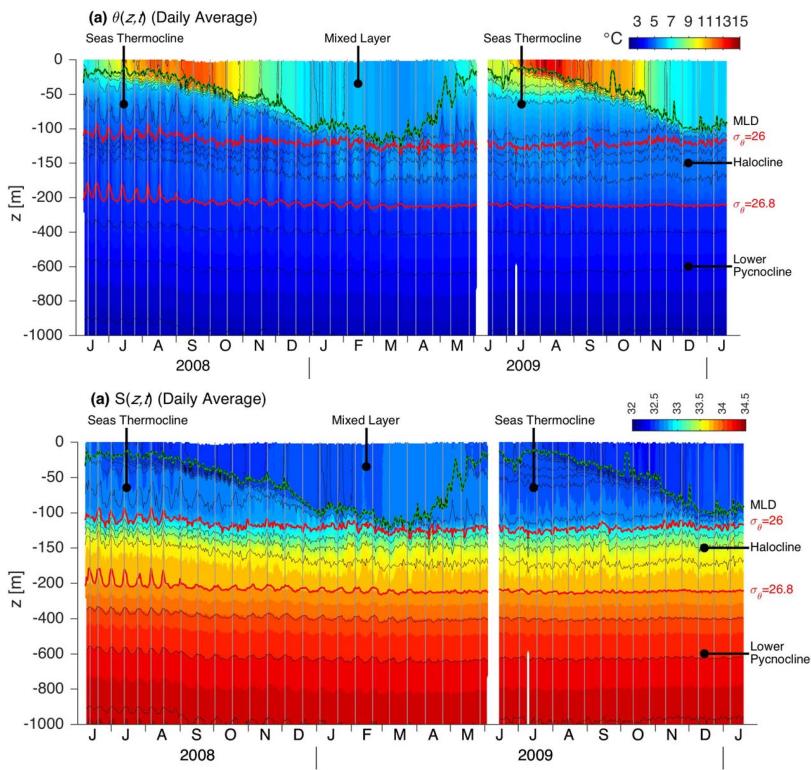


Figure 4.8: Temperature and Salinity in the upper ocean over an annual cycle at Station Papa (Northeast Pacific Ocean: 50 N, 145 W) [Pelland et al., 2016]

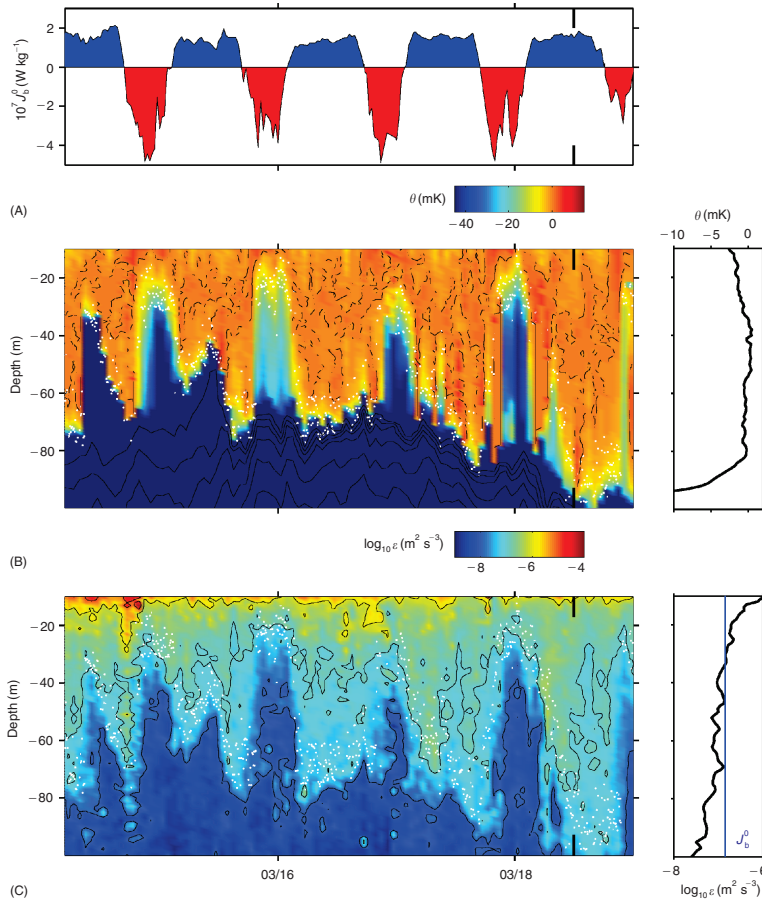


Figure 4.9: Mixing in the upper ocean in NE Pacific summer. A) heat flux, red being ocean heating, blue cooling. B) Temperature anomaly relative to depth-mean. So this shows the vertical variation, but not the cooling and heating with time. White dots indicate the base of the mixed layer. C) Turbulence dissipation rate.

Given the variety of forcings it is not surprising that the ocean mixed layer has a wide variety of depths through the world's oceans (figure 4.10). Depths are greatest in the winter, and reach quite great depths near the poles. Depths also tend to be largest on the windward side of the basins, where there are the greatest heat fluxes.

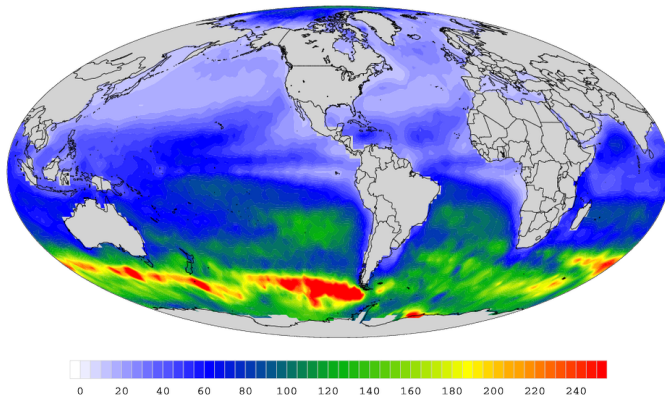
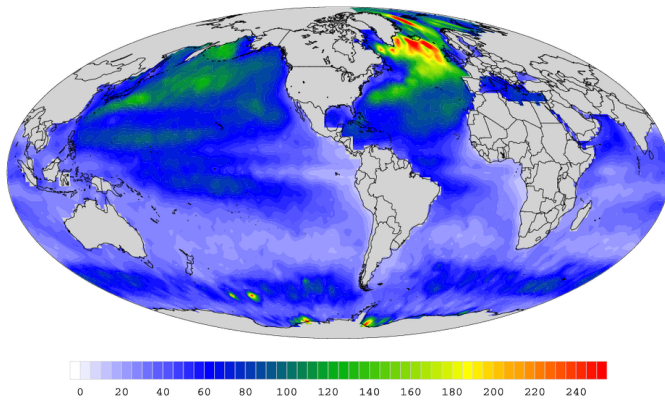
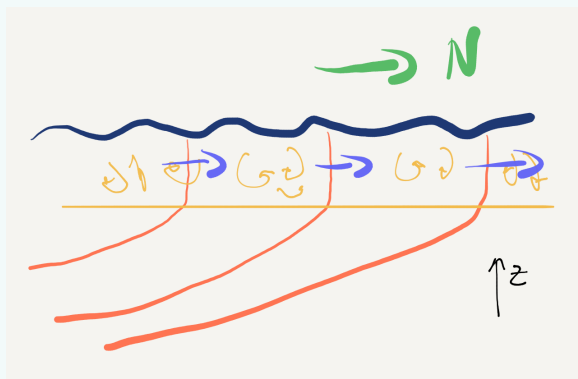


Figure 4.10: Mixed layer depth in the boreal and austral winters.

Box 4.3.1: Restratification of the mixed layer



A north-south section of the ocean in the northern hemisphere will tend to look like the schematic above. If there were no mixing in the upper ocean, the orange isopycnals would tend to flatten, driving a flow to the North. This happens all the time in the upper ocean where there is a warmer (lighter) mixed layer equatorward of a point. Hence heat is being constantly fluxed poleward by this restratification, and if the mixed layer is to stay mixed, it must mix via turbulence and lose heat to the atmosphere. So, when the north Pacific warms in the summer, it is not only the result of the local warming by the sun and lack of heat losses due to evaporation, but is also due to a northwards transport of heat by this restratification.

4.4 Property-property plots: θ - S plots

As noted, the water masses tend to have particular characteristics. Another useful tool for tracking water masses is to look at the data as property-property plots, and the most basic of these is a $\theta - S$ plot where potential temperature is plotted on the y axis, and salinity on the x-axis. From this we can clearly see the differences between the different water masses from south to north. At intermediate depths we can see the clear difference between warmer and fresher Pacific Intermediate Water at 34 psu and 7 degrees C, compared to the Antarctic Intermediate Water (34.25, 5 degrees C).

Looking deeper, below 2000 m, we can see that the water in the Southern Ocean is substantially different than the water in the rest of the Pacific Ocean, with a large salty bulge at around (34.75 psu, 2 degrees C). This distinct water is actually North Atlantic Deep Water that is found in the Southern Ocean, but does not make it into the rest of the Pacific Ocean. The very densest water, at the bottom of the

T-S curves, gets lighter both by warming and freshening.

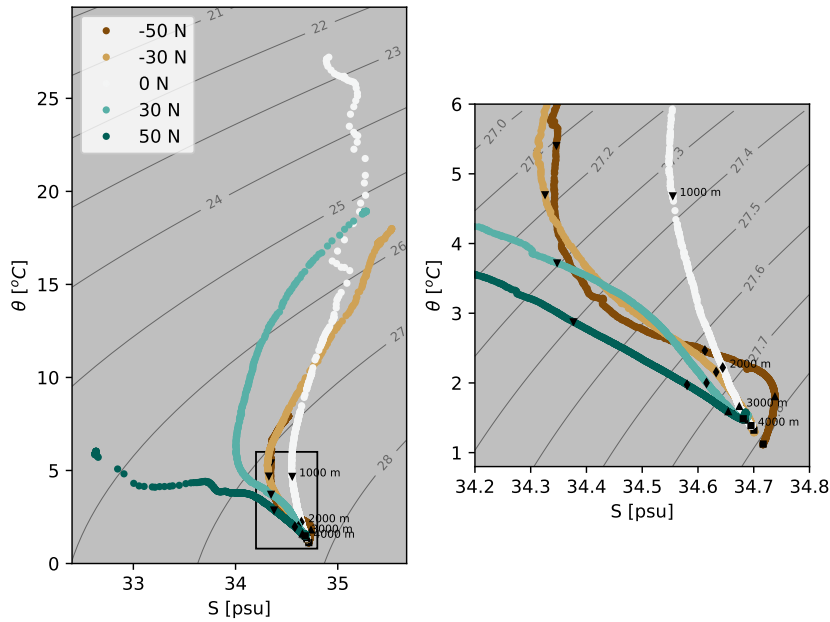


Figure 4.11: Example T-S plots from along P16 in the Pacific, from the profiles shown in figure 4.6. The depth of the data are shown with symbols on each curve, and the right hand side is meant to emphasize the properties in the deepest 1000 m. The white line has the depths labeled. Grey contours are potential density relative to the sea surface.

We can see how the properties vary smoothly with latitude by considering all the T-S curves along P16 (figure 4.12). The cold and very fresh surface waters near the poles show up as large anomalies. The anomalies are quickly eroded but still show up as the intermediate water masses. These intermediate water masses disappear, becoming more salty as the equator is approached.

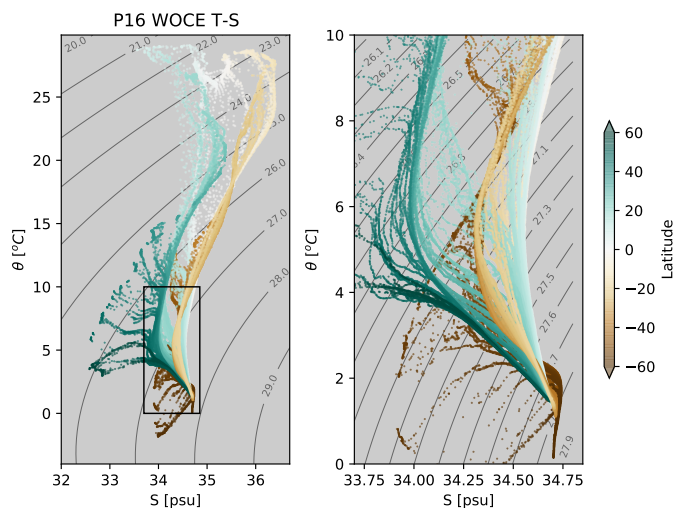


Figure 4.12: WOCE $\theta - S$ properties along P16. Data is color-coded by latitude.

The power of looking at T-S diagrams is that water should maintain its temperature and salinity properties away from the surface

of the ocean, except via mixing between the water masses. Mixing can be inferred from *end members* which tend to mix along straight lines in T/S space. For instance, if we mix equal parts water with salinity and temperature S_1 and θ_1 with a second water mass S_2, θ_2 , then the mixture will have a new salinity $(S_1 + S_2)/2$, and potential temperature $(\theta_1 + \theta_2)/2$ (figure 4.13). This new water mass lies on the line connecting the two water masses in space. If there is more of one water mass in the mixture, the point will still be along the line connecting the two water masses in T/S space, but it will be closer to the dominant water mass.

Box 4.4.1: Quick proof that mixture is along line between endpoints

The line connecting S_1, θ_1 and S_2, θ_2 is given by

$$\theta = \frac{\theta_2 - \theta_1}{S_2 - S_1} (S - S_1) + \theta_1 \quad (4.1)$$

If we then substitute $S = \frac{aS_1 + bS_2}{a+b}$ we get

$$\begin{aligned} \theta &= \frac{\theta_2 - \theta_1}{S_2 - S_1} \left(\frac{aS_1 + bS_2}{a+b} - S_1 \right) + \theta_1 \\ &= \frac{\theta_2 - \theta_1}{S_2 - S_1} \left(\frac{-bS_1 + bS_2}{a+b} \right) + \theta_1 \\ &= \frac{b\theta_2 - b\theta_1 + a\theta_1 + b\theta_1}{a+b} \\ &= \frac{a\theta_1 + b\theta_2}{a+b} \end{aligned}$$

so $\frac{aS_1 + bS_2}{a+b}, \frac{a\theta_1 + b\theta_2}{a+b}$ lies along the line between the two water masses for any values of $a > 0$ and $b > 0$. If either a or b are less than zero, the point lies beyond the two end point, which is not a possible situation for mixing.

The same principle applies if there are more water masses, though this becomes more complicated. Usually, to start, the mixing is just between two water masses, and the newly mixed water falls along a T-S line; in figure 4.14 the second row of plots shows what happens after a moderate amount of mixing between three water masses. There are two T-S lines, and the data will follow a "V" shape. As more mixing occurs, the original water masses start to be mixed way, until the final steady state of complete mixing is reached (figure 4.14, last row, step=9999). Note that during this whole time the mixed product stays within the triangle defined by the three water masses we started with. Indeed, unless there are surface processes, the T-S

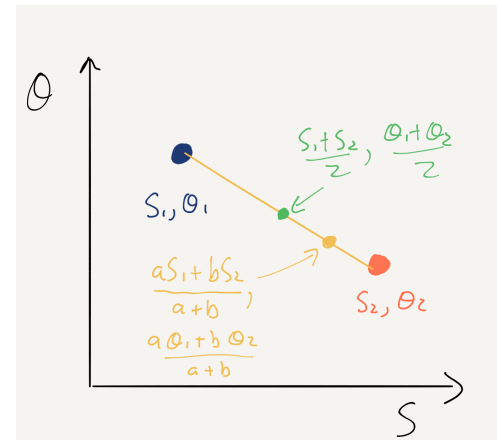


Figure 4.13: Result of mixing two water masses in T/S space. An equal mixture will lie midway on the line between the two water masses. An unequal mixture will also be along the line.

properties of any water parcel made up of these water masses *must* fall within this envelope.

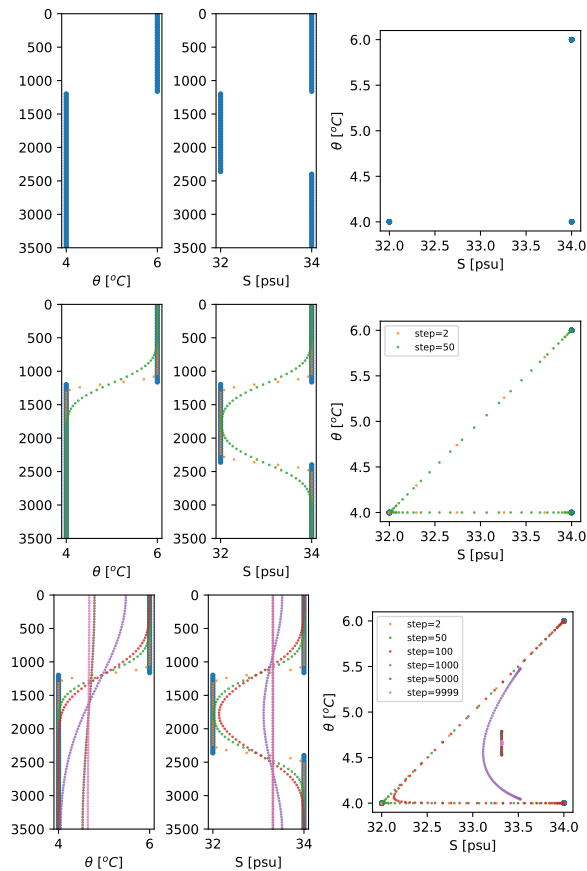


Figure 4.14: Result of mixing three water masses that are originally well mixed. The first row is the initial state. The second row is after some mixing has occurred, but all three water masses still exist. The last row is what happens after a long time. Eventually the temperature and salinity are well-mixed and all the points coalesce to a dot in T-S space.

We can then look at the WOCE data again, considering the origin of the water masses in the southern hemisphere (figure 4.15). If there were no North Atlantic Deep Water, there would be no kink in the T-S curves between $\gamma_N = 27.7$ and $\gamma_N = 27.8$. By the time we get to the equator (white line), the T/S curve looks a lot like the schematic shown in figure 4.14, where it curves between the bottom water and the surface towards the AAIW.

4.5 Summary

- The water properties in the ocean are largely set at the surface by heat and freshwater fluxes
- There are few locations where water is able to sink away from the surface, namely:
 1. the subpolar gyres: Intermediate waters

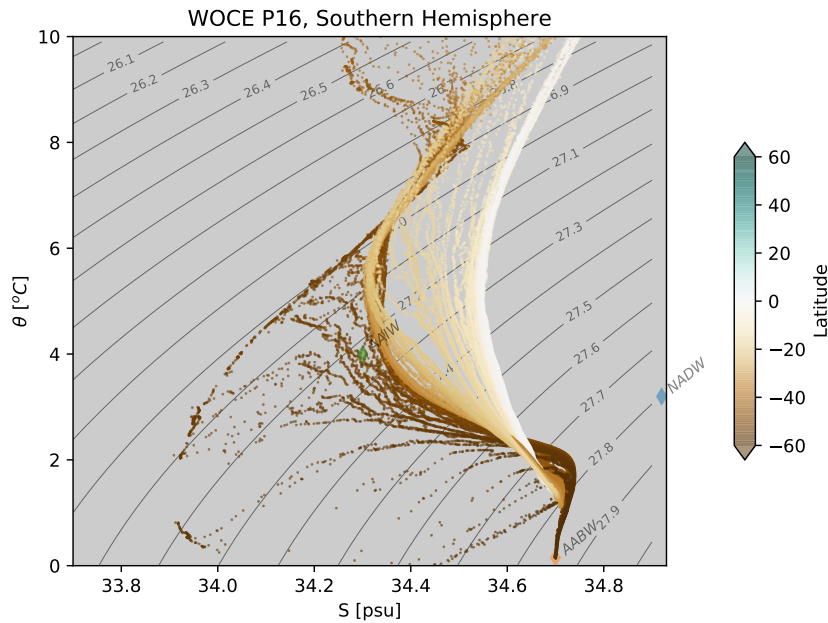


Figure 4.15: T/S diagram of the southern hemisphere Pacific, with core water masses indicated

2. marginal seas: i.e. Mediterranean and Red Seas
 3. high latitudes (also often marginal seas): Antarctic Bottom Water, and North Atlantic Deep Water.
- Subsurface waters can be traced over great areas in the world's oceans with identifiable *core waters*.
 - T-S properties are mixed along *mixing lines*.

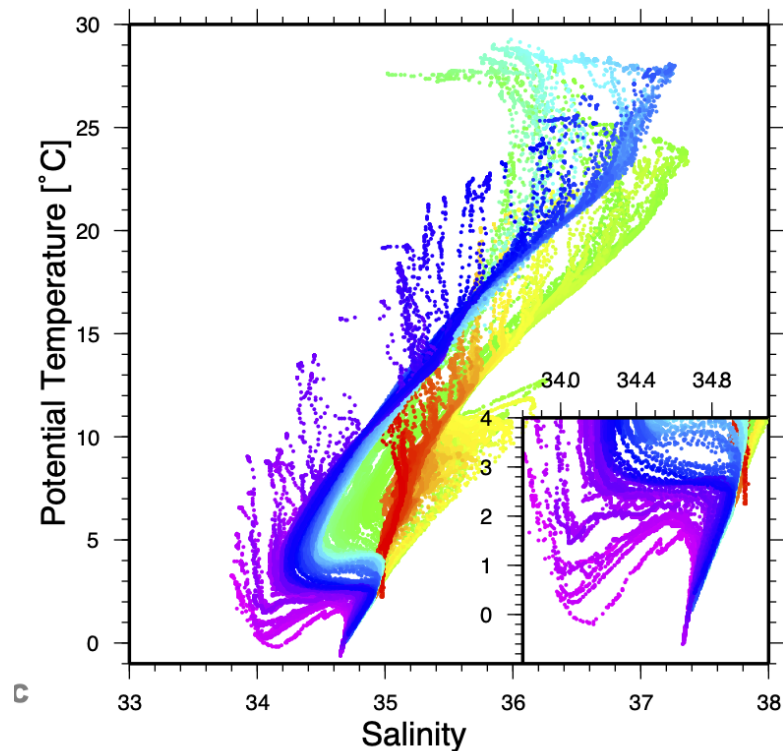
We will discuss in the next chapter where the deep waters arise and why they circulate as they do.

4.6 Exercises

Construct a T/S diagram Suppose we have a water column that initially is divided into three water masses:

z [m]	T [deg C]	S [psu]
0-10	20	30
10-20	10	31
20-30	5	30

- Sketch (or plot) the temperature and salinity vertical profiles ($T(z)$, $S(z)$) i) initially, ii) after they have undergone some mixing in the vertical, but there is still some 31-psu water that is unmixed; iii) after the 31 psu water has started to be mixed; iv) when the water is in steady state. NOTE: assume that the water column is not heated or cooled externally, and that there are no external salt sources or sinks.
- Draw the T/S diagram associated with each of your profile sketches.



Interpret a T/S diagram

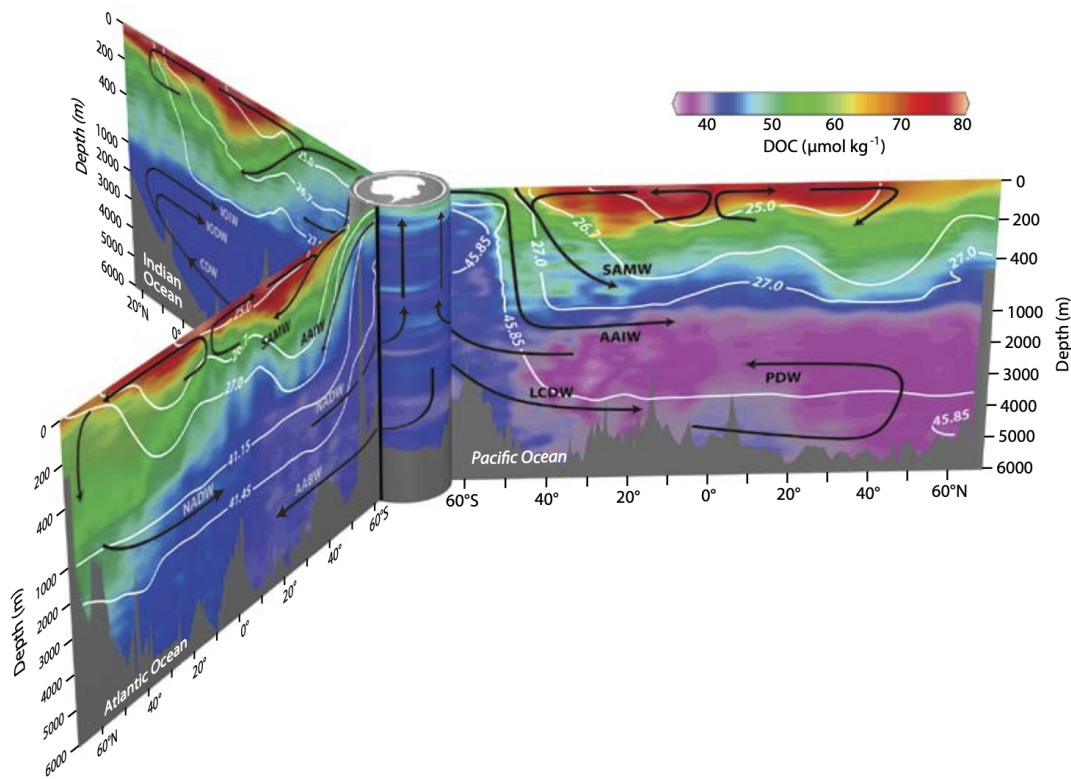
Consider the T-S diagram above.

- What do the colours represent? Explain why the different colors have different T/S properties

- Compare and contrast to the T/S diagram in figure 4.12. What different water masses can you see and which water masses are stronger and which are weaker?
- Identify, if possible, the major deep water masses.

5

Thermohaline overturning circulation



The water masses we saw in the previous chapter are the result of water formation at the ocean's surface, and for those that make it to depth, sinking of water. From the picture in figure 4.3a it is very evocative of the idea that dense water is created in the Southern Ocean and then sinks along the bottom to the north and fills the bottom basin of the Pacific. However, if that sinking of cold salty water happens all the time (and evidence is that it does), then there are two choices for where that water ends up eventually. The deep ocean could fill up with cold, salty water, or heat and fresh water can mix from above and modify it.

We sketch this here, where the 1.1°C isotherm is highlighted (figure 5.1). The dense water flows counter clockwise in this sketch, and must cross isotherms in order to complete the closed circuit. If water crosses an isotherm, it must warm, and the only way for this to happen is by vertical mixing. This chapter discusses this circulation, the evidence for it, and the mechanisms that drive it.

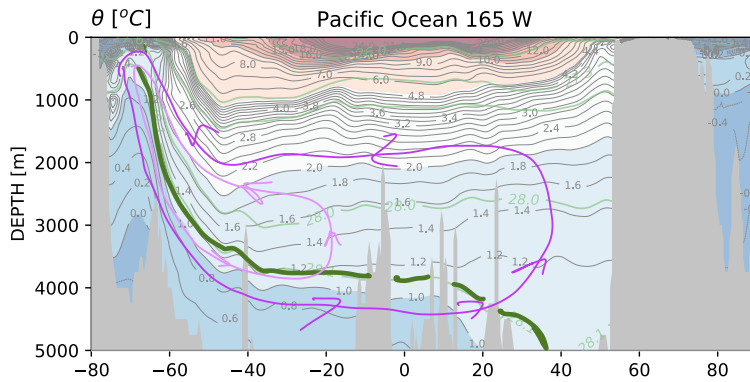


Figure 5.1: Sketch of deep overturning circulation in the Pacific. Green contour is the 1.1 degree-C isotherm (approximately) and the purple lines are idealized paths taken by the water.

5.1 Inferring the overturning circulation from other tracers

5.1.1 Bio-active tracers

The physical tracers like temperature and salinity are *conservative* in that they cannot be destroyed or consumed in the water column. This is not the case with bio-active tracers which change as the water is exposed to biological activity. In general, the upper ocean where sunlight can penetrate is dominated by photosynthesis, where plants, largely phytoplankton, convert CO_2 and nutrients to Oxygen. Outside the euphotic zone, the ocean is dominated by respiration, where animals and bacteria consume oxygen and respire CO_2 . This leads to the general picture in figure 5.2. The youngest water near the surface is high in O_2 and low in CO_2 and nutrients like Nitrate and Silica. The Antarctic Intermediate water is a clear plume of high- O_2 water being pushed south under the subtropical gyre. The Antarctic bottom water is seen pouring into the Pacific and losing oxygen as it moves north and gaining CO_2 . The lowest oxygen and highest CO_2 are found at around 1000 m in the north Pacific. Based on this logic alone we might argue that the oldest water is where this oxygen minimum is. That would not quite be correct - the oldest water is thought to be

about 1000 m deeper (see the next section), and that is because the net respiration rate tends to decrease with depth.

Nitrate and Silica are also highest at this point, though they have maxima at slightly different depths. Nutrients accumulate in the water column largely due to sinking of particles from the near-surface ocean. The particles that have large silica content like shells and bones tend to sink deeper than more labile material (bodies, fecal pellets) that contains significant nitrate. So, similarly to oxygen, the minima and maxima of the nutrients gives the correct sense of water sinking in the Southern Ocean and rising in the North Pacific, but the details depend on biological processes.

If we knew the rate of oxygen consumption, or the rate of particle fluxes in the deep ocean, we could use this information to estimate the strength of the overturning circulation. So if this rate were on average c $\mu\text{mol}/\text{kg}/\text{day}$, and there is 200 $\mu\text{mol}/\text{kg}$ difference between the AABW oxygen content and the oxygen minimum in the north Pacific, we could make an estimate of how many days it would take for the water to get to that minimum. Unfortunately, for most of the biological tracers, the consumption/production rates are poorly constrained, and understood to be spatially variable, so this approach is not typically used.

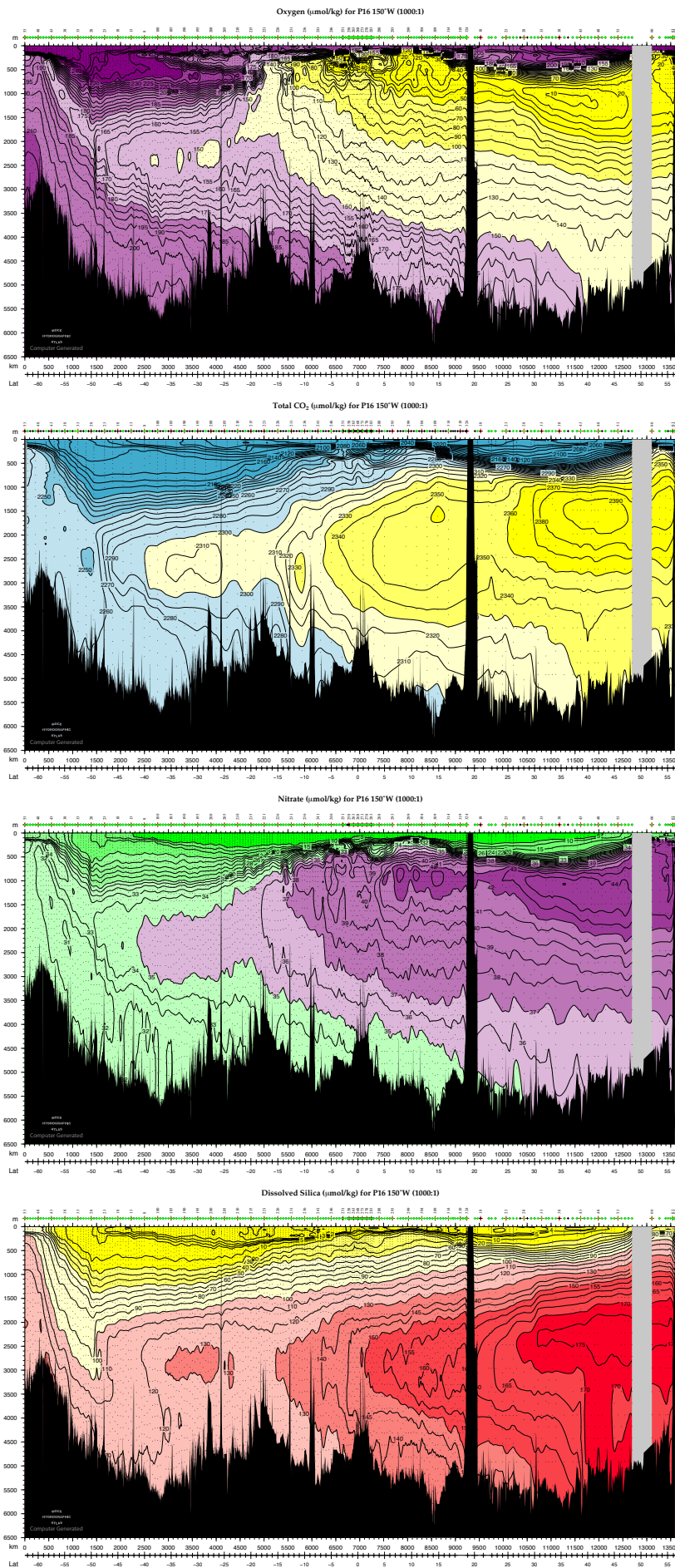


Figure 5.2: Bio-active tracers in the Pacific ocean along P16. From the WOCE Atlas of the Pacific.

5.1.2 *Radioactive and tracers from the crust*

The age of water can be relatively accurately determined by carbon data using the radioactive isotope ^{14}C . This carbon isotope is produced in the atmosphere when cosmic rays impact nitrogen molecules. As such, ^{14}C concentrations are highest in the surface ocean (figure 5.3). ^{14}C decays, but unlike bio-active tracers, it decays at a known steady rate, with a half-life of 5,730 years. Knowing this decay rate, and the relative abundance in the atmosphere, we can arrive at an average age for a water parcel, keeping in mind that there has necessarily been mixing with the water masses above. From this we can see that the oldest water in the Pacific is probably at about 2500 m depth in the North Pacific.

There are some caveats to looking at ^{14}C , the most obvious one is that the water signal can be contaminated by organic matter raining down from above. This organic matter will have younger ^{14}C in it, so the water will be deduced to be younger than it is. There is another bias that will make the water look younger, in that if young water is mixed with old water, the age is actually a logarithm of the concentration, and logarithms cannot be added linearly. This turns out to be a difficult problem, so that accurately estimating the age of the water requires complicated inverses of where the water has been and what water masses have mixed to produce it over its history.

Recent attempts to estimate water mass age using ^{14}C give estimates of water as old as 1500 y in the north Pacific, and at the north end of the Indian Ocean. Atlantic water tends to be younger, reaching about 700 years old, because it is heavily influenced by the shallower overturning of the North Atlantic Deep Water. These numbers speak to the sluggishness of the overturning circulation. In the Pacific, the bottom water is almost 1000 years old by the time it reaches the equator, or a speed of approximately 7.7 km-per-year in the horizontal, or $2.5 \times 10^{-7} \text{ m s}^{-1}$.

The isotope ^3He is an interesting tracer because it largely comes from ocean hydrothermal vents (figure 5.3c). The two large peaks in the middle of the section arise because the cruise passed close to the East Pacific Rise at these locations.

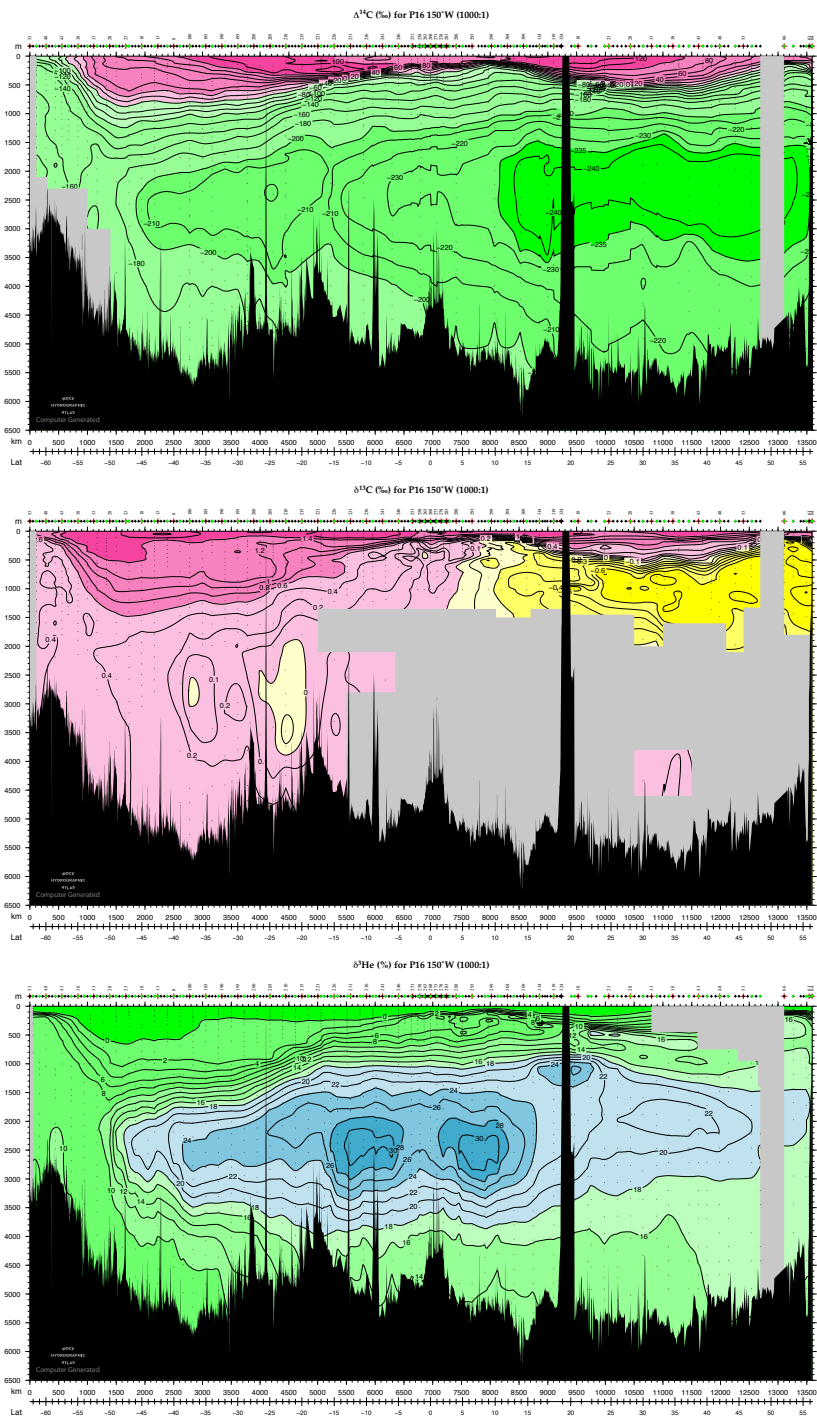


Figure 5.3: Radioactive and crust tracers in the Pacific ocean along P16. From the WOCE Atlas of the Pacific.

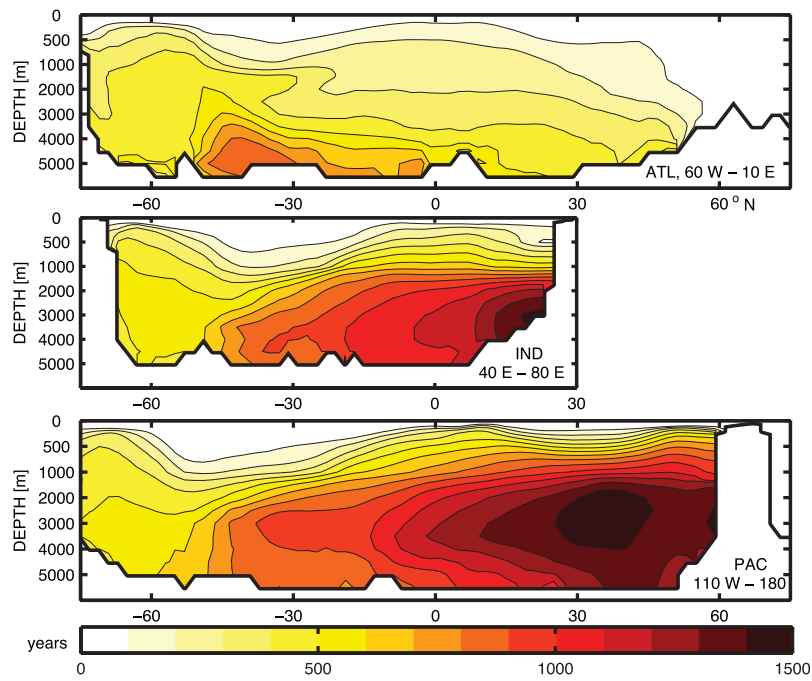


Figure 5.4: Average age of water in the three ocean basins as estimated from ^{14}C data [Gebbie and Huybers, 2012].

5.1.3 Man-made tracers

Anthropogenic tracers are also useful for tracking ocean processes. The only problem is that most of these are modern, and hence only track the upper ocean (figure 5.7). In fact these tracers give an idea of just how *slow* the circulation is. Tritium is largely a product of nuclear weapons testing, which was predominantly carried out in the atmosphere in the 1960s (figure 5.5). This makes for a nice tracer spike that shows how far water transited in the 35 years when the WOCE lines were run (figure 5.7). Similarly, CFC-11 and -12 saw an exponential increase in emissions until the 1970s when the danger of CFCs to the ozone layer was realized, and dropped off after the Montreal Protocol, when they were finally banned.

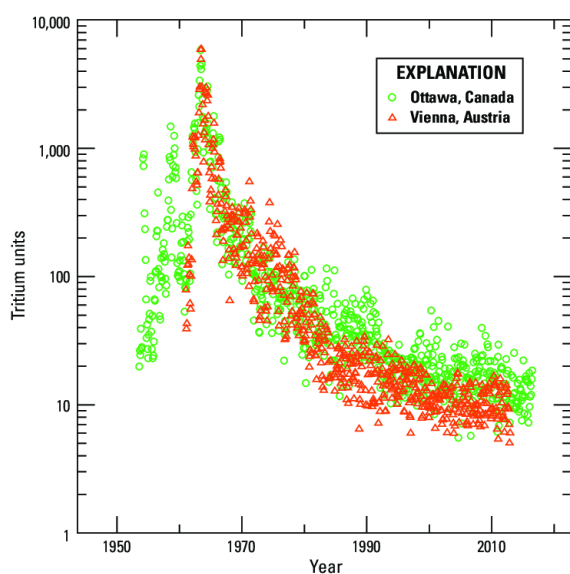


Figure 5.5: Tritium time series in the atmosphere measured at Ottawa and Vienna. Note the logarithmic vertical scale, so almost all the input was in the 1960s

All three man-made tracers had relatively minimal penetration into the deep ocean when the P16 lines were occupied, but *clearly* show up in the Southern Ocean as a plume of high concentrations. Of course the upper ocean has substantial quantities of these tracers.

The WOCE cruises along P16 spanned the years 1991-1993. These waters were resampled again as part of the CLIVAR/GO-SHIP program in 2014-2015 (figure 5.8) and the intervening 21-24 years do show some change. These changes are particularly pronounced in the intermediate waters with CFCs transiting substantially deeper and more equatorward. The CFCs also appear to have mixed from the surface ocean to deeper, with the CFC-gradient descending around 200 m in most of the basin. In the deep ocean, however, there is still little evidence of CFC penetration. Looking south of 60 S, there is

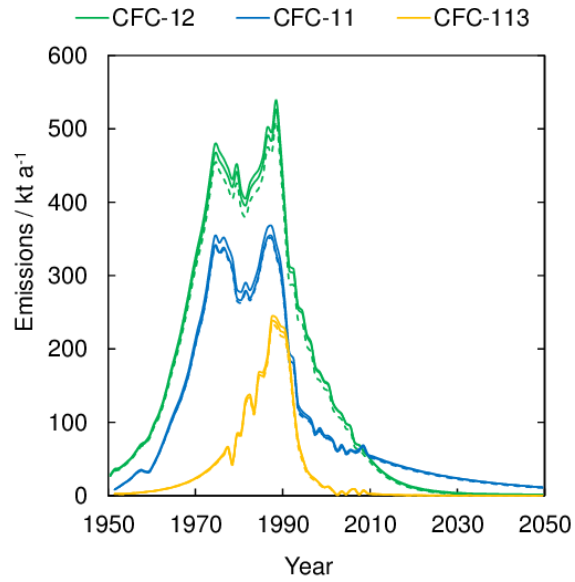


Figure 5.6: Global CFC emissions, estimated from atmospheric concentrations [Allin et al., 2015].

some evidence that high CFC waters are trying to push over the ridge, and there are perhaps some heightened values along the bottom south of 30 S, but if so, then these values are very diluted. Overall the manmade tracers show how old and slow the deep ocean bottom circulation is.

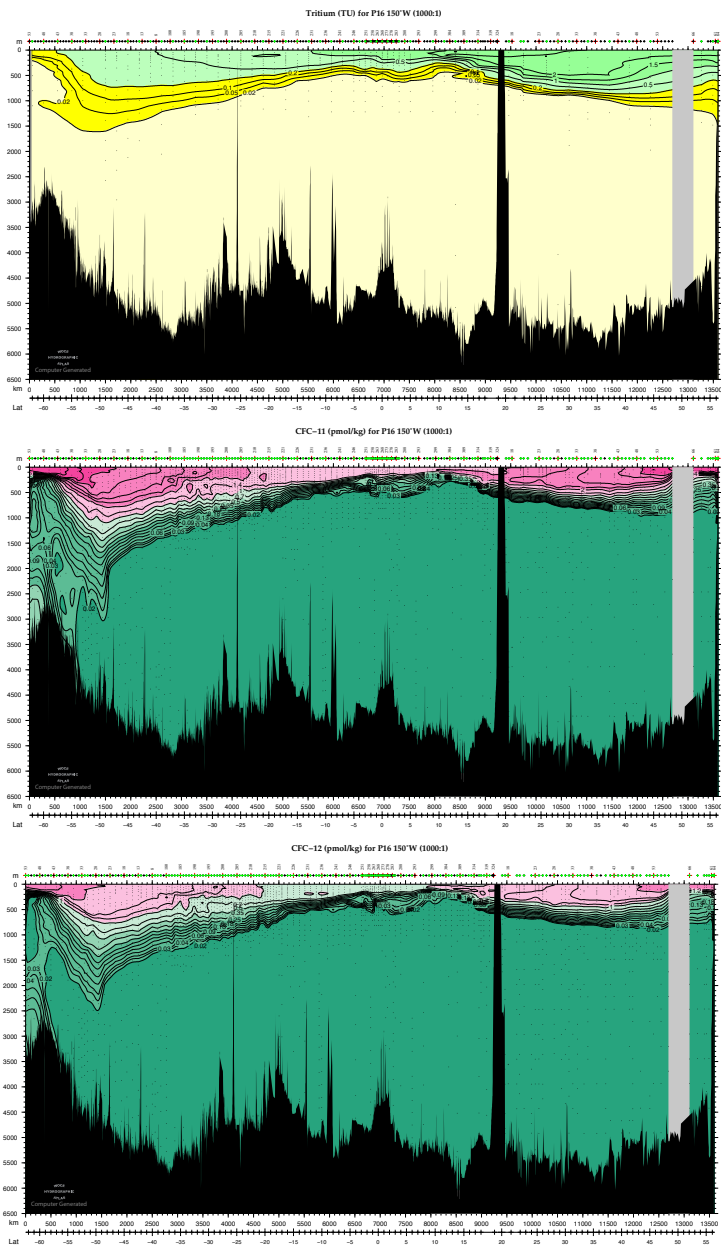


Figure 5.7: Man-made tracers along P16. From the *WOCE Atlas of the Pacific*. Note that this section was collected in 1991.

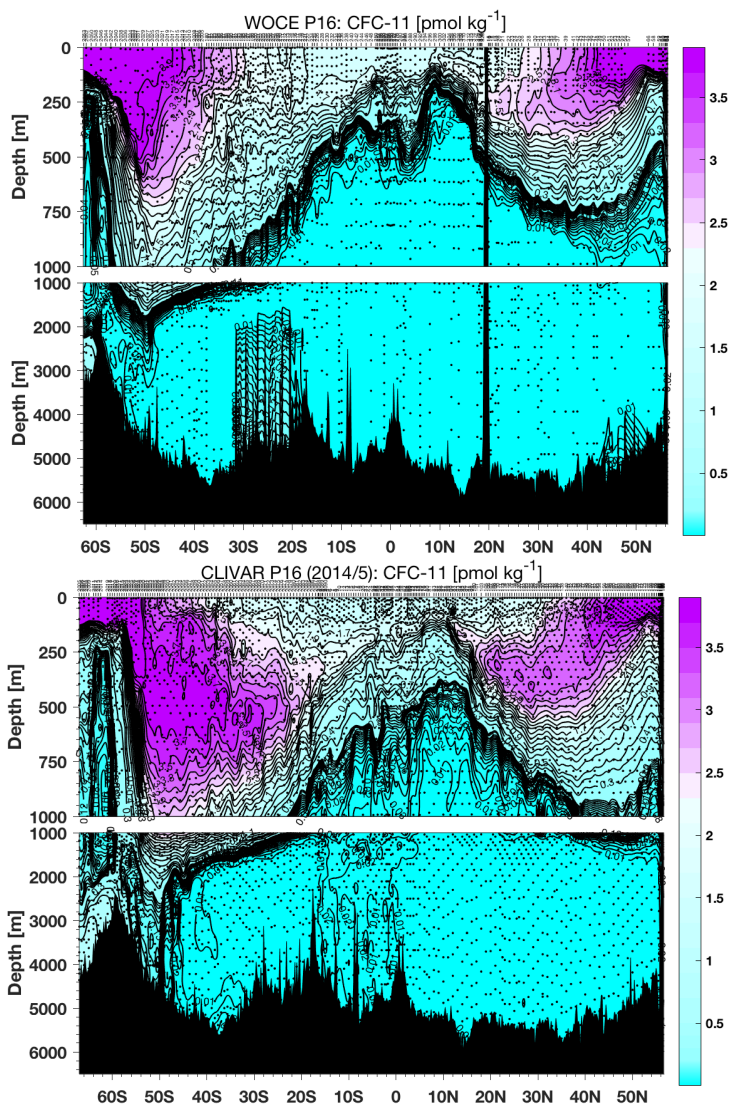


Figure 5.8: CFC-11 along P16, during WOCE (1991-93) and the GO-SHIP/CLIVAR re-occupation (2015-16). Note there are some poor-quality samples in the WOCE section deeper than 2000 m between 30S and 15 S. Figure courtesy S. Mecking.

5.2 Deep water formation processes

The densest water in the global ocean is formed at the high latitudes. The densest water is formed in the Wedell and Ross Seas in the southern ocean. Deep water formation processes are notoriously hard to observe, but the mechanisms are relatively well understood.

5.2.1 Antarctic Bottom Water

In the Antarctic, dry cold continental air blows off the continent figure 5.9. These winds can be quite strong and work to push sea ice off the landmass, often opening up *leads* and *polynyas*, despite the cold air. These polynyas are regions of very large heat loss, both latent and sensible. Further, they create more ice (which is then pushed offshore), and ice creation leads to brine rejection, which makes the water very salty.

Detailed observations in the Southern ocean make this process clear figure 5.10. In these observations, the cold water that comes from the shallower basins to the southeast are observed hugging continental slope. The very cold water at the bottom is colder than Antarctic Bottom Water, but mixes with the shallower as it descends the slope to make water that is between -1 and 0 C.

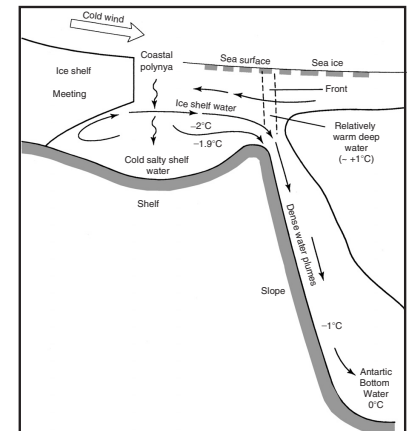


Figure 5.9: Schematic of deep water formation in the marginal seas of Antarctica [Gordon, 2001].

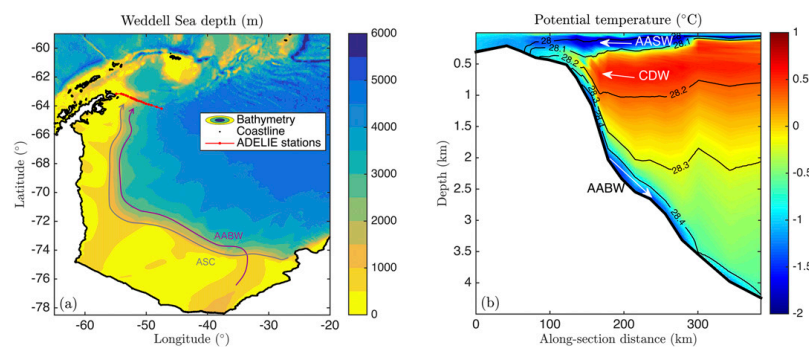


Figure 5.10: bathymetry of the Wedell Sea, and a section of density contours with temperature coloured underneath. Note the cold dense water sinking along the continental slope. [Stewart and Thompson, 2016].

5.2.2 North Atlantic Deep Water

North Atlantic Deep Water starts in a similar way to Antarctic Bottom Water, with an origin on the Barents Sea shelf. Conversely to the Antarctic, this water forms largely free from ice cover, and hence brine rejection is not too important a part of the process. This cold water flows into the Greenland Sea where it mixes with cold water experiencing convection (figure 5.11). This water pours over the Denmark Straits just east of Greenland, and is further diluted with warm

salty water from the North Atlantic. This current is added to from convection in the Labrador Sea.

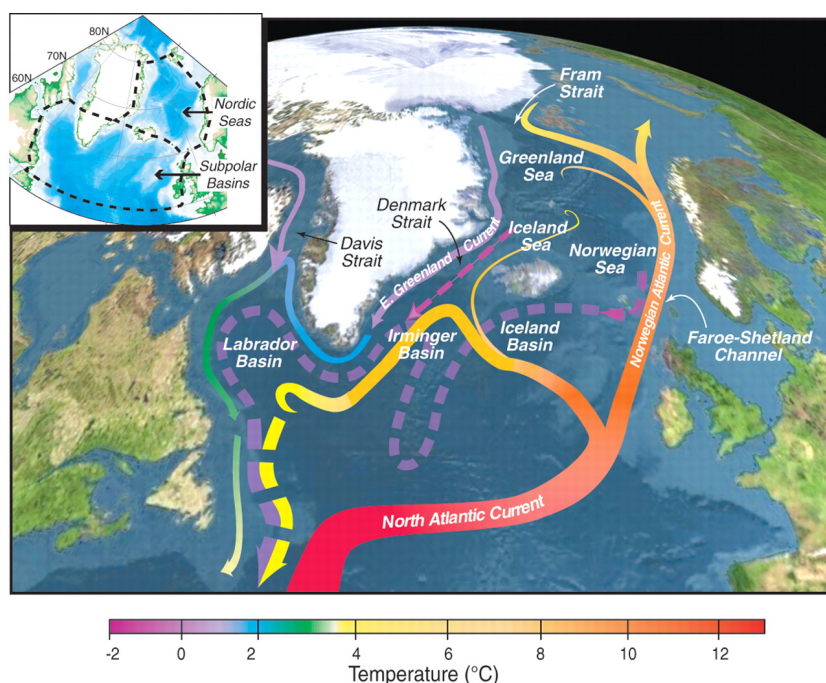


Figure 5.11: Sketch of paths taken by North Atlantic Deep Water. [Curry and Mauritzen, 2005]

Deep-water convection is very easy to observe in the Labrador Sea, between Labrador and Greenland. In the winter, convective mixing can create a mixed layer that is over 2000 m deep figure 5.12. This is caused by cooling, and mixing of relatively fresh water near the surface with warmer saltier water that comes in from the side. This process varies each year, and sometimes the convection is not as deep in one year as in other years (figure 5.13). In some years there is no convection at all, like 2007, whereas in others there is very deep convection, like in 2008.

This water flows South, hugging the western boundary of the Atlantic ocean in a narrow order 100-km wide flow, that mixes as it goes (figure 5.14). The boundary current is remarkably persistent, being traced as far south as Florida (figure 5.15), where bathymetry roughens and disperses the flow. The flow hugs this side of the basin due to the Coriolis force, and doesn't fall down the slope for the same reason. Bottom friction does cause it to move downslope slowly, but despite 1600 km of distance between the two sections, its clear that the current hasn't descended very much.

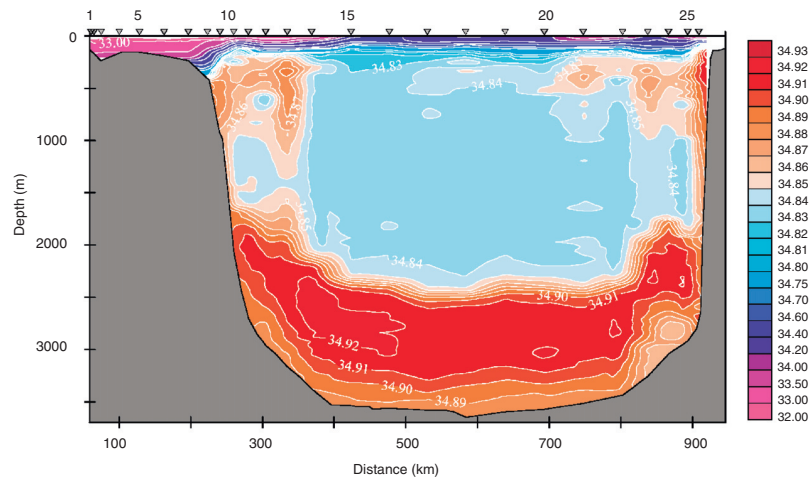


Figure 5.12: Evidence of convection in the Labrador Sea from a section across the Sea in June 1993. Note the very homogeneous water in the central Labrador Sea, with mixing deeper than 2000 m.

5.3 *Inferring the strength of the overturning circulation from data*

The strength of the overturning circulation is almost impossible to infer directly from measuring ocean velocities, and hence it is inferred from “inversions” of data collected on hydrographic cruises such as the WOCE and CLIVAR cruises mentioned above. We haven’t discussed geostrophic transport yet, but it will be discussed in future chapters. However, knowing the density distribution along a section will give us an estimate *within a constant* of the transport of water *across* that section (figure 5.16). This somewhat un-intuitive result is because the Coriolis force acting on the moving water balances the pressure gradients.

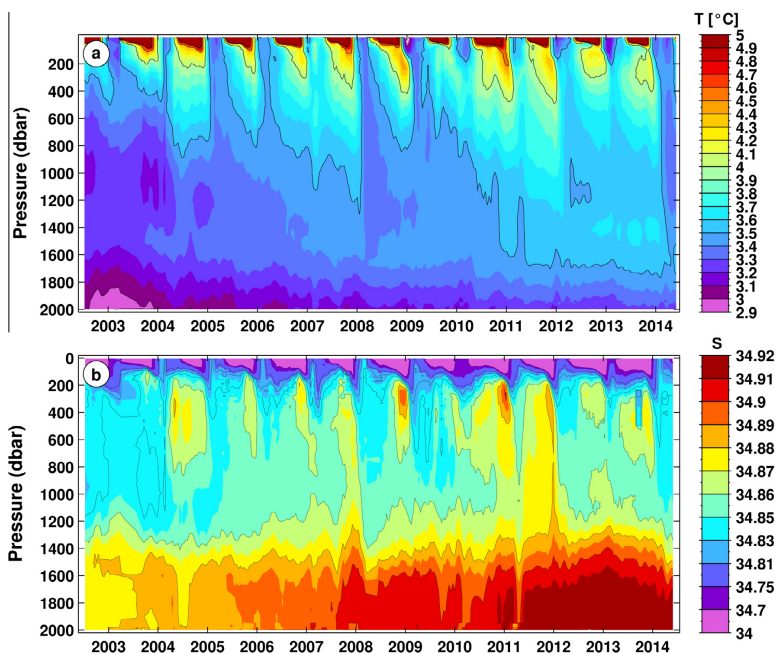


Figure 5.13: Time series of convection in the Labrador Sea as measured by autonomous Argo profiling floats [Kieke and Yashayaev, 2015]

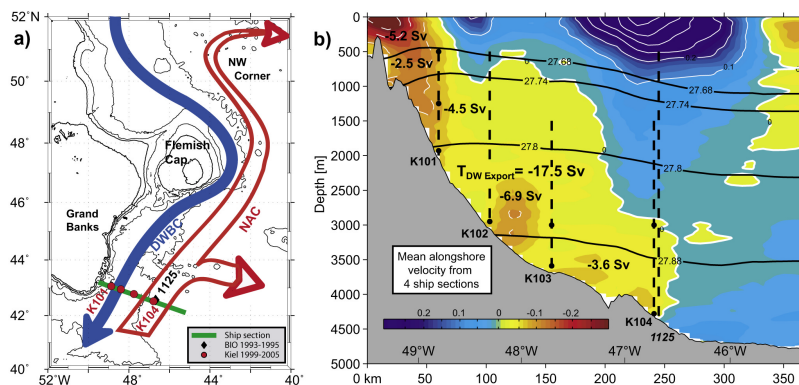


Figure 5.14: Observations of Deep Western Boundary Current off the Grand Banks.[Schott et al., 2006]

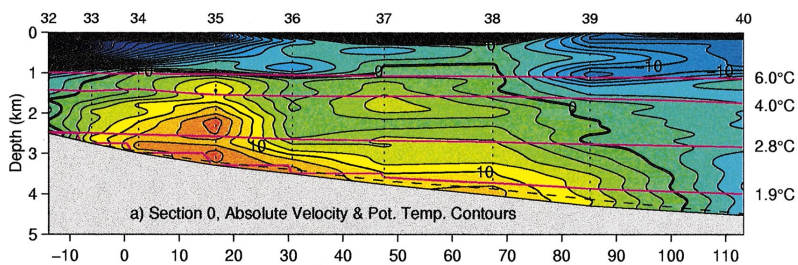


Figure 5.15: Observations of the Deep Western Boundary Current off Blake Outer Ridge (32 N) [Stahr and Sanford, 1999]

There are unknowns in making these estimates, which can be constrained for by making mass, heat, salt, and other tracers balance in the basins. We will discuss these results and how they are obtained briefly below.

5.3.1 Inverse results

The large amounts of data collected during the WOCE and CLIVAR cruises have undergone substantial analysis to determine the strength of the overturning circulation. The final result is what is described above, but quantified. Globally, there are two overturning cells, one that sinks in the southern ocean, and the other that sinks in the North Atlantic (figure 5.17). The Southern overturning cell is denser and flows under the North Atlantic cell on average. (The way these flows are contoured in figure 5.17 may be unfamiliar to some readers, so please see Box 5.3.1).

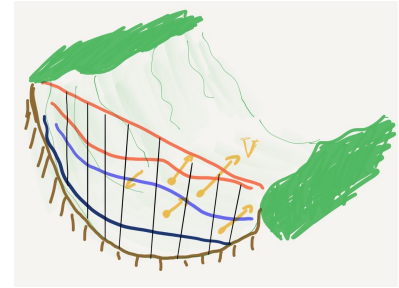
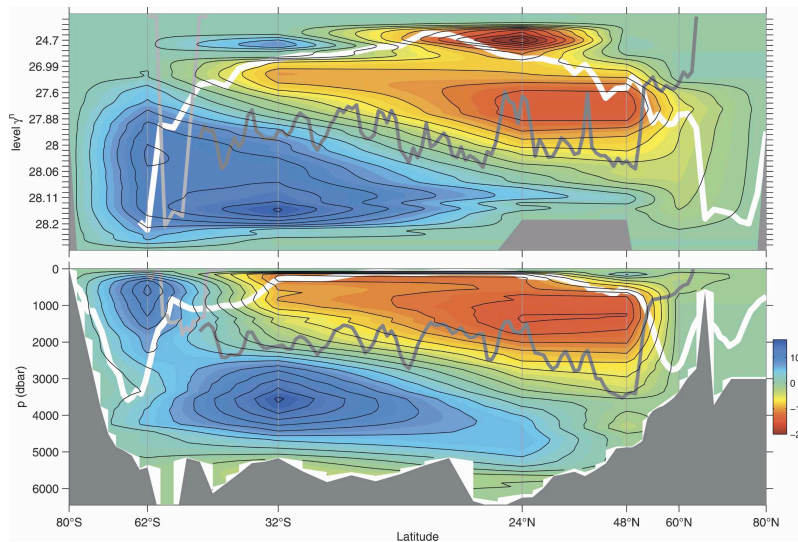
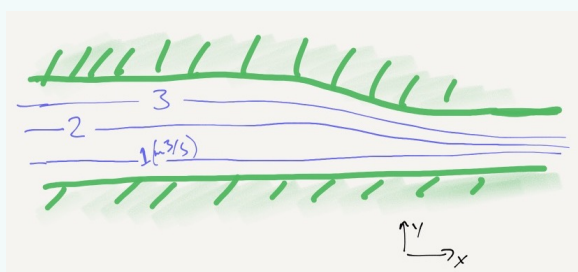


Figure 5.16: Sketch of cross section in a basin. A hydrographic cruise that has crossed the basin making measurements will give estimates of the pressure gradients along the section, which can be used to estimate the velocity across the section.

Figure 5.17: Estimate of the strength of the global overturning circulation plotted as a stream function. The upper plot is the streamfunction plotted with the density of the water as the vertical axes, whereas the lower plot is the depth of the ocean [Lumpkin and Speer, 2007]. The stream functions are plotted in units of Sv , where $1 Sv = 10^6 \text{ m}^3 \text{ s}^{-1}$

Box 5.3.1: Quantifying flows with streamlines

A “streamline” is a path followed by a parcel in a *steady* flow. These paths are plotted in 2-dimensions in figure 5.17 and represent the average path of the flow averaged around the world. This tells us qualitatively where the flow goes. Streamlines also receive a quantity proportional to the total water transported from the point of the streamline relative to some zero. So in the sketch below, showing an idealized river, the zero is the southward bank of the river. The $1 \text{ m}^3 \text{ s}^{-1}$ streamline denotes how far across the river you would need to go to get that much downstream (or along streamline) transport.



If the streamlines are drawn so that they have equal transport between them, then the spacing between streamlines is inversely proportional to the speed. So in the above plot the streamlines get closer together as the river narrows the speed necessarily increases.

Closed streamlines, as we see above (figure 5.17) indicate that the flow is circulating around a circuit. The more streamlines the stronger the recirculation.

The streamlines look different in the two plots of figure 5.17 because of the different averaging. However, the absolute values are the same - $20.9 \pm 6.7 \text{ Sv}$ for the Antarctic Bottom Water cell and $17.2 \pm 3.2 \text{ Sv}$ for the North Atlantic Deep Water cell (the unit Sv is called a *Sverdrup* after Harald Sverdrup and $1 \text{ Sv} = 10^6 \text{ m}^3 \text{ s}^{-1}$).

An important reason to plot figure 5.17 with density on the y-axis is to note where mixing is believed to happen. If water is going down in this reference frame, then it is getting denser, and that must be happening largely due to cooling or mixing with cold water. If water is going up along this axis it is being warmed by mixing with warm water above.

There is a stark difference in the overturning circulation between the Atlantic ocean and the Pacific and Indian due to Atlantic Deep

Water formation (figure 5.18). We see that the deep water in the Atlantic mostly moves south and that there is very little AABW recirculating in that basin. Conversely, in the Pacific the deep circulation is dominated by the AABW recirculating cell to quite low densities.

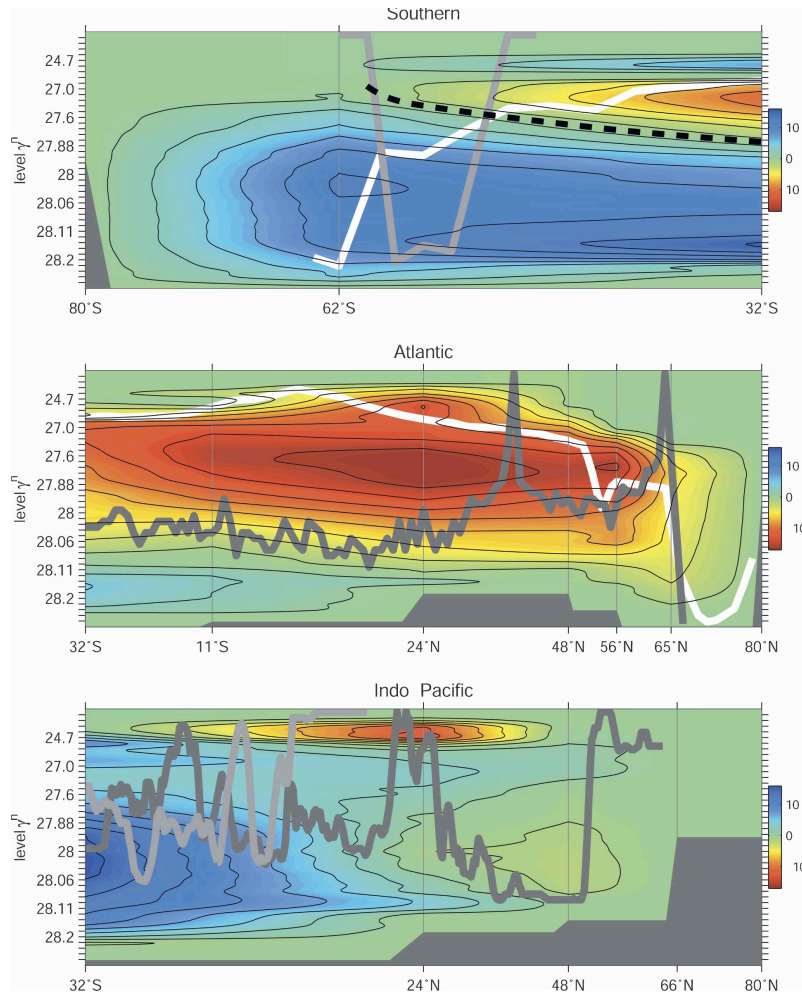


Figure 5.18: As in figure 5.17, but divided by ocean basin

The strength of the overturning, divided by basin, is shown in figure 5.19. The Pacific and Indian each support approximately 10 Sv of upwelling of AABW, while only 5 Sv is upwelled in the Atlantic. However, 17 Sv of NADW is also upwelled in the Atlantic, albeit from a less dense water mass. There are numerous complicated connections of the water in the upper ocean that must be tracked in order to balance the flux of water, including a very strong exchange between the Indian and Pacific oceans through Indonesia and near Australia.

Similar calculations can be presented in different ways. figure 5.20

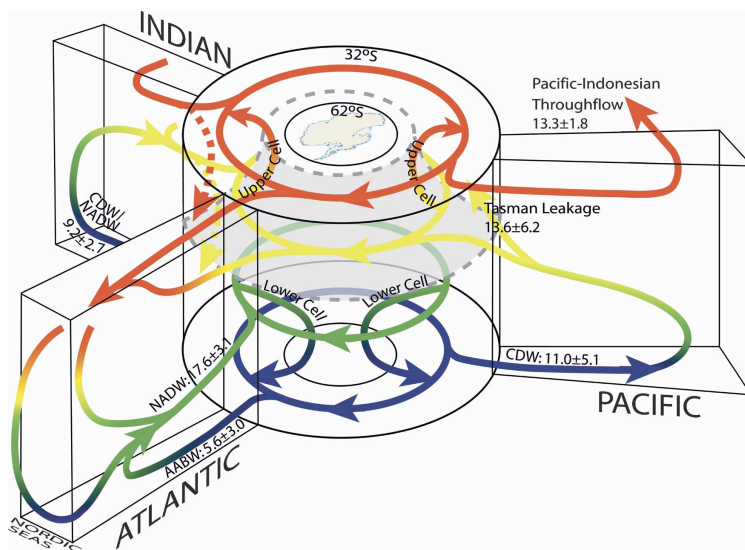


Figure 5.19: Strength of overturning circulation in various basins in Sv. Blue is the AABW, green is "deep water", yellow are "intermediate" waters, and orange surface water. [Lumpkin and Speer, 2007]

shows the transport of various water masses through the world's oceans. Sinking in the Southern ocean and Greenland-Iceland-Norway (GIN) seas then upwells in the various basins as shown by the green or blue arrows. Note that 15 Sv that is produced in the GIN seas eventually is transported to the Southern ocean where it either downwells again as AABW or upwells into the surface layer via mixing.

5.3.2 How to make an inverse calculation

The inverse calculations that go into creating the estimates above are simple in concept, but complicated in execution. The simplicity comes from just assuming a simple mass balances as we did in previous chapters, and assuming that the ocean is broadly in steady state.

A very simple example of such an inverse calculation comes from the flow of Antarctic Bottom Water into the Brazil Basin figure 5.21. Water colder than 1 deg C enters in the Vema Channel from the south, but is not observed to make it out of the Brazil Basin. This can be seen in figure 5.22, where water 1.2-degrees and colder is blocked at the north end of the basin.

Channels like the Vema Channel are nice, because the flow can be monitored with moorings, which was done in the late 70s [Hogg et al., 1982] and again late 90s [Morris et al., 2001]. These moorings found, on average, 3.7 Sv of water flowed in the channel that was

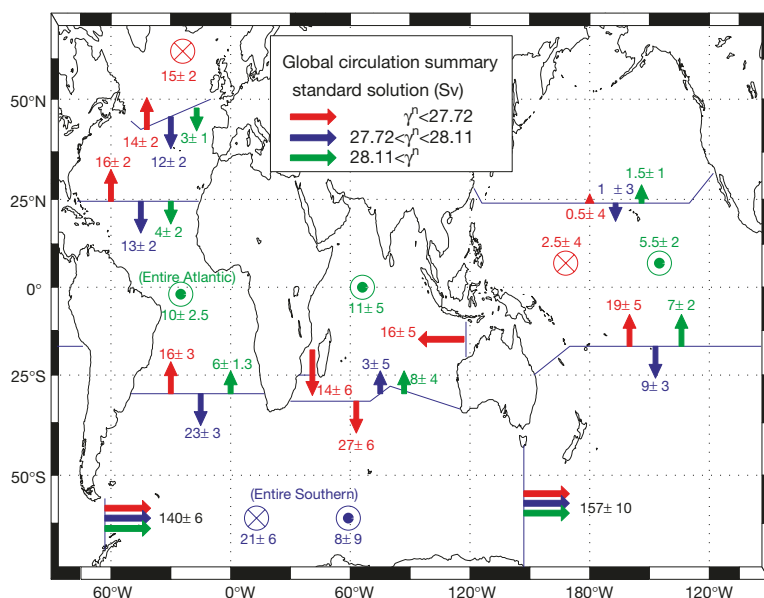


Figure 5.20: Arrows show lateral transport (in Sv) of upper- (red), mid- (blue), and deep (green) waters through WOCE hydrographic sections. X-symbols show flow downwards out of a layer into the next layer below. Dot-circle symbols show flow up out of a layer into the layer above. So the upwelling associated with AABW is shown with green dot-circle signals in the three oceans. [Ganachaud and Wunsch, 2000]

colder than 1.2 degrees [Morris et al., 2001]. This water, on average, is 0.2 degrees-C.

We can apply a volume budget and a heat budget to the problem, by considering a volume bounded by the Vema channel at the south, the north end of the Brazil Basin, and the 1.2 degree isotherm at the top. The volume budget is straight forward - if 3.7 Sv enters in Vema Channel and there is no outlet to the north, it must cross the 1.2 degree isotherm. $Q_{in} = Q_{out}$.

The heat budget is almost the same, but we need to include the heating due to diffusion at the top of our volume:

$$h_{in} + h_{diffusion} = h_{out} \quad (5.1)$$

where $h_{in} \approx 3.7\text{Sv} \cdot 0.0\text{C} = 0\text{Sv C}$, and $h_{out} \approx 3.7\text{Sv} \cdot 1.2\text{C} = 4.4\text{Sv C}$. This means that the residual has to come into the volume via diffusion:

$$h_{diffusion} = K \frac{d\theta}{dz} A \quad (5.2)$$

where $\frac{d\theta}{dz}$ is the average vertical temperature gradient at the top of the volume, and $A \approx 7 \times 10^{12}\text{m}^2$ is the area of the 1.2 degree isotherm in the basin. There were lots of hydrographic cruises made in the Brazil basin, such that the gradient was found to be $\frac{d\theta}{dz} \approx 2.1 \times 10^{-3}\text{C m}^{-1}$. This leaves us with only one unknown, K , the turbulent diffusivity necessary to mix the temperature gradient fast enough to counter the

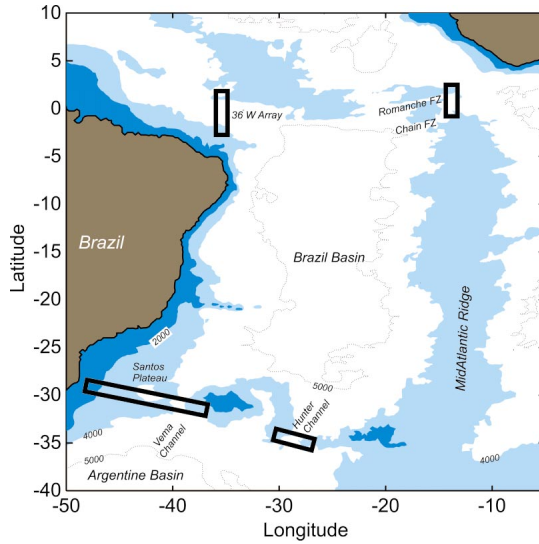


Figure 5.21: Map of the Brazil Basin
[Morris et al., 2001]

cold water coming into the basin from the south. And carrying out the math, we get a final answer of $K \approx 3 \times 10^{-4} \text{ m}^2 \text{ s}^{-1}$. Morris et al. [2001] divide the water in the basin into more layers and determine that the turbulent diffusivity is between 2 and $3 \times 10^{-4} \text{ m}^2 \text{ s}^{-1}$. Note that this is over 1000 times the molecular diffusivity of heat, so turbulence must be responsible for this inferred mixing.

The amount of turbulence required to maintain such a high turbulent diffusivity is moderately strong. Field work was carried out there to measure the turbulence directly using instruments called *shear probes*, which are 1-cm scale phonograph needles encased in a silicone tip. The results show that there is indeed substantial mixing in the Brazil Basin, but that it is not at all homogeneous, with the strongest mixing occurring on the east side where there is substantial roughness (figure 5.23). Indirect evidence is that this heightened mixing is due to tides moving back and forth over the rough bathymetry and creating turbulence with the stratified water above. Note that in most of the basin, even above the rough topography, the turbulence is substantially *lower* than the mean inferred from the inverse calculation. However, the mean is dominated by the few red and orange pixels in the data, and there are enough of those that the average comes out to $0.5 - 1.5 \times 10^{-4} \text{ m}^2 \text{ s}^{-1}$ [Polzin et al., 1997]. This is within a factor of two of the inverse estimate, and probably within error bounds of both. It is also likely that the Brazil Basin is under-sampled by the turbulence measurements and there is some mixing “hot spots” that the sampling missed.

Extending the inverse estimate made in the Brazil Basin to the global oceans is exactly what was done in section 5.3.1. Volumes

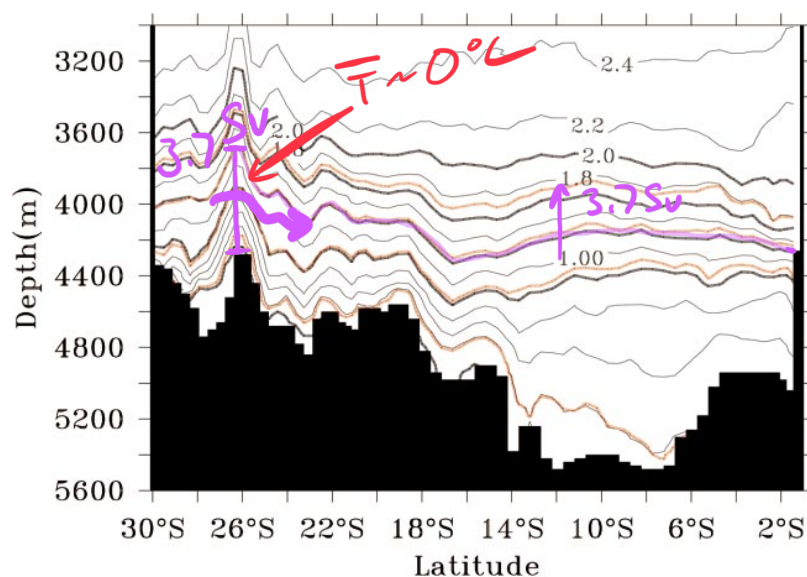


Figure 5.22: Hydrography along the Brazil Basin. Note that water colder than 1.2 degrees C does not make it out the north end. [Morris et al., 2001]

of the ocean were constrained by the cross-basin cruises. However, in addition to an unknown diffusivity in the ocean, there were unknown offsets in the velocity measurements (because we do not have current meters everywhere in the ocean), and sampling errors due to temporal variability. So, what is done for global estimates is to use substantially more data from other tracers. These tracers have their own uncertainties; for instance silicate is used, but the accumulation of silicate in the deep ocean is an unknown. C_{14} is used, but will be biased by particles raining down from the surface ocean. These data and unknowns are all put into a large matrix, and then the best solutions for the unknowns are inverted for by minimizing error in all the individual constraints. This was the procedure pioneered by Wunsch [1996], and followed by Lumpkin and Speer [2007] in the results above.

5.4 Theory of overturning circulation and Sandstrom's theorem

From the above, we might have the idea that the overturning circulation is driven by how much cold water you make. That's true to an extent - the heating gradient between the poles and the equator is one part of what drives the overturning circulation, and plus or minus any net heating or cooling, the heat transport in the ocean must balance the heating differential (figure 5.24).

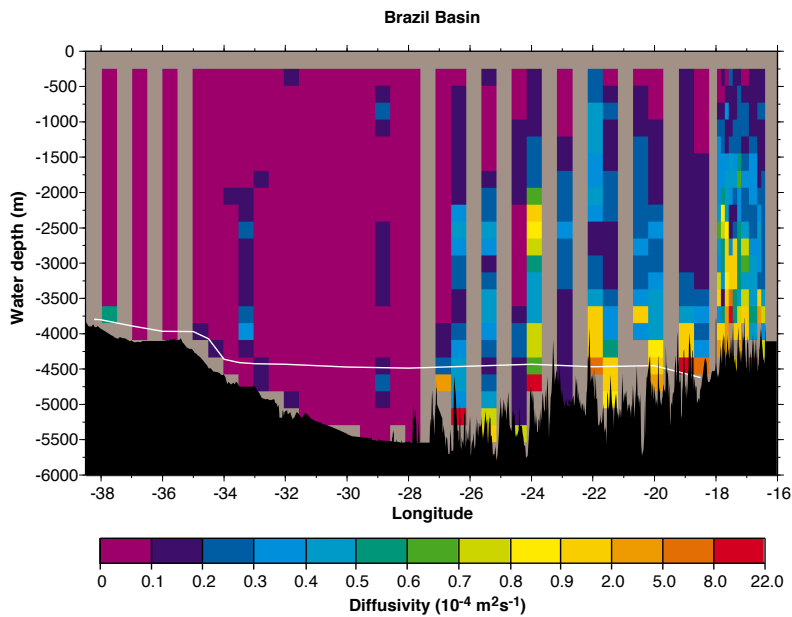


Figure 5.23: Turbulence diffusivity inferred from directly measuring turbulence. The cross section is made west-to-east across the Brazil Basin, and the 0.8-degC isotherm is shown in white. [Polzin et al., 1997]

However, just like a river pouring into an estuary, it's possible for that heat flux to be carried in a very shallow current and drive a very weak volume transport that only affects the very surface ocean. In such a world, all the deep ocean would be very cold, and a thin layer at the surface would be very warm (figure 5.25).

So for a given heat difference at the surface, what ultimately drives the strength of the overturning circulation is how strong mixing is in the ocean. By mixing the heat down, the ocean creates lateral density gradients, and lateral gradients create lateral pressure gradients that ultimately drive circulation (figure 5.25).

The other way to think of this is to think of the *potential energy* of the system. Recall from previous chapters that the isopycnals surfaces in figure 5.25 want to flatten out. This means that tilted isopycnals have potential energy that they would not have if the isopycnals were all flat. This idea of potential energy and the need to mix buoyancy to depth in the ocean is nicely encapsulated by *Sandstrom's theorem* which states that heating and cooling at the same depth will not drive a vigorous circulation in fluid. Essentially surface heating and cooling does not increase the potential energy of the system, and hence there is no strong circulation driven.

Conversely mixing of heat down from the equatorial regions *does* increase the potential energy. However, it is important energetically

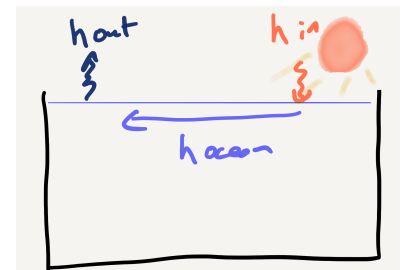


Figure 5.24: Sketch of heat input into a one-pole ocean. The heat flux in must be balanced by the heat flux out, and the ocean must transport that heat from the equator to the poles.

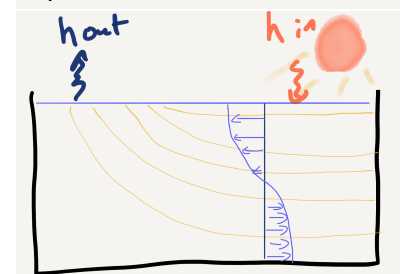


Figure 5.25: Sketch of two different oceans with the same external heat differential. The top panel shows weak mixing, and the bottom panel shows strong mixing. The heat transports from equator to pole are the same, but the

to realize that this mixing cannot arise because of the overturning circulation itself. i.e. the 20-30 Sv of overturning noted above cannot create the turbulence that drives the overturning. This would be the equivalent of the ocean lifting itself by its own bootstraps. Instead the energy for the overturning circulation must come from other sources of deep ocean mixing. This again is directly analogous with the situation in an estuary - the estuarine circulation is catalyzed by mixing in the estuary.

This dependence of the overturning circulation on the strength of the turbulence has been tested numerically. Stronger mixing transports heat deeper in the ocean (figure 5.26) making for stronger lateral gradients. This drives a more vigorous overturning circulation (figure ??). The scaling of the overturning circulation with the vertical diffusivity K is approximately $K^{1/3}$ (figure 5.27). These integrations were carried out many years ago, but the basic results have held up well to more sophisticated treatments.

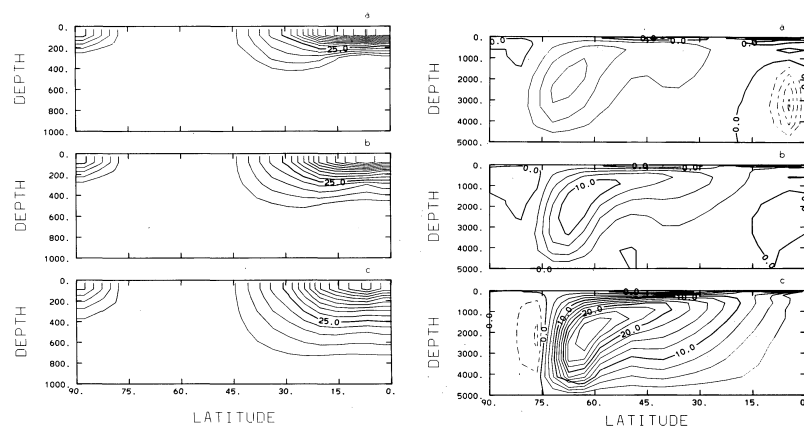


Figure 5.26: Left panels: Potential temperature cross section in a numerical ocean with different vertical diffusivities: $0.1, 0.5$ and $2.5 \times 10^{-4} \text{ m}^2 \text{ s}^{-1}$. Right panels: Overturning streamfunctions. [Bryan, 1987]

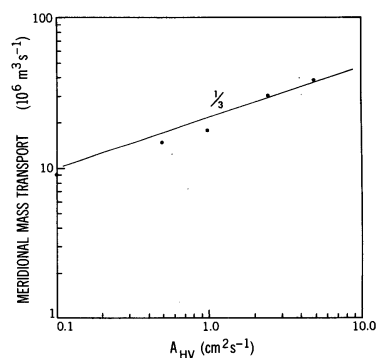


Figure 5.27: Dependence of the overturning circulation strength on the vertical diffusivity used in the idealized model [Bryan, 1987].

The tides and wind are believed to be the energy source for the

mixing that drives the overturning circulation. Because the fluid is stratified, energy is able to radiate into the interior from the boundaries as **internal waves**. There are many sources and pathways of internal waves, and their importance to the overturning circulation has catalyzed a significant research into their properties (figure 5.28).

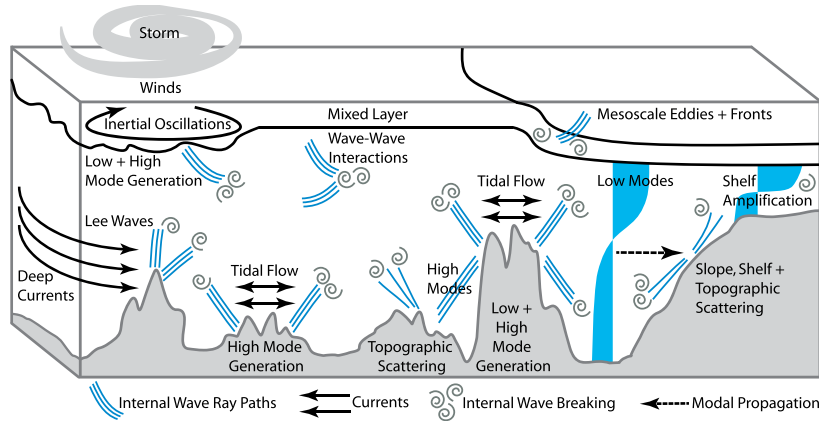


Figure 5.28: Schematic of the zoo of ocean mixing processes [MacKinnon et al., 2017].

5.5 Exercises

Inverse modelling Suppose we have a rectangular basin that runs north-south, is 3000 km long and is 1000 km wide at each end. There is an isopycnal in this basin that intersects each of the ends (and of course the side walls). We use the open ends, the sidewalls, to constrain the sides of a volume of water, and the sea floor and the isopycnal to constrain the bottom and top of the volume.

The average temperature along the bounding isopycnal is 7 degrees C, and $dT/dz = -10^{-3}$ deg/m at that isopycnal.

At the south end section: the thickness of the layer defined by the isopycnal is 2500 m, the average temperature in the section beneath the isopycnal is $T=3.2$ deg C, the average salinity, $S=33$ psu, and the average speed through the section is $V=0.02$ m/s (positive to the north)

North end section, the isopycnal layer is thinner at 2200 m, with an average temperature of $T= 3.3$ deg C, and average salinity of $S = 33.01$ psu. The average velocity is $V=0.0226$ m/s, to the north.

- What is the average velocity out the top of the bounding box?
- What is the average turbulent diffusivity of temperature along the isopycnal?

- What is the salinity of the top of the surface, assuming $dS/dz = 0$ there (i.e. no diffusive flux in or out the top).

6

Climate Change; The Effect on the Overturning Circulation and Sea Level



There are numerous effects of climate change on the ocean, but perhaps two of the most fundamental are the effect of (all) melting ice on the thermohaline circulation, and the effect of melting land-fast ice and ocean warming on sea-level.

6.1 Effect of melting on the overturning circulation

North Atlantic Deep Water (NADW) is produced because it is salty and cold. As discussed in chapter 5, NADW sinks near Greenland and Iceland, and descends along the Western Boundary Current to depths of approximately 2500 m. Warm water from equatorward moves in to replace the sinking water. The overturning circulation in the North Atlantic is about 15-20 Sv and carries 1-1.5 PW of heat northwards [Bryden et al., 2020].

If there is a change of the freshwater cycle or sudden introduction of fresh water in the northern hemisphere, say due to melting Arctic ice, or the Greenland ice sheet, then the overturning circulation can be suppressed, or stopped altogether (figure 6.2a, figure 6.1b). This stops the transport of heat northwards due to the overturning circu-

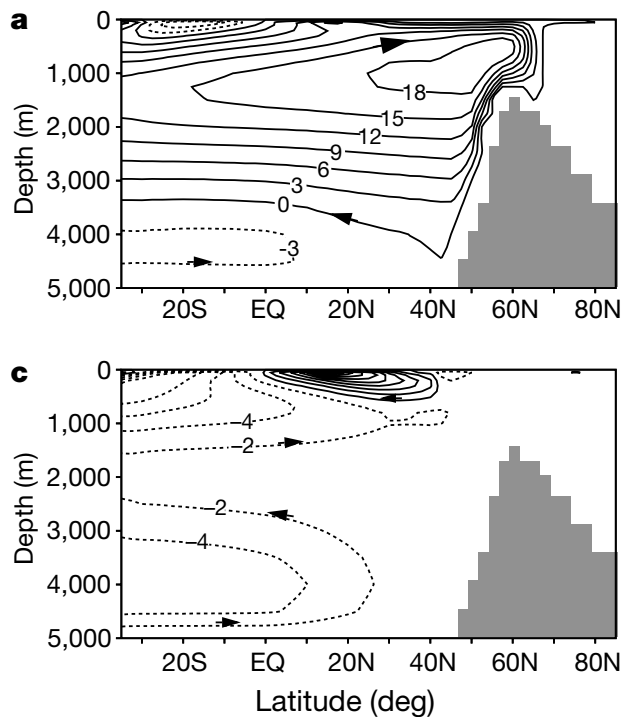


Figure 6.1: Overturning stream functions in the North Atlantic for a) the modern simulation (figure 6.2, 20 Sv overturning, 0 Sv fresh water flux anomaly, and c) when the overturning circulation has been turned off due to fresh water fluxes in the Northern hemisphere Ganopolski and Rahmstorf [2001].

lation, and has a dramatic effect on the temperature of the northern hemisphere, causing a cooling over the Atlantic in the simulation of up to 6 °C (figure 6.2c).

The role of the AMOC in warming the North Atlantic is relatively clear, but its role in sequestering anthropogenic CO₂ is less-well understood. However, it can readily be imagined that shutting off one of the sinking regions for surface water may indeed cause a decrease in the rate of ocean uptake of CO₂, leading to a deleterious feedback of warming the ocean further.

This remarkable re-arrangement of the circulation cannot persist without a large-scale change of the hydrological cycle, but it can introduce changes on decadal-to-century time scales. There is substantial evidence of rapid freshening of the North Atlantic during glacial times, in what are called **Heinrich Events**. These were originally discovered as open-ocean deposits of terrigenous rocks by large icebergs that broke off continental glaciers. While the chronology is not perfect, these events were also correlated with cooling, as inferred in Greenland ice cores. These coolings are known as **Dansgaard-Oeschger events**, and are largely confined to the northern hemisphere (figure 6.3). These oscillations represent about 8 degrees of cooling over a short period, and are strong evidence for a reduc-

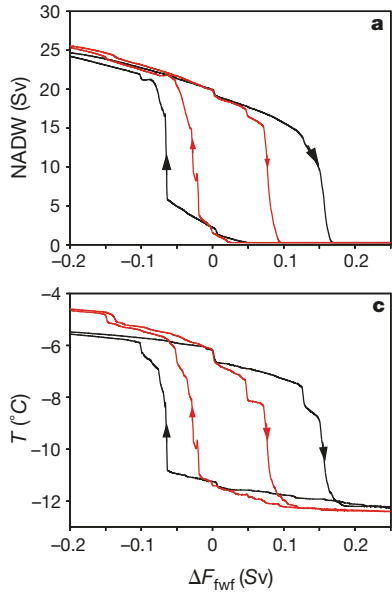


Figure 6.2: Effect of increasing fresh-water flux on a) the North Atlantic overturning circulation, and b) North Atlantic air temperatures 60-70 N [Ganopolski and Rahmstorf [2001]. Red curves are fresh water introduced north of 50 N, black are south of 50 N. Note that restoring the freshwater flux to modern values does not allow the overturning circulation to immediately restart.

tion of the transport of warm water to the North Atlantic.

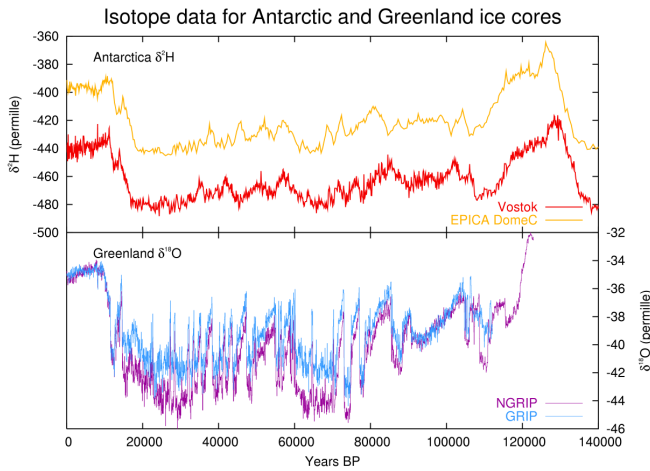


Figure 6.3: Ice core records of δO^{18} , a proxy for atmospheric temperature, with high values representing warmer atmosphere. (Leland McInnes at English Wikipedia <https://commons.wikimedia.org/wiki/File:Ice-core-isotope.png>)

Given the importance of the AMOC for our climate, there have been modern attempts to constrain its magnitude. These attempts actually contain a bit of a cautionary tale; considering 5 cruises from 1957 to 2004, [Bryden et al., 2005] inferred a substantial slowdown of the transport across 24.5 N, from 23 to 15 Sv in the upper 1000 m (figure 6.4), and an accompanying slowdown of heat transport of approximately 1 PW.

Such a slow down was considered quite alarming and spurred better observations. Since 2004, the same line at 25 N was occupied,

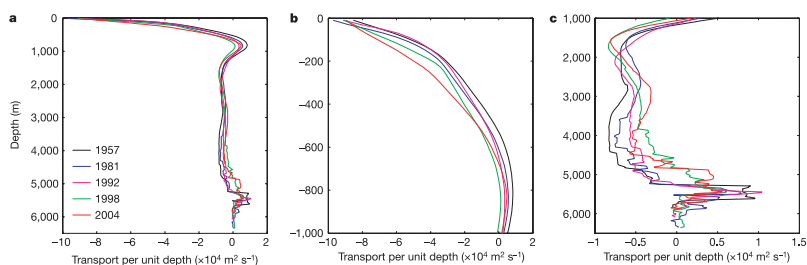


Figure 6.4: Transport as a function of depth across 24.5 N (approximately) [Bryden et al., 2005].

and supplemented by a mooring array to constrain the transport better. At the same time, estimates have been made at 35 S, 16 N, and approximately 55 N (figure 6.5). These demonstrate remarkable inter-annual variability, such that the result in [Bryden et al., 2005] is likely a sampling error due to infrequent ship-based sampling. It is of note, however, that these four timeseries are not very well correlated, indicating substantial error and/or natural variability. There has been some argument that there has been slowdown in the RAPID array data, but much more subtle than that previously argued. Conversely, the array at 16N indicates an increase in the overturning circulation. Continuing to monitor this overturning circulation is a large enterprise in global oceanography at present, with most Atlantic nations (including Canada) contributing.

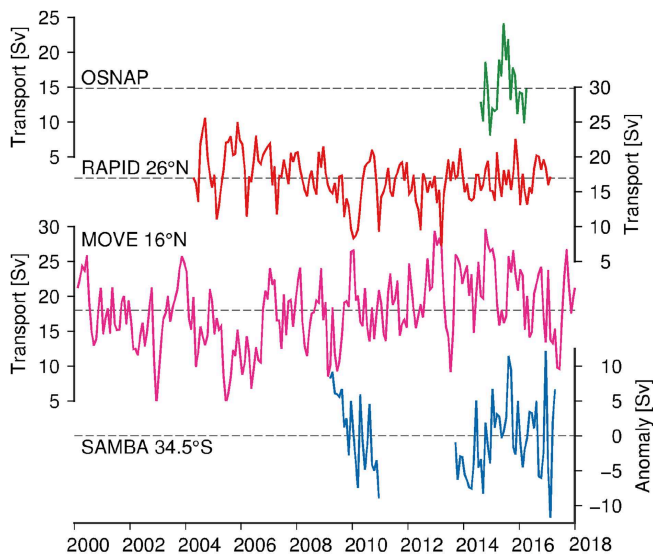


Figure 6.5: Northwards AMOC transport timeseries at 4 latitudes in the Pacific (OSNAP is approximately 55 N). Data gaps are due to arrays not being in place at those times.

6.2 Sea level change

A major physical effect on the ocean due to climate change is an increase in sea level, or ocean volume. This happens due to melting of land-fast ice (“Eustatic change”) and due to heating of the ocean water mass (“Steric change”). Since 1900, sealevel is believed to have increased by 20 cm. Over the last 20 years, melting has been estimated to be responsible for approximately 6 cm of sea level rise, whereas heating has been responsible for 3 cm.

GLOBAL SEA LEVEL

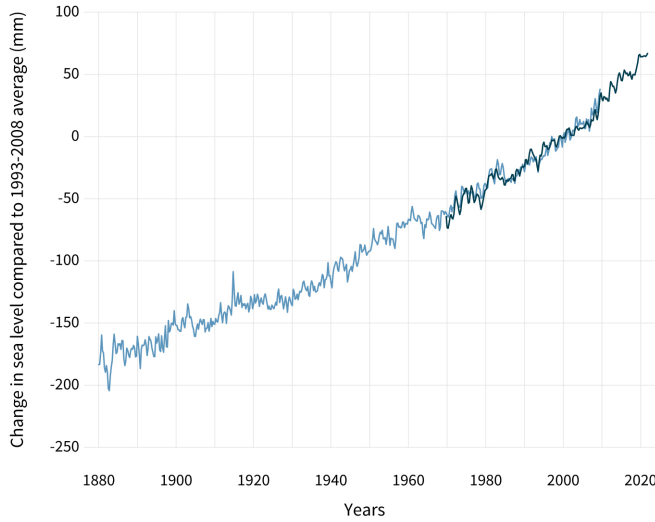


Figure 6.6: Global sea level change since 1880; blue is largely from tide gauges, black from satellite record (from <https://www.climate.gov/news-features/understanding-climate/climate-change-global-sea-level>, long timeseries is from [Church and White, 2011]).

Contributors to global sea level rise (1993-2018)

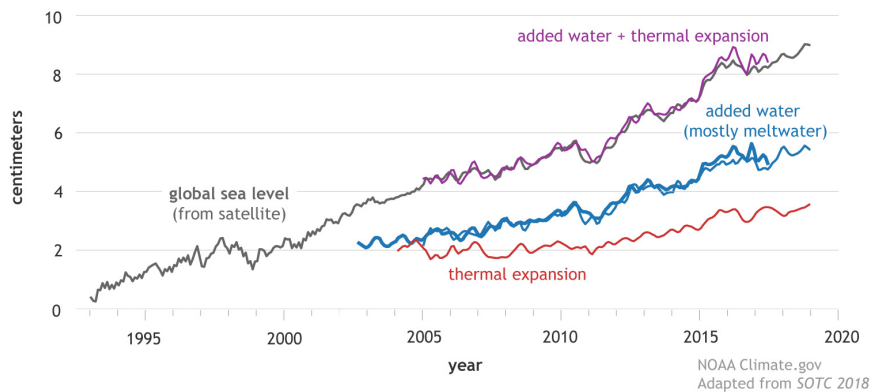


Figure 6.7: Contributions to sea level rise since 1993 (from <https://www.climate.gov/news-features/understanding-climate/climate-change-global-sea-level>).

6.2.1 Land-fast ice

Melting of landfast ice is responsible for something close to $2/3$ of the sealevel rise observed in the last 20 years, and responsible for much of the change since 1900. Of course, floating ice is melting as well, but it displaces its own weight in water, so when it melts it does not add to the total volume of the oceans. Tracking where this water has come from is a major undertaking in glaciology.

The biggest advances in monitoring the landfast ice sheets have used satellite measurements using either lasers, radars, or gravimeters to determine changes in ice cover. These methods are in general agreement, and indicate that 4000 Gt of ice were lost from both ice sheets, with substantially more lost from Greenland than the Antarctic. Distributed over the area of the oceans this contributed 1 cm of sea level rise between 1990 and 2010.

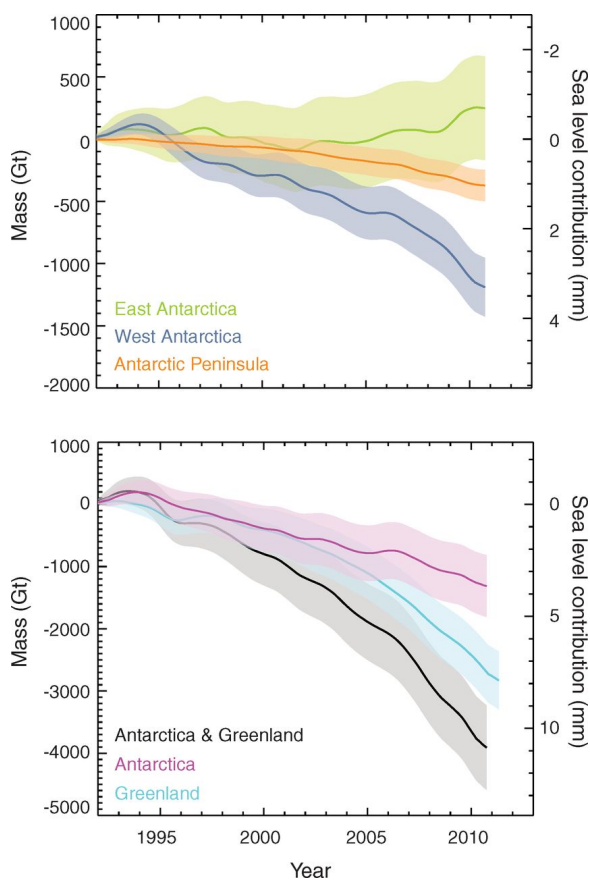


Figure 6.8: a) Cumulative ice sheet mass loss over time in regions of Antarctica, b) all Antarctica and Greenland [Shepherd et al., 2012].

6.2.2 Thermal expansion (steric change)

The other way that the ocean is expanding is due to thermal expansion as the ocean has warmed. The ocean has warmed about 2×10^{23} J between 1960 and today (figure 6.9). This means that, roughly, the ocean has increased its average temperature 0.03 °C.

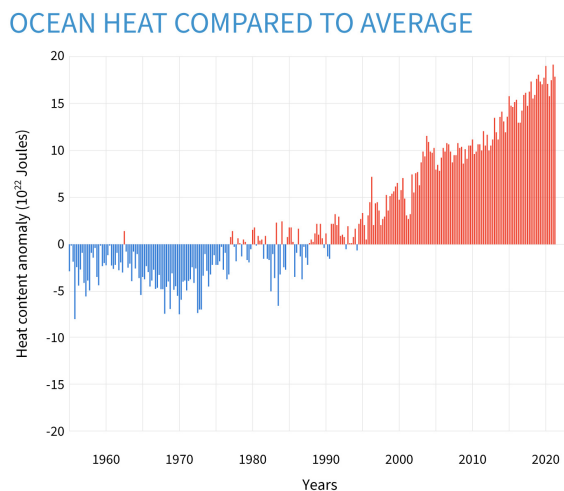


Figure 6.9: From <https://www.climate.gov/news-features/understanding-climate/climate-change-ocean-heat-content>

The warming effect is relatively easy to understand; suppose you have 1 L of 32 pus water at 20 degrees C - its density is $1022.504 \text{ kg m}^{-3}$. If we warm it 0.03 degrees, the new density is 1022.496. The mass will not have changed, so its new volume will be 1.0000078 L. If we multiply this over the whole ocean, we get a 3 cm of change over 4000 m. These rough numbers are similar to what is shown in figure 6.7.

This heat change is difficult to measure over the whole globe, and requires integrating temperature estimates from many measurements. Ship measurements get to the deepest depths, and then the more variable surface waters are more comprehensively measured with a fleet of autonomous profiling floats called Argo floats <https://argo.ucsd.edu>. These floats work by adjusting their buoyancy and collecting CTD data profiles to 2000 m every 10 days (figure 6.10).

6.3 Future sea level rise

Sea level is predicted to keep rising as melting of ice caps and heating of the ocean continues. The extent of the sea level change depends on amount warming and thus the amount of greenhouse gasses that will be put into the atmosphere. The best predictions

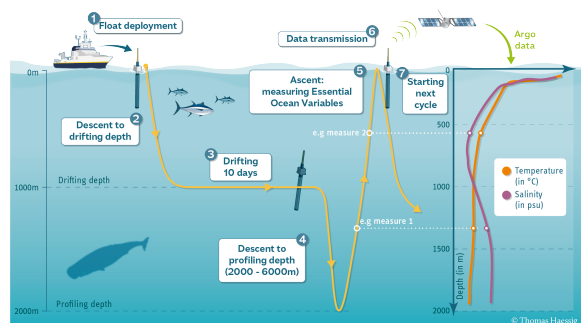


Figure 6.10: From <https://argo.ucsd.edu/how-do-floats-work/>

are shown in the IPCC technical report figure 6.11, where two scenarios are presented, RCP8.5, which is for poor mitigation of CO₂ use, and RCP2.6, which is for a scenario where all CO₂ emissions have stopped by 2100. The totals by 2100 are 0.84 m and 0.43 m, all of which is “locked in” because of the warming will not reverse itself just because CO₂ emissions stop.

The sea level rise due to increasing heat content is relatively well constrained by the models. Predicting future heat fluxes into the ocean is not perfectly known, but is probably known well enough that these error bars are relatively narrow.

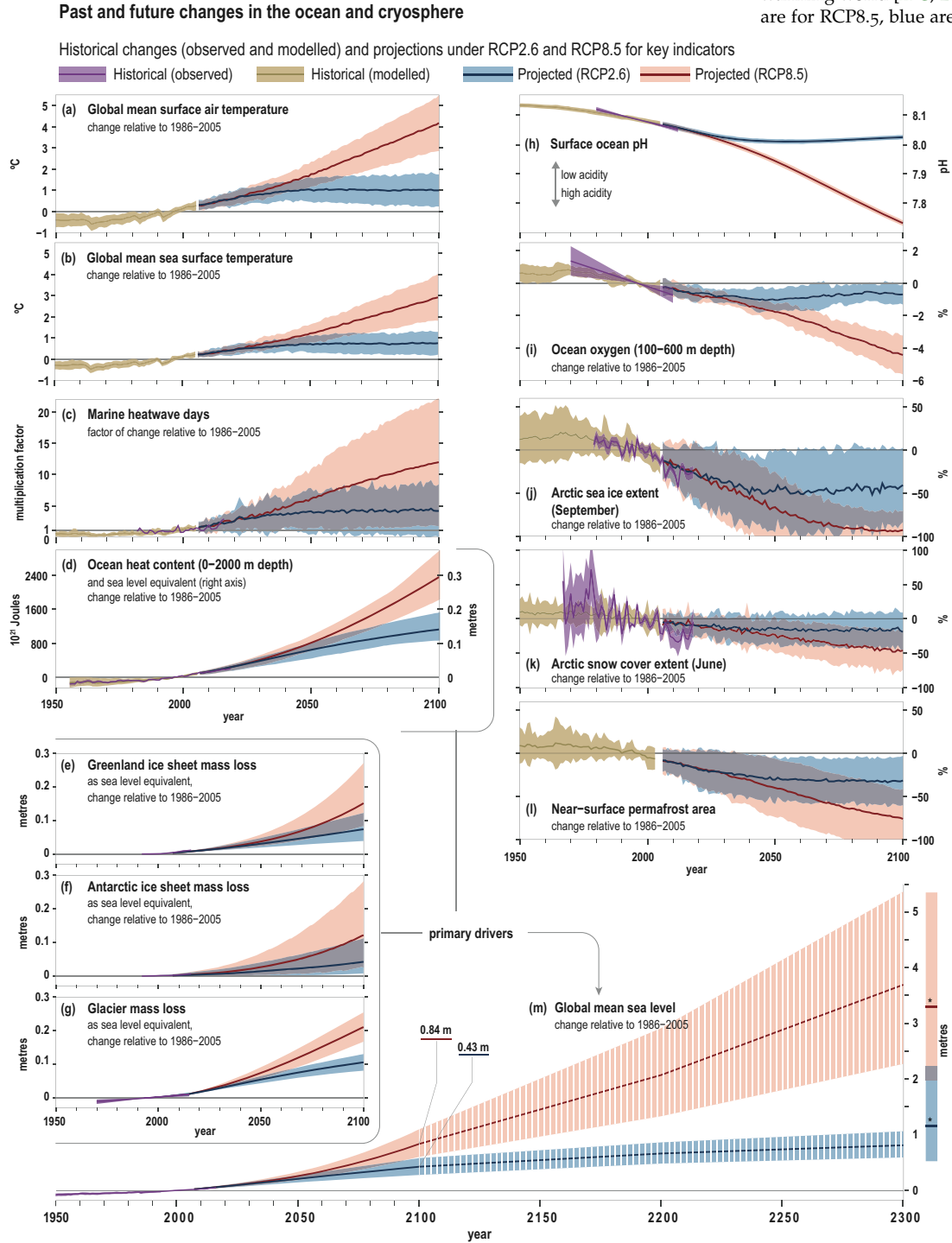
Conversely, the error bars of sealevel rise due to melting polar caps is quite poorly constrained. That is because there are numerous complex processes that lead to landfast ice melting. Atmospheric warming matters, but less well known is the lubricating effect on glacier movement of melt water reaching the base of the glacier (processes A–C in figure 6.12). This makes ice sheets more unstable and prone to calving off as icebergs that are quickly melted.

Similarly, many land-fast icesheets have ice shelves that extend over the ocean. These shelves are subject to thermal forcing from the warming ocean, as well as wind and tidal forcing (process E and the numbered processes in figure 6.12). Again, as these thin and break off, they stop supporting ice that is higher up on land, and can lead to increased rates of calving. These are all very hard to parameterize in large scale estimates, hence the large uncertainties in figure 6.11 for the ice-sheet terms.

6.4 Other reading

- <https://www.climate.gov/news-features/understanding-climate/climate-change-global-sea-level>
- <https://www.climate.gov/news-features/understanding-climate/climate-change-ocean-heat-content>

Figure 6.11: IPCC Ocean changes in warming world [IPC, 2022]. Red curves are for RCP8.5, blue are for RCP2.6.



Ice / Ocean interaction at the 79°N Glacier, East Greenland

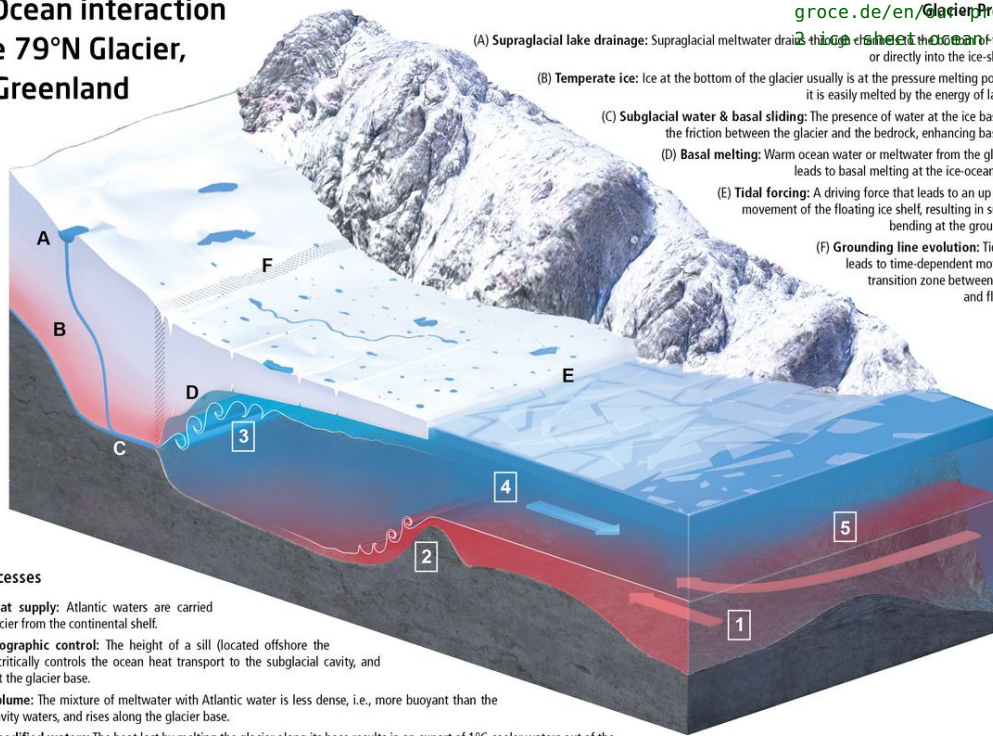


Figure 6.12: Ocean-glacier interactions (from <https://groce.de/en/GlacierProcesses/2-ice-sheet-ocean-interaction/>).

(A) **Supraglacial lake drainage:** Supraglacial meltwater drains either directly into the ice-shelf cavity.

(B) **Temperate ice:** Ice at the bottom of the glacier usually is at the pressure melting point, where it is easily melted by the energy of latent heat.

(C) **Subglacial water & basal sliding:** The presence of water at the ice base reduces the friction between the glacier and the bedrock, enhancing basal sliding.

(D) **Basal melting:** Warm ocean water or meltwater from the glacier itself leads to basal melting at the ice-ocean interface.

(E) **Tidal forcing:** A driving force that leads to an up and down movement of the floating ice shelf, resulting in subsequent bending at the grounding line.

(F) **Grounding line evolution:** Tidal forcing leads to time-dependent motion of the transition zone between grounded and floating ice.

Ocean Processes

- [1] **Ocean heat supply:** Atlantic waters are carried toward the glacier from the continental shelf.
- [2] **Local topographic control:** The height of a sill (located offshore the glacier front) critically controls the ocean heat transport to the subglacial cavity, and thereby melt at the glacier base.
- [3] **Ice shelf plume:** The mixture of meltwater with Atlantic water is less dense, i.e., more buoyant than the surrounding cavity waters, and rises along the glacier base.
- [4] **Glacially modified waters:** The heat lost by melting the glacier along its base results in an export of 1°C cooler waters out of the subglacial cavity.
- [5] **Critical layer thickness:** Large-scale hydrographic variations, reflected by changes in the Atlantic water layer thickness, are subject to local topographic control and thereby determine the heat supply below the glacier tongue.

Part II

Waves and Tides

7

Surface gravity waves



Waves are the phenomena that carry energy from one place to another, and occur in all branches of physics, from sound waves, to the wave-like nature of light. The ocean supports waves, both at its surface, and on density interfaces within the ocean as touched on briefly in the previous part. Here we deal just with surface waves though many of the same concepts apply to underwater waves and waves in the atmosphere. We also restrict the discussion to high-frequency waves, and do not consider so-called “planetary waves” or waves that are strongly affected by rotation.

7.1 Characterizing waves

Waves are often described in terms of sinusoids. If we write out the equations that govern waves displacements the solutions are sinusoids, and indeed most waves we observe in nature are well approximated by sinusoids, *except* near the shore, where non-linear effects can lead to breaking.

So, if we took a photograph of a wave from the side, and froze it in time, the wave would be described by the height of the waves, or the *amplitude*, A , and the distance between the wave crests (or troughs), or the *wavelength*, λ . The amplitude A is usually the height of the wave crest from the resting interface of the water, and is half the crest-to-trough *wave height* or H figure 7.1.

To fully specify a wave on the surface of the ocean, we need two other pieces of information. First, we need to specify where the crests are relative to where we define $x = 0$. That sounds abstract, but all it means is that we would like to know not only how high and far apart crests are, but also where they are at any given time. Second, we need to know the direction the wave is travelling. Usually, we will just consider waves travelling in one-dimension in the class, but bear in mind that in figure 7.1 the direction that x points along is usually taken to be in the direction of wave propagation (or its opposite). If we took it to be at a different angle, then the wave crests would appear further apart than they are in the direction of propagation (figure 7.2).

Mathematically, we therefore write the description of the sea surface displacement η wave as $\eta(x) = A \sin\left(\frac{2\pi}{\lambda}x + \phi\right)$, where ϕ is the phase that describes where the zero crossing will be. The term $\frac{2\pi}{\lambda}$ comes up all the time so we define $k = \frac{2\pi}{\lambda}$, where k is called the *wavenumber* and has units of rad m^{-1} . Using this shorthand, we see can rewrite the sinusoid as $\eta(x) = A \sin(kx + \phi)$.

Waves also have time dependence. So if we were looking at one spot we would see the wave moving up and down such that it completes a complete cycle in one *period*, which we usually denote with a T . Mathematically, the time dependence can be written as $\eta(t) = A \sin\left(\frac{2\pi}{T}t + \phi_2\right)$, or in terms of an angular frequency $\omega = \frac{2\pi}{T}$ (rad s^{-1}): $\eta(t) = A \sin(\omega t + \phi_2)$. Note that if it is the same wave as we took the spatial snapshot of, then the amplitude A will be the same in both frames of reference, but the phase ϕ will be different.

This is two ways of looking at the same wave, so combining them, we say that

$$\eta(x, t) = A \sin(kx - \omega t + \phi) \quad (7.1)$$

where $\eta(0, 0) = A \sin \phi$ is the height of the sea surface at $x = 0, t = 0$. If the frequency is not zero, then the wave propagates in space. If

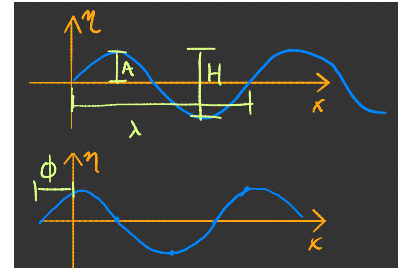


Figure 7.1: Sketch of sinusoidal wave forms that are frozen in time. The bottom sketch has a different phase ϕ than the top sketch.

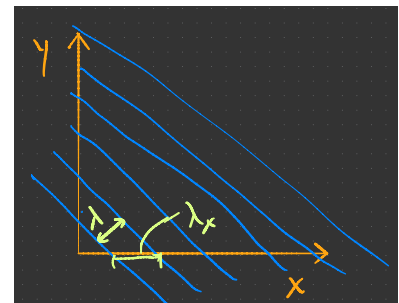


Figure 7.2: Schematic of wave crests at an angle to the "x" axis. Note that the wavelength λ is shorter than it would appear if we looked at the waves along the x axis λ_x .

$k > 0$ then the wave will propagate to the right (figure 7.3). Rather than drawing the curve many times, we can also plot as an *Hovmöller diagram* and trace the crests as a series of highs and troughs as lows (figure 7.3). The crests and troughs are examples of *lines of constant phase* (as are the "nulls", coloured as white here), and for a wave in a homogenous medium they follow straight lines. The slope of these lines is given by T/λ , and is inversely proportional to how fast the phases (e.g. the crests) of the wave move. So, we say that the *phase speed* of the wave is $c_p = \lambda/T$, or $c_p = \omega/k$.

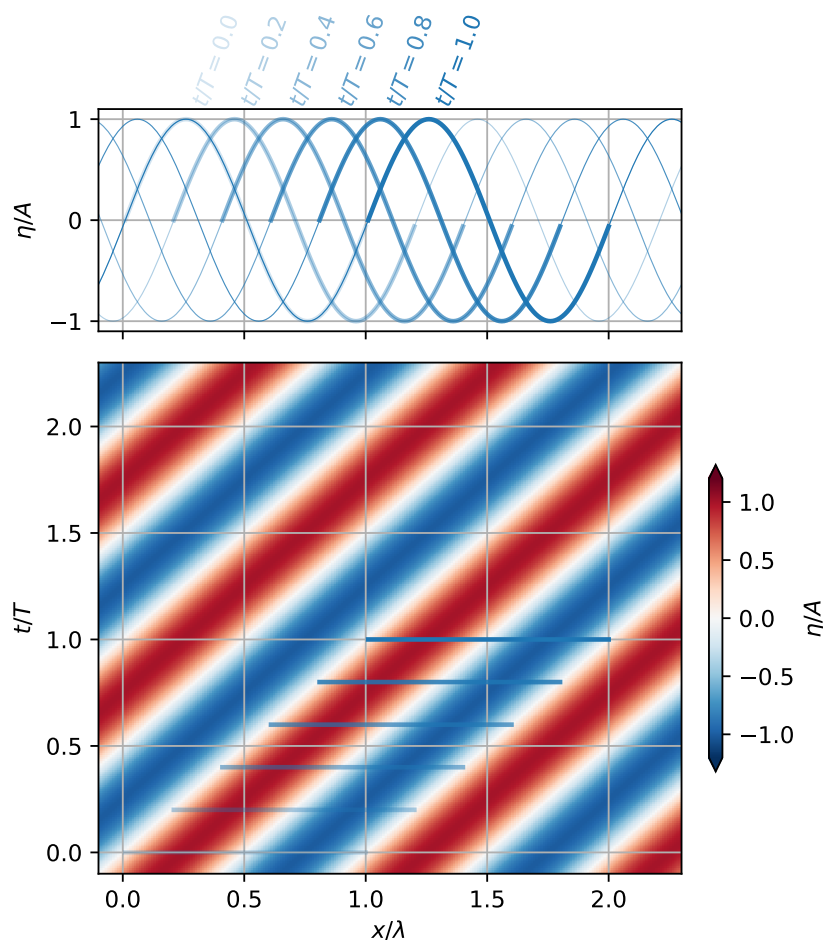


Figure 7.3: Upper panel: Schematic of a propagating wave, where the trace gets darker as time progresses. For this wave $k > 0$, so the wave crests propagate to the right. Note also that we have drawn this with $\phi = 0$ if the wave is described by equation (7.1). Lower panel: Hovmöller diagram of a wave propagating to the right in x . Peaks of the wave are red, and troughs blue. Blue lines on this panel correspond to the thick blue traces on the panel above.

7.2 Causes

Waves are caused by some sort of unsteady forcing - if you wanted to make a wave in a bathtub, you would move your hand back and

forth at a particular frequency. This would raise and lower the water level in front of your hand, and then the wave would propagate away.

In the ocean, most waves are caused by the wind (tsunamis caused by earthquakes are thankfully rare). The process by which waves develop is a continuum of processes, but the basic idea is that initially “cat’s paws” develop making small *capillary waves*. These waves actually have surface-tension as a restoring force, and have wavelengths of the order centimeters. On a calm day with small gusts of wind you can see these as local patches of roughness on the water.

If the wind is sustained, resonances with some wavelengths will lead to a growth of those waves. These resonances put energy in at all scales, but do so more efficiently at some, and waves with those wavelengths grow the fastest. The simplest way to think about the resonances is in terms of *Jeffrey’s sheltering theory*. As waves grow in size, the flow on the upstream side is blocked by the wave, and the downstream side is “sheltered” by the wave (figure 7.4). This creates high pressure on the windward face and low pressure on the downwind side, and this acts to steepen the wave. It is a resonance, because if the wave gets steeper, the effect grows stronger, and the wave continues to grow. How quick this resonance is, and what wavelength waves are affected the quickest depend on the wind speed.

Waves are only able to grow to be so steep before they break. the criteria for breaking in the open ocean is that the amplitude of the wave A cannot be much more than $1/15$ th the wavelength of the wave. This is actually quite large, and a 100-m horizontal scale wave will not break on its own unless its amplitude reaches 7 m or 14 m height. Waves tend to break before this due to the wind pushing the crests over, or waves interacting with each other to produce localized breaking regions.

Waves get larger, but also longer, as the wind speed increases. That is because the shorter waves tend to break sooner, and dissipate out of the system. A “fully-developed” sea is one in which the wind has been blowing a sufficiently long time that the waves have reached a steady state. In that situation the ocean will take on characteristic wave sizes, and amounts of breaking (figure 7.5).

Of course waves have spatial dependence as well, just as the storms that make them have spatial dependence. A snapshot from a model shows that the waves track the storms quite closely (figure 7.6), but you can also see bands of energy leaking North from the southern ocean. These are propagating waves, radiating energy from their source. (For a movie visit https://csdms.colorado.edu/wiki/Movie:Global_Wave_Power_2012.) Indeed, the longest waves are the fastest (as we will see below), and can sometimes outrun the storms

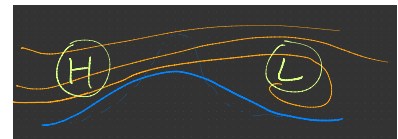


Figure 7.4: Sketch of the streamlines of air over a relatively steep wave (orange) and the pressure difference they would experience.

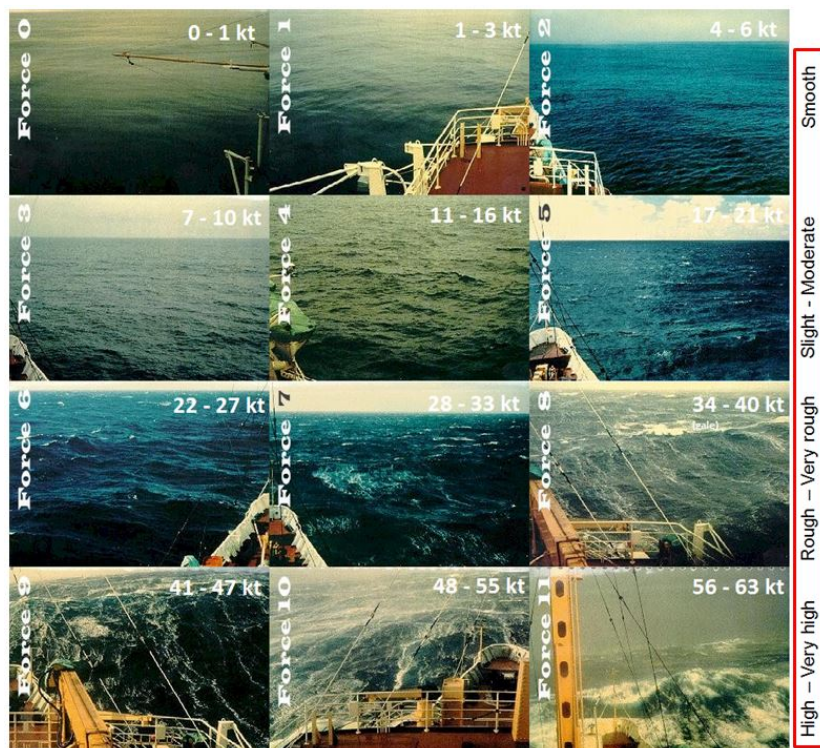


Figure 7.5: Pictures of fully-developed seas at increasing wind strengths.

that create them. We see this quite often on the West Coast, where swell will arrive a day or so before a winter storm.

7.3 Dispersion relation, phase speed, and particle motion

So far we have discussed the wavelength and period of the wave like they are independent, but in reality they depend on each other. Most people would expect that longer waves (large λ) will tend to have longer periods T . You can try this at home with a bathtub or sink - the wavelength of the waves you make depends on the frequency you slash with, not with how far you move your hand or paddle.

The relationship between the period and the wavelength is called the *dispersion relation*, and depends on the properties of the fluid and the physics of the waves. We are considering surface gravity waves, so of course this relationship depends on the strength of the gravity: $g = 9.8 \text{ m s}^{-2}$. It also depends on the water depth, which we will call h , and the wavelength of the wave λ . The general dispersion relation is a bit complicated:

$$\omega^2 = gk \tanh kh \quad (7.2)$$

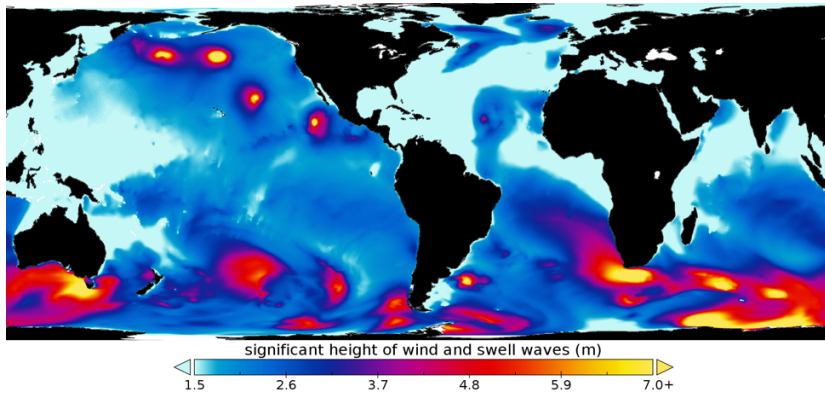


Figure 7.6: Snapshot of global wave heights during the boreal summer.

but it has two much simpler asymptotes that are applicable depending on the ratio of the wavelength to depth (or the product of kh (figure 7.7). If $kh \ll 1$ then the waves are “long” compared to the water depth, or we can also call the “shallow” water. In that case $\tanh kh \rightarrow kh$, and the dispersion relation is

$$\omega = \sqrt{gh} k \quad (7.3)$$

(blue line in figure 7.7). The phase speed of these waves are all the same, and only depend on the water depth $c_p = \omega/k = \sqrt{gh}$. We see then from this that as waves move into shallower water waves will get slower.

Deep water waves are quite different. They do not feel the bottom, so their phase speed only depends on the water depth. As $kh \gg 1$, then $\tanh kh \rightarrow 1$ and

$$\omega = \sqrt{gk} \quad (7.4)$$

and hence their phase speed is $c_p = \sqrt{g/k}$. So as k gets larger, the wavelength of the waves is shorter, and they move more slowly.

7.4 Orbital motions: velocity of water parcels

It is important to bear in mind that linear waves do not carry water with them. Non-linear waves do, and much of our intuition is from beaches where waves obviously push the water up the beach. But in open water where the waves are more likely to be linear, the water in a wave crest moves with the wave, but the water in the trough moves against the wave, so that over a wave period there is no net water motion. So while the wave crests move at the phase speed of the wave, the actual water does not move when averaged over a wave period.

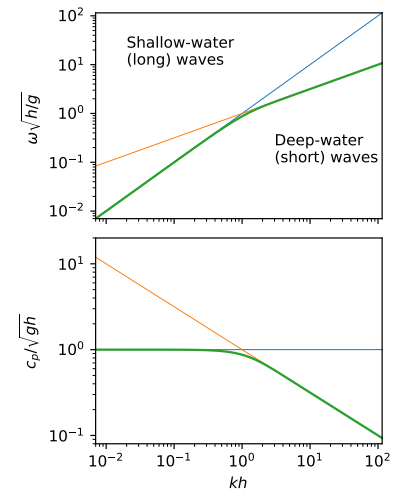


Figure 7.7: Upper panel: Dispersion relation for surface gravity waves (green), with the long-wave (blue) and short-wave (orange) asymptotes. Note the logarithmic scale used. Lower panel: dispersion relation expressed as phase speed.

In deep water, the velocity induced by the waves decays with depth with a vertical scale proportional to k^{-1} . So, longer wavelengths are felt to deeper depths (figure 7.8). This is why when scuba diving you often do not feel the surface waves. This also provides some physical justification for the different physics of “deep” versus “shallow” waves - deep waves do not feel the sea floor, whereas shallow ones do. In deep water, parcels of water make perfect circles, but as the water gets more shallow these circles are compressed by the bottom and become ellipses, and eventually there is almost no vertical motion and the water just moves back and forth.

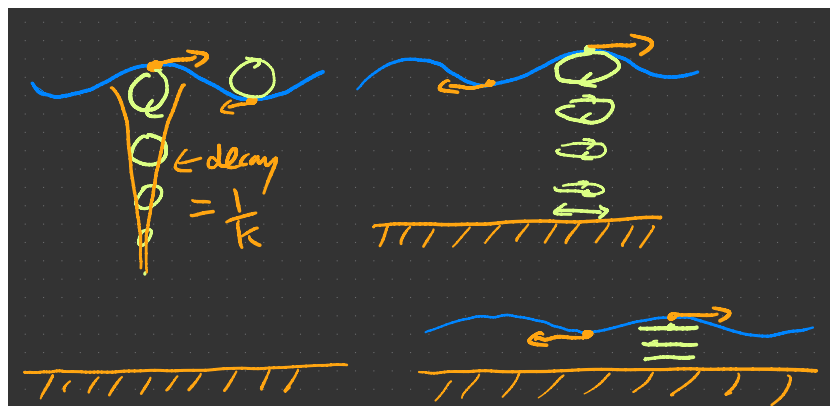


Figure 7.8: Sketch of orbital velocities of waves in three different depths: deep, intermediate and shallow.

Thinking about the velocity of water parcels also helps us understand why waves propagate. The flows are in opposite directions beneath the crest and the trough, and hence there is a convergence there (figure 7.9), and the peak moves in the direction of the flow under the crest. Note that for a left-going wave the flow direction under the crest is to the left, and the same argument applies.

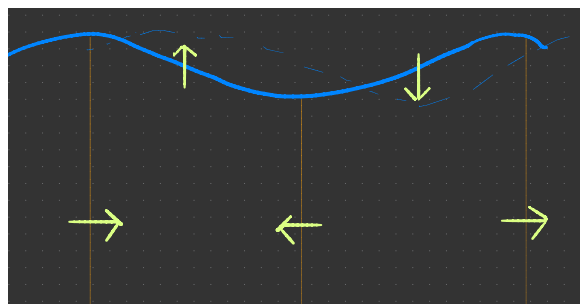


Figure 7.9: Sketch of how convergence and divergence in a wave causes it to propagate.

7.5 Group speed

Deep-water waves (or short waves) are examples of *dispersive* waves, in that the longer wavelengths and lower frequencies travel faster than the shorter. This leads to interesting effects when we consider packets or *groups* of waves.

A sine-wave describes an infinite disturbance - the wave oscillates for ever and for all values of x . Of course real wave packets or *groups* are finite in extent because the storms that make them are finite. One way to make a group of waves is to add together many sine waves with different amplitudes, wavenumbers, and phases, so that they *interfere* with one another such that when you add them together, they make a group. The simplest group occurs when we add two sine waves together with different wavelengths, and equal amplitudes. This creates infinite repeating groups, but is the easiest way to get the idea (figure 7.10). The waves in this figure have two slightly different wavelengths, and they are in 3.5 m of water, so the $\lambda > h$ and the phase speed of the waves is $\sqrt{gh} = 5.9 \text{ m s}^{-1}$. Adding these two waves together gives peaks and nulls as the waves constructively and destructively interfere with one another.

After 25s, both waves crests have travelled at 147 m at their phase speed. The crests are still in phase, and so the group has also moves 147 m. Because the waves stay in phase, we say they are *non-dispersive*.

Conversely, consider two deepwater waves with the same wavelengths. Here the phase speed is faster for the longer wave ($c_1 = \sqrt{g\lambda_1/2\pi} = 5.6 \text{ m s}^{-1}$) compared to the shorter ($c_2 = 5.3 \text{ m s}^{-1}$). That means that after 25 s they have travelled 140 m and 132.5 m respectively, and moved 7.5 m out of phase (figure 7.11). This means that when we add the two waves together, the peak in the interference pattern has fallen behind the two waves that made the peak in the first place. Hence, for *dispersive waves* the group speed is different than the phase speed. In the case of deep-water waves is exactly half the phase speed, and we can clearly see that the peak of the group is at about 70 m, whereas the original wave crests are at about 140 m.

The speed of the group is given by the derivative of the dispersion relation: $c_g = \frac{d\omega}{dk}$ which is called the *group speed*.

	long (shallow water)	all waves	short (deep water)
dispersion	$\omega = k\sqrt{gh}$	$\omega^2 = gk \tanh kh$	$\omega = \sqrt{gk}$
phase speed (c_p)	\sqrt{gh}	$\sqrt{g/k} \tanh^{1/2} kh$	$\sqrt{g/k}$
group speed (c_g)	c_p	$\frac{c_p}{2} \left(1 + \frac{2kh}{\sinh 2kh}\right)$	$\frac{c_p}{2}$

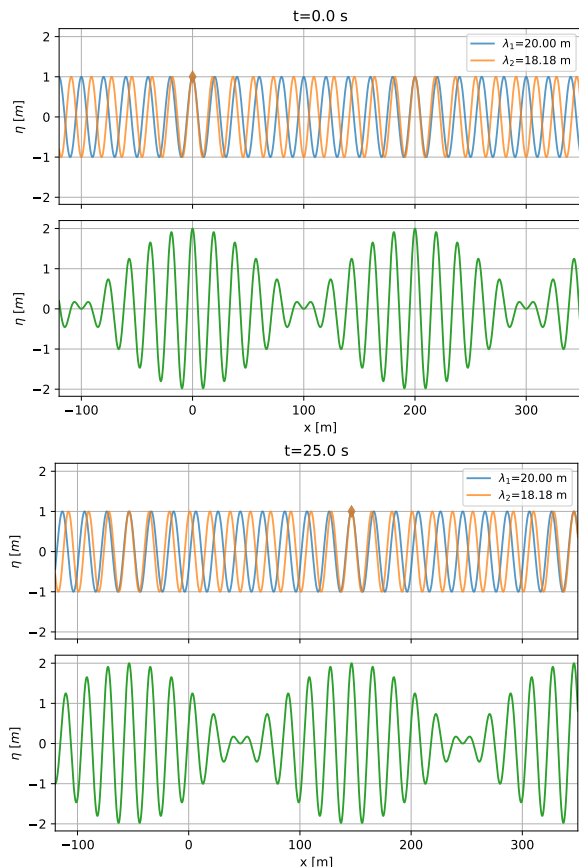


Figure 7.10: Two non-dispersive waves added together to make group. The crests are in phase at $x = 0$ at $t = 0$. 25 s later, both crests have traveled the same distance, and the “group” has moved with them.

Box 7.5.1: Derivation of group speed

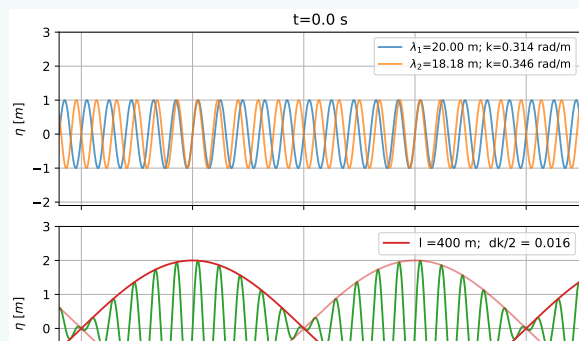
The group speed is given by $c_g = \frac{d\omega}{dk}$ which can easily be seen by considering the summation of two sine waves with slightly different wavelengths (and hence frequencies):

$$\eta = A \sin((k + \delta k)x - (\omega + \delta\omega)t) + A \sin((k - \delta k)x - (\omega - \delta\omega)t)$$

Using the angle identity $\sin \theta + \sin \phi = 2 \sin\left(\frac{\theta + \phi}{2}\right) \cos\left(\frac{\theta - \phi}{2}\right)$ we get

$$\eta = 2A \sin(kx - \omega t) \cos\left(\frac{\delta k}{2}x - \frac{\delta\omega}{2}t\right)$$

and we see that the combination of the waves is a convolution of a carrier wave with wavenumber k , frequency ω and an envelope with wavenumber $\delta k/2$ and frequency $\delta\omega/2$.



Seeing the difference between the two types of waves is another useful application of a Hövmoller diagram (figure 7.12). For the non-dispersive waves we can easily see that the crests of the individual waves follow the group, whereas for the deep-water dispersive waves, the group is propagating at half the speed.

In the real ocean, the packets do not repeat like they do when we just add two waves together. A more isolated group can be created if we consider summing together even more wavenumbers. The same group speed applies, but since longer waves have a faster group speed, the packet will spread with time as the longer waves outrun the shorter (figure 7.13).

Note that for dispersive waves, there is the un-intuitive phenomena that wave crests and trough emerge from the back of the packet, move faster than the packet and then disappear at the front of the packet. This is unintuitive, but is fundamentally because waves are not particles, but the result of convergences and divergences. These convergences and divergences simply get weaker towards the front of the packet until they are gone.

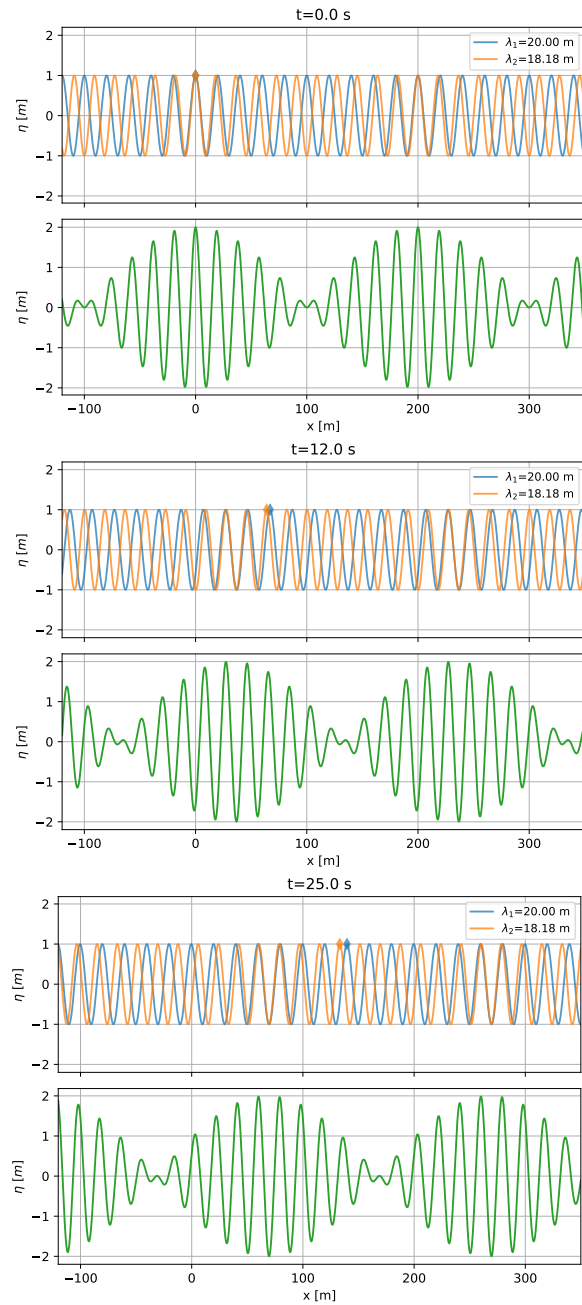


Figure 7.11: wo non-dispersive waves added together to make groups. The crests are in phase at $x = 0$ at $t = 0$. However, the longer wave moves faster than the shorter, and the crests move out of phase (diamonds), hence the interference pattern between the two falls back.

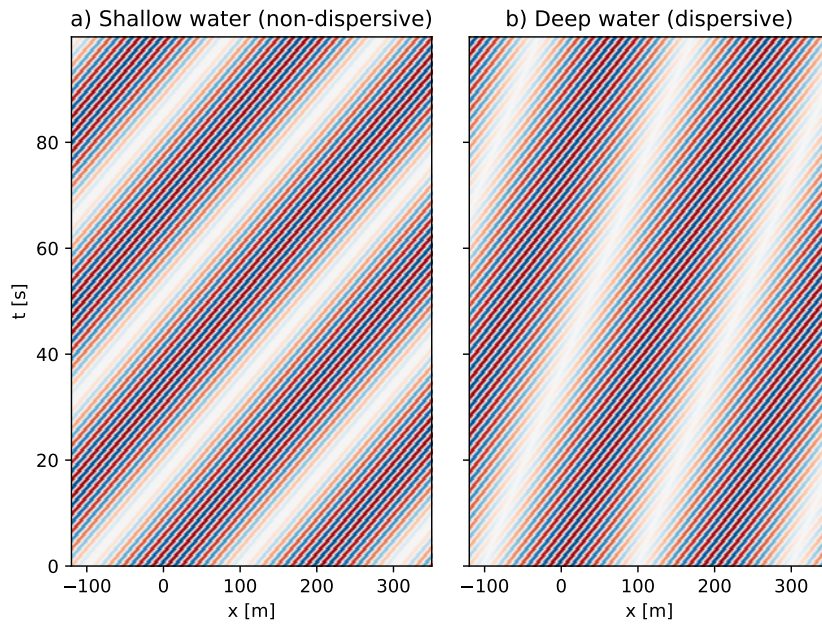


Figure 7.12: a) Hövemoller diagram for two shallow water, non-dispersive waves with the same wavelengths as figure 7.10 b) for deep-water dispersive waves (same two as figure 7.11).

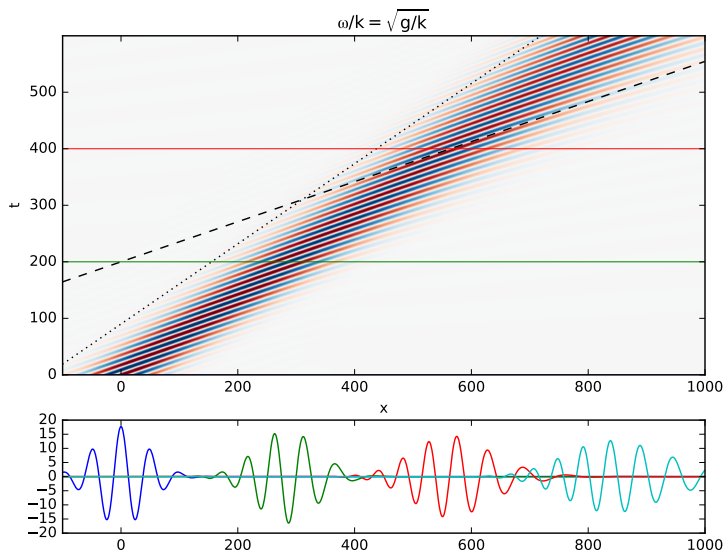


Figure 7.13: A very localized wave packet in deep water. Note how the group “disperses” as time goes forward, and that the larger wavelengths are at the front of the packet, and shorter at the back.

7.6 Energy conservation

Parcels of water are not carried by the waves, but *energy* is definitely carried by the waves. The speed at which the energy is carried is the group speed, as should be obvious by the fact that the disturbance created by the waves moves at that speed. If the speed of the energy is c_g , then we need only know the energy density to get a flux or transport due to the waves.

The energy density of waves is usually averaged over a period or wavelength. Within a period or wavelength the wave energy peaks twice, once at the crest and once at the trough, both times when there is potential energy (because the water is displaced) and kinetic energy (because the water is moving). We cannot derive the average energy density here, but for linear waves it is, per surface area of the ocean:

$$E = \frac{1}{2}\rho g A^2 \quad [\text{J m}^{-2}] \quad (7.5)$$

where remember that $A = H/2$ is the amplitude of the waves, and ρ is the density of the water. The energy flux is then

$$F = c_g E \quad [\text{W m}^{-1}] \quad (7.6)$$

where this is the flux per meter perpendicular to the direction the waves are travelling.

Considering the conservation of energy helps us understand some behaviour of waves as they are concentrated, either in shallower water or as a water way narrows. In both cases the energy density must increase to account for the reduced ability of the water to transport the waves.

So, for the first case, suppose we have a shallow-water wave propagating from $h_1 = 50\text{m}$ of water to a region where the water is only $h_2 = 10\text{m}$ deep. If we assume there is no energy loss between the two water depths, then the *fluxes* are equal, and

$$c_{g1} E_1 = c_{g2} E_2 \quad (7.7)$$

or,

$$E_2 = \sqrt{\frac{h_1}{h_2}} E_1 \quad (7.8)$$

from which we get that the amplitude in the shallower water has increased

$$A_2^2 = \sqrt{\frac{h_1}{h_2}} A_1^2 \quad (7.9)$$

because $\sqrt{\frac{h_1}{h_2}} = \sqrt{5} > 1$. Of course we see this at the beach, where very small swell in deeper water amplifies and steepens as it reaches shore (e.g. figure 7.14).



Figure 7.14: Waves approaching a beach. Note how offshore it is hard to see any waves (though of course its also further away). [Wikipedia](#)

A similar concentration of energy will happen in a narrowing channel (figure 7.15), even if the water depth stays constant. In this case we need to take into account the width of the channel, which is perpendicular to the wave propagation, to get:

$$W_1 F_1 = W_2 F_2 \quad W \quad (7.10)$$

But because c_g is constant in this case,

$$A_2^2 = \frac{W_1}{W_2} A_1^2 \quad (7.11)$$

and, again, if $W_1 > W_2$, then $A_2 > A_1$ and the amplitude must increase.

One small note here is that in order for these energy relations to be easy to follow like this, the change of the bathymetry or the width of the channel must be gradual relative the the wavelength of the waves. If it is not, then there will be some reflection from the bathymetry and wave energy will bounce backwards. Of course energy is still conserved, but you can end up with a partially standing wave.

7.7 Refraction and diffraction

When standing at the seashore, waves are almost always coming towards the beach, and this is because of *refraction*, the tendency of a wave to turn towards regions where the wave moves more slowly. Because shallow water wave phase speed depends on the square root

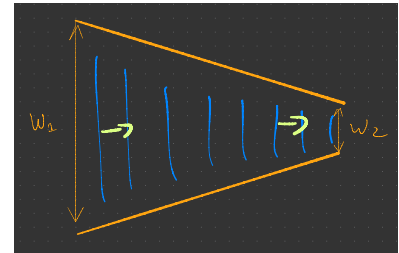


Figure 7.15: Waves propagating into a narrowing channel

of the water depth, waves in shallower water move more slowly than they do in deeper water.

Consider a wavefield heading towards a shoreline at an oblique angle (figure 7.16). In order to stay in a straight line all parts of the wavefront must move at the same speed. However, the shoreward end of the waves hits the shallow/slow part of the water first and slows down and falls behind the straight line, bending the line with the wavecrests towards the shoreline. This continues to happen, and if the change of bottom depth is gradual enough the waves will eventually be parallel to the shore. Of course if the beach is quite steep, this won't happen perfectly, but the tendency is usually there for most beaches.

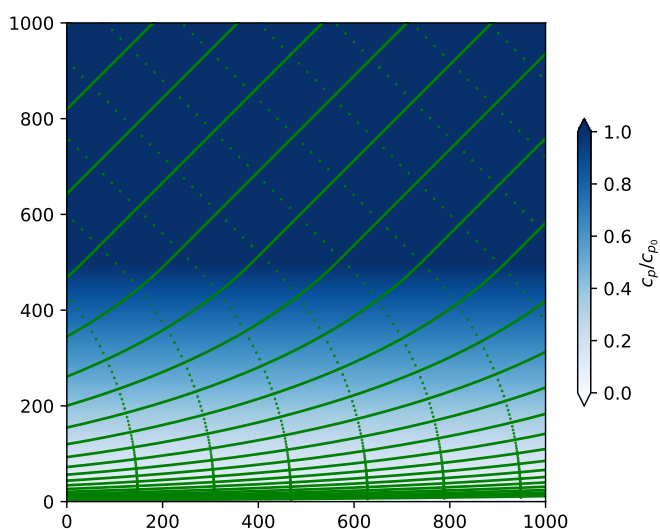


Figure 7.16: Crests of waves moving into shallower water (as indicated by the blue colors). Initially parallel out at sea, the waves crests bend in towards the shoreline. Dashed lines are wave “rays”, and identify where a certain point along the crest propagates to. “rays” are perpendicular to the wave crests everywhere.

The refraction of waves explains why “point breaks” often have more stronger surf than “beach breaks” (figure 7.17). As waves are bent towards the headland there is a convergence of energy as rays become closer together that is added to the convergence of energy as the water gets shallower. Of course point breaks are also favoured by surfers because the wave that breaks at the point then progressively breaks as it moves on shore, lending for a longer ride into shore (figure 7.18).

Diffraction also leads to bent wavefronts, but is fundamentally due to cylindrical spreading of the wavefront. We know that when we drop a pebble into a pool cylindrical waves will radiate from where

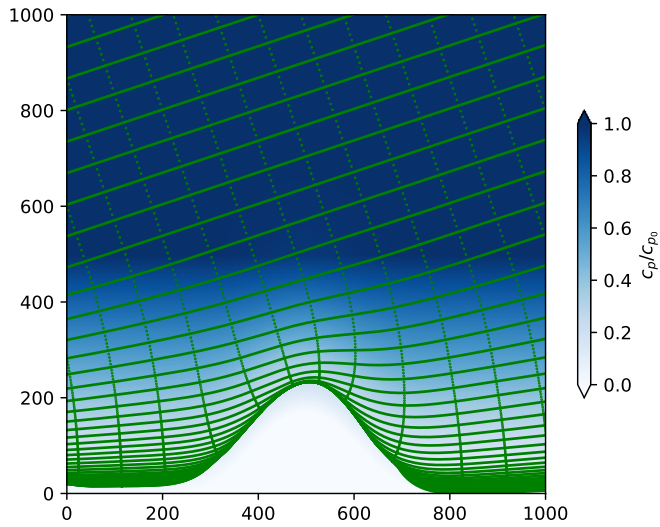


Figure 7.17: Crests of waves moving towards a headland. Note the headland extends underwater (colors). Note the concentration of rays at the wave-ward side of the headland.

the pebble hits the surface. A related effect will occur on the lee side of a barrier like an island or a breakwater. The corner of the island is like a wave source for the calm water beyond, and the waves will spread out to fill the calm water in a cylindrical pattern (figure 7.19). This will happen, even if the water is all one depth, so it is not due to refraction, though both phenomena can happen at the same time.

7.8 Non-linearity

The physics we have discussed so far applies to linear waves, i.e. waves for which the amplitude of the wave is much less than the water depth. If the wave amplitude becomes comparable to the water depth, the waves will become non-linear. Usually non-linear waves require some sort of numerical simulation, but we can readily see how non-linear waves might steepen and break on a beach by considering the phase speed of the crest versus the trough.

Normally, we consider the phase speed constant, however if the water depth changes drastically due to the, the water depth will be significantly larger at the crest h_C than in the trough h_T (figure 7.20). This leads to steepening as the crest overtakes the trough, eventually leading to a vertical wave face and breaking.



Figure 7.18: Long period swell at Rincon (southern California), a classic point break.

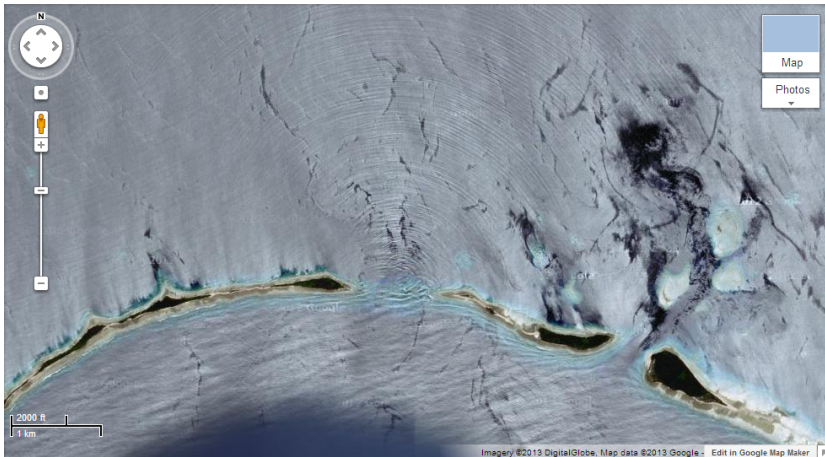


Figure 7.19: Wave diffraction through a gap between two islands. The swell is coming from the SSE and hits the gap from which radiates waves as approximate cylinders. [From Reddit!](#)

There are other forms of non-linear behaviour, including when waves interact with one another, but this is the most straight forward and largely responsible for breaking waves and bores.

7.9 Exercises

Swell prediction If a storm sets up in the Gulf of Alaska, 4000 km from Tofino, with wind speeds of 24 m/s:

- how long until surfers can expect good waves? (hint, figure out the wave height from the Beaufort scale, assuming a well-developed sea, use the ratio of height to wavelength to figure out the wavelength).

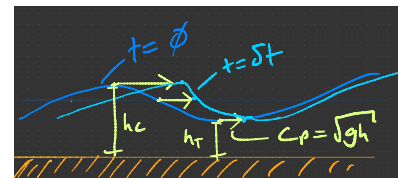
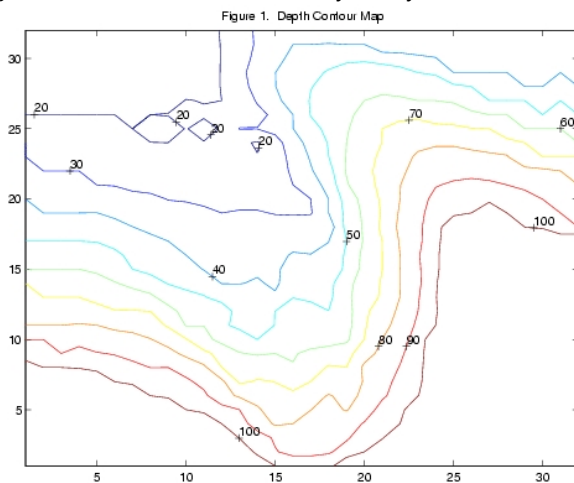


Figure 7.20: Sketch of steepening wave at two different times. The crest moves faster than the trough because the water depth is greater, and hence the wave steepens.

- What will the period of these deep-water waves most likely be?
- Those are pretty decent waves. They would be even better if they were 15-s waves. How fast would the wind need to be?
- Suppose the 24 m/s waves are travelling, and gradually move from 4000 m of ocean to 20 m. What would you expect the wave height to be (assume they become “shallow-water” waves, and that they don’t change their frequency). Hint: Conserve wave energy into the shallow water, but remember that the group speed also changes!
- Try to explain why waves that start in the gulf of Alaska often do not have such large amplitudes when they reach our shores?

Refractions Consider the bathymetry (of Jaws in Hawaii) below.



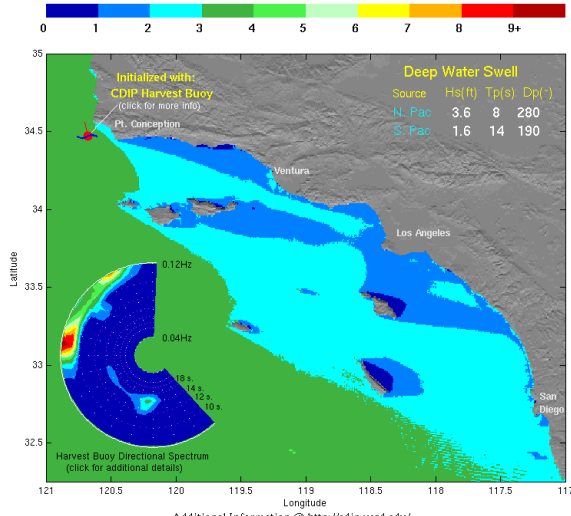
- If the waves approach from the south, where would you expect the strongest waves to be? Sketch lines of wavecrests.

More swell prediction Describe the last plot below. Where are the waves coming from, and what is their period? Briefly explain the patterns of green, blue and cyan. Why does the blue change back to cyan?



Analysis Time - 9 JUN 2007 : 1223 PST

Swell Height (ft) - Southern California Bight



8

Tides



Tides are an important ocean phenomena. In many places in the ocean they are the dominant source of ocean currents, and we have briefly touched on the fact that they drive mixing in both estuaries and the global ocean. Here we briefly describe how the various tides arise due to astronomical forcing, and discuss how they manifest in the real ocean.

Tides are generally caused by the co-orbiting of the moon and the earth, and the earth and the sun. These orbits cause gravity and centrifugal forces to act on the ocean, and the ocean responds to the forcing with a relatively complex set of waves that move around ocean basins. Ultimately such waves can only be predicted numerically, but the basic idea behind the forcing can be easily understood.

8.1 Tidal example and describing tides

A (somewhat) typical tidal signal is shown in figure ???. There are approximately two high tides a day, one is usually higher than the other. The high tides are move later in the day, indicating that their period is greater than 12 h. The amplitude of the tide also modulates over the 8 days shown here, with the tidal amplitudes large at the

beginning of the time period and becoming more modest towards the end of the time period. Note that there was a full moon on 1 August.

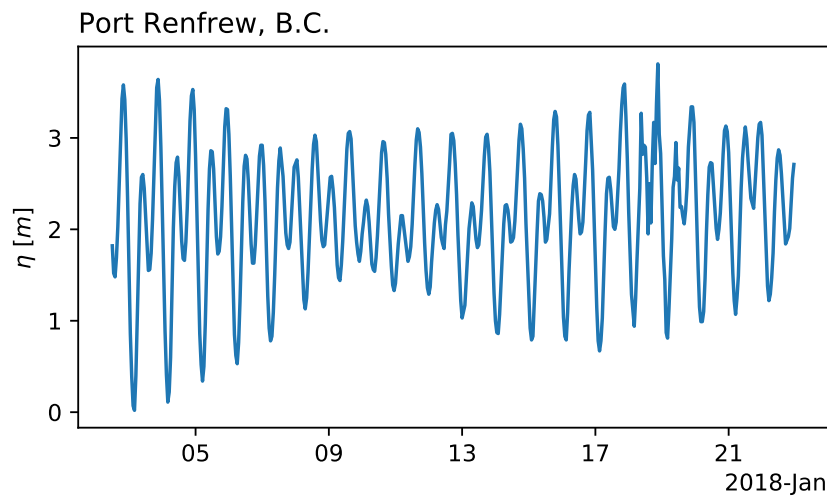


Figure 8.1: Tides observed at Port Renfrew, BC.

When discussing tides it is natural to use the language of waves we saw in the previous chapter (chapter 7). We saw that if we add two waves together of different wavelengths or frequencies we will get an interference pattern. Using that, we can fit a tidal signal to frequencies we expect from the astronomical forcing, and combine them with the proper amplitude and phase to get a tidal prediction into the future (figure 8.2).

The tides are dominated by frequencies that represent the *semi-diurnal* tides, which are twice a day, and *diurnal* tides, which are once a day (table 8.3). In general, it is the interference of M_2 and N_2 , for instance, which give a substantial portion of the spring-neap cycle.

8.2 Tidal forces: Gravity and centrifugal forces on co-orbiting bodies

The tides are driven by the fact that the earth and the moon orbit around one another and the sun and the earth orbit around each other. We usually think of the moon orbiting around the earth every 27.3 days, but the earth also orbits around the center of mass of the earth-moon system every 27.3 days. The point they both orbit around is called the **barycenter**, and for the earth and the moon, it is 4670 km from the center of the earth, which is less than the radius of the earth, so the orbit causes the earth to wobble.

The earth moves around this barycenter maintaining its orientation

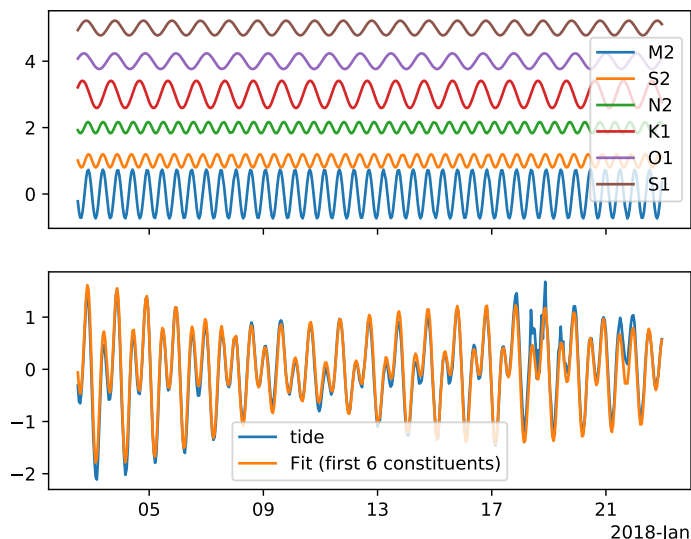


Figure 8.2: Harmonic fit of tides at Port Renfrew, BC. Upper panel are 6 tidal harmonics with their amplitude and phase fit to the signal in figure 8.1. Lower panel is the original signal (blue) and the fit (orange).

	period (h)	Fit at PR (m)	Origin
M_2	12.421	0.74	Principal lunar semidiurnal
S_2	12.000	0.20	Principal solar semidiurnal
N_2	12.658	0.17	Larger lunar elliptic semidiurnal
K_1	23.934	0.41	Lunar diurnal
O_1	25.819	0.24	Lunar diurnal
S_1	24.000	0.22	Solar diurnal

Figure 8.3: First 6 tidal constituents, and their amplitude at Port Renfrew BC.

in space. This is shown schematically in figure 8.4, where we have used squares instead of circles to represent the bodies, because it helps makes the orientation of the earth relative to the barycenter. In each frame, the green dot points "up". Hence the green dot traces exactly the same size circles as the red dot and the center of mass of the earth. Note that the moon behaves differently. The same face is always angled towards the earth, so that face will make a smaller circle, and the far face will make a larger one. This phenomena is called **tidal locking** and is why we only see one side of the moon.

The fact that the earth maintains the same orientation in space during its orbit around the barycenter means that every point on the planet feels an identical **centrifugal force**. This acceleration tends to fling particles away from the axis of rotation with a value

$$a_c = \omega^2 r \quad (8.1)$$

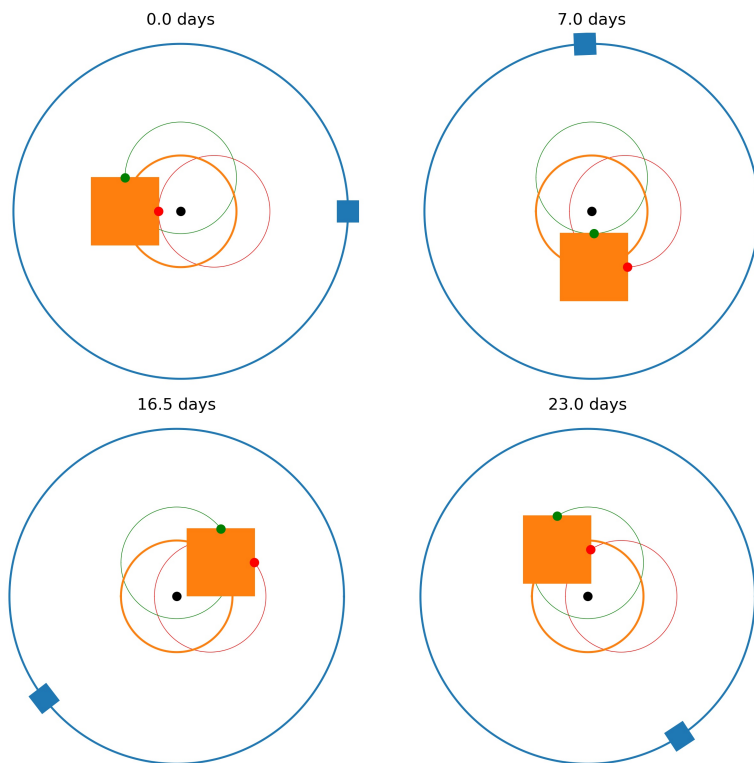


Figure 8.4: Schematic of a square earth co-rotating around its barycenter, with a square moon. The orbits of two points on the earth are also shown with red and green circles, as is the center of mass of the earth (orange line) and the moon (blue line).

where $\omega = 2\pi/27.3d$ and $r = 4670$ km is the distance from the center of the earth to the moon-earth barycenter, so this acceleration is $3.3 \times 10^{-5} \text{ m/s}^2$.

At the center of mass of the earth, this centrifugal acceleration is balanced by the force of gravity of the moon, pulling the earth towards it. This acceleration is given by Newton's law of universal gravitation:

$$a_g = \frac{Gm_{\text{moon}}}{R^2} \quad (8.2)$$

where G is a constant, m_{moon} the mass of the moon, and R the distance from the moon's center of mass to any point on (or in) the earth.

So the centrifugal force, a_c , is the same everywhere on the earth, but the gravitational attraction due to the moon is definitely not, because R varies over the earth, so that points further from the moon experience less gravitational pull than points closer (figure 8.5). In addition, points on the earth that are not on the earth-moon axis are pulled towards that axis. The net effect is that the earth bulges towards *and away* from the moon.

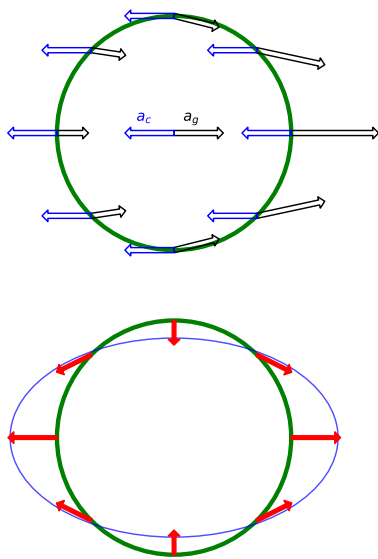
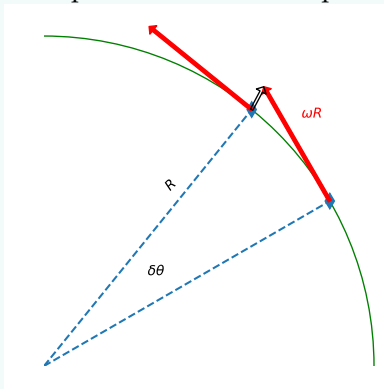


Figure 8.5: Sketch of Net tidal forces on earth due to moon. Centrifugal accelerations are shown in blue, and are the same everywhere. Gravitational accelerations are shown in black, and vary with the inverse square of distance from the moon, and point towards it. The bottom panel shows the direction of the net forces when the satellite is very far away and a schematic of the tendency of the earth to bulge toward and away from the satellite.

Box 8.2.1: Centrifugal force

The centrifugal force is an *apparent* force (a term I prefer to “fictitious”) that arises when a co-ordinate system is rotating. Consider a counter-clockwise rotating system as shown below. At the first arrow, an object orbiting in the co-ordinate system is moving with speed ωR , where $\omega = 2\pi/T$ is the rotation frequency of the rotating system and R is the distance to the axis of rotation. The direction that this particle is moving is tangential to the arc of the circle.

If there were no forces acting on the particle at this point, it would travel in a straight line tangential to the circle (along the arrow). A particle that travelled with the circle would still be on the orbit and would be travelling in a different direction (with the same speed) since the circle bends. Thus the particle with no external forces is accelerated away from the axis of rotation, and we call this acceleration the “centrifugal force”. In order for a particle to continue to move in a circle, there has to be compensating **Centripetal force** pulling the particle towards the axis of rotation. If the particle were the moon, the centripetal force would be provided by the earth’s gravity.



Deriving the acceleration is relatively straight forward. The angle difference between the two velocity vectors is $\delta\theta$, so the velocity difference is $\delta v = \omega R \sin(\delta\theta)$, and if $\delta\theta$ is small $\delta v \approx \omega R \delta\theta$, or dividing by the time it took to traverse the small change in angle, δt : $a_c = \omega R \delta\theta / \delta t = \omega^2 R$, with the direction away from the axis of rotation.

8.3 The reason for various tidal frequencies

The various frequencies observed in the tides arise naturally from the net tidal forces (i.e. the tidal bulges) caused by the moon and the sun. Understanding their origin requires remembering some basic things

about the orbit of the moon around the earth and the earth around the sun. But a few things to keep in mind are

- orbital planes are not along the earth's equator, so the tidal bulges are not usually centered at the equator; as we will see below this causes a once-a-day modulation of the tides.
- orbits are not perfect circles, but rather ellipses, so there are modulations if the earth is closer or further away from the sun or moon.

8.3.1 Twice a day tides

$M_2 = 12.42\text{h}$: *lunar semi-diurnal* The tidal bulge made between the moon and the earth means that as the earth spins on its axis, a given point on the earth passes through two high points in the bulge and two low points in the bulge every time that point catches up to the moon (figure 8.6). Because the earth and the moon rotate in the same direction, this means that the moon has done $1/29.53$ of its orbit in one 24 h period, and hence the bulge has rotated. The time it takes for the earth to catch up with the moon again is given by $t\omega_E = t\omega_M + 2\pi$ or in terms of the periods:

$$t = \frac{T_M T_E}{T_M - T_E} = 24.84 \text{ h} \quad (8.3)$$

or a high and low tide every 12.42 h.

Note that we have used the *synodic month* or *lunar month* of 29.53 days for the period of the moon, despite the fact we said the moon orbits the earth every 27.3 days. The moon actually does travel 360 degrees around the earth in 27.3 days, but the earth moves relative to the sun, so the moon has to orbit further to be at the same orientation of the earth and sun, and this takes 29.53 days; for a nice animation see [here](#). Note that this is derived with the same equation as above with $T_M = 27.321 \text{ d}$, and $T_S = 365.256 \text{ d}$, to yield a period of 29.53 days.

$S_2 = 12 \text{ h}$; *solar semi-diurnal: spring-neap cycle* In exactly the same way as the moon, the sun creates a tidal bulge, and this leads to a 12-h tide as the earth turns to face the sun every 24 h, leading to the S_2 tide. The strength of the S_2 tide is generally weaker than the M_2 tide, because the moon is closer, even though much less massive than the sun. The relative strengths vary, depending on the time of month, time of year, etc, but we saw above in table 8.3 that S_2 was less than $1/3\text{rd } M_2$; globally they average out to be about half the lunar tide.

Nonetheless, the interference of S_2 and M_2 create a modulation to the M_2 tides that we call the *spring-neap cycle* to the semi-diurnal tide. As the moon orbits the earth, the tidal bulge moves with it, but

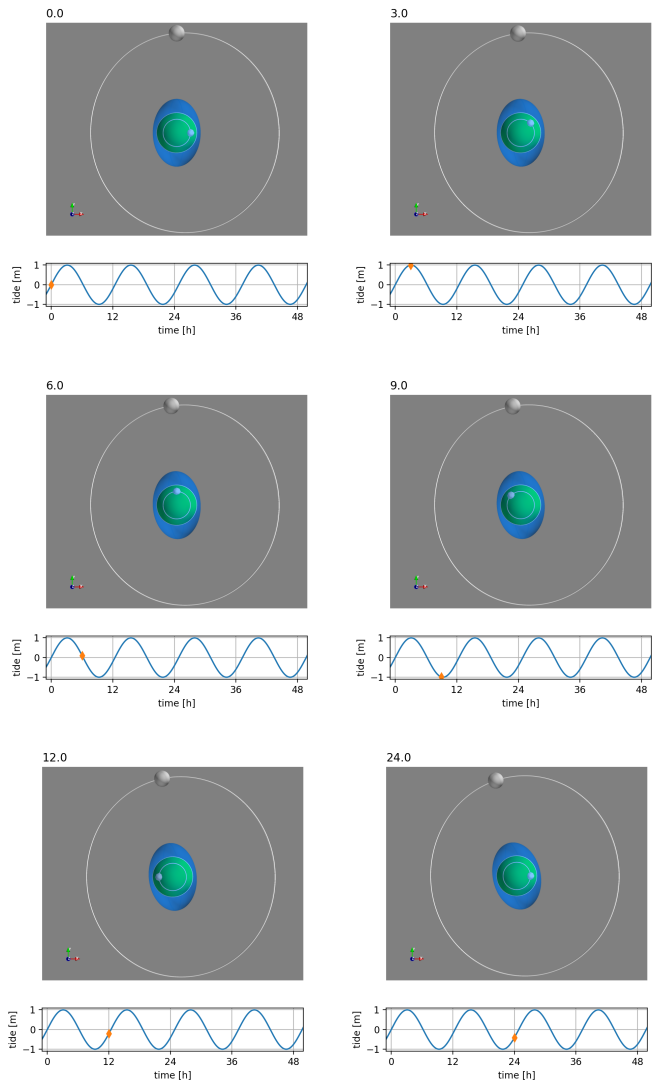
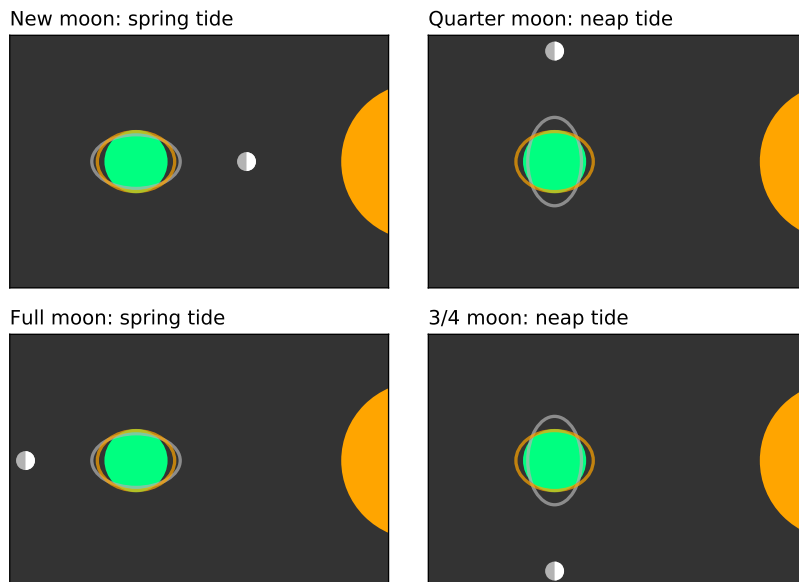


Figure 8.6: Origin of twice-a day tides from the moon. Looking at North pole, moon moves counter clockwise. Earth also spins counter-clockwise.

the tidal bulge due to the sun only moves slowly as the earth orbits the sun, and the moon and sun's tidal effects are in quadrature ever half lunar synodic orbit ($29.53/2 = 14.77$ days).



Mathematically, we can see that adding an S_2 and M_2 tide gives us a modulation with a period of $S_2 M_2 / (M_2 - S_2) = 14.75$ days, which is the half the synodic orbit (the one relative to the sun, which we have to line up with) period of the moon (figure 8.7).

8.3.2 Daily tides (diurnal): Tides due to non-equatorial orbits

The moon's orbit is not along earth's equator, and the earth is tilted relative to the sun. So the tidal bulges that these bodies cause are not centered on the equator, but rather are tilted. As the earth spins through these bulges, there are still two high tides, but one of them will be larger than the other, adding a **diurnal** component to the tides.

Moon's declination The moon's orbit is at an angle to the equator. Currently that angle is about 21 degrees, but it varies between 18 and 28 degrees on a 18.6-year time scale (figure 8.8). This precession of the moon's orbit leads to an 18.6-y cycle in the tides that must be kept track of!

The result of this tilt relative to the equator means that the tidal bulge is also inclined between 18 and 28 degrees from the equator.

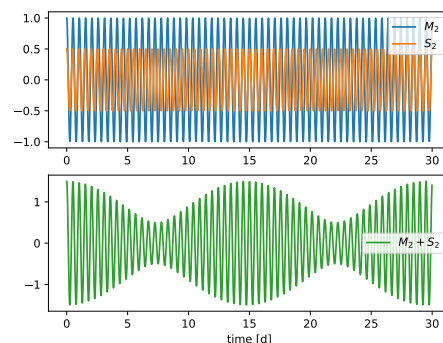


Figure 8.7: Adding an M_2 and S_2 wave together, giving a spring-neap cycle that repeats every 14.77 days.

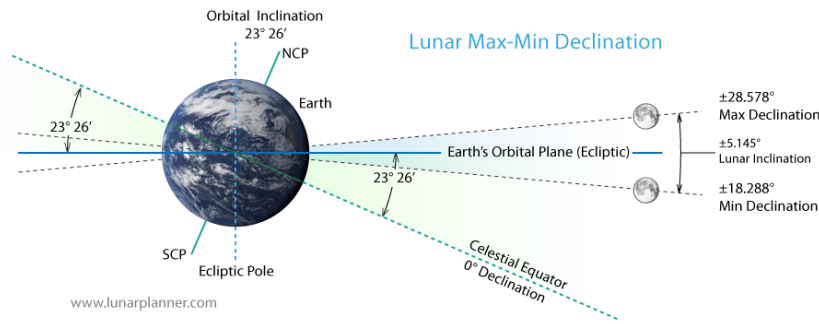


Figure 8.8: Schematic of the lunar declination, and the earth's tilt relative to its orbital plane around the sun. Note these tilts mean that the tidal bulges are not symmetric about the earth's equator.

As a point on the norther hemisphere spins through this bulge, there are still two high tides, but one will be larger than the other (figure 8.9).

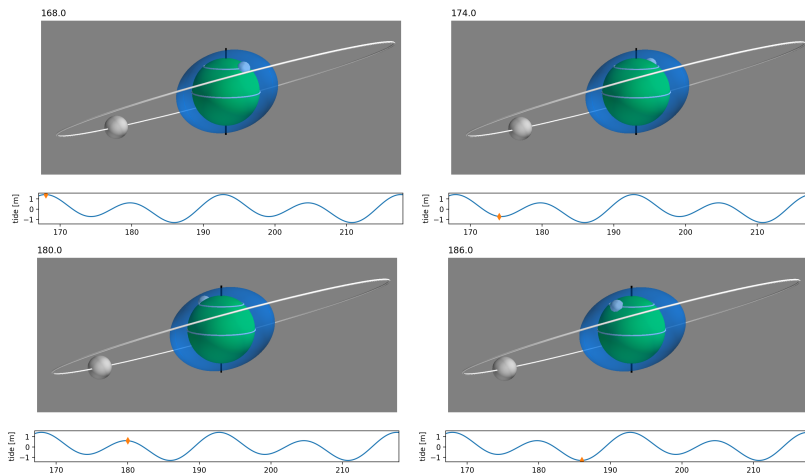


Figure 8.9: Origin of once-a-day tides from the moon. Here the moon is at the point of its orbit when it is 20 degrees below the equator. So the tidal bulge is large on the northern hemisphere away from the moon. An observer on the northern hemisphere sees a larger high tide when pointed away from the moon, and a lower high tide on the side nearest the moon.

Mathematically, we represent this as a daily modulation on the twice-a-day tide by adding a "diurnal" component to the tide (figure 8.10). This has the obvious effect of making the high tide higher once every two high tides. Note also that there is an asymmetry to the high-high and low-low tides just from these two components that make the high-highs larger ever two weeks, and the low-lows larger on opposite weeks. Note, however, that this does *not* happen with the real moon, because the real moon changes its angle throughout the orbit of the moon, and the strength of the K_1 diurnal component is modulated by the O_1 . Note that the K_1 and O_1 tides create a 13.66 day beat, which is half of the *sidereal* (or from space, versus relative to the sun) orbit period of the moon of 27.3 days.

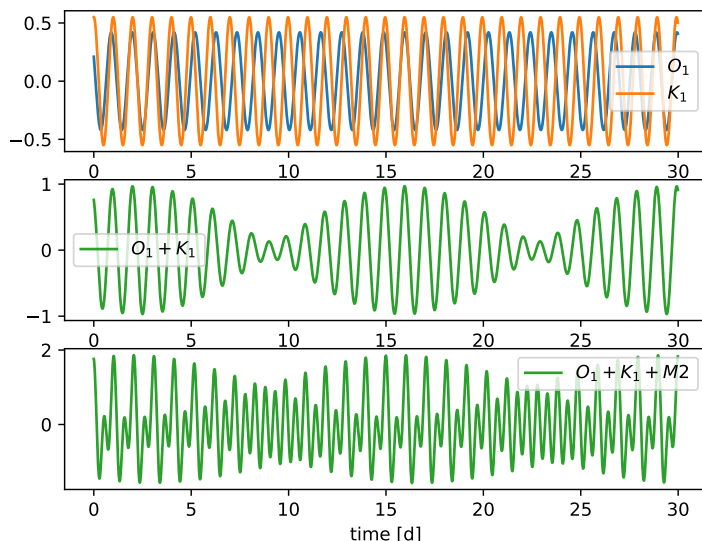


Figure 8.10: Adding a diurnal frequency tide to a semi-diurnal that varies in strength every two weeks. $K_1 = 23.934$ h and $O_1 = 25.819$ h are lunar-diurnal tides and added together they are modulated every 13.66 days

Solar declination Similarly, the earth is inclined towards the sun, with the northern hemisphere tilted 23.43 degrees towards the sun in the northern hemisphere summer solstice. This similarly causes an asymmetry in the solar tidal bulge, and a diurnal component to the solar tides. These have a similar character to the changes due to the moon's declination, however, their strength varies through the *year* rather than through the lunar month. The solar diurnal component pair are $S_1 = 24$ h and $P_1 = 24.06588766$ h, and the beat between them is one year.

8.3.3 Longer period tides

Finally, there is a weak dependence of the tide on how close the moon is and how close the earth is to the sun. When the moon is close to the earth it is called *perigee*, and the opposite is *apogee*. The perigee is about 10% of the moon's mean orbit of about 400,000 km, so this has a significant effect on the tides. The perigee and apogee precess with time, so they are not tied to the declination, and have a period of 27.554 days. This precession has a period of about 4 years.

The equivalent frequency is an annual change in the earth's distance from the sun, or perihelion and aphelion. The difference is about 2.5 million km out of 149.5 million km, so a much less pronounced of an ellipse than the lunar orbit. Currently, perihelion

occurs the first week of January (5 January for 2020) and aphelion the first week of July (4 July, 2020). That it occurs near the solstices is a co-incidence, though, and the ellipticity of the earth's orbit around the sun varies on a time scale of 22,000-26,000 years.

As noted above the declination of the moon varies on an 18.6 year time scale between 18 and 28 degrees with respect to the equator, so we expect lunar diurnal tides to vary on this time scale as well. The importance of this is hard to see, but there is evidence that this change in tides affects the strength of ocean mixing, particularly in straits that have strong diurnal tides, and that this can have a noticeable affect on ocean temperature [McKinnell and Crawford, 2007], and oxygen levels [?], possibly due to mixing in the Sea of Okhotsk [Yasuda et al., 2006].

Finally, the tilt of the earth varies with a period of about 41,000 y. These variations are thought to have only been between 22 and 24 degrees, but are thought to have long-timescale climatic effects, called Milankovitch cycles.

8.4 *Dynamic theory of the tides*

If a real tidal bulge were to travel around the earth, it would need to travel 40,000 km around the equator in 24 h, or travel at a speed of 465 m/s. Assuming this is a shallow water wave, the ocean would have to be 22km deep. Further, of course, the ocean would have to be continuous, with no land masses blocking the progress of the wave. Therefore, instead we should think of the tidal bulge as a forcing that the ocean responds to. The details of that response depend on the shape of basin, and sources of loss from the surface tide to other smaller scale processes (e.g. friction, making internal tides, etc).

8.4.1 *Tidal Resonance*

The most obvious example of the tidal response depending on the shape of the basin is to think about what happens in a fjord. Consider a fjord that is approximated as a long rectangular basin, say $H = 200$ m deep, with a mouth into a much deeper and larger ocean. The tidal forces act on the small fjord, but are completely swamped by the tides that the mouth of the fjord sees. So this is a situation where the body doesn't even notice the astronomical forcing by the tides, let alone be driven by them. Similarly, the ocean barely notices the presence of the fjord, and the tides in the ocean can ignore the motions in the fjord.

In this idealization, we can prescribe the forcing at the mouth of the fjord in terms of a sea level change that is a sine wave in time,

e.g. $\eta(x = L, t) = \eta_0 \sin(\omega t)$ (figure 8.11). The *response* of the fjord is simply a pair of waves, one propagating into the fjord, and one reflecting. Because no energy is lost, both waves have the *same* amplitude, but can have different phases:

$$\eta = A \sin(\omega t - kx + \phi_{in}) + A \sin(\omega t + kx + \phi_{out}) \quad (8.4)$$

where $\omega/k = \sqrt{gH}$ because the tidal waves are examples of shallow-water waves. In order to solve for A and the phases, we need a second boundary condition, this one is at the head of the fjord ($x = 0$), where we know that the flow must be zero: $u = 0$. Recall that the speed of a wave is proportional to the derivative of the seasurface height, so we can rewrite this as $\frac{d\eta}{dx} = 0$. Using both these conditions and our double angle identities, we can write the solution as:

$$\eta = \frac{\eta_0}{\cos kL} \sin \omega t \cos kx \quad (8.5)$$

Hopefully, it's readily apparent that this solution satisfies the conditions above at $x = -L$ and $x = 0$.

This solution is a **standing wave**. Notice that everything in the fjord rises and falls at the same time, so high tide happens everywhere at the same time. Another way of saying this is that there is no change of phase of the tide in the fjord. Another feature is that the amplitude of the sea surface height at the head of the fjord is larger than the amplitude at the mouth; the opposite applies to the velocities, which are zero at the head, and largest at the mouth.

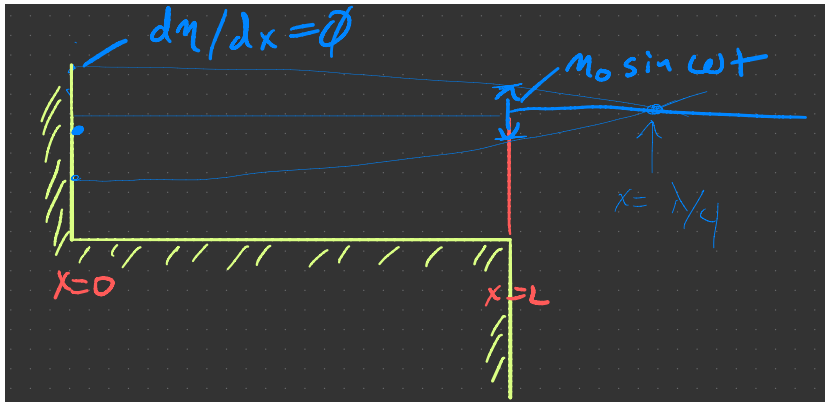


Figure 8.11: A fjord with a wall at $x = 0$ and an ocean at $x = L$. The wavelength $\lambda = \frac{2\pi}{k}$ is set by the water depth and the frequency of the tide: $k = \frac{\omega}{\sqrt{gH}}$

The solution depends significantly on the quantity kL . As $kL \rightarrow n\pi/2$ the response in the fjord becomes infinite because $\cos kL \rightarrow 0$. This is called *quarter-wave resonance*, and is the same resonance that you get when blowing over a bottle at the right frequency to make a

musical note. Any length L fjord with a depth H has *resonant frequencies* given by $\omega = \frac{n\pi}{2L} \sqrt{gH}$, where n is any integer. A useful way to think about this is that the response is a sine wave with wavenumber k , and if the mouth of the Inlet falls on a "node" of the sine wave, then a resonant response is achieved. As an example, consider a tide with $T = 12.4$ h in a fjord with a water depth of 200 m, then the wavelength of the wave is about 2000 km, and a resonant fjord would have a wavelength of about 500 km (or 1500 km, or 2500 km, etc, but those would be *very* long fjords!).

Note that as a fjord that is longer than $\lambda/4$ (but shorter than $3\lambda/4$) then the head of the fjord and the mouth are 180 degrees out of phase, with the head rising while the mouth sinks.

8.4.2 Frictional effects

A frictionless flow is often a reasonable approximation of a deep fjord. If there is friction, then the reflected wave is weaker than the incoming wave, and the tide will have a *progressive* character with phase changing as the wave propagates into the fjord. It is possible that the wave is damped completely so that there is no standing component, and the amplitude falls to zero at the head of the fjord.

8.4.3 Global response

The global response to tidal forcing is quite complex due to the bathymetry and shapes of the ocean basins (figure 8.12). In general, the tides create a wave that propagates clockwise around the basin in the northern hemisphere, and counter-clockwise in the southern. The clockwise circulation (NH) is because of the Coriolis force creating a wave that always has land on its right side (NH). This can be seen by the increasing value of the phase contoured in figure 8.12. The response is such that there are "nulls" in the pattern, called **Amphidromic points** where the amplitude of the tide is zero. Conversely the tides tend to be largest at boundaries of basins.

The surface M_2 tide in 4000-m of water has a wavelength of $\approx 8,800$ km, and the K_1 tide is 17,000 km, so a wave "fits" in the basins very imperfectly. You can see that, because of its longer wavelength, the K_1 tide has fewer amphidromic points than the M_2 tide.

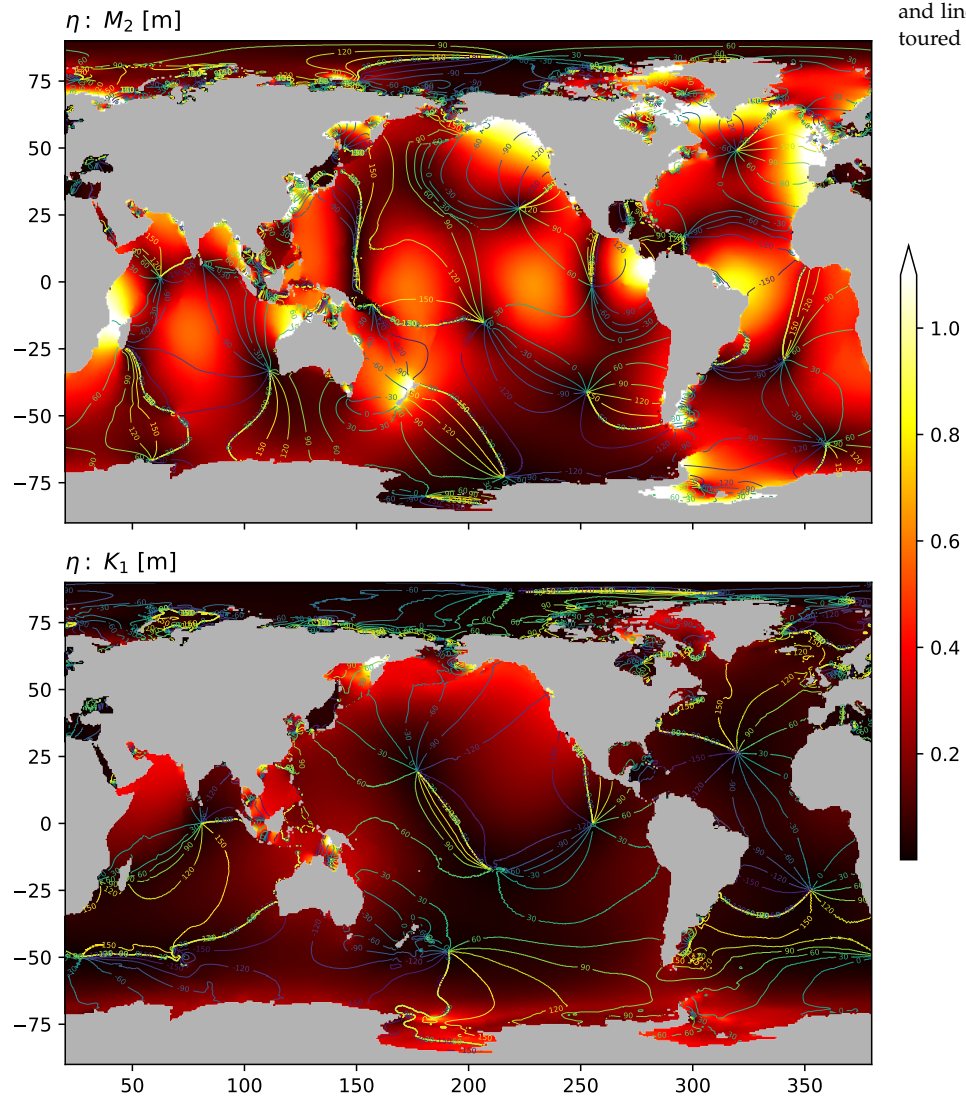
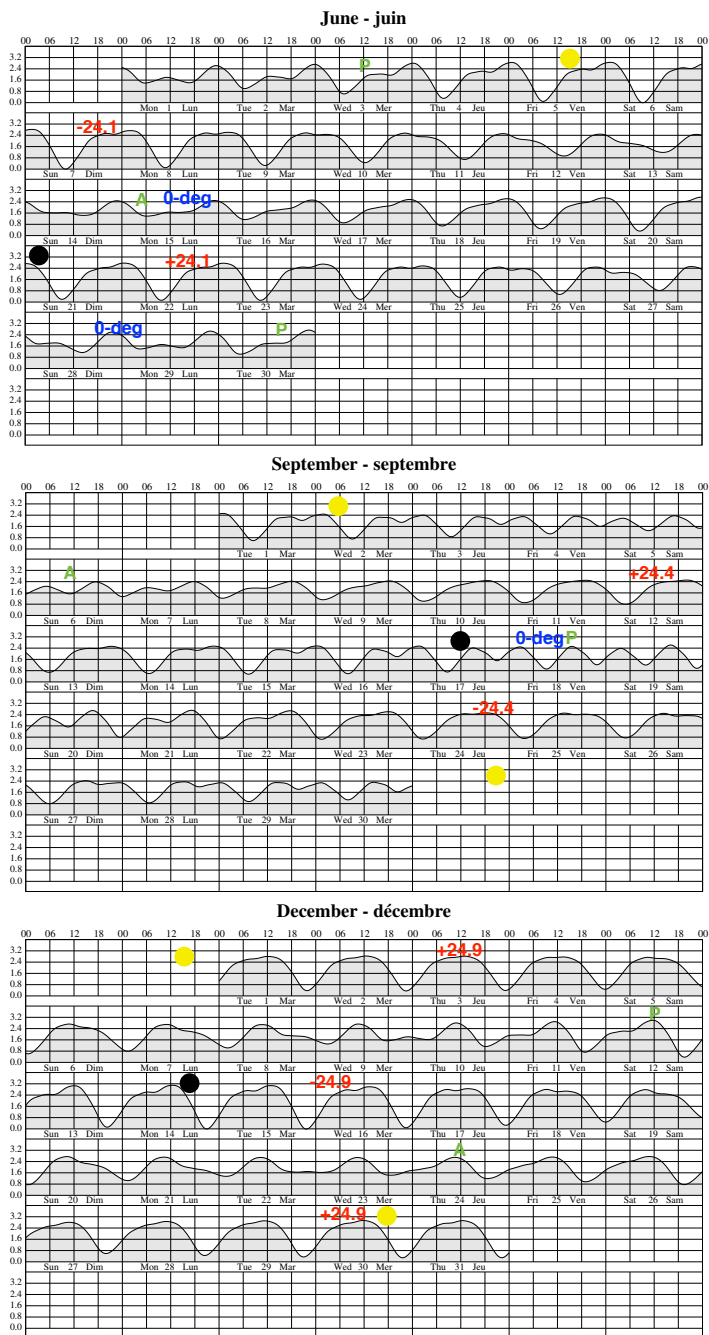


Figure 8.12: Amplitudes are coloured, and lines of constant phase are contoured in degrees.

8.5 Exercises

Consider the tidal calendars for Victoria BC, 2020. Full and new moons are marked (circles), lunar perigee and apogees are marked (P/A), as are the peaks of the moon's declination relative to the equator.



Using what you learned in this chapter, describe as many features

of the tides at Victoria as possible by comparing and contrasting the months, and the lunar and solar orbit characteristics.

Part III

Wind-driven circulations

9

Wind-driven circulation overview

As discussed the overturning circulation is rather weak in the global ocean, but is very important for the climate as that is how deep water stores heat and carbon. However, the major ocean currents (other than tides) are typically driven by the winds.

This chapter provides some data with minimal discussion that shows two example flows that we are interested in for the following chapters. The first is wind blowing along a coast. Such a wind drives coastal upwelling and downwelling and is very important for the ecosystem of the coast. The second is the large-scale circulation of the North Pacific basin.

9.1 Coastal upwelling

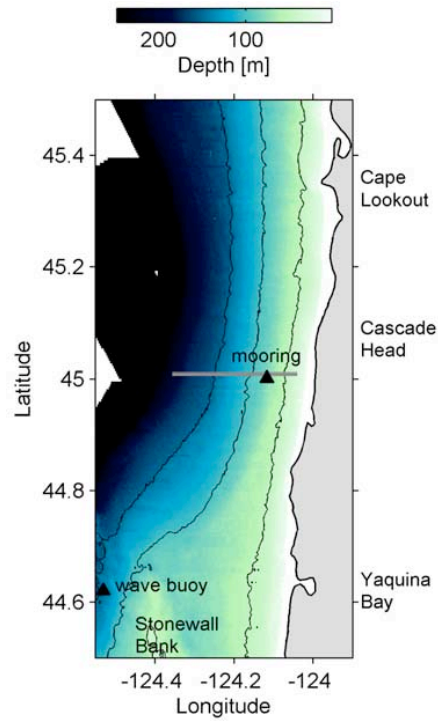


Figure 9.1: Location of coastal observations. A ship transited the line at 45 N repeatedly over an 8-day period.

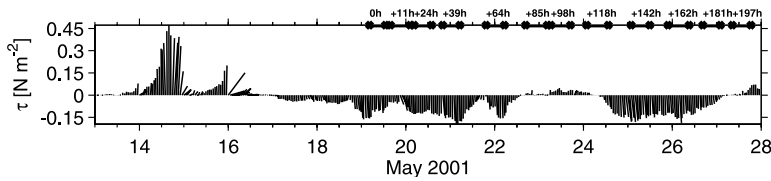


Figure 9.2: Wind stress arrows, where the wind direction is indicated by the arrow direction, and is mostly north (positive) and south (negative). During the cruise (dots along top axes), winds were mostly towards the south, except for a brief reversal 23-24 May.

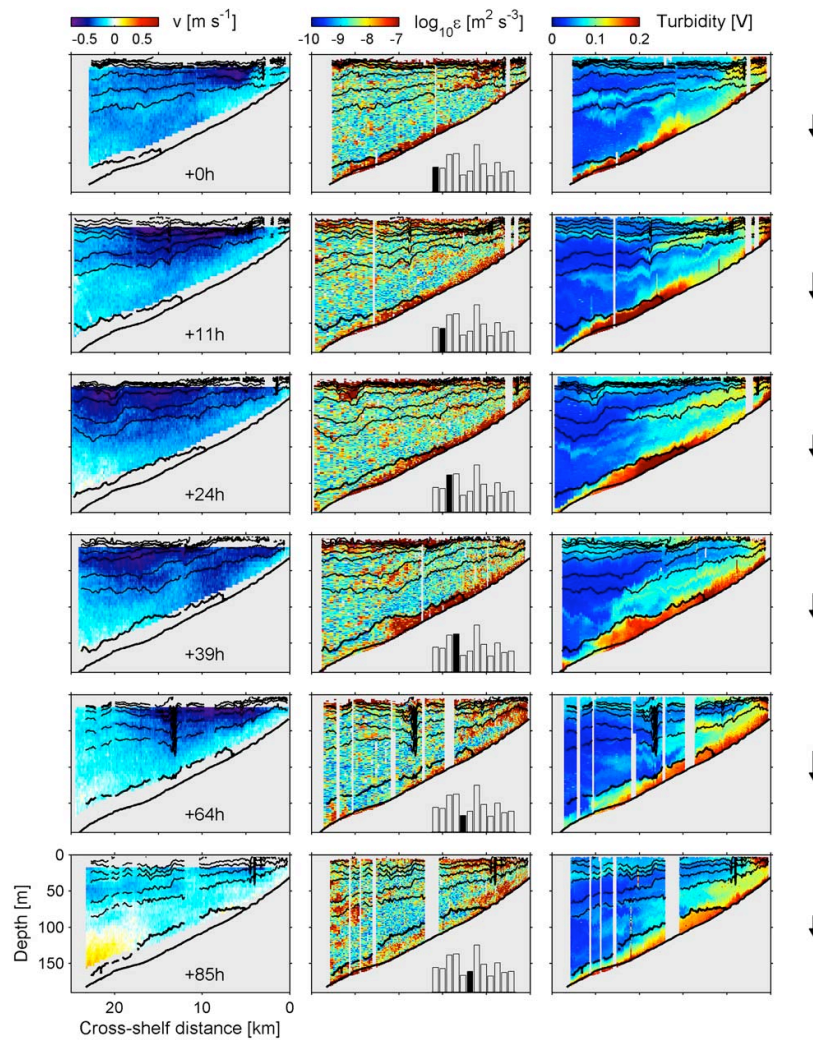


Figure 9.3: Observations from the ship. Black contours are potential density. The left column shows along-shelf current speed, blue meaning towards the south. The middle column shows the strength of turbulence in the water column, yellow/red being more turbulent. The right column shows turbidity, a measure of particles suspended in the water column. the arrows on the far right are the wind stress vectors.

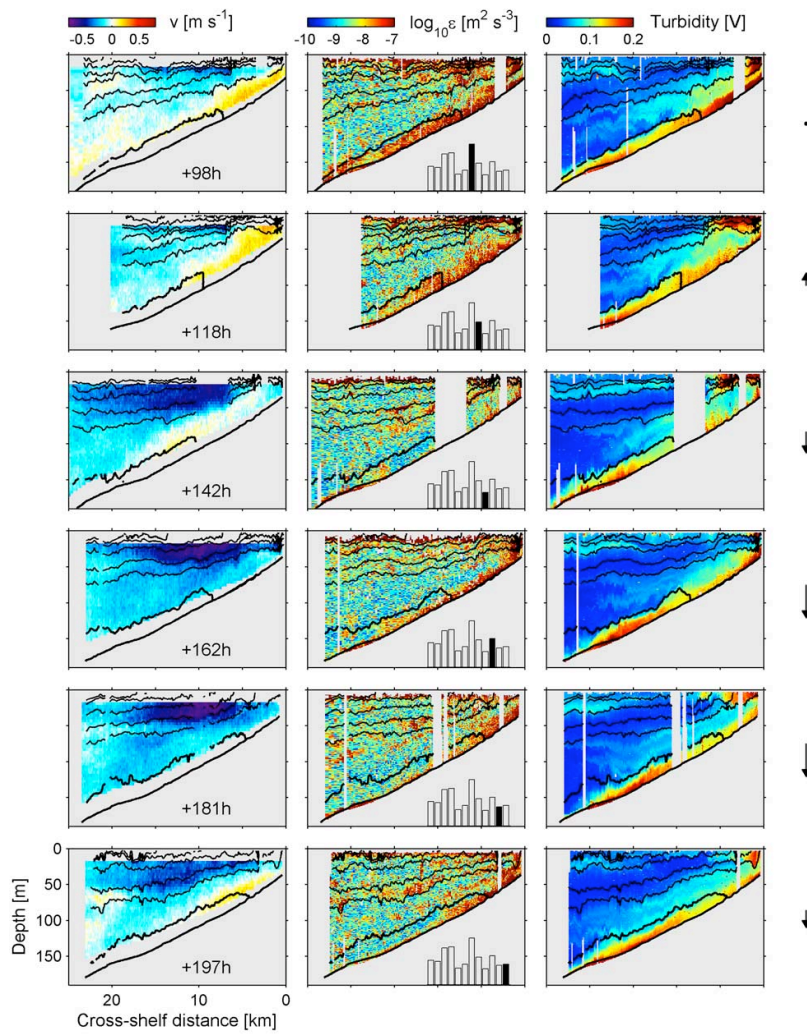


Figure 9.4: As in figure 9.3. Note the wind reversal and then resumption of wind blowing to the south.

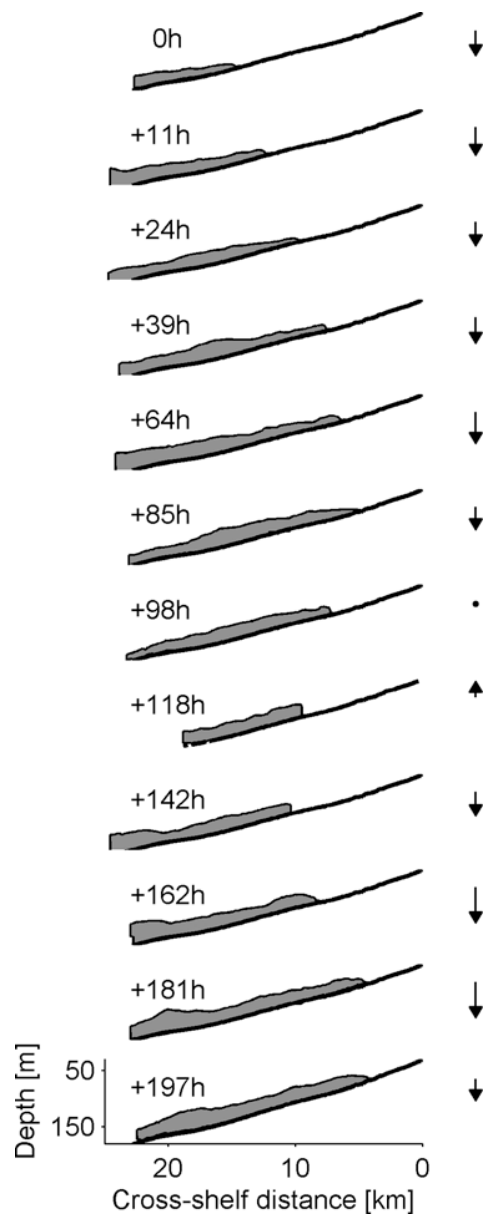
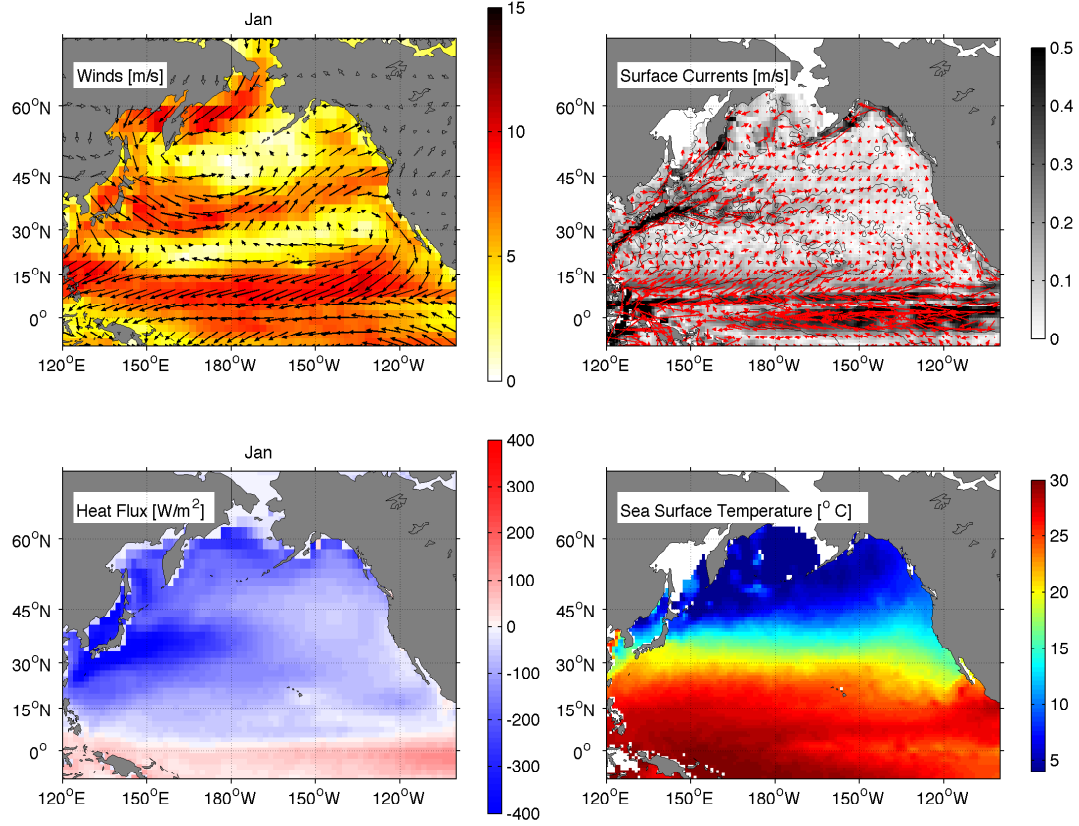
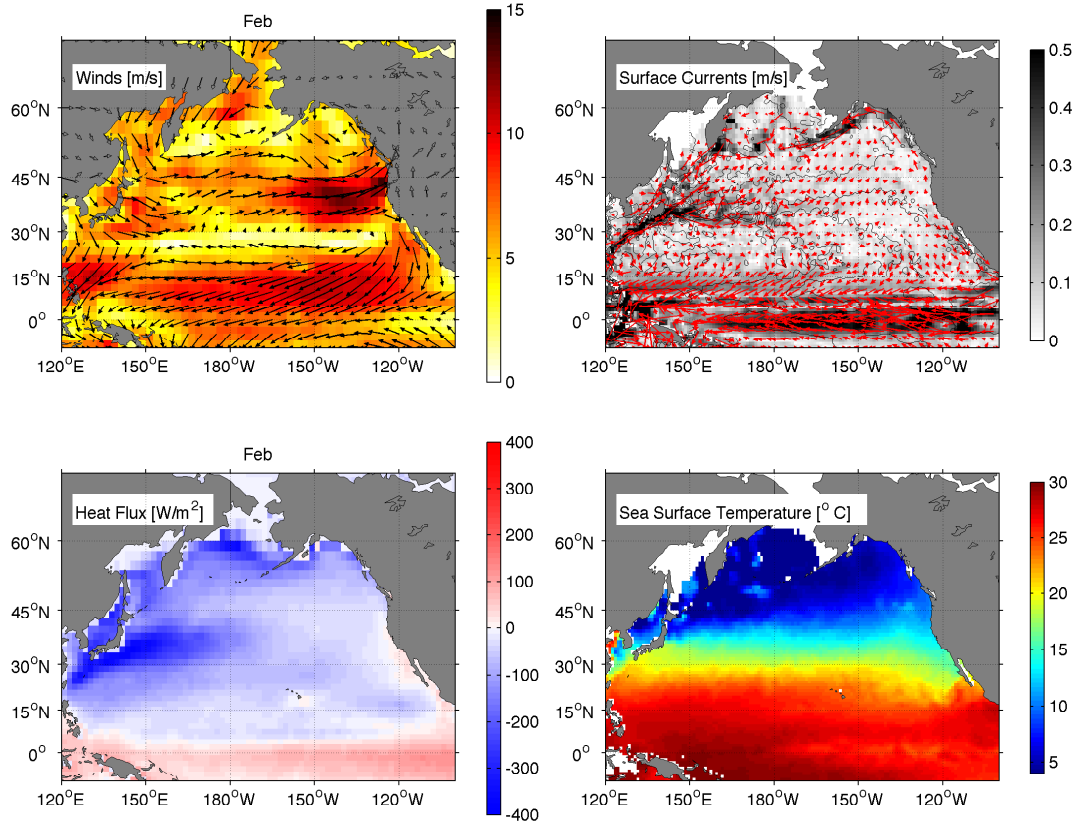
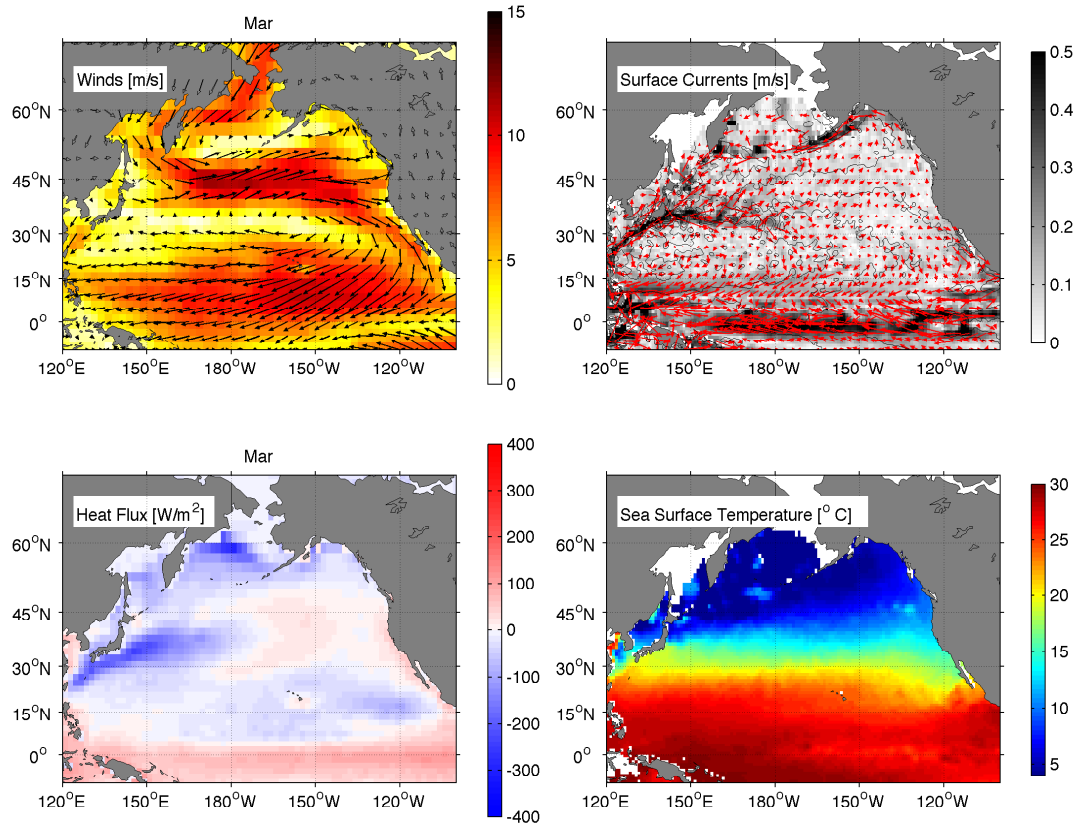


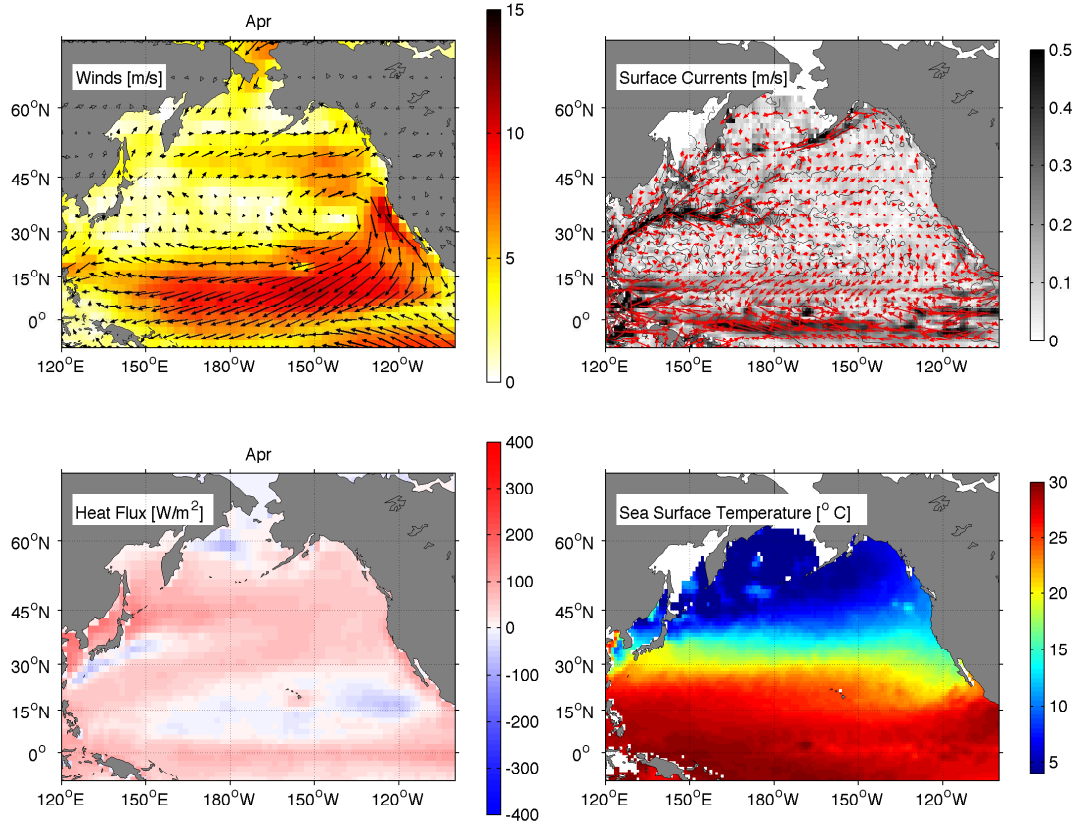
Figure 9.5: Same density data as figure 9.3 and figure 9.4, highlighting the motion of the bottom boundary layer up and down the shelf. During peak upwelling the speed is about 6 km/d.

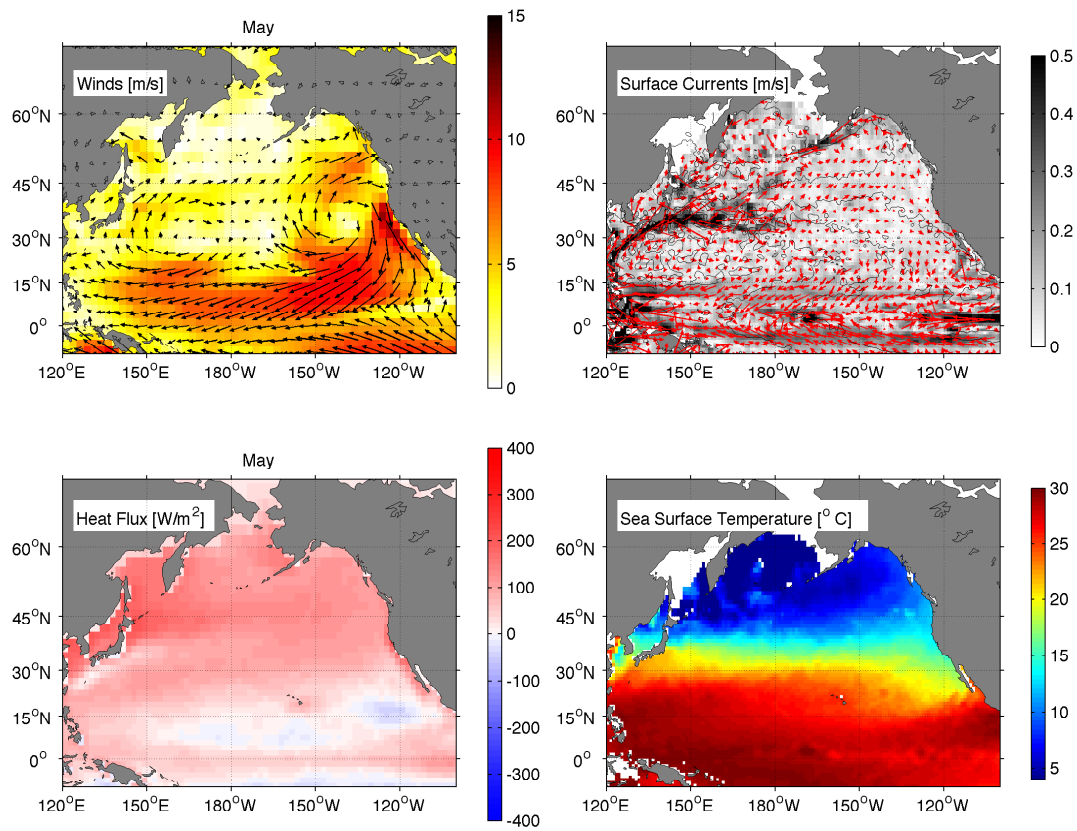
9.2 North Pacific observations

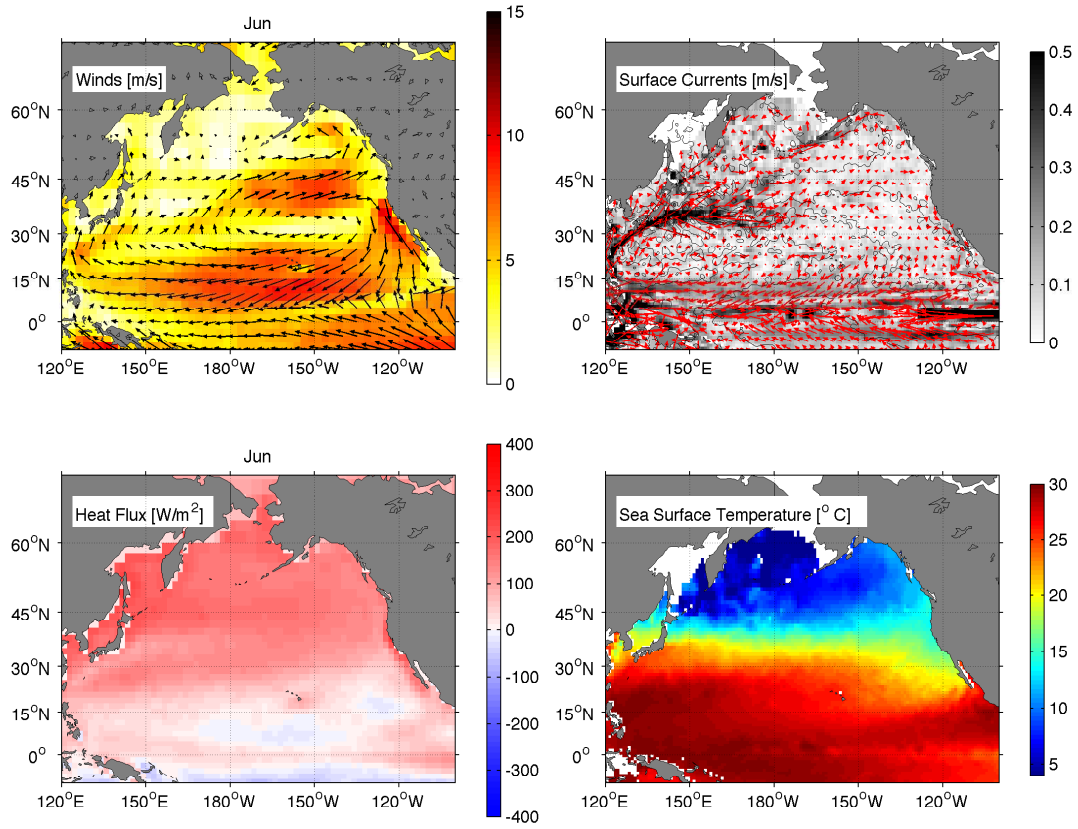


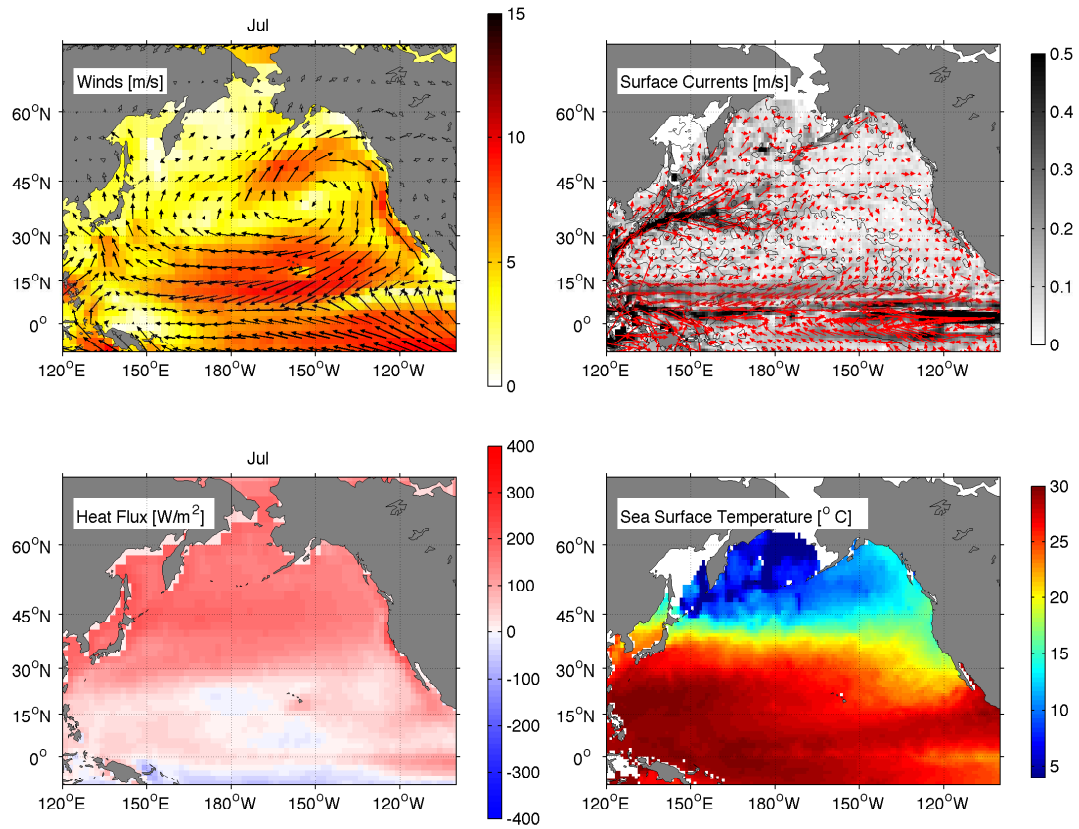


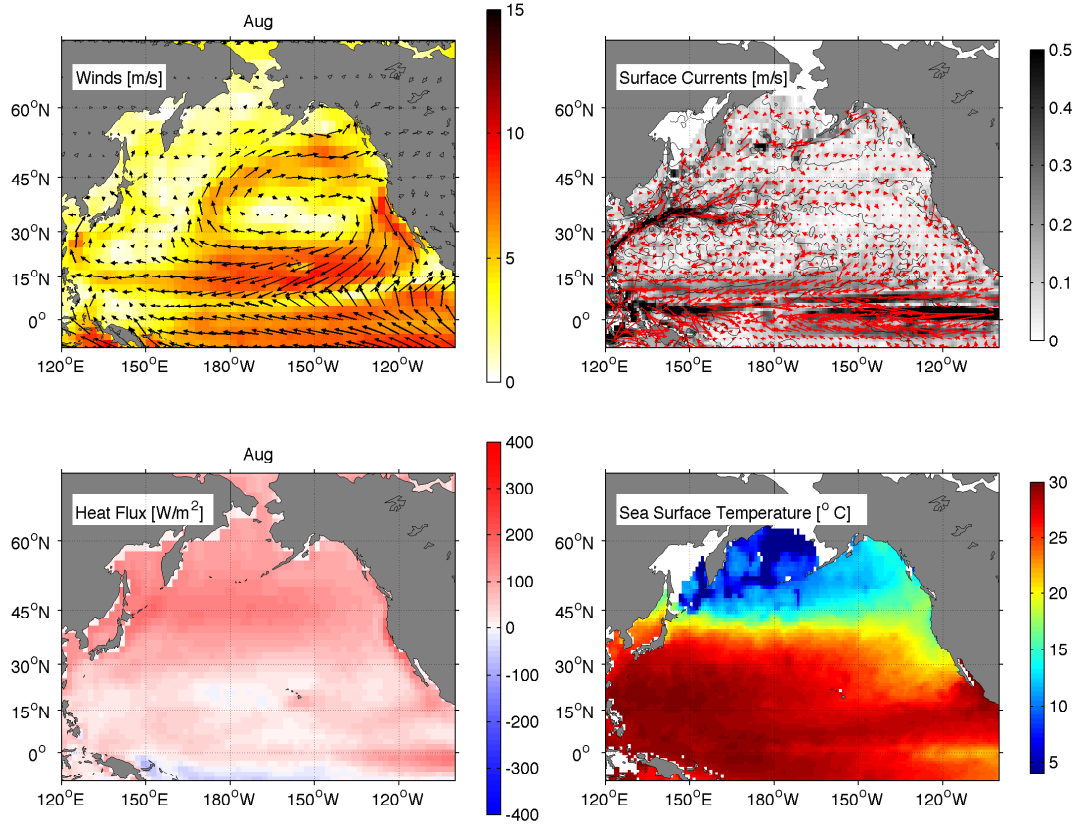


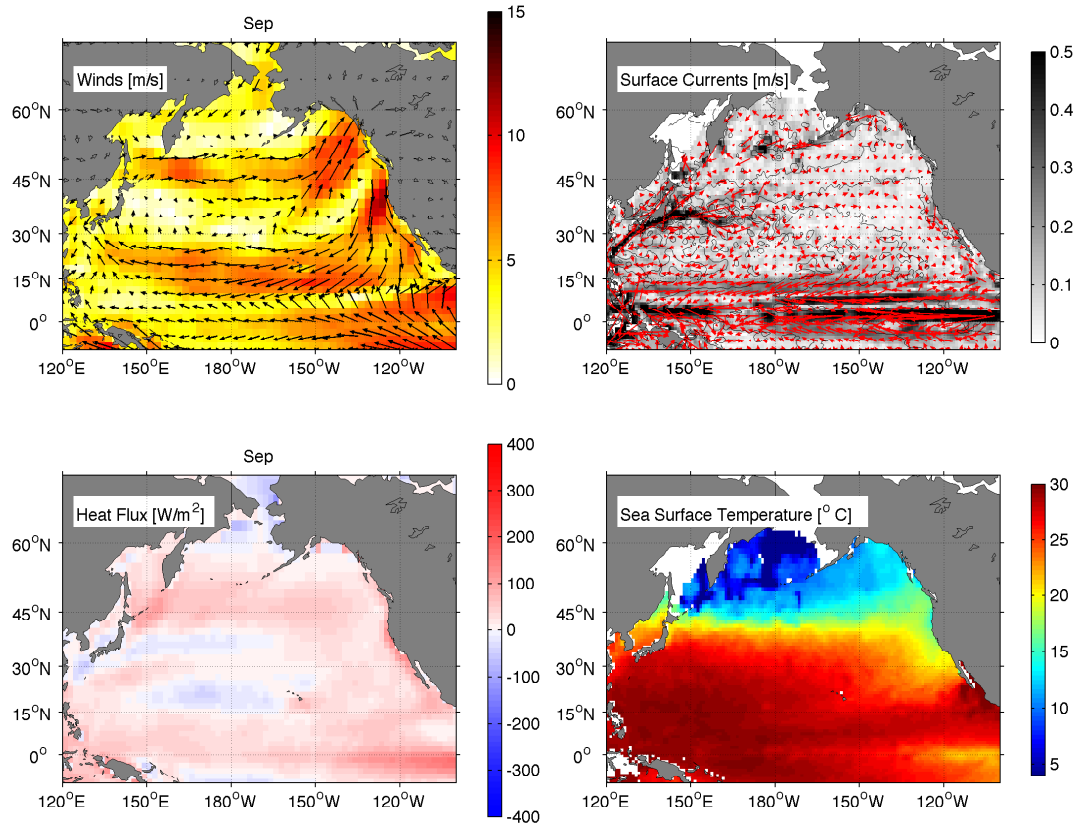


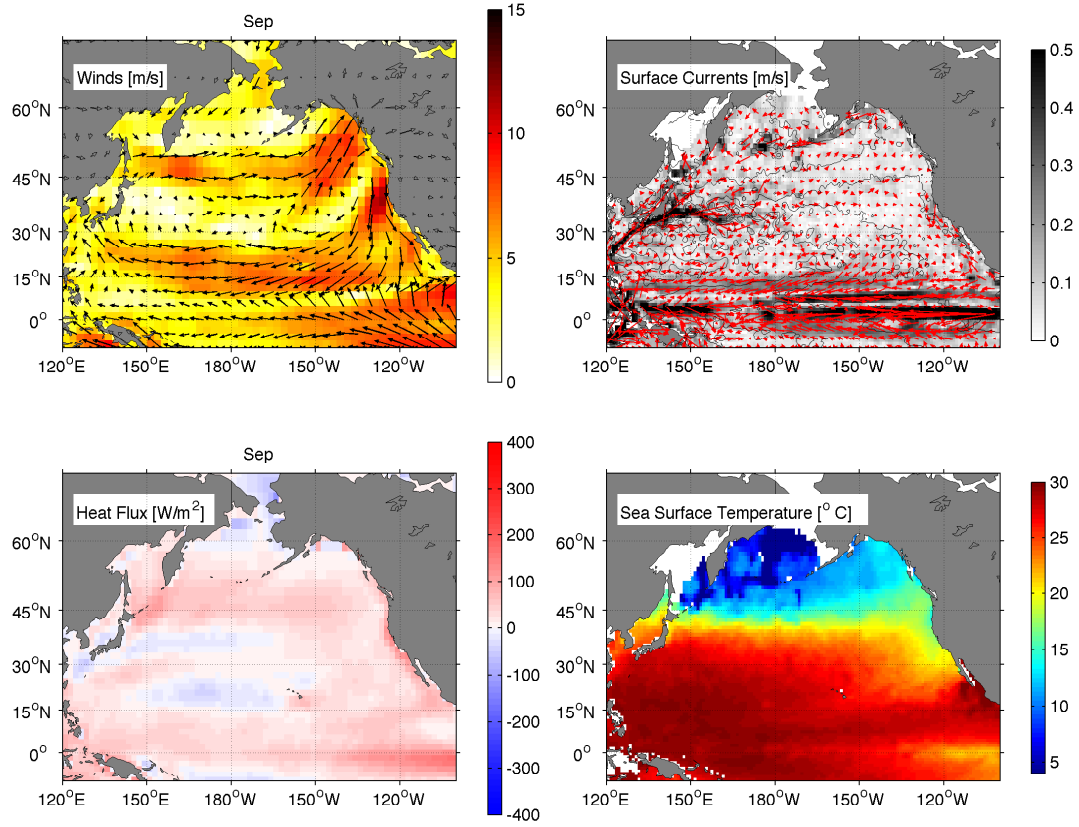


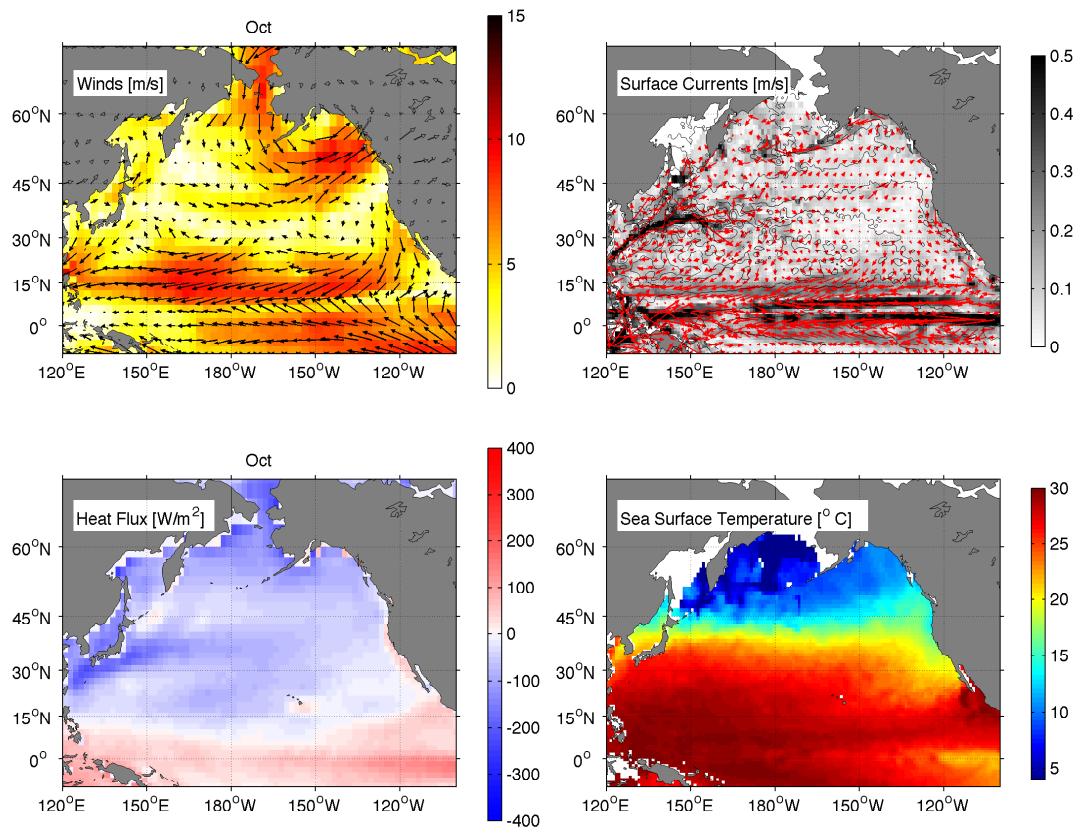


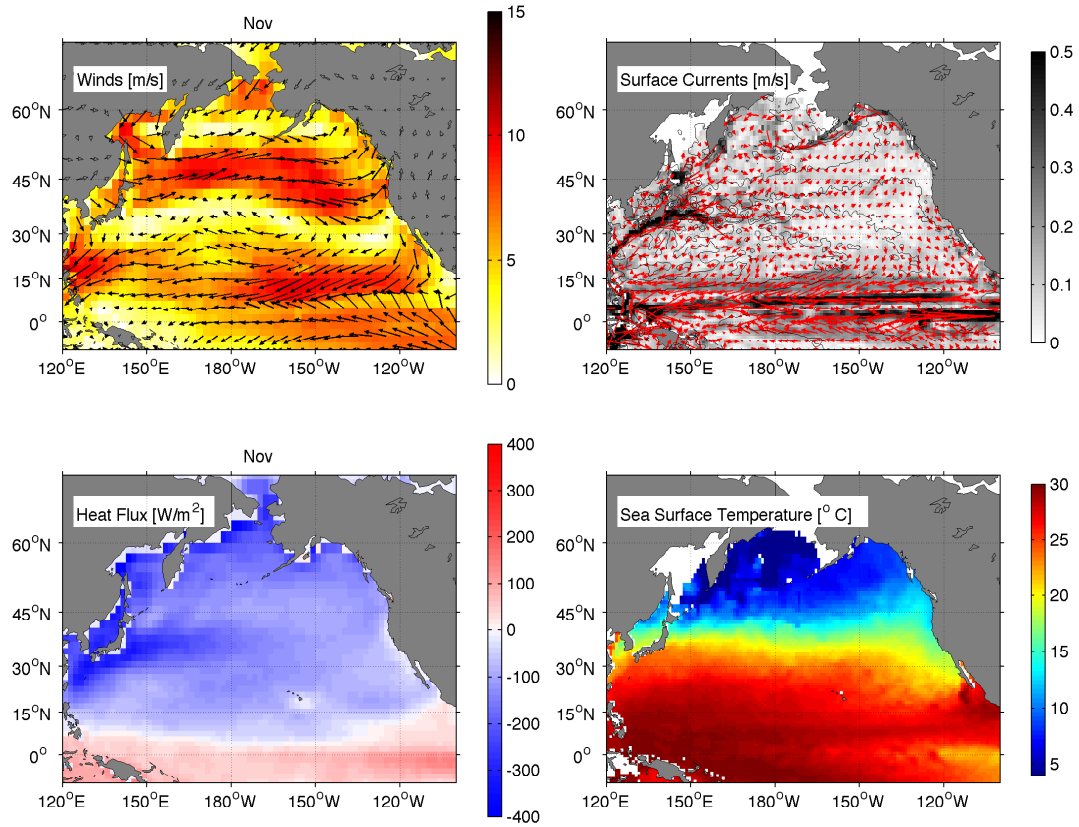


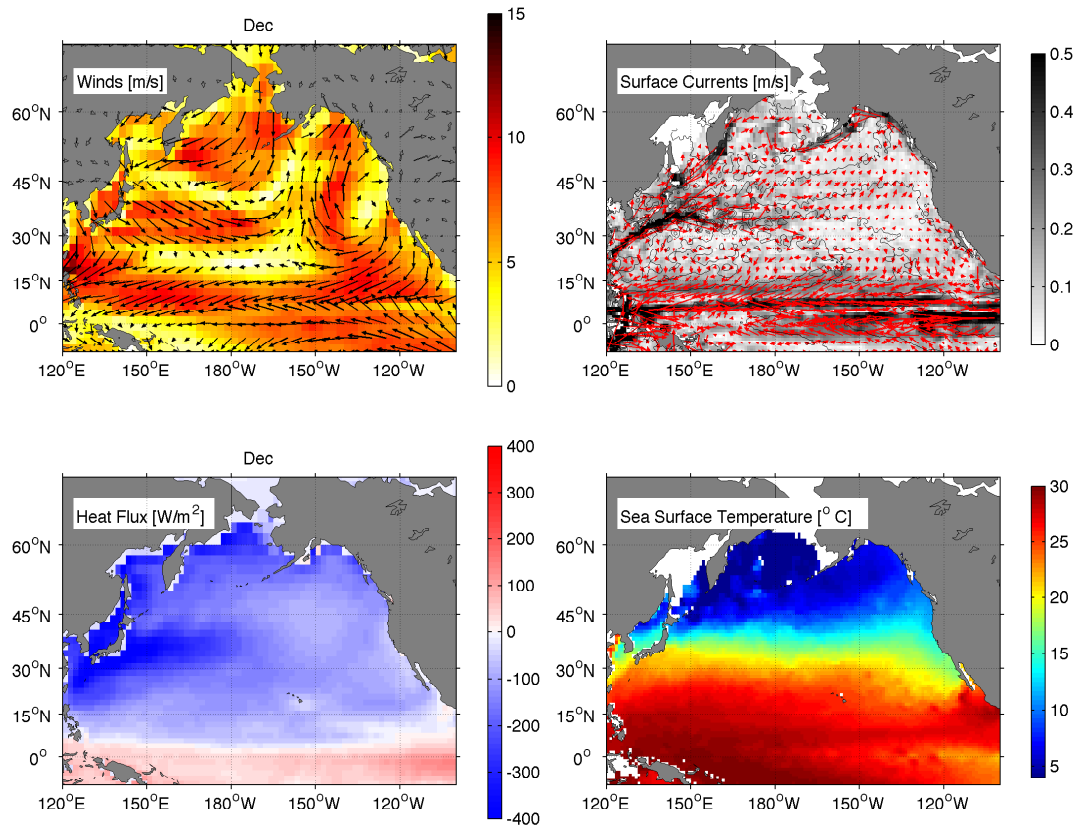












Coriolis force and Ekman Balance



The large-scale circulation of the ocean occurs on spatial scales spanning the size of ocean basins and temporal scales of hours to decades. On these scales, the earth's rotation matters at leading order to the dynamics of the motions, via an apparent force we call the **Coriolis force**.

10.1 Quick review of forces and apparent forces

First, it's helpful to quickly review forces, and then discuss what we mean by an **apparent force**.

Newton's second law says that the rate of change of a body's velocity (\mathbf{u}) is proportional to the *net* force exerted on it:

$$\sum \mathbf{F}_i = m \frac{d\mathbf{u}}{dt} \quad (10.1)$$

where we have used bold to remind ourselves that the *direction* of the force matters. As with concentrations, in fluid mechanics it is more natural to consider force per mass, or

$$\sum \mathbf{a}_i = \frac{d\mathbf{u}}{dt}. \quad (10.2)$$

It is possible for a body to have forces being exerted on it, but those forces be in “balance” so that the acceleration of the body is zero (or approximately zero). A common example from physics classes is a falling body that has reached its **terminal velocity**, which is a balance between the force of gravity pulling the body down, and friction resisting the downward motion:

$$\frac{dw}{dt} = -g + Fr \approx 0 \quad (10.3)$$

where w is the vertical component of velocity, and Fr is the wind friction at the terminal velocity (figure 10.1).

Newtons laws of motion apply to an **inertial reference frame**, i.e. a reference frame that is not accelerating. An east way to think about this is to consider a cup of coffee on the dashboard of your car. If you are travelling a constant speed, the coffee travels with your dashboard and there are the only forces on it are vertical (gravity and the normal force, figure 10.2, left-top). Now suppose the car accelerates with acceleration a . From an outside observer’s point of view, the cup continues to move at the same speed, but the car starts to accelerate away from the coffee cup (figure 10.2, left-middle sketch). However, if you are sitting in the car, it is like a force pushed the cup so that it accelerates towards the back of the car (figure 10.2, left-bottom sketch). This would be an **apparent force** in the accelerating reference frame of the car.

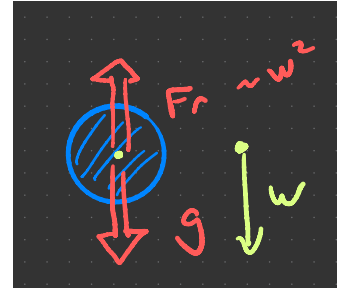


Figure 10.1: Sketch of terminal velocity force balance. In balance, the gravity force g is equal and opposite to the friction force (Fr).

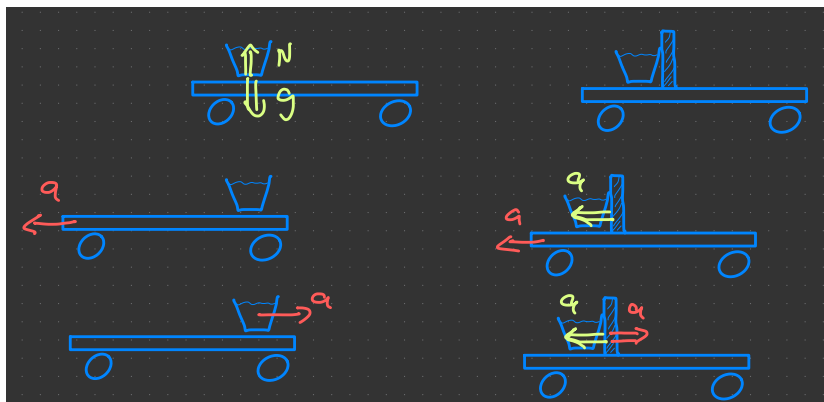


Figure 10.2: Apparent force on a cup in a car. Left side are frictionless cups (or a ball if you prefer) on an accelerating car. Right hand side is a cup held laterally by a cup holder.

If the cup moves with the car, then something has to supply a lateral force to cause that acceleration. So, imagine a wall that the coffee can push against, or a cupholder (figure 10.2, top-right). From an outside observers point of view, there is only one force acting on the cup, a to the left supplied by the cup holder, accelerating the cup at the same rate the car is being accelerated. However, someone

inside the car may very well feel that there is a force pushing the cup to the back of the car, and infer an equal-and-opposite force towards the front, so the cup does *not* accelerate in this frame of reference.

Hopefully this change of reference frames makes sense to you. If you are sitting in a car and the driver slams on the brakes, you don't say that you were "slowed down more slowly than the car", you say that you were "thrown forward". Of you accelerate very quickly, you say you were "pushed back in your seat".

The application to the earth is hopefully obvious - the earth is constantly rotating, and hence any point rotating with the earth is constantly changing its velocity (but not its speed!), and hence the rotating frame is not an inertial frame of reference.

10.2 Centrifugal and Coriolis forces

A rotating reference frame gives rise to *two* apparent forces, the **centrifugal force** and the **Coriolis force**. The centrifugal force is felt everywhere on the planet and is a constant that depends on position, so we actually roll it into our definition of gravity and promptly forget about it (except perhaps on an exam). The Coriolis force only arise if a body is moving relative to the rotating frame.

In oceanography, when we say a parcel of water moves at 1 m/s, it is doing so in the rotating frame. From space it is moving at 132 m/s (at 49 N), where most of that is the earth's rotation. Doing everything from a frame that is out in space is possible, but extremely awkward!

10.2.1 Centrifugal force

The earth spins about its axis every 24 h, such that it spins counter clockwise when looking down on the north pole. Because this is an important constant it gets a capital $\Omega = 2\pi/24h = 7.27 \times 10^{-5} \text{ rad s}^{-1}$. The radius of the earth is $R = 6731 \text{ km}$, and the radius at any given latitude λ is given by $r = R \cos(\lambda)$. As pointed out in Box 8.2.1, the linear speed of a particle is given by ωr and the velocity is tangential to the circle. The acceleration needed to keep going in a circle is readily shown to be $a_c = r\omega^2$. A mass on the rotating system that suddenly becomes unglued will be flung away from the axis of rotation, and we call this the **centrifugal force** (figure 10.3).

So, as you sit in your chair (or comfy sofa) reading this, what keeps you rotating around the axis of the earth's rotation? There needs to be a centripetal force to counteract the centrifugal force that wants to fling you into space. This force, at 49 degrees of latitude is

$$a_{cent} = R \cos(\lambda) \omega^2 = 0.0107 \text{ m s}^{-2} \quad (10.4)$$

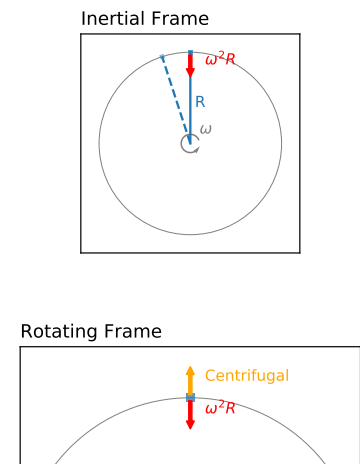


Figure 10.3: Forces on a rotating reference frame observed from an inertial reference frame (i.e. from space). There needs to be a centripetal force applied to any object going around the circle or it will be flung off the orbit. An observer in the rotating frame sees two forces: the centripetal force and an apparent centrifugal force that works against the centripetal force to keep the body in place on the rotating frame.

so its small compared to gravity, but is not non-zero. You may argue that it is friction with your chair that keeps you in place, but that doesn't apply if your chair has wheels, or to a hockey puck on an ice rink. The answer is that the earth is not a sphere, and bulges out at the equator, precisely because it is spinning; the equatorial radius is 22 km more than the polar radius.

This leads to a centripetal force because there is an imbalance between the normal force exerted by the earth's spheroidal surface and the direction that gravity points. First, consider the forces on a body sitting on a perfect sphere as observed from an inertial frame (i.e. space; figure 10.4 left panel). There are two real forces acting on the body - gravity pulls towards the center of the earth, and there is a normal force due to the body of the earth that pushes back. Because this is a perfect sphere the normal force is in the same direction as the gravity force, pointing away from the center of the sphere. Combined, then there are no net forces on the object, and hence the object will *not* orbit with the spinning of the earth.

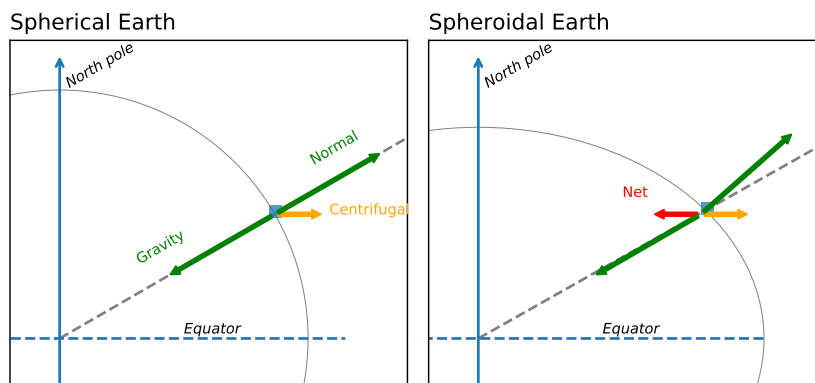


Figure 10.4: Left panel: forces on an object on a perfect sphere. There is a normal force that is exactly equal and opposite to the gravity force because the normal on a perfect sphere points towards the centre of the sphere. Right panel: the same forces on an oblate spheroid; the normal force and the gravity force are at angles to one another leading to a net force towards the axis of rotation.

Naturally, this does not happen on the real earth - if somehow we started with a spinning perfect sphere earth it would tectonically shear apart until it made a bulge at the equator that balanced the spinning. Such a bulge is in rotational equilibrium when the normal force at any point on its surface points at an angle to the center of the earth so that the sum of the two forces result in a net force towards the axis of rotation (figure 10.4, right panel). The faster a planet spins, the larger this bulge is. Of course there are irregularities on a real planet, like mountains, but if you put your chair on the mountain side, you would roll off.

Now consider a plumb bob hanging above the surface of the earth.

It is *not* just pulled down towards the center of the earth, but also is flung out slightly by the centrifugal acceleration. Hence it will fall parallel to the normal line in figure 10.4, (right side), and not towards the center of the earth. Hence we call this direction "down" and "up" and we slightly modify the value of gravity to account for the centrifugal acceleration. Hence you will find gravity calculators that depend on the latitude λ .

10.2.2 Coriolis force

The **Coriolis force** is the second apparent force in a rotating reference frame. It only occurs if the object has a velocity relative to the rotating frame. It is quite unintuitive, and has no easy analogue like in the accelerating car. i.e. the cup feels the same acceleration whether it is already moving in the car or not.

The Coriolis force acts exactly 90 degrees to the right of the velocity vector in the Northern hemisphere, and to the left in the Southern. The strength of the force is linearly proportional to the velocity:

$$|\mathbf{F}_{\text{Coriolis}}| = f|\mathbf{u}| \quad \text{to the right of } \mathbf{u} \quad (10.5)$$

Understanding how this force arises is not terribly difficult (and the math is even easier if you know some vector calculus). First, consider a hockey player shooting a puck along a frictionless ice rink. That person is rotating on the earth, and hence is being pulled into the center of the earth by the net centripetal acceleration (figure 10.5). You can think of this as the summation of two vectors, the tangential motion of the hockey player at travelling a distance $\omega r \delta t$, and the motion towards the axis of rotation $0.5\omega^2 r \delta t^2$.

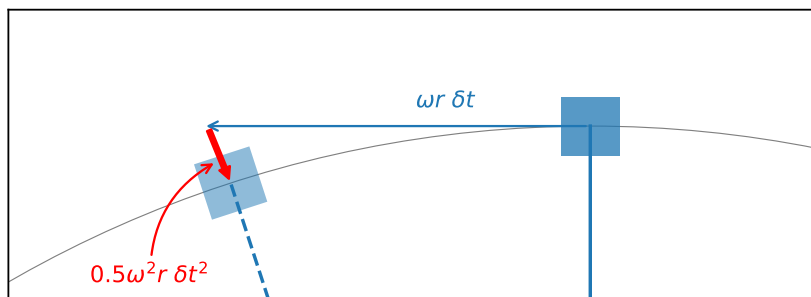


Figure 10.5: Forces on a person who is stationary in the rotating frame.

Now, suppose they aim the puck away from the axis of motion, which on the northern hemisphere is like aiming at a target to the south (figure 10.6). Note that the target moves further to the left than

the hockey player, and then is pulled back into orbit by a stronger centripetal force because it is further from the axis of rotation. The hockey player shoots the puck with enough velocity to hit the target, and the aim directly away from the axis of rotation.

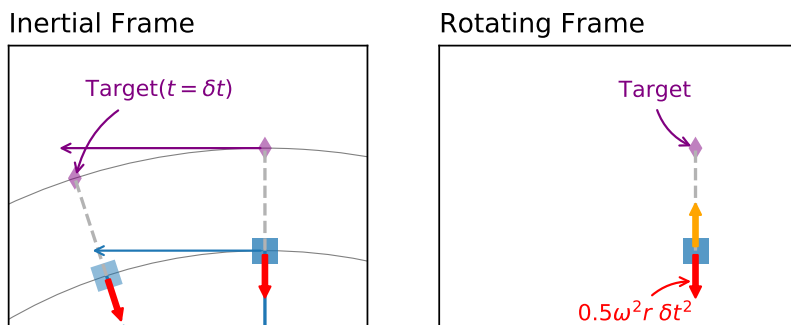


Figure 10.6: Left panel: forces in the inertial frame of a hockey player aiming at a target further from the axis of rotation. Note that the target has a *faster* tangential velocity than the hockey player. Right panel: setup in the rotating frame observed by the hockey player.

What happens when the player shoots the puck is that everything continues to rotate because of the centripetal force, but the puck does not have enough tangential velocity to hit the target. In figure 10.7, the puck ends up at the summation of three vectors - the first two are (ahem, almost) the same as the hockey players, the tangential distance $\omega r \delta t$, and the motion towards the axis of rotation $0.5\omega^2 r \delta t^2$. The third is the velocity component $U \delta t$ imparted by the player when they shot the puck. Adding these three together, it should be clear that the puck can't keep up with the target, and ends up "behind" it, or to the right of the velocity (figure 10.7, Rotating Frame).

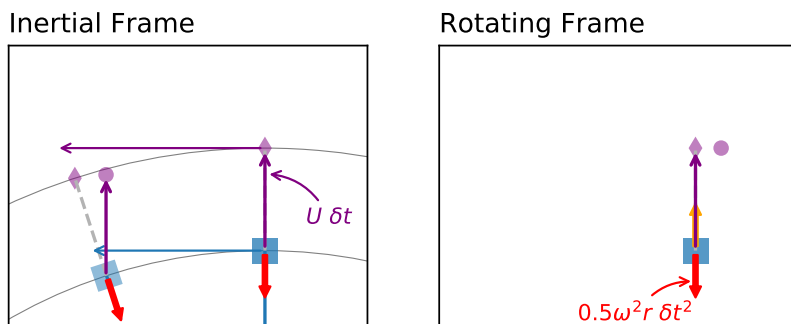


Figure 10.7: Left panel: The result of the shot after a time δt in the rotating frame, where the circle is the puck. the puck doesn't have enough velocity to the "left" to keep up with the target and falls behind. Right panel: in the rotating frame, the puck veers to the right of the target.

Why does a greater velocity result in a greater Coriolis force? Quite simply the puck would get further away from the axis of ro-

tation in time δt , and would fall even further behind the new, more distant target.

A similar effect happens if the throw is in the tangential direction. In this case this would be to the “east” if the shot was taken in the Northern hemisphere. In this case, the puck is given too much tangential velocity (figure 10.8). It still gets pulled in towards the axis of rotation the same amount as the hockey player, but it has more tangential velocity so it ends up further from the axis of rotation. The hockey player sees it fly to the right.

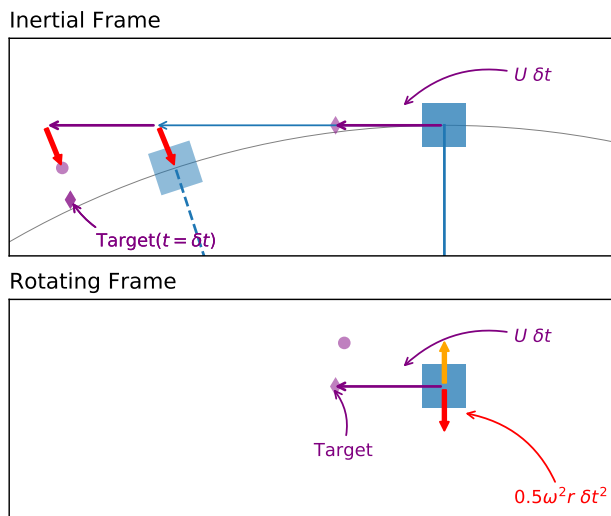


Figure 10.8: Upper plot: a shot in the same direction as rotation. The puck has (approximately) the same centripetal acceleration towards the axis of rotation, but has too much momentum to be pulled back to the original orbit, and hence moves in a net sense away from the axis of rotation. Lower plot: as observed by the hockey player, the puck veers to the right of the target.

the astute reader will note that the puck now has a component of velocity that has turned to the right of its original motion. This should mean the Coriolis force turns to the right at the same time. Indeed what happens is that the Coriolis force pushes the particle around a circle with a frequency given by the proportionality constant f . This type of motion is regularly seen in the ocean (figure 10.9), and is called an **inertial oscillation**.

It is interesting to note that the Coriolis force is the same *everywhere* in the rotating reference frame, and depends only on the velocity and the angle of the velocity with the axis of rotation. However, as the earth is a sphere, and we specify our velocities as horizontal velocities along the sphere (eastward: u , northward: v) and upwards perpendicular to the geoid (w). Usually the Coriolis force due to motions in the vertical is very small ($w \ll u$), so we only deal

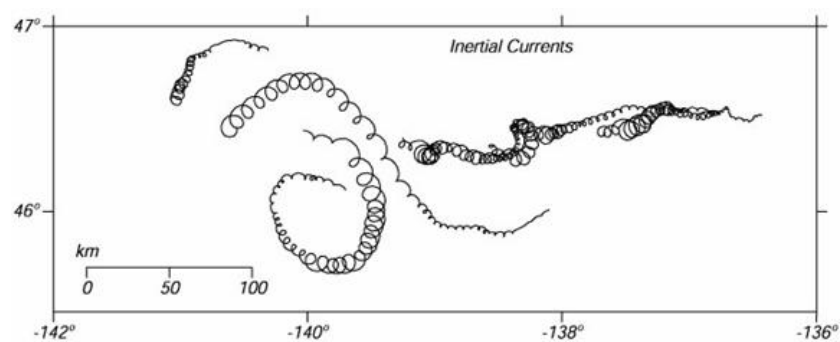


Figure 10.9: Response of surface drifters in the ocean to a sudden windstorm. Note the circular motion superimposed on the mean currents.

with the horizontal terms, but these make an angle to the axis of rotation everywhere on the sphere, except right at the poles. That angle means that the horizontal component of the Coriolis force is $f = 2\Omega \sin \lambda = 1.45 \times 10^{-4} \text{ rad s}^{-1}$, where λ is the latitude. So, $f = 2\Omega$ at the north pole, 0 at the equator, and -2Ω at the south pole. At the mid latitudes ($\lambda = 45^\circ \text{ N}$) $f \approx 10^{-4} \text{ rad s}^{-1}$.

The minus sign in the southern hemisphere means that inertial motions are counter clockwise. This is just because "up" points closer to the south pole than towards the north pole. A puck pushed eastward in the southern hemisphere is still flung away from the axis of rotation, its just that away from the axis of rotation in the southern hemisphere means moving northward instead of southward. You can also think of this as looking down at the earth spinning from the south pole, in which case it appears to turn clockwise and we can think of the rotation rate as being $-\Omega$.

Mathematically, we write the horizontal equations of motion as

$$\frac{du}{dt} = +fv - \frac{1}{\rho} \frac{dP}{dx} + \sum F_x \quad (10.6)$$

$$\frac{dv}{dt} = -fu - \frac{1}{\rho_0} \frac{dP}{dy} + \sum F_y \quad (10.7)$$

where F_x and F_y are the friction forces in x and y .

Box 10.2.1: Non-linearity of equations of motion

The equations in equation (10.6) are adequate for our needs, but note that these are the equations following a parcel of water, just like in classical mechanics how we would follow the forces on a single ball. In fluid mechanics we call this the **Lagrangian reference frame** and usually specify with a capital D instead of lower case d (i.e. $\frac{Du}{Dt} = \dots$).

However, we usually cannot follow a parcel of water, so the derivatives at a point have terms that are due to the water moving from one point to another. This is called the Eulerian reference frame, and is what makes water flow so complicated because there are nonlinear terms:

$$\frac{Du}{Dt} = \frac{\partial u}{\partial t} + u \frac{\partial u}{\partial x} + v \frac{\partial u}{\partial y} + w \frac{\partial u}{\partial z} \quad (10.8)$$

Including these terms makes mathematically solving the equations of motion very difficult!

10.3 Friction force

Now we only need to consider the final terms in equation (10.6), the friction forces. Friction forces are quite complicated in general, but let's consider a simpler flow. Suppose there is a flow in the x -direction, and that it has **shear** in the vertical such that the faster flow is above the slower (figure ??). Because the fluid is viscous, the faster flow above will exert a stress to the right on the flow below, and the slower flow will exert a stress to the left on the faster flow. This will decelerate the upper flow and accelerate the lower flow (figure 10.10). This transfer of momentum occurs at a rate proportional to the shear and the viscosity of the fluid:

$$\frac{\tau_{xz}}{\rho} = \nu \frac{du}{dz} \quad (10.9)$$

where the subscript xz means transfer of x momentum in the z -direction. Here ν is the kinematic viscosity and has a molecular value of $\nu \approx 10^{-6} \text{ m}^2 \text{ s}^{-1}$. Note that the units are the same as for a diffusion co-efficient, and can be thought of as a diffusion of x -momentum in the vertical.

The net force at any point depends on the difference of the stresses in the vertical (figure 10.11). The parcel gains momentum from above, but loses it below. So in this simplified flow

$$F_x = \frac{1}{\rho} \frac{d\tau_{xz}}{dz} + \text{other friction in } x = \nu \frac{d^2u}{dz^2} + \text{other friction in } x \quad (10.10)$$



Figure 10.10: Left: Velocity in x-direction with faster flow above slower (blue arrows). Right: velocity after there has been a downward transfer of x-momentum (τ_{xz}); the faster velocity has slowed, and the slower velocity accelerated.

So just like for diffusion, the flow needs to have some curvature ($\frac{du}{dz} \neq 0$) for there to be a net effect on the velocity due to friction.

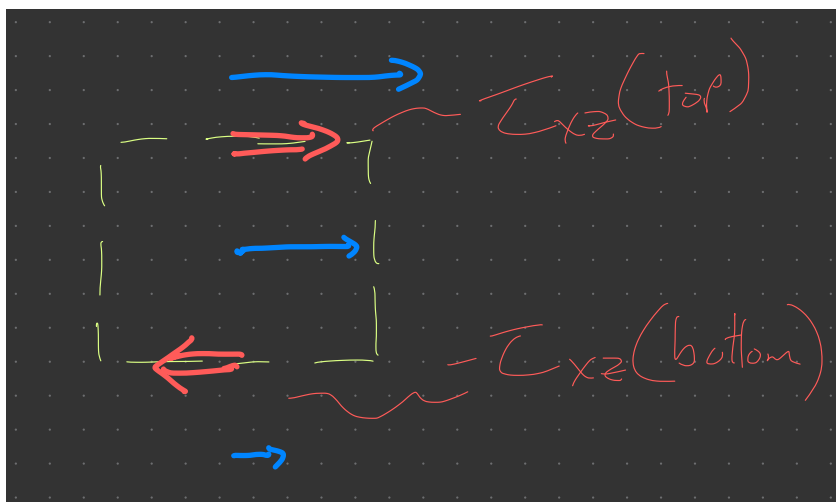


Figure 10.11: Net stress on a parcel (yellow dashes) in a sheared flow (blue velocity arrows) is the difference in the stress from top to bottom (red arrows). The water above speeds up the parcel, but the water below slows it down.

X-direction momentum doesn't just diffuse in the vertical direction. If we re-drew figure 10.10 with y replacing z the same physics would apply, and similarly in the x-direction, so the full value of of the friction in x is:

$$F_x = \frac{1}{\rho} \left(\frac{d\tau_{xz}}{dz} + \frac{d\tau_{xy}}{dy} + \frac{d\tau_{xx}}{dx} \right) \quad (10.11)$$

and similar equations apply for F_y and F_z , leading to nine total terms.

10.3.1 External stresses

Water can have one of two boundary conditions - constant velocity (usually not moving), or constant stress. Constant velocity means that

at the boundary the fluid moves with the boundary, and is usually applicable to solid boundaries.

Constant stress is often applied at the air-sea boundary as a “wind stress”. As the wind blows over the top of the ocean, it imparts some momentum to the ocean (and vice-versa). We usually use the symbol τ_x^w for the x-direction wind stress and τ_y^w where it is understood that the stress is being transmitted vertically.

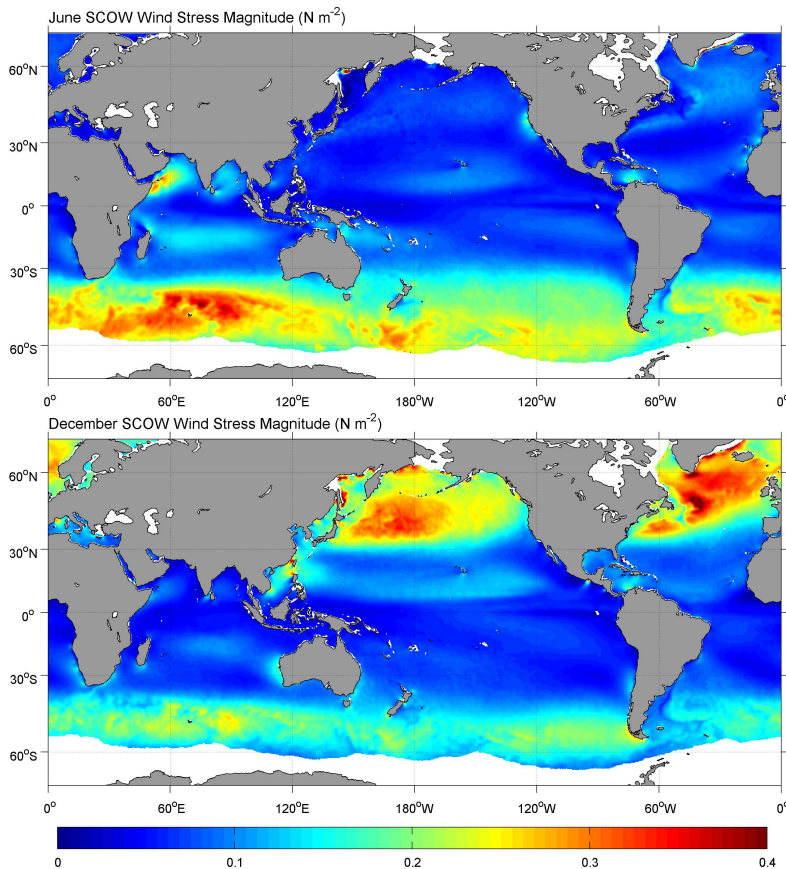


Figure 10.12: Wind stress amplitude, averaged for June and December.

10.4 Ekman balance

In physics it is often helpful to determine if a steady state exists. In physical oceanography this means times when $du/dt = 0$. We saw in the previous chapter that the flow in the large-scale ocean actually *does* change relatively slowly, so on long time scale this is approximately true. Even in the coastal flow, the flow evolved slowly enough that the dominant balances are obeyed. There are two such

balances. The Ekman balance is between the Coriolis and friction and friction forces, and the **Geostrophic balance** is between Coriolis and the pressure gradient force:

$$\frac{du}{dt} = \underbrace{-\frac{1}{\rho_0} \frac{dP}{dx} + fv + \frac{1}{\rho} \frac{d\tau_{xz}}{dz}}_{\text{Ekman}} \quad (10.12)$$

$$\frac{dv}{dt} = \underbrace{-\frac{1}{\rho_0} \frac{dP}{dy} - fu + \frac{1}{\rho} \frac{d\tau_{yz}}{dz}}_{\text{Ekman}} \quad (10.13)$$

Here we discuss the first of these two balances, the Ekman balance.

The Ekman balance typically occurs near the boundaries where the shear stresses in the ocean are the largest. In this region we assume that the friction is balanced by the Coriolis force, and ignore the pressure gradient force:

$$\frac{1}{\rho} \frac{d\tau_{xz}}{dz} = -fv \quad (10.14)$$

$$\frac{1}{\rho} \frac{d\tau_{yz}}{dz} = -fu \quad (10.15)$$

The stress profile can be complicated, but if we integrate from some depth where $\tau_{xz} = 0$, say at $z = -D$ to the sea surface, then we can write:

$$\frac{1}{\rho} \tau_x^w = -f\bar{v}D \quad (10.16)$$

$$\frac{1}{\rho} \tau_y^w = f\bar{u}D \quad (10.17)$$

where $\bar{u} = \frac{1}{D} \int_{-D}^0 u \, dz$ is the average velocity in the surface layer (same for \bar{v}). In the coastal upwelling example, $D \approx 20$ m is probably appropriate, because that is the region where the turbulence is enhanced. The terms $\bar{v}D$ and $\bar{u}D$ are called the Ekman transport and represent a 2-D transport with units of $\text{m}^2 \text{s}^{-1}$.

So, for example in the coastal upwelling case, the wind is blowing from north to south, so the net force on the upper ocean is to the south (figure 10.13). If this force is in balance with the Coriolis force, then the Coriolis force must be towards the north. Since the Coriolis force is to the north, that means there must be a net flow to the west (assuming this is northern hemisphere). The other way to remember this is that the Ekman transport is to the right of the stress.

Stress can also be exerted at the sea floor by friction of the mean flow with the bottom. Suppose, as in the coastal circulation example, the flow is towards the south. Then there will be a friction to

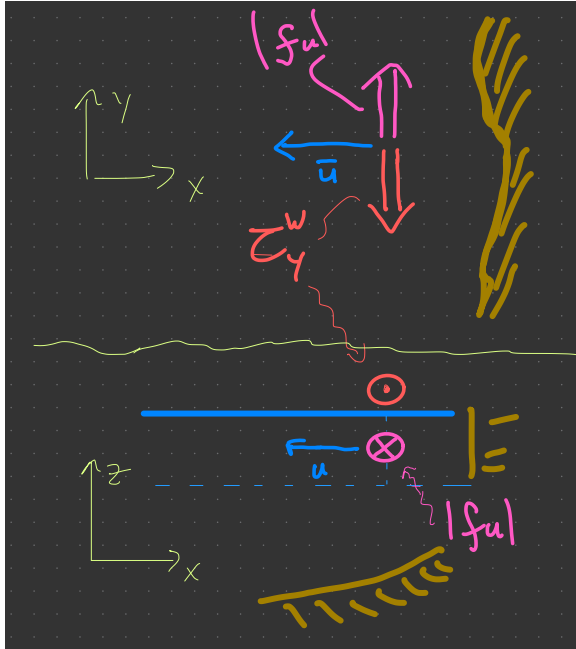


Figure 10.13: Sketch of the depth-integrated force balances in the Ekman layer in the coastal-upwelling case. Upper is looking from above, and lower sketch is looking from the south.

the north tending to slow this flow down, which we represent as a bottom stress τ_y^B . We saw in the observations that there is indeed heightened turbulence near the sea floor. This also results in an Ekman layer, but now the stress is to the north (figure 10.14), so the Ekman transport $\bar{u}D$ is to the east, or onshore.

Putting some values on these transports, usually we can estimate the windstress or bottom stress from the speed of the water or wind. For the Oregon shelf case, the bottom stress is estimated to be something like $\tau_B^W \approx 0.1 \text{ N m}^{-2}$, so

$$\bar{u}D = \frac{\tau_B^W}{\rho_0 f} = \frac{0.1}{10^3 \times 10^{-4}} = 2 \text{ m}^2 \text{ s}^{-1} \quad (10.18)$$

where this is transport per along-shore distance. If we average this over 20 m, then the average speed of this layer is 0.1 m s^{-1} , or about 8 km/d. We saw from the observations that dense water was seen moving up the shelf at approximately 7 km/d, so this is in agreement with our observations. (Note that the surface mixed layer was very hard to observe in these observations so we don't make a direct comparison of its motion.)

10.4.1 The Ekman spiral: fact and fiction

Above we elided the structure of the Ekman flow and skipped to the net transport by integrating from $z = -D$ to the surface (or over

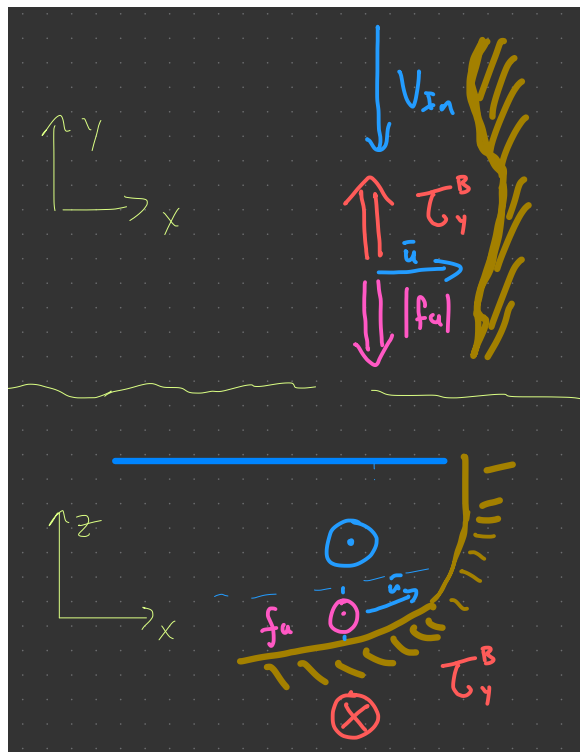


Figure 10.14: Sketch of the depth-integrated force balances in a bottom Ekman layer in the coastal-upwelling case. Upper is looking from above, and lower sketch is looking from the south. The bottom stress is the net stress acting to slow down the southward interior current.

the bottom Ekman layer). The details of the Ekman flow are quite interesting, but in the end frustratingly hard to quantify and observe.

The coastal upwelling example clearly shows the effect of Ekman transport pushing water up the shelf. However, note that the observations did not directly observe the velocity associated with this transport because the Doppler current profiler has a technical limitation near the seafloor. So we infer the net motion from the transport of dense water up the shelf. I would argue that this transport is the important factor, and details of the currents in the Ekman layer are of secondary importance.

Regardless, even elementary text books discuss the **Ekman spiral** which has a very idealized shape. In this idealization, the surface currents flow at 45 degrees to the wind, and then smoothly spirals to clockwise as it decays with depth (figure 10.15). This ideal solution depends on a constant viscosity ν in the upper ocean. However, that is rarely the case as the viscosity is usually a turbulent viscosity and the turbulence in the upper water column varies due to many factors. Hence observed Ekman spirals are usually found to have more veering than predicted, and a compressed decay scale (figure 10.16).

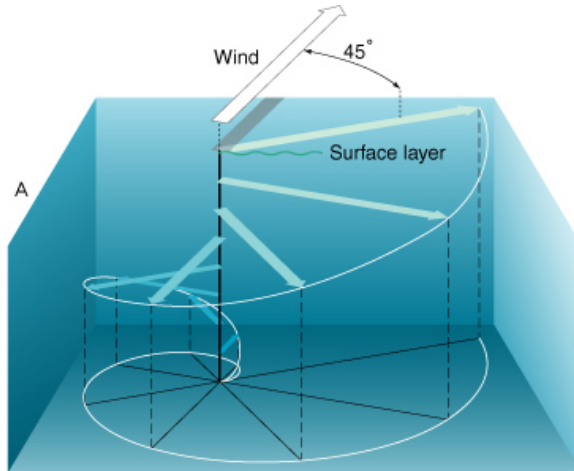


Figure 10.15: Idealized Ekman spiral for flow with a constant viscosity. <http://oceanmotion.org/html/background/ocean-in-motion.htm>

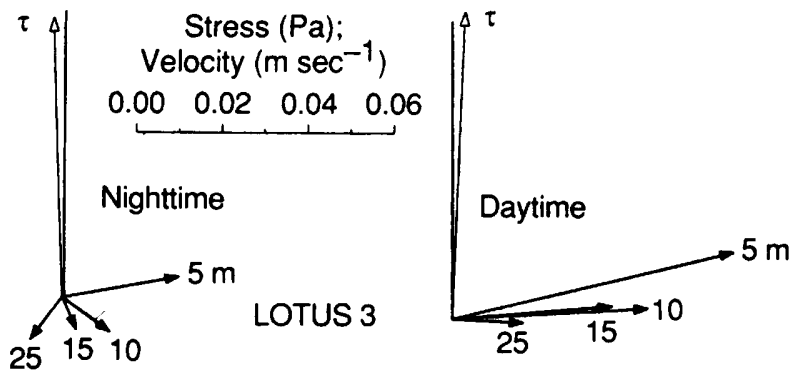


Figure 10.16: Observed Ekman spiral from direct measurements in the upper ocean divided into flow at night and during the day. Daytime stratification compresses the Ekman layer to the upper ocean. [Price et al., 1987]

10.5 Ekman convergence and divergence

Ekman transports tend to only affect a thin region through the upper ocean, or near the seafloor. However, because they move water around they can make convergences and divergences. In a convergence water piles up and then is pushed downwards, in a divergence the sea level tends to drop, and then water is pulled up from depth. This creates pressure gradients that can then be felt from the top of the water column to the bottom.

First, if there is a coast, steady offshore Ekman transport leads to a divergence at the coast. This will tend to make the water level drop at the coast relative to offshore (figure 10.17), until there is replacement flow from below. It is important to remember this cross-shore pressure gradient is caused *before* any replacement flow happens, and

indeed this pressure gradient is what ultimately causes the replacement flow. That there must be a replacement flow should be clear - suppose $1 \text{ m}^2 \text{ s}^{-1}$ of offshore transport (see calculation above for bottom boundary layer), and suppose this is applicable 10 km offshore. Over this 10 km, the water level will drop at a rate 10^{-4} m s^{-1} , or 8 m a day. While winds clearly blow for more than a day, the sea-surface is never drawn down 8 m at the coast. As we will see in the next chapter, the replacement flow is due to coastal upwelling in the bottom boundary layer, but there is one more step in the process that we will cover next chapter. However, if we know the offshore transport, we can infer the vertical upwelling rate as 10^{-4} m s^{-1} .

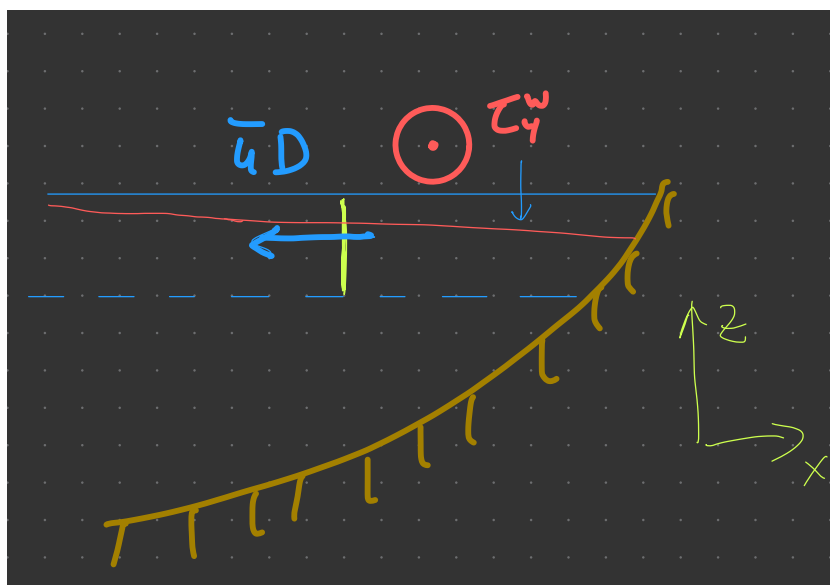


Figure 10.17: Sketch of divergence on the coast due to a southward wind (τ_y^w). Average offshore transport is everywhere except at the coast, leading to the sea surface dropping.

Ekman convergences and divergences are also crucially important in the interior of the ocean, away from boundaries. In this case the convergences must be caused by changes in the wind stress. When discussing the wind-driven flow in the North Pacific, we noted that the westerlies are concentrated at 45 N, and the trades at 15 N (figure 10.18). The Ekman transport in the westerlies is to the south, and in the trades it is to the north (figure 10.18, blue arrows), so everywhere between these two latitudes, we have an Ekman convergence or **Ekman pumping**. The convergence causes the sea surface to be high in the middle of these winds (as observed) and drive a flow downwards.

In fact, everywhere that there is a gradient in the windstress, there will either be a convergence or a divergence. If the wind stress gradi-

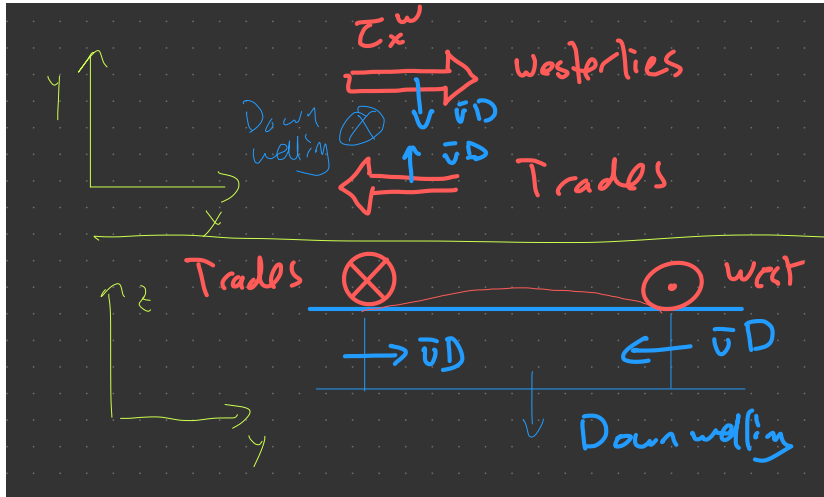


Figure 10.18: Sketch of winds in the Pacific, looking from above (top) and from the east (bottom). There is a convergence between the Westerlies and Trades (red arrows) due to the converging Ekman transports. This leads to high sea level between these latitudes, and downwelling or Ekman pumping into the interior.

ents are mostly north-south, then we can write:

$$\bar{w} \delta y = \bar{v}D|_{y+\delta y} - \bar{v}D|_y = -\frac{1}{\rho_0 f} (\tau_x^w(y + \delta y) - \tau_x^w(y)) \quad (10.19)$$

or if we allow δy to become very small:

$$w = -\frac{1}{\rho_0 f} \frac{d\tau_x^w}{dy} \quad (10.20)$$

So in the N. Pacific, the distance between 15 and 45 N is 3300 km, so $\frac{1}{\rho_0 f} \frac{d\tau_x^w}{dy} \approx 10^{-6} \text{ ms}^{-1}$, or close to 0.1 m per day. Integrated over the basin this represents $30 \times 10^6 \text{ m}^3 \text{ s}^{-1}$.

Note that the full Ekman vertical velocity is given by the **curl** (mathematics) of the wind vector, so winds that spin in a clockwise direction tend to drive water towards the center, and winds that spin counter clockwise pull water from the center:

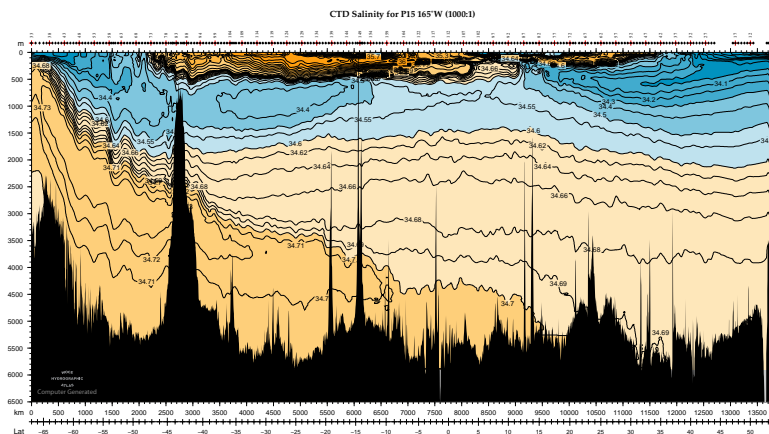
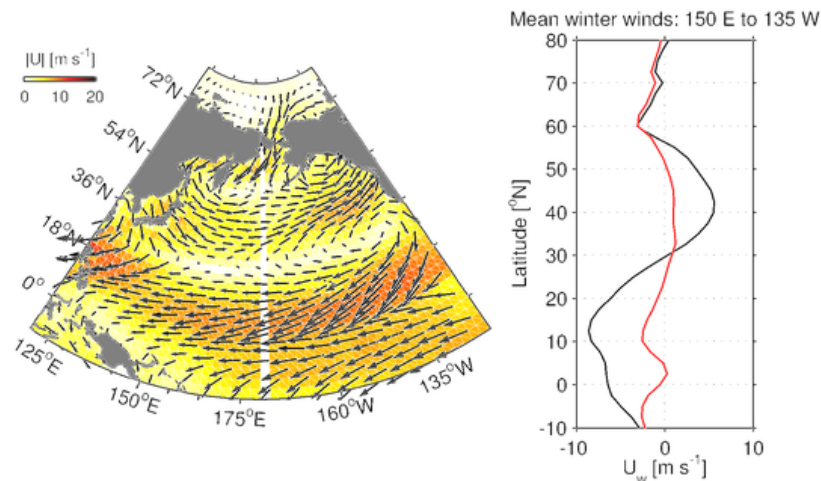
$$\text{curl}\tau^w = \frac{d\tau_y^w}{dx} - \frac{d\tau_x^w}{dy} \quad (10.21)$$

10.6 Exercises

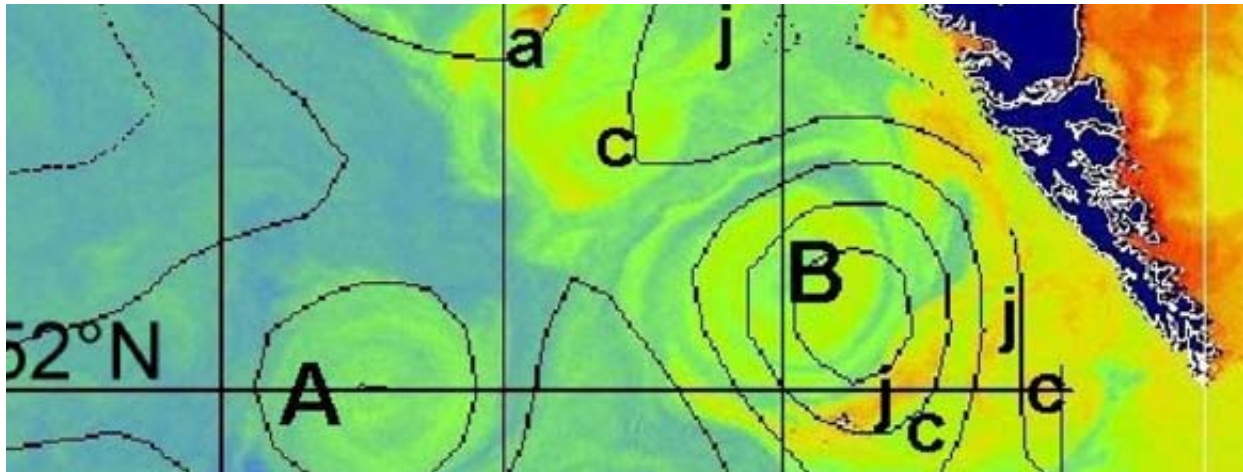
Coriolis to west Using the logic above, and a sketch, argue that shooting a hockey puck towards a target to the west (i.e. a tangential shot against the direction of rotation) will lead to a Coriolis force to the north (or towards the axis of rotation).

Calculate Ekman convergence and divergence Suppose we have a wind from the west that increases to the north so that at 30 N it blows at 0.1 N m^{-2} . At a point 50 km north it blows at 0.2 N m^{-2} , and 100 km north it blows at 0.3 N m^{-2} . What is the average rate of Ekman “pumping” between the wind measurements (in m/s)? Sketch.

Where is the Ekman pumping in N. Pacific? Based on the figure below, where is there Ekman pumping and suction (by latitude) in the North Pacific? How well does this correspond to the shape of the isohalines of the upper ocean in the salinity section below?



Geostrophic balance and coastal flow



11.1 Geostrophic balance

The second balance that involves the Coriolis force is the **Geostrophic balance**, and is when the Coriolis force is in “balance” with the pressure gradient:

$$\frac{du}{dt} = \underbrace{-\frac{1}{\rho_0} \frac{dP}{dx}}_{\text{geostrophic}} + \underbrace{fv + \frac{1}{\rho} \frac{d\tau_{xz}}{dz}}_{\text{Ekman}} \quad (11.1)$$

$$\frac{dv}{dt} = \underbrace{-\frac{1}{\rho_0} \frac{dP}{dy}}_{\text{geostrophic}} - \underbrace{fu + \frac{1}{\rho} \frac{d\tau_{yz}}{dz}}_{\text{Ekman}} \quad (11.2)$$

in which case the equations of motion simplify to:

$$-\frac{1}{\rho_0} \frac{dP}{dx} \approx -fv$$

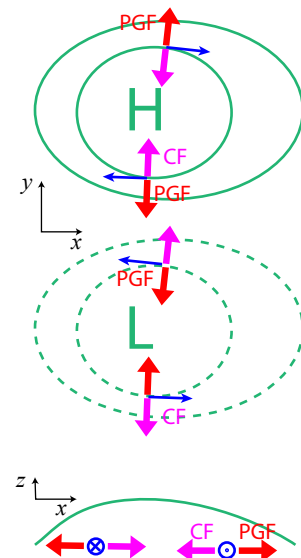


Figure 11.1: Sketch of geostrophic force-balance for a sea-level high and a sea-level low in the northern hemisphere, looking from above, and from the south for the high. The flow will be clockwise around a high and counter-clockwise.

$$-\frac{1}{\rho_0} \frac{dP}{dy} \approx +fu$$

In the northern hemisphere ($f > 0$) this says that water turns to the right as it moves from high pressure to low. This gives a clockwise circulation around an isolated high, or a counter-clockwise around an isolated low (figure 11.1)

Crucially, if we know the pressure gradient, we can directly calculate the geostrophic flow perpendicular to that pressure gradient from the equations above. So, suppose the high in the cover figure is 16 cm, over 100 km. The pressure difference due to this flow gives us an estimate of the velocity (assuming $f = 10^{-4} \text{ rad s}^{-1}$)

$$|u| = \left| \frac{1}{f\rho} \frac{dP}{dx} \right| = \frac{1}{f\rho} \frac{\Delta P}{\Delta x} = \frac{g}{f} \frac{\eta_C - \eta_E}{\Delta x} \approx 0.16 \text{ m s}^{-1} \quad (11.3)$$

The equation applies everywhere in the fluid, and is only made complex by the presence of water with different densities making the flow have a pressure gradient that changes with depth. An observation of this can be seen in figure 11.2, where there is a sea-surface high in the middle, but the pressure gradient inside the eddy is the other direction. This causes the pressure gradient force to decrease with depth, and hence the geostrophic flow decays with depth as well.

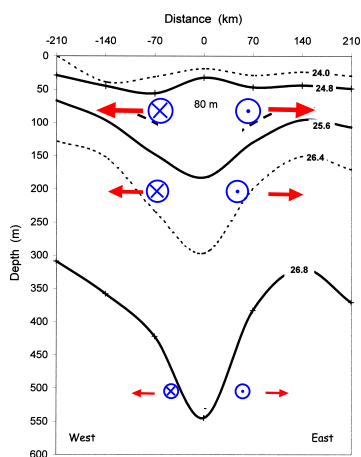


Figure 11.2: Observations of density inside an Eddy. Note how the density contours tend to counteract the high sea-surface height. Blue circles with crosses are into the page, and with dots are out of the page, and the size is sketched to be proportional to the speed of the flow.

As discussed in chapter 2, calculating the pressure gradient is simply a matter of calculating the pressure at two locations, and differencing, where the pressure is given by:

$$P(z)/\rho_0 = \frac{1}{\rho_0} \int_z^\eta \rho g \, dz \approx g\eta + \frac{1}{\rho_0} \int_z^0 \rho g \, dz \quad (11.4)$$

So imagine one flank of the eddy, and that the eddy is made of two densities $\rho_1 < \rho_2$ (figure 11.3). In the upper layer

$$-\frac{1}{\rho_0} \frac{dP}{dx}(z = z_1) = -\frac{1}{\Delta x} g(\eta_B - \eta_A). \quad (11.5)$$

In the lower layer, things are a bit more complicated, so we just do it step by step:

$$P_A(z = z_2) = \rho_1 g(\eta_A - Z_A) + \rho_2 g(Z_A - z_2) \quad (11.6)$$

$$P_B(z = z_2) = \rho_1 g(\eta_B - Z_B) + \rho_2 g(Z_B - z_2) \quad (11.7)$$

So the total pressure gradient in the lower layer is approximated as

$$-\frac{1}{\rho_0} \frac{P_B - P_A}{\Delta x} = \overbrace{-\frac{1}{\Delta x} g(\eta_B - \eta_A)}^{\text{Surface}} - \overbrace{\frac{1}{\Delta x} g \frac{(\rho_2 - \rho_1)}{\rho_0} (Z_B - Z_A)}^{\text{Internal}} \quad (11.8)$$

According to the geostrophic balance, then, the flow in the upper layer is into the page, and the one in the bottom layer is either into the page, but more slow, or even out of the page.

11.1.1 Thermal wind

The example above makes it clear that lateral density differences can drive velocity differences in the vertical if the flow is in geostrophic balance. This can easily be extended to the continuous case with some manipulation of the momentum equations. If we take the vertical derivative of the x- and y-momentum equations we arrive at:

$$-\frac{1}{\rho_0} \frac{d^2 P}{dx dz} = -f \frac{dv}{dz} \quad (11.9)$$

$$-\frac{1}{\rho_0} \frac{d^2 P}{dy dz} = f \frac{du}{dz} \quad (11.10)$$

but $P = \int_z^\eta \rho g dz$, so we get the **thermal wind** relation.

$$-\frac{1}{\rho_0} \frac{d\rho}{dx} = -f \frac{dv}{dz} \quad (11.11)$$

$$-\frac{1}{\rho_0} \frac{d\rho}{dy} = f \frac{du}{dz} \quad (11.12)$$

so, if we know the horizontal pressure gradient, we can immediately say how the velocity changes with depth (though we do not know the absolute velocity).

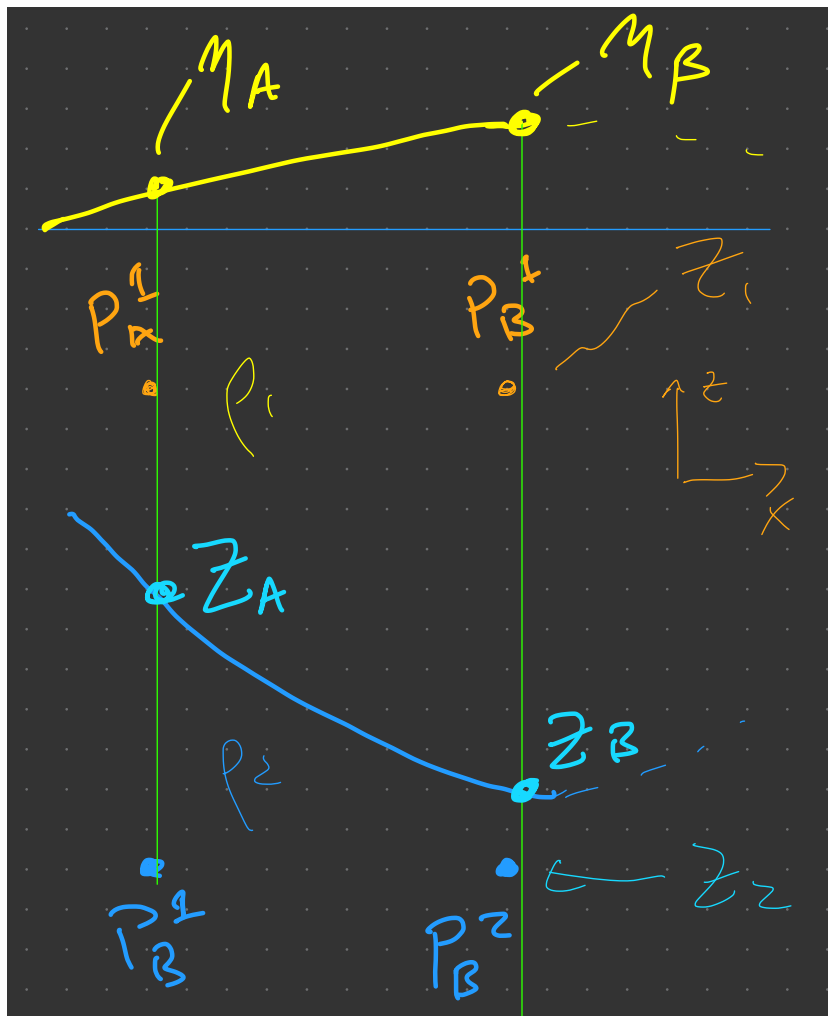


Figure 11.3: Two-layer approximation of pressure gradients in an eddy.

11.1.2 Level of no motion and “dynamic height”

Back in the pre-satellite days, all oceanographers would have had to rely on measurements of the density under the ocean, like those in figure 11.2. Estimating the sea-surface height was impossible; imagine detecting 15 cm over 100 km in an ocean that is otherwise also moving due to tides, surface waves, relative to a poorly-constrained geoid. However, oceanographers noted that most ocean currents, like the eddy, had tilted density surfaces, and that the currents at depth go to approximately zero.

Under these assumptions, oceanographers would assume that the pressure gradient at a “level of no motion” was zero, so that the geostrophic flow was zero there as well. In order to get this level of no motion the pressure gradients inferred from the interior density

measurements were assumed to be balanced by a pressure gradient from the surface at that depth. So, for instance, in the simple two-layer case the equation (11.8), the *Surface* term was equal and opposite in sign to the *Internal* term, if the deep layer was assumed to be not moving. Note that this allows an estimate of the surface pressure gradient, and using the geostrophic balance, the surface velocities. This surface pressure gradient is of course supplied by the sealevel interface being tilted, and calculating these gradients is like calculating a “dynamic height” of the ocean.

An example in figure 11.4, calculated in the 1980s looks strikingly similar to the sea surface heights in chapter 9. In particular, where there is Ekman convergence in the subtropics there is a high of up to 2 m, and a low in the sub-polar regions where there is Ekman divergence. The highs and lows are displaced to the west sides of the basins. The steepest change in dynamic height correspond to the strongest currents, again largely concentrated on the west side of the basins, and associated with the Gulf Stream, Kurishio, East Australian current etc.

Just to summarize again how this is done:

1. An interior pressure gradient is calculated at two “stations” as a function of depth using the density data from CTDs or other measurements.
2. At a “depth of no motion” the pressure gradient is assumed to be zero, so a surface pressure gradient is added to the two points to make that be the case.
3. If there are multiple stations in a line the surface pressure gradient is integrated to make a dynamic height with an arbitrary zero at some location.

We will come back to *why* the dynamic height looks the way it does in the next chapter.

11.2 Coastal upwelling, complete picture

Using the Ekman and geostrophic balances we are now in a position to explain the coastal upwelling example in detail (i.e. figure 9.3, one snapshot in detail in figure 11.5).

First, the wind starts to blow towards the south; this sets up a southwards windstress τ_y^w (figure 11.6, red circle). When this flow is in a steady-state Ekman balance there will be an equal and opposite Coriolis force to the north (figure 11.6, magenta circle). That implies

an offshore Ekman transport to the west given by

$$u_{Ek}D = \frac{\tau_y^w}{\rho_0 f} \quad (11.13)$$

The offshore Ekman transport drops the sealevel at the coast (figure 11.7, surface interface). This creates a surface pressure gradient force that acts to push water back towards the coast (figure 11.7, red arrow). Again, in *steady state* geostrophic balance, the pressure gradient force is balanced by a Coriolis force offshore, which must be generated by a geostrophic velocity to the south. Note that this evolves in time with the deep water *initially* moving onshore, but then being turned south (to the right) by the Coriolis force.

At this point the flow cannot be in steady state because we are transporting water offshore in the surface Ekman layer, but not having any onshore transport to replace it. Without this return flow, the sea surface will continue to increase its tilt. The return flow happens in the bottom Ekman layer. The interior geostrophic flow moves south, so there is a corresponding bottom stress to the north τ_y^B (figure 11.2, red circle at bottom). In a steady Ekman balance, this implies a Coriolis force to the south, which implies a net Ekman transport onshore (figure 11.2, blue arrows, bottom), given by

$$u_{Ek}D = \frac{\tau_y^B}{\rho_0 f} \quad (11.14)$$

The offshore Ekman transport drops the sealevel at the coast (figure 11.2)

When is the whole flow balanced? When $\tau^B = \tau^W$ so that the transport in the bottom Ekman layer is the same as the transport in the surface Ekman layer. So, if we know the wind stress, and have a good estimate of the bottom drag co-efficient, $C_D \approx 10^{-3}$, then we can guess what the mean geostrophic velocity is, and hence the size of the sea surface tilt. For the Oregon shelf, $\tau_y^W \approx -0.15 \text{ N m}^{-2}$ (minus means to the south). That means that the geostrophic velocity $v_g \approx 0.35 \text{ m s}^{-1}$ in order for $\rho_0 C_D |v_g|^2$ to be large enough to provide the bottom stress to match. This is approximately the same as the observations near the bottom.

We can further calculate the sea-surface height drop across the 20-km width of the shelf from $g \frac{d\eta}{dx} = f v_g$ or $\Delta\eta = 0.08 \text{ m}$ across the shelf.

11.2.1 Internal dynamics on shelf

The final thing we notice about the shelf observations is that the flow is slower towards the sea-floor than at the surface. This is also largely

explained by the geostrophic balance. Note that the isopycnals tilt up towards the coast, counteracting the surface pressure gradient (also sketched in figure 11.8). This means that the surface tilt is actually larger than we calculated above if the bottom velocity is to remain 0.38 m s^{-1} , leading to faster velocities near the surface.

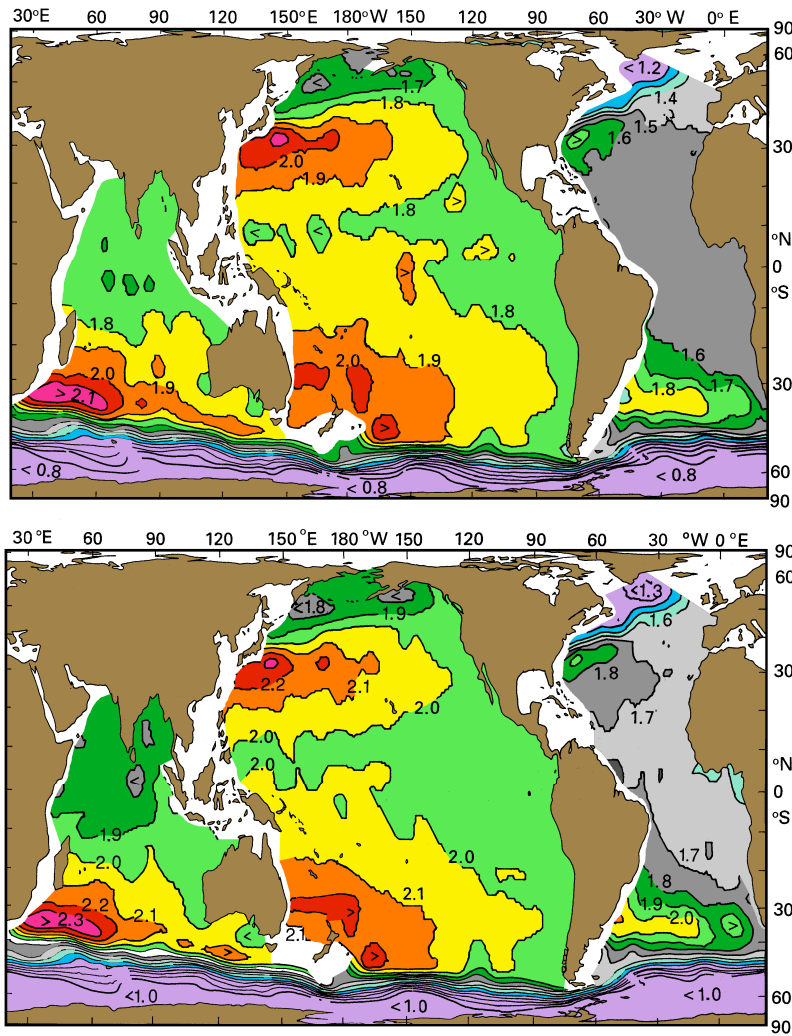


Figure 11.4: Dynamic height with a level of no motion at 1500 m (top) and 2500 m (bottom). Note these are quite similar, strongly indicative that the dynamics are largely above these depths.

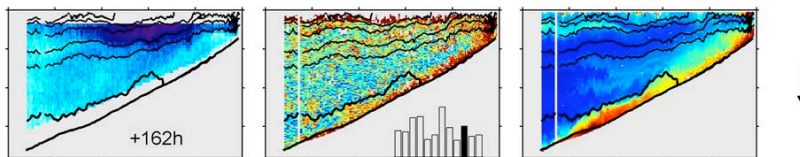


Figure 11.5: Data from figure 9.3.

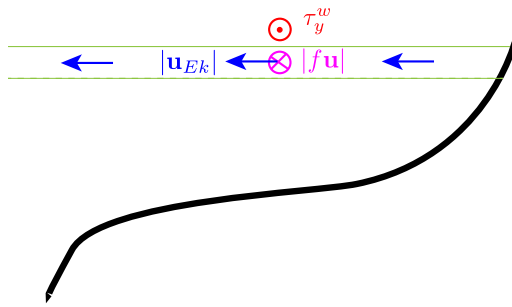


Figure 11.6: On a continental slope, initially at rest, a wind stress blows from north to south (dotted red circle)

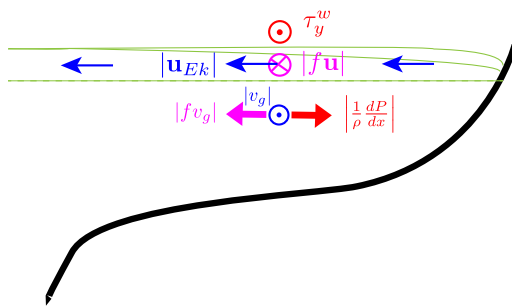


Figure 11.7: After the Ekman transport has been active for a while, the sea level drops at the coast (green surface), and an interior geostrophic balanced flow is set up.

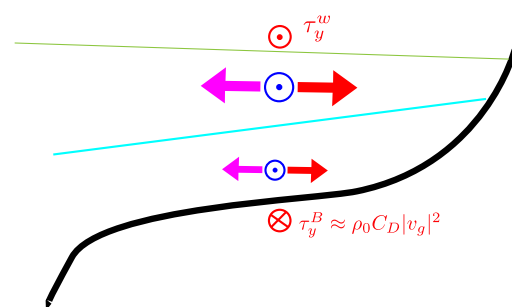
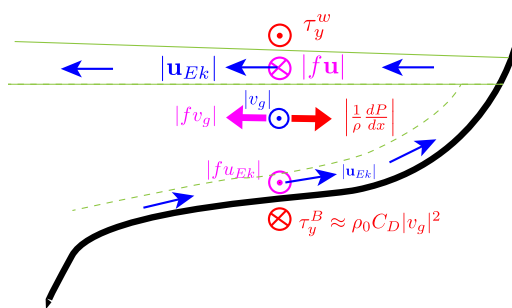


Figure 11.8: Sketch of pressure gradient changes if there are tilted isopycnals (cyan line) in the section, as observed in the coastal data. The tilted isopycnal counteracts the surface tilt, slowing the barotropic flow.

11.3 Exercises

Geostrophic balance two stations Calculate the geostrophic flow at two stations 50 km apart, assuming $f = 10^{-4} \text{ rad s}^{-1}$. Approximate the density measured at each location as 50-m blocks of homogeneous density:

z [m]	ρ_A [kg m ⁻³]	ρ_B [kg m ⁻³]
0–50	1021	1020
50–100	1022	1021
100–150	1024	1023
150–200	1025	1024

- If the surface pressure gradient is zero, what is the internal pressure gradient at 50, 100, 150, and 200 m? (do not drop too many decimal places!)
- What is the direction and strength of the *geostrophic* velocity at the 4 depths?
- If there is a pressure gradient, what must its direction and strength be so that the geostrophic flow is zero at 200 m?
- How large must the surface difference be at the two stations?
- What is the new flow at the other depths in the presence of this surface gradient?

Geostrophic flow Gulf Stream Consider the temperature section across the Gulf Stream (figure 11.9). Assuming a level of no motion at approximately 1500 m, what does

- the sea-surface tilt look like?
- the interior velocity look like (just a sketch)?
- where would you expect the Gulf Stream to be the fastest?

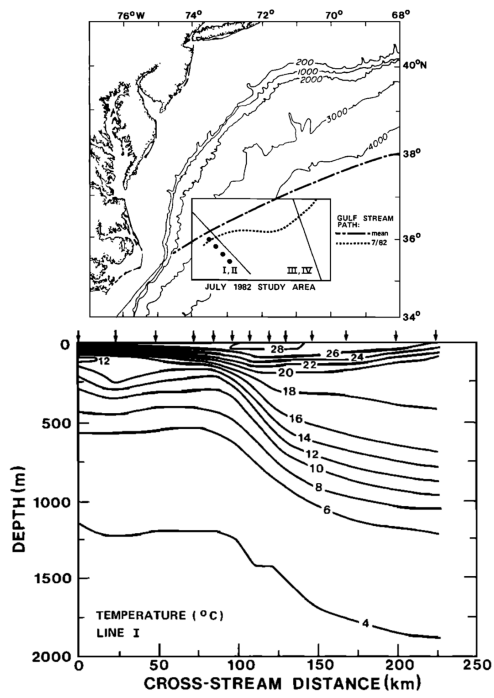
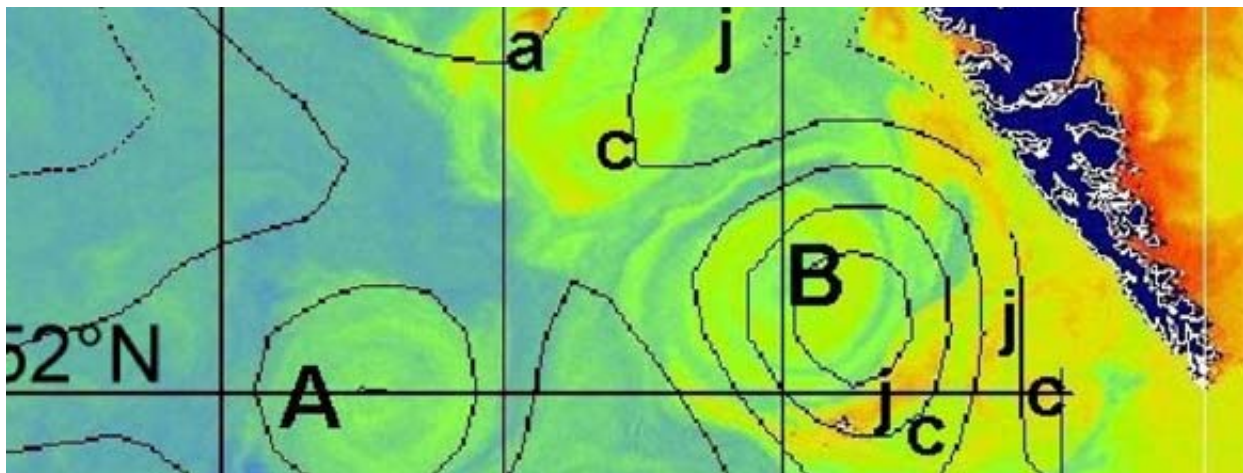


Figure 11.9: Location of measurements in the Gulf Stream, and plot of temperature across the section [Johns et al., 1995].

12

Sverdrup balance and basin-scale circulation



We saw above that the Ekman balance can drive convergences and divergences in the ocean, and that these cause the water to pile up preferentially creating pressure gradients. The pressure gradients are then balanced by the Coriolis force, in the geostrophic balance, and water flows parallel to lines of constant pressure, clockwise around highs in the Northern hemisphere.

This *all* happens on the large scale. If we consider the subtropical gyre, between 15 and 45 degrees, there is an Ekman convergence towards the centre of the gyre, and that causes there to be a sea-surface high there. The water will flow around that sea-surface high in a clockwise direction (northern hemisphere). However that leaves two questions:

1. How strong will the flow be? Alternately, how high will the highs in the middle of the gyre be?
2. Why is the gyre asymmetric east-west?

The answer is, as we will see below, that the flow is driven by the conservation of angular momentum acting in the presence of

basin-scale changes in the Coriolis frequency. Water with a negative (clockwise) torque exerted on it can either spin with negative (clockwise) angular momentum, or it can move to a region with lower background “planetary” angular momentum.

12.1 Circulation

Idealizing the winds and seafloor in the subtropical gyre we have the idea that the winds blow from west to east in the westerlies (45 N) and east to west in the Trades (15 N; figure 12.1). Based on the dynamics as we’ve understood them so far, this leads to an Ekman convergence everywhere in the gyre, and a raising of the seafloor height, and causing a downwelling.

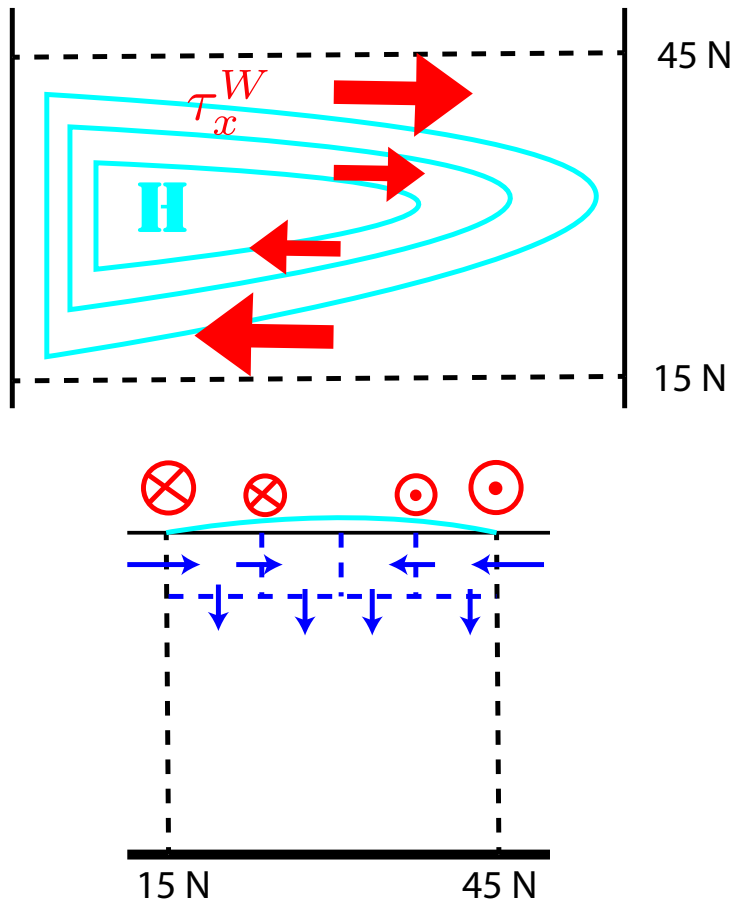


Figure 12.1: Idealized sketch of the wind stress in the subtropical gyre (northern hemisphere). Top panel is from above, with coasts on the west and east side. Westerlies peak at 45 N, and the trades at 15 N. This makes a high in the middle, but offset to the west. Bottom panel is the same situation looking at the side from the east towards the west. The Ekman layer is shown with the blue arrows, noting that there is downwelling throughout this gyre.

However, the observed gyre is asymmetric, with the high concentrated near the western boundary. This implies that the velocity is largely equatorward everywhere in the gyre, except to the west of the high, along the **Western boundary**. The real situation is even more asymmetric than pictured in figure 12.1. If we remember that the geostrophic interior velocity is proportional to the strength of the pressure gradient, then we would expect very slow flow towards the south in the interior, and very fast flow along this western boundary. The western boundary current in the N. Pacific subtropical gyre is the **Kuroshio**; the **Gulf Stream** is the corresponding current in the Atlantic.

12.2 Conservation of potential vorticity

The way to understand the gyre circulation is to consider the conservation of angular momentum, or in fluid mechanics we call it **potential vorticity**. Just like any angular momentum, the potential vorticity changes in response to torque, in this case from the wind and seafloor. A simplified version, useful for our case is:

$$\frac{d}{dt} \left(\frac{\zeta + f}{H} \right) = \frac{1}{H^2 \rho_0} \left[\frac{d\tau_y^W}{dx} - \frac{d\tau_x^W}{dy} + \frac{d\tau_y^B}{dx} - \frac{d\tau_x^B}{dy} \right] \quad (12.1)$$

Here the term on the left side of the equation is the potential vorticity, and the term on the right side the torque due to the wind stress (τ_x^W, τ_y^W) and bottom friction (τ_x^B, τ_y^B) . H is the water depth, and f is the Coriolis parameter, which we keep in mind varies with latitude, or y . We call this the *planetary vorticity* and is the vertical angular momentum due to the earth's rotation.

The term ζ is the **relative vorticity** of the flow and is defined as:

$$\zeta = \frac{dv}{dx} - \frac{du}{dy} \quad (12.2)$$

where u and v are the x - and y -components of velocity. It is relatively straight forward to see how this relates to a spinning flow (figure 12.2). Consider a flow spinning in a counter-clockwise manner. The velocity gradients in such a flow are such that $\zeta > 0$. This uses the **right-hand rule**, which says that if you curl your right hand fingers in the direction of rotation, your thumb will point up for positive vorticity and down for negative vorticity (this is just a convention, and could have just as easily been the other way, but it is useful to choose one convention and stick with it). Of course a clockwise flow has a negative vorticity.

The same logic and sign convention applies to torque. In the gyre sketched in figure 12.1, the gradients in τ^W are such that $\frac{d\tau_x^W}{dy} < 0$, so the wind is exerting a negative torque on the water.

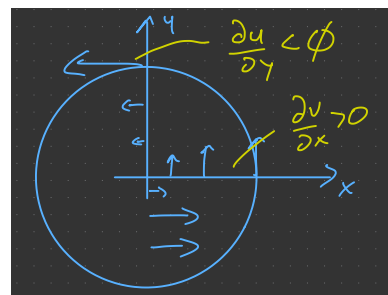


Figure 12.2: Sketch of velocity gradients in a counter clockwise flow. Note $\zeta > 0$ in this flow.

Box 12.2.1: Derivation of potential vorticity

Potential vorticity for a barotropic fluid is relatively straight forward to derive. We need the momentum equations and the continuity equation:

$$\begin{aligned} \frac{du}{dt} &= -\frac{1}{\rho} \frac{dP}{dx} + fv + \frac{1}{\rho} \frac{d\tau_x}{dz} \\ \frac{dv}{dt} &= -\frac{1}{\rho} \frac{dP}{dy} - fu + \frac{1}{\rho} \frac{d\tau_y}{dz} \end{aligned}$$

If we take $-d/dy$ of the first equation and d/dx of the second and add them, then the pressure term drops out:

$$\frac{d}{dt} \left(\frac{dv}{dx} - \frac{du}{dy} \right) = -f \left(\frac{du}{dx} + \frac{dv}{dy} \right) + \frac{1}{\rho} \left(\frac{d^2\tau_y}{dz dx} - \frac{d^2\tau_x}{dz dy} \right) \tag{12.3}$$

and we note that the first term is just the derivative of ζ with time.

We integrate this vertically from the sea-floor to sea surface, and assume that the water is H deep, including any sea-surface displacements.

$$H \frac{d\zeta}{dt} = -fH \left(\frac{du}{dx} + \frac{dv}{dy} \right) + \frac{1}{\rho} \left(\frac{d\tau_y^W}{dx} - \frac{d\tau_x^W}{dy} \right) + \frac{1}{\rho} \left(\frac{d\tau_y^B}{dx} - \frac{d\tau_x^B}{dy} \right) \tag{12.4}$$

So now we use the fact that $\frac{du}{dx} + \frac{dv}{dy} = -dW/dz = H^{-1} \frac{dH}{dt}$.
 TODO: finish

We saw in the classroom demo a consequence of the conservation of potential vorticity: when water that is initially not moving in a rotating reference frame moves from shallow water to deep water, the water column deepens, so H increases (figure 12.3). There are no substantial bottom or surface friction, so no external torque on the water column. However, it does have initial *planetary vorticity*, f from the rotation of the reference frame. Since there is no torque we can write:

$$\frac{\zeta_0 + f_0}{H_0} = \frac{\zeta_F + f_F}{H_F} \tag{12.5}$$

Now initially the water is not moving, and f is constant, so we can solve for ζ_F to find that the water is spinning with a vorticity that has the same sign as f :

$$\zeta_F = f \left(\frac{H_F}{H_0} - 1 \right) \tag{12.6}$$

and because $H_F > H_0$ this is a positive number. This is all directly analogous to the spinning ice skater who draws in their arms, and

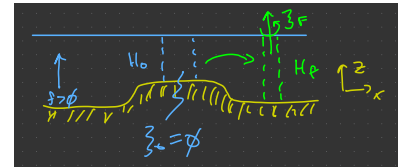


Figure 12.3: Sketch of parcel of water moving from shallow to deep region. As it moves to deep region its planetary vorticity is stretched and manifests as an eddy rotating in the same direction as the planetary vorticity.

makes themselves thinner, and hence spin faster, just here the effect is caused by the earth spinning rather than the skater.

On the large scale, ie. our basin, it is important to bear in mind two facts. First, f varies with latitude - it is higher at the poles and zero at the equator. So that means when we think about $\frac{f+\zeta}{H}$ changing with time following a parcel of water, we need to remember that f can change too. Second, On large scales $\zeta \approx 0$, and in fact if ζ is large, like in an eddy or cyclone, it will tend to move poleward if it is a cyclone, and equatorward if an anti-cyclone. To see why this is, consider ζ_0 which is large at a latitude where $f = f_0$. Supposing H is constant, then for ζ_F to be driven to zero we have an expression for f_F :

$$\zeta_0 + f_0 = f_F \quad (12.7)$$

So for a hurricane $\zeta_0 > 0$, they always move poleward, and die out, partially because they are moving to a region with higher planetary vorticity.

12.3 Sverdrup transport

The Sverdrup transport is a straight-forward application of the conservation of potential vorticity equation (12.1), if we realize a few things. First, let us approximate the ocean depth as a constant. Second, we assume bottom friction is generally quite small, so $\tau_x^B \approx \tau_y^B \approx 0$. Third, note that on the scale of the whole Pacific, the relative vorticity is substantially smaller than f , so we can write $f + \zeta \approx f$. To see this, consider the scale of the fastest velocity in the ocean, which is about $U \sim 1 \text{ m s}^{-1}$. This is spread over a distance of $L \sim 10,000 \text{ km}$, so the scale of vorticity is $U/L \sim 10^{-7} \text{ s}^{-1}$. Compare to $f \approx 10^{-4} \text{ s}^{-1}$, and it is clear that on large scales (say scales $> 10 \text{ km}$), $f \gg \zeta$. Finally, lets only consider that the wind is in the x-direction as sketched in figure 12.1. These assumptions simplify equation (12.1) significantly:

$$H \frac{df}{dt} = -\frac{1}{\rho_0} \left[\frac{d\tau_y^W}{dx} \right] \quad (12.8)$$

So what this says is that the rate of change of f is proportional to the wind torque. In the sketch above (figure 12.1) the torque is clearly negative, so this equation says that f must decrease with time following a parcel of fluid. The way that f decreases with time is by moving South because f is a sinusoid centered at the equator.

Indeed the torque tells us how fast the water will move north or south under the Sverdrup balance. If v is the north-south velocity,

It is actually the same math if the eddy starts spinning so it has *relative vorticity* as well as having *planetary vorticity*, there is just an extra term:

$$\zeta_F = \frac{H_F}{H_0} (\zeta_0 + f) - f$$

Of course a cyclone will also die out due to friction, and loss of warm water feeding the low pressure system in its centre, but the tendency to move North is because of the conservation of potential vorticity.

then

$$\frac{df}{dt} = v \frac{df}{dy} \quad (12.9)$$

where y is in m. df/dy is a function of latitude, but we often can make the **beta-plane** approximation and assume it's a constant β . At 30 degrees latitude (the middle of the subtropical gyre) $\beta \approx 2.3 \times 10^{-11} \text{ [(ms)}^{-1}\text{]}$. This gives us the Sverdrup relation:

$$Hv \approx -\frac{1}{\beta\rho_0} \left[\frac{d\tau_y^W}{dx} \right] \quad (12.10)$$

So, in the case where the torque is negative the velocity v is negative, and thus to the south.

Box 12.3.1: Calculating Beta

The rate of change of f with the y coordinate, $\beta = \frac{df}{dy}$ is readily calculated from f and the radius of the Earth, R . $f = 2\Omega \sin \lambda$ and $y = R\lambda$, so

$$\begin{aligned} \beta &= \frac{df}{dy} \\ &= \frac{df}{d\lambda} \frac{d\lambda}{dy} \\ &= \frac{2\Omega}{R} \cos \lambda \end{aligned}$$

So with $R = 6371 \text{ km}$ and $2\Omega = 1.45 \times 10^{-4} \text{ s}^{-1}$, then at 30 N, $\beta \approx 2.3 \times 10^{-11} \text{ [(ms)}^{-1}\text{]}$.

So let us apply to our wind torque pictured in figure 12.1. If we assume that the wind stress profile is given by $\tau_x^W(y) = \tau_0 \sin\left(2\pi \frac{y-y_{30}}{2L}\right)$, where $\tau_0 = 0.1 \text{ N m}^{-2}$, and $L = 3300 \text{ km}$ is the north-south extent of the basin (see figure 12.4). So the gradient is given by

$$-\frac{d\tau_x^W}{dy} = -\tau_0 \frac{\pi}{L} \cos \pi \left(\frac{y-y_{30}}{L} \right) \quad (12.11)$$

So, the transport is given by

$$Hv \approx \left(4.14 \text{ m}^2 \text{ s}^{-1} \right) \cos \pi \left(\frac{y-y_{30}}{L} \right) \quad (12.12)$$

So, at 30-degrees, the 2-D transport is $4.14 \text{ m}^2 \text{ s}^{-1}$. Averaged over the 4000-m water depth we can arrive at an average velocity of $v \approx 1 \text{ mm s}^{-1}$, though the actual wind-driven transport tends to be surface intensified. Integrated across the Pacific, with a width of 10,000 km this yields a total 3-D transport of $4.14 \times 10^7 \text{ m}^3 \text{ s}^{-1}$, or 40

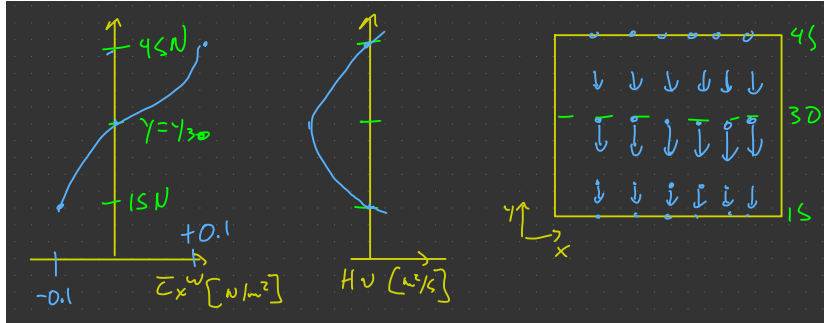


Figure 12.4: Sketch of shape of wind stress (left), shape of Sverdrup transport (middle), and arrows indicating what that transport looks like when looking from above (right).

Sv. Note that as we get closer to the bottom ($\lambda = 15N$) and the top ($\lambda = 45N$) the transport drops to zero (figure 12.1).

Note that this sense of transport agrees with observations of a sea-surface high displaced to the west of the gyre. Of the flow is clockwise around the high, then all the water to the east of the high will be moving southwards. This estimate also accords with our best estimates of the transport in the gyre from calculating geostrophic velocities (

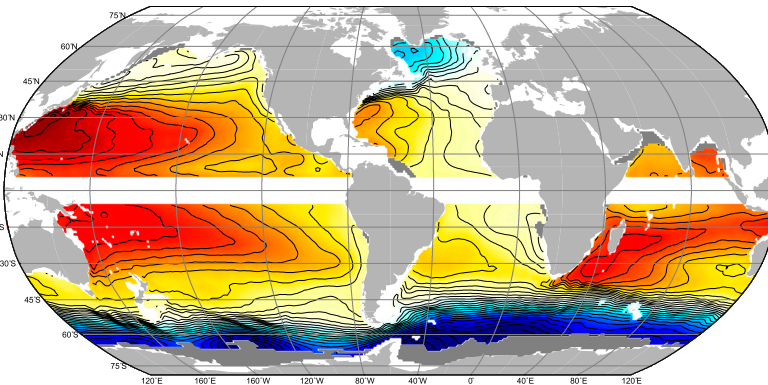


Figure 12.5: Geostrophic streamfunction at 5 dbar in m^2s^{-2} , estimated from Argo floats. Red high, clockwise flow. [Gray and Riser, 2014]

12.3.1 Alternative derivation: Ekman pumping

An alternative way to think about the Sverdrup balance is to separate the upper-ocean Ekman layer from the interior of the ocean. In this case, the interior of the ocean does not feel the wind friction, and hence has no mechanical torque acting on it. However, there is a constant downwelling of water from the Ekman pumping. This causes the water already in the interior to be squished, so $dH/dt < 0$, and the water will tend to move south.

In terms of the vorticity equation, we can write it with no torques and small relative vorticity as

$$\frac{d}{dt} \frac{f}{H} = 0 \quad (12.13)$$

or using the fact that $d(ab)/dt = adb/dt + bda/dt$:

$$Hv\beta = f \frac{dH}{dt} = fw \quad (12.14)$$

where the rate of squishing of the deeper water is w , the rate of Ekman pumping (figure 12.6).

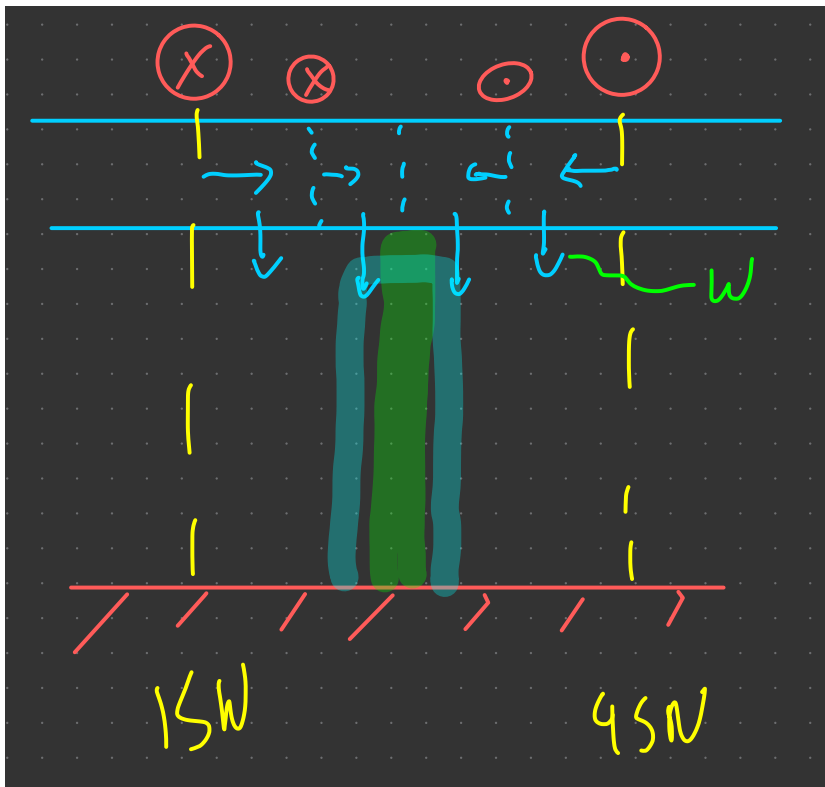


Figure 12.6: Sketch of how Ekman pumping pushes down on the water in the interior, causing H to decrease, and hence the water to tend to flow south to compensate.

We noted in that the rate of Ekman pumping is related to the curl of the wind stress:

$$w = -\frac{1}{f\rho_0} \frac{d\tau_x^W}{dy} \quad (12.15)$$

or,

$$Hv\beta = f \frac{dH}{dt} = -\frac{1}{\rho_0} \frac{d\tau_x^W}{dy} \quad (12.16)$$

just like in the derivation above.

12.4 Return flow

Remember that the Sverdrup balance applies from the top to the bottom of the water column, so if all the water between 15 and 45 N is flowing south under the Sverdrup balance, there has to be a return flow to the north somewhere. The shape of the sea-surface height in figure 12.5 indicates that the northward flow is on the west side of the basin, and indeed we can easily argue that this is indeed true.

In order for flow to move north, it needs a positive torque. The wind torque is negative, so the opposing torque must be from friction and tend to spin the water counter-clockwise. If we assume the torque comes from the sides, we simply check the sign of the torque exerted by a parcel of water moving north on either sidewall (figure 12.7). If the return flow were in the east, then the friction force would be on the east side of a parcel of water, and there would be no friction force on the left side. This would tend to spin the water in a clockwise sense, or with negative torque. This is, of course, the wrong sense, because we need a positive torque. If we consider a return flow on the west side, the friction is on the west side of a parcel moving north, and there is no friction on the east side, so the parcel will tend to be torqued in a counter-clockwise direction, and hence this is where the return flow must be.

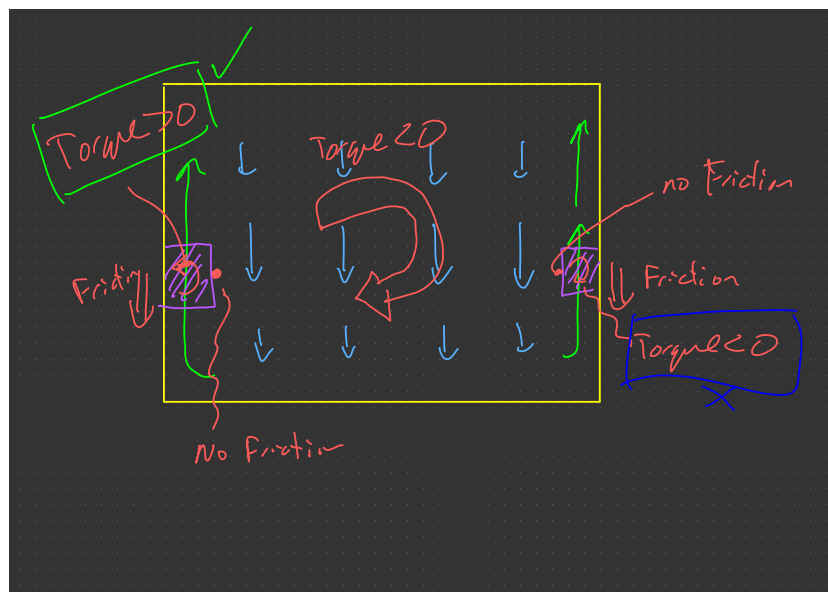


Figure 12.7: Sketch of sidewall torque on two alternate return flows in a subtropical gyre.

The final missing piece is that water must move from the interior to and from the western boundary current. just using conservation

of volume, we can readily infer that the water south of 30 N must be moving west, and the water north must be moving east. Thus the flow follows the geostrophic contours as plotted in figure 12.5, moving around the high sealevel in a clockwise fashion. Where the sea level gradient is steepest, the flow is the fastest, in the Western Boundary current.

Looking at figure 12.5, it is apparent that there is a western boundary current in both the northern and southern hemispheres, and in all the ocean basins. In the subtropical gyres, these currents carry water from the equator towards the poles, and in the subpolar gyres, they do the opposite. Its worth testing your knowledge by considering the wind patterns in the southern hemisphere, or the subpolar gyre, and see if the sign of the torque accords with figure 12.5.

Bibliography

- Technical summary. In *The Ocean and Cryosphere in a Changing Climate*, pages 39–70. Cambridge University Press, apr 2022. DOI: 10.1017/9781009157964.002. URL <https://doi.org/10.1017/9781009157964.002>.
- S. J. Allin, J. C. Laube, E. Witrant, J. Kaiser, E. McKenna, P. Dennis, R. Mulvaney, E. Capron, P. Martinerie, T. Röckmann, and et al. Chlorine isotope composition in chlorofluorocarbons cfc-11, cfc-12 and cfc-113 in firn, stratospheric and tropospheric air. *Atmospheric Chemistry and Physics*, 15(12):6867–6877, Jun 2015. ISSN 1680-7324. DOI: 10.5194/acp-15-6867-2015. URL <http://dx.doi.org/10.5194/acp-15-6867-2015>.
- J.O. Blanton, M.A. Ferreira, and F.A. Andrade. Effect of a broad shallow sill on tidal circulation and salt transport in the entrance to a coastal plain estuary (Mira: Villa Nova De Milfontes, Portugal). *Estuaries*, 23(3):293–304, 2000.
- Frank Bryan. Parameter sensitivity of primitive equation ocean general circulation models. *J. Phys. Oceanogr.*, 17(7): 970–985, Jul 1987. ISSN 1520-0485. DOI: 10.1175/1520-0485(1987)017<0970:psopeo>2.0.co;2. URL [http://dx.doi.org/10.1175/1520-0485\(1987\)017<0970:PSOPEO>2.0.CO;2](http://dx.doi.org/10.1175/1520-0485(1987)017<0970:PSOPEO>2.0.CO;2).
- Harry L. Bryden, Hannah R. Longworth, and Stuart A. Cunningham. Slowing of the atlantic meridional overturning circulation at 25°n. *Nature*, 438(7068):655–657, Dec 2005. ISSN 1476-4687. DOI: 10.1038/nature04385. URL <http://dx.doi.org/10.1038/nature04385>.
- Harry L. Bryden, William E. Johns, Brian A. King, Gerard McCarthy, Elaine L. McDonagh, Ben I. Moat, and David A. Smeed. Reduction in ocean heat transport at 26°n since 2008 cools the eastern subpolar gyre of the north atlantic ocean. *Journal of Climate*, 33

- (5):1677–1689, mar 2020. DOI: 10.1175/jcli-d-19-0323.1. URL <https://doi.org/10.1175%2Fjcli-d-19-0323.1>.
- John A. Church and Neil J. White. Sea-level rise from the late 19th to the early 21st century. *Surveys in Geophysics*, 32(4-5):585–602, mar 2011. DOI: 10.1007/s10712-011-9119-1. URL <https://doi.org/10.1007%2Fs10712-011-9119-1>.
- Ruth Curry and Cecilie Mauritzen. Dilution of the northern North Atlantic Ocean in recent decades. *Science*, 308(5729):1772–1774, Jun 2005. ISSN 1095-9203. DOI: 10.1126/science.1109477. URL <http://dx.doi.org/10.1126/science.1109477>.
- A. J. Elliott. The circulation and salinity distribution of the Upper Potomac Estuary. *Chesapeake Science*, 17(3):141–147, 1976.
- Alexander Ganachaud and Carl Wunsch. Improved estimates of global ocean circulation, heat transport and mixing from hydrographic data. *Nature*, 408:453–457, 2000.
- Andrey Ganopolski and Stefan Rahmstorf. Rapid changes of glacial climate simulated in a coupled climate model. *Nature*, 409(6817):153–158, jan 2001. DOI: 10.1038/35051500. URL <https://doi.org/10.1038%2F35051500>.
- A.E. Gargett, D. Stucchi, and F. Whitney. Physical processes associated with high primary productivity in Saanich Inlet, British Columbia. *Est. Coast. and Shelf Sci*, 56(5–6):1141–1156, 2003. DOI: 10.1016/S0272-7714(02)00319-0.
- Geoffrey Gebbie and Peter Huybers. The mean age of ocean waters inferred from radiocarbon observations: Sensitivity to surface sources and accounting for mixing histories. *J. Phys. Oceanogr.*, 42(2):291–305, Feb 2012. ISSN 1520-0485. DOI: 10.1175/jpo-d-11-043.1. URL <http://dx.doi.org/10.1175/JPO-D-11-043.1>.
- W. Rockwell Geyer and David M. Farmer. Tide-induced variation of the dynamics of a salt wedge estuary. *J. Phys. Oceanogr.*, 19:1060–1072, 1989.
- A.L. Gordon. Bottom water formation. *Encyclopedia of Ocean Sciences*, pages 415–421, 2001. DOI: 10.1016/b978-012374473-9.00006-0. URL <http://dx.doi.org/10.1016/B978-012374473-9.00006-0>.
- Alison R. Gray and Stephen C. Riser. A global analysis of Sverdrup balance using absolute geostrophic velocities from Argo. *J. Phys. Oceanogr.*, 44(4):1213–1229, apr 2014. DOI: 10.1175/jpo-d-12-0206.1. URL <https://doi.org/10.1175%2Fjpo-d-12-0206.1>.

N. Hogg, P. Biscaye, W. Gardner, and W. J. Schmitz, Jr. On the transport and modification of Antarctic bottom water in the Vema Channel. *J. Mar. Res.*, 40(Suppl.):231–263, 1982.

WE Johns, TJ Shay, JM Bane, and DR Watts. Gulf Stream structure, transport, and recirculation near 68 w. *J. Geophys. Res.*, 100:817–817, 1995.

Dagmar Kieke and Igor Yashayaev. Studies of Labrador Sea Water formation and variability in the subpolar North Atlantic in the light of international partnership and collaboration. *Progress in Oceanography*, 132:220–232, Mar 2015. ISSN 0079-6611. DOI: 10.1016/j.pocean.2014.12.010. URL <http://dx.doi.org/10.1016/j.pocean.2014.12.010>.

Ming Li, Liejun Zhong, and William C. Boicourt. Simulations of Chesapeake Bay estuary: Sensitivity to turbulence mixing parameterizations and comparison with observations. *J. Geophys. Res.*, 110 (C12004):doi:10.1029/2004JC002585, 2005.

Rick Lumpkin and Kevin Speer. Global ocean meridional overturning. *J. Phys. Oceanogr.*, 37:2550–2562, 2007.

Jennifer A. MacKinnon, Matthew H. Alford, Joseph K. Ansong, Brian K. Arbic, Andrew Barna, Bruce P. Briegleb, Frank O. Bryan, Maarten C. Buijsman, Eric P. Chassignet, Gokhan Danabasoglu, and et al. Climate process team on internal-wave driven ocean mixing. *Bull. Am. Meteorol. Soc.*, Mar 2017. ISSN 1520-0477. DOI: 10.1175/bams-d-16-0030.1.

Dianne Masson and Patrick F. Cummins. Observations and modeling of seasonal variability in the Straits of Georgia and Juan de Fuca. *J. Mar. Res.*, 62:491–516, 2004.

Stewart M. McKinnell and William R. Crawford. The 18.6-year lunar nodal cycle and surface temperature variability in the northeast pacific. *J. Geophys. Res.*, 112(C2), Feb 2007. ISSN 0148-0227. DOI: 10.1029/2006jc003671. URL <http://dx.doi.org/10.1029/2006JC003671>.

Michele Y. Morris, Melinda M. Hall, Louis C. St. Laurent, and Nelson G. Hogg. Abyssal mixing in the Brazil Basin. *J. Phys. Oceanogr.*, 31(11):3331–3348, Nov 2001. ISSN 1520-0485. DOI: 10.1175/1520-0485(2001)031<3331:AMITBB>2.0.CO;2. URL [http://dx.doi.org/10.1175/1520-0485\(2001\)031<3331:AMITBB>2.0.CO;2](http://dx.doi.org/10.1175/1520-0485(2001)031<3331:AMITBB>2.0.CO;2).

Noel A. Pelland, Charles C. Eriksen, and Meghan F. Cronin. Seaglider surveys at ocean station papa: Circulation and water

- mass properties in a meander of the north pacific current. *Journal of Geophysical Research: Oceans*, 121(9):6816–6846, Sep 2016. ISSN 2169-9275. DOI: 10.1002/2016jco11920.
- K.L. Polzin, J.M. Toole, J.R. Ledwell, and R.W. Schmitt. Spatial variability of turbulent mixing in the abyssal ocean. *Science*, 276:93–96, April 1997.
- J. F. Price, R. A. Weller, and R. R. Schudlich. Wind-driven ocean currents and ekman transport. *Science*, 238(4833):1534–1538, Dec 1987. ISSN 1095-9203. DOI: 10.1126/science.238.4833.1534. URL <http://dx.doi.org/10.1126/science.238.4833.1534>.
- Raymond Schmitt. The ocean's role in climate. *Oceanography*, 31(2), Jun 2018. ISSN 1042-8275. DOI: 10.5670/oceanog.2018.225. URL <http://dx.doi.org/10.5670/oceanog.2018.225>.
- Friedrich A. Schott, Jürgen Fischer, Marcus Dengler, and Rainer Zantopp. Variability of the Deep Western Boundary Current east of the Grand Banks. *Geophysical Research Letters*, 33(21), Oct 2006. ISSN 0094-8276. DOI: 10.1029/2006gl026563. URL <http://dx.doi.org/10.1029/2006GL026563>.
- J.R. Schubel and D.W. Pritchard. Responses of upper Chesapeake Bay to variations in discharge of the Susquehanna River. *Estuaries*, 9(4A):236–249, 1986.
- Harvey E. Seim and Michael C. Gregg. Detailed observations of a naturally occurring shear instability. *J. Geophys. Res.*, 99(C5):10049–10073, 1994.
- Andrew Shepherd, Erik R. Ivins, Geruo A, Valentina R. Barletta, Mike J. Bentley, Srinivas Bettadpur, Kate H. Briggs, David H. Bromwich, René Forsberg, Natalia Galin, Martin Horwath, Stan Jacobs, Ian Joughin, Matt A. King, Jan T. M. Lenaerts, Jilu Li, Stefan R. M. Ligtenberg, Adrian Luckman, Scott B. Luthcke, Malcolm McMillan, Rakia Meister, Glenn Milne, Jeremie Mouginot, Alan Muir, Julien P. Nicolas, John Paden, Antony J. Payne, Hamish Pritchard, Eric Rignot, Helmut Rott, Louise Sandberg Sørensen, Ted A. Scambos, Bernd Scheuchl, Ernst J. O. Schrama, Ben Smith, Aud V. Sundal, Jan H. van Angelen, Willem J. van de Berg, Michiel R. van den Broeke, David G. Vaughan, Isabella Velicogna, John Wahr, Pippa L. Whitehouse, Duncan J. Wingham, Donghui Yi, Duncan Young, and H. Jay Zwally. A reconciled estimate of ice-sheet mass balance. *Science*, 338(6111):1183–1189, nov 2012. DOI: 10.1126/science.1228102. URL <https://doi.org/10.1126%2Fscience.1228102>.

- J. O. Shin, S. B. Dalziel, and P. F. Linden. Gravity currents produced by lock exchange. *Journal of Fluid Mechanics*, 521:1–34, Dec 2004. ISSN 1469-7645. DOI: 10.1017/S002211200400165X.
- W. D. Smyth, J.D. Nash, and J.N. Moum. Differential diffusion in breaking Kelvin-Helmholtz billows. *J. Phys. Oceanogr.*, 35:2753–2766, 2005. DOI: 10.1175/JPO2739.1.
- Frederick R. Stahr and Thomas B. Sanford. Transport and bottom boundary layer observations of the north atlantic deep western boundary current at the blake outer ridge. *Deep Sea Research Part II: Topical Studies in Oceanography*, 46(1-2):205–243, Jan 1999. ISSN 0967-0645. DOI: 10.1016/S0967-0645(98)00101-5. URL [http://dx.doi.org/10.1016/S0967-0645\(98\)00101-5](http://dx.doi.org/10.1016/S0967-0645(98)00101-5).
- Andrew L. Stewart and Andrew F. Thompson. Eddy generation and jet formation via dense water outflows across the antarctic continental slope. *J. Phys. Oceanogr.*, 46(12):3729–3750, Dec 2016. ISSN 1520-0485. DOI: 10.1175/jpo-d-16-0145.1. URL <http://dx.doi.org/10.1175/JPO-D-16-0145.1>.
- Bruce A. Warren. Transpacific hydrographic sections at lats. 43 °s and 28 °s: the scorpio expedition—ii. deep water. *Deep Sea Research and Oceanographic Abstracts*, 20(1):9–38, Jan 1973. ISSN 0011-7471. DOI: 10.1016/0011-7471(73)90040-5.
- Martin Wild, Doris Folini, Maria Z. Hakuba, Christoph Schär, Sonia I. Seneviratne, Seiji Kato, David Rutan, Christof Ammann, Eric F. Wood, and Gert König-Langlo. The energy balance over land and oceans: an assessment based on direct observations and cmip5 climate models. *Climate Dynamics*, 44(11):3393–3429, 2015. DOI: 10.1007/s00382-014-2430-z. URL <https://doi.org/10.1007/s00382-014-2430-z>.
- Carl Wunsch. The ocean circulation inverse problem. Jun 1996. DOI: 10.1017/cb09780511629570. URL <http://dx.doi.org/10.1017/CB09780511629570>.
- Ichiro Yasuda, Satoshi Osafune, and Hiroaki Tatebe. Possible explanation linking 18.6-year period nodal tidal cycle with bi-decadal variations of ocean and climate in the north pacific. *Geophys. Res. Lett.*, 33(8), 2006. ISSN 0094-8276. DOI: 10.1029/2005gl025237. URL <http://dx.doi.org/10.1029/2005GL025237>.

Index

license, [2](#)